

# Concept of Modular Kinematics to Design Ultra-high Precision Parallel Robots

THÈSE N° 5377 (2012)

PRÉSENTÉE LE 8 JUIN 2012

À LA FACULTÉ DES SCIENCES ET TECHNIQUES DE L'INGÉNIEUR  
LABORATOIRE DE SYSTÈMES ROBOTIQUES 2  
PROGRAMME DOCTORAL EN SYSTÈMES DE PRODUCTION ET ROBOTIQUE

ÉCOLE POLYTECHNIQUE FÉDÉRALE DE LAUSANNE

POUR L'OBTENTION DU GRADE DE DOCTEUR ÈS SCIENCES

PAR

**Murielle RICHARD**

acceptée sur proposition du jury:

Prof. H. Bleuler, président du jury  
Prof. R. Clavel, directeur de thèse  
Prof. J. Giovanola, rapporteur  
Dr P. Helmer, rapporteur  
Dr S. Henein, rapporteur



ÉCOLE POLYTECHNIQUE  
FÉDÉRALE DE LAUSANNE

Suisse  
2012



# Version Abrégée

La miniaturisation sera le défi clé de la prochaine décennie dans de nombreux domaines industriels tels que la microélectronique, l'optique et le biomédical. Bien que la plupart de leurs produits atteignent déjà des empreintes de quelques millimètres carrés, la tendance actuelle visant à intégrer le maximum d'éléments dans un volume minimal nécessite des composants encore plus compacts. Ce phénomène crée par conséquent un besoin croissant de robots industriels capables d'effectuer des tâches de micromanipulation et de micro-assemblage avec une précision sub-micrométrique. Toutefois, la conception de telles machines est actuellement gourmande en temps et en argent, principalement à cause de la double complexité de leur développement : d'un point de vue cinématique d'abord, l'utilisation d'une structure parallèle consiste en une approche particulièrement intéressante pour la construction de robots d'ultra-haute précision. La synthèse d'une telle cinématique se révèle néanmoins particulièrement délicate pour les machines de plus de 3 degrés de liberté. De plus, les robots ainsi créés ne permettent guère de s'adapter à des modifications du cahier des charges industriel : s'il venait à changer, impliquant par exemple l'ajout d'un degré de liberté ou le déplacement d'un centre de rotation, le processus de conception devrait être entièrement recommencé. Le deuxième défi consiste à concevoir et réaliser des mécanismes à guidages flexibles : ce type d'articulations, basées sur l'élasticité de la matière, permettent d'obtenir des mouvements sans frottement, sans jeu et sans usure. Leur utilisation est nécessaire pour obtenir la précision sub-micrométrique visée. Bien que la synthèse de structures planes et à faible mobilité sont maintenant largement étudiées, le développement d'un robot tridimensionnel entièrement constitué de guidages flexibles est encore rare, en particulier dans le contexte industriel.

Cette thèse présente ainsi une **méthodologie de conception modulaire qui diminue significativement le temps de développement (time-to-market) des robots d'ultra-haute précision**. Cette procédure peut être comparée à un **Lego robotique**, où un **nombre fini de briques de construction conceptuelles** permet d'aisément construire et modifier des robots parallèles. De plus, ce travail montre que les machines créées grâce à cette approche présentent des **performances similaires, voire même supérieures**, à celles de robots développés de manière plus traditionnelle.

Le **concept de cinématiques modulaires** constitue l'aspect clé de cette thèse : il vise à faciliter la synthèse de cinématiques parallèles grâce à des catalogues de solutions. A ce stade de la méthodologie, les briques de construction conceptuelles et les cinématiques sont entièrement indépendantes de toute réalisation mécanique. Elles peuvent donc être utilisées

pour concevoir une large variété de robots, allant de la machine-outil aux robots d'échelle micrométrique. Un premier catalogue de solutions conceptuelles regroupe exhaustivement les cinématiques générées par la combinaison des briques de construction. Un catalogue de solutions réduit pour l'ultra-haute précision a également été établi : basé sur des critères de sélection liés à la conception et l'usinage de structures flexibles, il permet de réduire le nombre total de solutions et d'ainsi faciliter l'utilisation pratique du concept.

La deuxième partie de ce travail traite de la *conception mécanique des briques de construction*, dont le principal défi consiste à augmenter le rapport entre le volume de travail d'un mécanisme et son encombrement. Une ou plusieurs réalisations à guidages flexibles ont été développées pour chaque brique motorisée : l'accent a notamment été mis sur l'utilisation originale d'un Centre de Rotation Déporté, permettant d'atteindre de grands angles de rotation tout en réduisant drastiquement les translations parasites. Le développement d'une sous-brique d'actionnement, commune à toutes les briques motorisées, introduit un nouveau niveau de modularité, accroissant ainsi encore la flexibilité de la méthodologie. De plus, de nouvelles réalisations, ainsi que des utilisations originales de mécanismes bien connus, sont proposées pour les briques non-motorisées.

Une *étude de cas sur un robot à 5 degrés de liberté, le Legolas 5*, illustre enfin l'utilisation pratique de la méthodologie. Tout d'abord, la sélection d'une cinématique du catalogue de solutions adaptée au cahier des charges est détaillée. Ensuite, le développement du prototype du Legolas 5 met en évidence la conception mécanique des briques de construction ainsi que des subtilités d'assemblage, telles que l'alignement des forces et la compensation de la gravité, permettant de judicieusement construire un robot de haute performance. La caractérisation de cette machine a permis de mesurer une résolution et une répétabilité de mouvement de 50 nm en translation et de 1.9  $\mu$ rad en rotation (limitées par la résolution des capteurs).

Cette étude de cas a engendré *la famille Legolas, nouvelle famille de robots parallèles d'ultra-haute précision*, qui inclut notamment la version orthogonale de la cinématique du Delta. En utilisant seulement 6 briques de construction, une solution peut être réalisée pour chacune de 19 mobilités possibles du robot. La caractérisation prometteuse du Legolas 5 laisse présager que les robots de cette famille seront des candidats sérieux pour satisfaire la demande croissante en machines industrielles d'ultra-haute précision, rapidement conçues et hautement performantes.

**Mots-clés :** Robotique parallèle, Robotique industrielle, Cinématique, Modularité, Ultra-haute précision, Méthodologie de conception, Conception mécanique, Guidages flexibles, Mécanismes à guidages flexibles.



# Abstract

Miniaturisation will be the key challenge for the next decade in numerous industrial fields, such as microelectronics, optics and biomedical engineering. Although most of their products already achieve footprints of some square millimeters, the trend towards the integration of a maximum number of elements in a minimal volume requires even more compact components. This tendency creates a growing need for industrial robots able to perform micromanipulation and microassembly tasks with a submicrometric precision. Nonetheless, the design of such machines is nowadays costly, both in time and money, mostly because of the twofold complexity of their development: first, from a kinematic standpoint, the use of a parallel structure consists in a particularly interesting approach to build ultra-high precision robots. However, the synthesis of such a kinematics proves especially challenging for machines presenting more than 3 degrees of freedom. Moreover, the resulting robots are scarcely flexible: if the industrial specifications are modified, which for example necessitates to add a degree of freedom or to change the position of a rotation centre, the design process has to be restarted, often from the very beginning. The second challenge consists in the mechanical design of flexure-based mechanisms: flexure hinges are joints which are based on the elasticity of the matter. They allow to perform motions which are without friction, backlash and wear; their use is thus mandatory to achieve the aimed submicrometric precision. Albeit the synthesis of planar and low-degree of freedom structures is now widely investigated, the development of a whole tridimensional flexure-based robot is still infrequent, especially in the industrial context.

This thesis thus introduces a ***modular design methodology which significantly reduces the time-to-market of ultra-high precision robots***. This procedure can be compared to a ***robotic Lego***, where a ***finite number of conceptual building bricks*** allows to easily design and modify parallel robots. Furthermore, this work shows that the machines resulting from this approach present ***similar or even improved performances*** compared to robots developed more traditionally.

The key aspect of this thesis consists in the *concept of modular kinematics*, which aims at facilitating the synthesis of parallel kinematics thanks to solution catalogues. At this step of the methodology, the conceptual building bricks and the kinematics are totally independent from any mechanical design: they can thus be used to synthesise a large variety of robots, from machine-tools to microscale robots. An exhaustive conceptual solution catalogue groups all kinematics generated by the combination of the building bricks. Then, a reduced solution catalogue for ultra-high precision is proposed: based on selection criteria

linked with the design and machining of flexure-based mechanisms, it allows to reduce the total number of solutions and thus facilitates the practical use of the concept.

The second part of this work details the *mechanical design of the building bricks*, whose main challenge consists in increasing the ratio between the working ranges of the mechanisms and their overall size. One or more flexure-based solutions have been developed for each motorised brick: a special emphasis is given to the original use of a Remote Centre of Motion, which allows to achieve high rotation angles while drastically reducing parasitic translations. The development of a standardised actuation sub-brick, common to all motorised bricks, introduces a new level of modularity, thus increasing even more the flexibility of the methodology. As for non-actuated bricks, original designs and uncommon uses of well-known mechanisms are proposed.

A case study on a 5-degree of freedom robot, *Legolas 5*, finally illustrates the practical use of the methodology: first, the selection in the solution catalogue of a kinematics adapted to the specifications of the robot is detailed. Then, the development of the *Legolas 5* prototype highlights the mechanical design of the necessary building bricks, as well as assembly subtleties, such as force alignment and gravity compensation, which allow to shrewdly design a high-performance robot. The measurements of this machine have shown motion resolution and repeatability of 50 nm in translation and 1.9  $\mu$ rad in rotation (limited by the sensor resolution).

This case study has generated *the Legolas family, a new family of ultra-high precision parallel robots*, which notably includes the orthogonal version of the Delta kinematics: using only 6 of the conceptual building bricks, one solution can be built for each of the 19 possible robot mobilities. The promising characterisation of the *Legolas 5* tends to suggest that the robots from this family will be interesting candidates to fulfill the upcoming need for quickly designed and high-performance industrial ultra-high precision machines.

**Keywords:** Parallel robotics, Industrial robotics, Kinematics, Modularity, Ultra-high precision, Design methodology, Mechanical design, Flexure hinges, Flexure-based mechanisms

# Acknowledgements

In the first place, I would like to thank my thesis director, Prof. Reymond Clavel, for having given me the opportunity to do this thesis, and for letting me freely choose the research directions to investigate, while being always ready for instructive brainstorm sessions. Besides, the four years spent under his supervision have allowed to add *vaudois* to my language skills!

Then, I would like to express my thankfulness to the members of my thesis jury, namely Prof. Hannes Bleuler, Prof. Jacques Giovanola, Dr. Patrick Helmer and Dr. Simon Henein, for the meticulous reading of the manuscript and for their constructive comments. Special thanks to the two latter, Dr. Helmer and Dr. Henein, who took an early and lively interest in my research; I am grateful for their trust and for the very helpful advice they gave me.

A big thank you to all colleagues met during these years at the Laboratoire de Systèmes Robotiques (LSRO), who are way too numerous to be all named here, for the large range of activities performed together, from technical discussions to table football sessions. In particular, I would like to thank:

The Ph.D. students of the LSRO, especially the two current and last ones, namely Florent Cosandier and Philipp Kobel, for sharing experience, advice, brainstorms and doctoral courses, as well as for the helping hands given for my precision measurements.

Dr. Mohamed Bouri for the control hardware and software, Jacques Fournier for the electronics, and Willy Maeder who has nearly always the thing you are looking for hidden somewhere in his office, in the manner of Riki the pelican in the Petzi comics, who always has a brace or some other tool in his beak!

Olivier Chappuis for the development of the Matlab algorithm featured in Appendix A, which proved the exhaustiveness of the solution catalogue, and for his dexterity with a keyboard, especially with the delete key.

Sylvain Tozzini for the help with the wiring of the control hardware.

Carole Weissenberger, the lab secretary, for her obligingness and precious help, especially for the quick and efficient *ibicotting* of my thesis report copies.

Dr. Emanuele Lubrano, who has too many *casquettes*: former colleague, friend and undisputed master of the toy machine! More seriously, his knowledge and experience of high precision measurement and calibration have been more than useful, and he greatly contributed to create the cheerful work atmosphere in the lab.

Furthermore, I would like to thank:

The semestre project students Arnaud Müller, who contributed to the development of the robot mock-up, and Raphaël Waldis, whose presence of mind saved the Legolas prototype from a starting fire in the middle of the night.

The workshops for the numerous hours spent on the machining of the Legolas mock-up and prototype: Marc Salle and his staff from the ATME, Alfred Thomas and his staff from the ATPR.

The administration of the EDPR doctoral program, especially Claire Chabanel, Prof. Max-Olivier Hongler and Dr. Eric Boillat.

Last but not least, I wish to express my gratefulness to my family and friends for their unwavering support; special thanks to my sister Joëlle for proof-reading the manuscript and to my parents, who have always encouraged me in everything I have undertaken, including my scientific career, even when it meant spending endless times in technical museums or coping with improbable experiments involving the kitchen oven!

These acknowledgments would not be complete without symbolic thanks to the music groups which I have been listening to while performing my research; if I had to retain only one song, it would be the following, which illustrates well what thoughts came to my mind at the time I faced what seemed endless and insurmountable problems:

*The pouring rain sticks my hair to my face  
An empty gaze is all I have left  
The stars that once led my way  
Have dimmed, the sky turned grey  
The path once so clear faded away  
Blessed are the days when life is intent and clear  
No falter or doubt, I know the way*

[...]

*Stand up and fight!  
Stand up and look into the light  
Pushing the clouds away  
Stand up and fight!  
Stand up and see the sky turn bright  
Fight for a better day*

[...]

Turisas, *Stand Up and Fight*, from the eponymous album, Century Media, 2011.

*Everything should be made as simple as possible, but not simpler.*

Albert Einstein

*On ne chatouille pas impunément le nanomètre.*

Reymond Clavel



# Contents

- Version Abrégée** **i**
- Abstract** **iii**
- Acknowledgements** **v**
- 1 Introduction** **1**
  - 1.1 General introduction . . . . . 1
  - 1.2 Preliminary definitions . . . . . 2
    - 1.2.1 Degrees of Freedom (DOF) and mobility . . . . . 2
    - 1.2.2 Resolution, precision, repeatability and accuracy . . . . . 3
    - 1.2.3 Parallel robots . . . . . 4
    - 1.2.4 Flexure hinges . . . . . 5
    - 1.2.5 Modularity of industrial robots . . . . . 7
  - 1.3 Objectives . . . . . 7
  - 1.4 Postulate . . . . . 8
  - 1.5 Main contributions . . . . . 8
  - 1.6 Structure of the thesis report . . . . . 9
- 2 State of the art** **11**
  - 2.1 Modular design methodologies . . . . . 11
    - 2.1.1 Design methodologies of parallel robots . . . . . 11
    - 2.1.2 Concepts of serial modular robots . . . . . 13
    - 2.1.3 Concepts of parallel modular robots . . . . . 13
      - 2.1.3.1 Methodologies based on the Stewart platform . . . . . 13
      - 2.1.3.2 Methodologies based on libraries of modules . . . . . 16
  - 2.2 Flexure-based mechanisms . . . . . 21
    - 2.2.1 Design methodologies . . . . . 21
    - 2.2.2 Modelisation . . . . . 21
    - 2.2.3 Examples of flexure-based designs . . . . . 22
  - 2.3 High precision and ultra-high precision robots . . . . . 25
    - 2.3.1 Delta<sup>3</sup> robots family . . . . . 25
    - 2.3.2 Sigma 6 robot . . . . . 26
    - 2.3.3 Academic high precision robots . . . . . 28

2.3.4	Commercial high precision and ultra-high precision robots . . . . .	29
2.4	Conclusion . . . . .	30
<b>3</b>	<b>Concept of modular kinematics</b>	<b>33</b>
3.1	Modular parallel robot and building bricks . . . . .	33
3.1.1	Conceptual building bricks . . . . .	34
3.2	Generation of the exhaustive conceptual solution catalogue . . . . .	40
3.2.1	Active bricks arrangements . . . . .	41
3.2.1.1	First example: planar joint mobility . . . . .	41
3.2.1.2	Second example: 4-DOF mobility . . . . .	43
3.2.2	Passive bricks arrangements . . . . .	44
3.2.3	Automatic generation of the conceptual solution catalogue . . . . .	46
<b>4</b>	<b>Reduced solution catalogue for ultra-high precision</b>	<b>49</b>
4.1	Hypotheses for ultra-high precision . . . . .	49
4.2	Building bricks for ultra-high precision . . . . .	50
4.2.1	Active bricks . . . . .	50
4.2.2	Passive bricks . . . . .	53
4.3	Reduced conceptual solution catalogue . . . . .	56
<b>5</b>	<b>Mechanical design of the building bricks</b>	<b>59</b>
5.1	Challenges in flexure-based brick design . . . . .	59
5.2	Mechanical design of the active bricks for ultra-high precision . . . . .	60
5.2.1	Actuation sub-brick . . . . .	60
5.2.1.1	Linear flexure-based guiding mechanism . . . . .	61
5.2.1.2	Linear actuator . . . . .	63
5.2.1.3	Linear position sensor . . . . .	64
5.2.2	Active bricks design . . . . .	65
5.2.2.1	$R_{\parallel}$ and $R_{\perp}$ bricks . . . . .	65
5.2.2.2	$T_{\parallel}$ and $T_{\perp}$ bricks . . . . .	67
5.2.2.3	$T_{\parallel 1}T_{\parallel 2}$ and $T_{\parallel}T_{\perp}$ bricks . . . . .	67
5.2.2.4	$T_{\parallel}R_{\perp}$ , $T_{\perp}R_{\parallel}$ and $T_{\parallel 1}R_{\parallel 2}$ bricks . . . . .	68
5.2.2.5	$T_{\parallel 1}T_{\parallel 2}R_{\perp}$ and $T_{\parallel 1}T_{\perp}R_{\parallel 2}$ bricks . . . . .	69
5.3	Mechanical design of the passive bricks for ultra-high precision . . . . .	70
5.3.1	$r_{\parallel}$ and $r_{\perp}$ bricks . . . . .	71
5.3.2	$t_{\parallel}$ and $t_{\perp}$ bricks . . . . .	73
5.3.3	$t_{\parallel 1}t_{\parallel 2}$ and $t_{\parallel}t_{\perp}$ bricks . . . . .	73
5.3.4	$t_{\parallel 1}r_{\parallel 1}$ and $t_{\perp}r_{\perp}$ bricks . . . . .	73
5.3.5	$t_{\parallel}r_{\perp}$ , $t_{\perp}r_{\parallel}$ and $t_{\parallel 1}r_{\parallel 2}$ bricks . . . . .	74
5.3.6	$r_{\parallel 1}r_{\parallel 2}$ and $r_{\parallel}r_{\perp}$ bricks . . . . .	74
5.3.7	$t_{\parallel}t_{\perp}r_{\perp}$ , $t_{\parallel 1}t_{\perp}r_{\parallel 1}$ and $t_{\parallel 1}t_{\parallel 2}r_{\parallel 1}$ bricks . . . . .	74
5.3.8	$t_{\parallel 1}t_{\perp}r_{\parallel 2}$ and $t_{\parallel 1}t_{\parallel 2}r_{\perp}$ bricks . . . . .	76
5.3.9	$t_{\perp}r_{\parallel 1}r_{\parallel 2}$ and $t_{\parallel 1}r_{\parallel 2}r_{\perp}$ bricks . . . . .	76
5.3.10	$t_{\perp}r_{\parallel}r_{\perp}$ , $t_{\parallel 1}r_{\parallel 1}r_{\perp}$ and $t_{\parallel 1}r_{\parallel 1}r_{\parallel 2}$ bricks . . . . .	76



5.3.11	$t_{\parallel}t_{\perp}r_{\parallel}r_{\perp}$ , $t_{\parallel}t_{\perp}r_{\parallel}r_{\parallel}$ and $t_{\parallel}t_{\parallel}r_{\parallel}r_{\perp}$ bricks	77
5.3.12	$t_{\parallel}t_{\perp}r_{\parallel}r_{\perp}$ and $t_{\parallel}t_{\parallel}r_{\parallel}r_{\parallel}$ bricks	77
5.3.13	$t_{\perp}r_{\parallel}r_{\parallel}r_{\perp}$ and $t_{\parallel}r_{\parallel}r_{\parallel}r_{\perp}$ bricks	78
5.3.14	$t_{\parallel}t_{\perp}r_{\parallel}r_{\parallel}r_{\perp}$ and $t_{\parallel}t_{\parallel}r_{\parallel}r_{\parallel}r_{\perp}$ bricks	79
5.3.15	$t_{\parallel}t_{\parallel}t_{\perp}r_{\parallel}r_{\perp}$ and $t_{\parallel}t_{\parallel}t_{\perp}r_{\parallel}r_{\parallel}$ bricks	80
5.4	Discussion	80
<b>6</b>	<b>Case study: 5-DOF ultra-high precision robot</b>	<b>83</b>
6.1	Robot specifications	83
6.2	Kinematics synthesis	84
6.2.1	Active bricks arrangements	84
6.2.2	Passive bricks arrangements	85
6.2.3	Legolas, ultra-high precision parallel robots family	89
6.3	Mechanical design	91
6.3.1	Active bricks design	91
6.3.1.1	Actuation sub-brick	91
6.3.1.2	$T_{\parallel}$ active brick	93
6.3.1.3	$T_{\parallel}R_{\perp}$ active brick	94
6.3.2	$t_{\parallel}t_{\perp}r_{\parallel}r_{\parallel}$ passive brick design	95
6.3.3	Design and assembly subtleties	96
6.3.3.1	Leaf spring assembly	96
6.3.3.2	Actuators adjustment	96
6.3.3.3	Gravity compensation	98
6.3.4	Legolas 5 prototype	99
6.3.4.1	Force alignment	100
6.4	Characterisation and results	101
6.4.1	Actuation sub-bricks	102
6.4.1.1	Single translation actuation sub-bricks	103
6.4.1.2	Translation and rotation actuation sub-bricks	106
6.4.1.3	Eigenfrequencies	108
6.4.2	Legolas 5 prototype	109
6.4.2.1	Workspace	109
6.4.2.2	Resolution and repeatability	112
6.4.2.3	Eigenfrequencies	120
6.5	Discussion	126
<b>7</b>	<b>Conclusion</b>	<b>129</b>
7.1	General conclusion	129
7.2	Original contributions	130
7.3	Perspectives	131
7.4	Final note	132

<b>Appendix</b>	<b>134</b>
<b>A Automatic generation of the exhaustive conceptual solution catalogue</b>	<b>135</b>
A.1 Generation of the active bricks arrangements . . . . .	135
A.1.1 Active mobility bricks generation . . . . .	136
A.1.2 Establishment of the active bricks arrangements catalogue . . . . .	138
A.2 Generation of the passive bricks arrangements . . . . .	140
<b>B Exhaustive conceptual solution catalogue</b>	<b>145</b>
<b>C Reduced solution catalogue for ultra-high precision</b>	<b>205</b>
<b>D Mechanical design of the active bricks for ultra-high precision</b>	<b>231</b>
D.1 $R_{\parallel}$ and $R_{\perp}$ bricks . . . . .	231
D.2 $T_{\parallel}$ and $T_{\perp}$ bricks . . . . .	233
D.3 $T_{\parallel 1}T_{\parallel 2}$ and $T_{\parallel}T_{\perp}$ bricks . . . . .	233
D.3.1 Solution featuring two collinear actuators . . . . .	233
D.3.2 Solution featuring two orthogonal actuators . . . . .	234
D.4 $T_{\parallel}R_{\perp}$ , $T_{\perp}R_{\parallel}$ and $T_{\parallel 1}R_{\parallel 2}$ bricks . . . . .	235
D.5 $T_{\parallel 1}T_{\parallel 2}R_{\perp}$ and $T_{\parallel 1}T_{\perp}R_{\parallel 2}$ bricks . . . . .	236
<b>E Legolas, ultra-high precision parallel robots family</b>	<b>239</b>
E.1 1 DOF: $R_x$ . . . . .	241
E.2 1 DOF: $T_x$ . . . . .	241
E.3 2 DOF: $T_x, T_y$ . . . . .	242
E.4 2 DOF: $T_x, R_x$ . . . . .	242
E.5 2 DOF: $T_x, R_y$ . . . . .	243
E.6 2 DOF: $R_x, R_y$ . . . . .	243
E.7 3 DOF: $T_x, T_y, T_z$ . . . . .	244
E.8 3 DOF: $T_x, T_y, R_x$ . . . . .	245
E.9 3 DOF: $T_y, T_z, R_x$ . . . . .	245
E.10 3 DOF: $T_z, R_x, R_y$ . . . . .	246
E.11 3 DOF: $T_x, R_x, R_y$ . . . . .	247
E.12 3 DOF: $R_x, R_y, R_z$ . . . . .	248
E.13 4 DOF: $T_x, T_y, T_z, R_x$ . . . . .	249
E.14 4 DOF: $T_x, T_z, R_x, R_y$ . . . . .	250
E.15 4 DOF: $T_x, T_y, R_x, R_y$ . . . . .	251
E.16 4 DOF: $T_x, R_x, R_y, R_z$ . . . . .	252
E.17 5 DOF: $T_x, T_y, R_x, R_y, R_z$ . . . . .	253
E.18 5 DOF: $T_x, T_y, T_z, R_x, R_y$ . . . . .	254
E.19 6 DOF: $T_x, T_y, T_z, R_x, R_y, R_z$ . . . . .	255
<b>Bibliography</b>	<b>257</b>
<b>Curriculum Vitae</b>	<b>265</b>

# Chapter 1

## Introduction

### 1.1 General introduction

Miniaturisation will be the key challenge of the next decade in numerous industrial domains, such as microelectronics, optics and biomedical engineering. Although most of their products already achieve footprints of some square millimeters, the trend towards the integration of a maximum number of components in a minimal volume still demands more compact devices. Subsequently, *the current manufacturing processes and machines will soon be overtaken by this decrease in the size of the products: this tendency thus creates an urgent need for new production methods*. Two possible directions to solve this issue are currently investigated: the bottom-up and the top-down approaches. Bottom-up manufacturing is based on atomic and molecular manipulation: techniques such as self-assembly, chemical synthesis and positional assembly, which consists in building devices atom by atom, are the main investigation fields of this avenue. On the other hand, the top-down approach consists in removing and shaping material using ultra-high precision techniques. Usual cleanroom processes (lithography, etching) and classical material removal manufacturing methods (turning, milling, grinding, laser beam machining, electro-discharge machining), are included in this approach [92]. Furthermore, both philosophies notably share the objective of miniaturising the whole production line, thus using down-scaled pick-and-place machines, conveyers, and miniaturised specific operation robots, intended for tasks such as manipulation, packaging, or dispensing. Consequently, new production plant concepts emerge, such as microfactories: they consist in tabletop production lines, often combined with mini-cleanroom modular production cells, and have already been investigated for several years [49, 93].

The main implication of both new manufacturing approaches for small devices is *the creation of a need for robots able to perform micromanipulation and microassembly tasks with a submicrometric precision*. Typical requirements of such machines are performing more than 3 Degrees of Freedom (DOF), with strokes of some millimeters in translation and of more than  $5^\circ$  in rotation. The aimed precision order of magnitude is 10 to 100 nanometers and  $1 \mu\text{rad}$ . Furthermore, the total volume of the robot should be minimised to permit the miniaturisation of the production line.

Nonetheless, *the design of such machines is nowadays costly, both in time and money*, mostly because of the twofold complexity of their development: first, from a kinematic standpoint, the *use of a parallel structure* consists in a particularly interesting approach to build ultra-high precision robots. However, *the synthesis of such a kinematics proves especially challenging for machines presenting more than 3 degrees of freedom*. Numerous design methodologies have been developed, for example in [24, 31, 34]. However, these share the common drawback that *the resulting machines are scarcely flexible*: if the industrial specifications change, requiring for example to add a degree of freedom or to change the position of a rotation centre, the synthesis process has to be restarted, often from the very beginning.

Then, the second challenge consists in the *mechanical design of flexure-based mechanisms*: flexure hinges are joints which are based on the elasticity of the matter. They allow to perform motions which are without friction, backlash and wear; their use is thus mandatory to achieve the aimed submicrometric precision. Albeit the synthesis of planar and low-degree of freedom structures is now widely investigated, the development of a whole tridimensional flexure-based robot is still infrequent, especially in the industrial context.

This thesis thus introduces a *modular design methodology*, which drastically decreases the time-to-market of ultra-high precision robots. This procedure can be compared to a *robotic Lego*, where a *finite number of conceptual building bricks* allows to easily design and modify parallel robots. Furthermore, this work aims at proving that the machines resulting from this approach present *similar or even improved performances* compared to more traditionally developed robots.

## 1.2 Preliminary definitions

### 1.2.1 Degrees of Freedom (DOF) and mobility

The number of *degrees of freedom (DOF)* of a rigid body is the number of independent parameters needed to uniquely describe its kinematical behaviour in a tridimensional space. The maximal number of DOF is thus 6, as the behaviour of a free rigid body is characterised by 3 components in translation, describing its position, and 3 in rotation, expressing its orientation [34]. In this thesis, the following definitions and notations will be used:

- The *degrees of freedom of a robot or a mechanism* refer to the independent parameters needed to describe the behaviour of its output. The output of a robot is specifically named *end-effector*, and is defined as the rigid body which is in contact with the object to manipulate or assemble, possibly through a tool or a gripper [34]. In this thesis, *mobility* will be used as a synonym of degrees of freedom.
- The *internal degrees of freedom* of a robot or a mechanism are motions which are possible within the system without influencing the kinematic behaviour of the output.
- In this thesis, the notation of the 6 possible degrees of freedom of a robot or mechanism is the following:  $T_x$ ,  $T_y$  and  $T_z$  represent the components in translation, whereas  $R_x$ ,  $R_y$  and  $R_z$  stand for the components in rotation.

### 1.2.2 Resolution, precision, repeatability and accuracy

The positioning capability of a robot is usually described in terms of resolution, precision, repeatability and accuracy. These concepts, as well as their use in this thesis, need to be clearly defined.

- **Resolution** refers to the *minimal motion a robot or a mechanism can perform*. This denomination is also used for sensors, where it represents the *smallest change in the quantity which can be measured*. The overall resolution of a closed-loop system, for example a robot, depends on the performances of its sensors, actuators, mechanical design and controller: the minimal achievable motions of the robots considered in this thesis are only limited by the resolution of its sensors, thanks to a smart mechanical design.
- **Precision** and **repeatability** (*précision relative* et *répétitivité* in French) are used as synonyms and represent the *statistical measure of how much a robot actual motions differ from each other when the robot is commanded to repeat a single desired motion* [2, 54]. Note that this quantity is usually evaluated with a measuring device which is external to the robot. Moreover, the repeatability of a robot cannot be smaller than its resolution.
- **Accuracy** (*précision absolue* in French) refers to the difference between the desired position which a robot is commanded to achieve, and the actual position which it actually reaches; this quantity cannot be smaller than the robot repeatability.

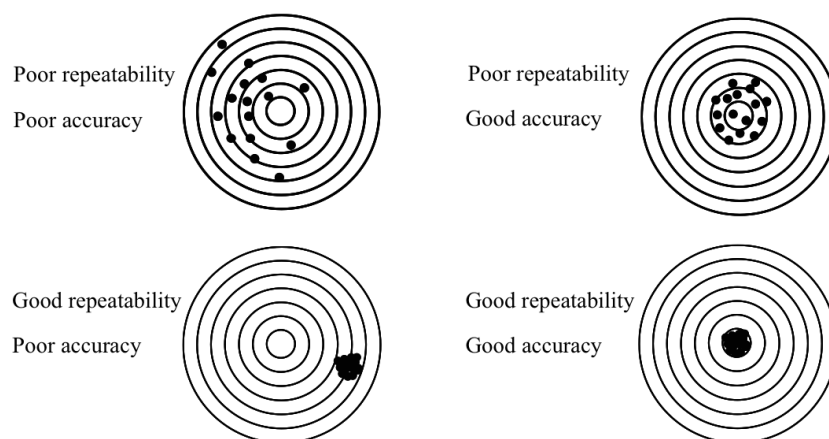


Figure 1.1: *Illustration of the repeatability and accuracy concepts with the analogy of a shooter* [30]

Figure 1.1 illustrates the difference between repeatability and accuracy by analogy with a shooter. Moreover, precision and repeatability differ from accuracy on a key aspect: the first concepts are characteristics which are intrinsic to the robot design and assembly, whereas the second is strictly linked to the mathematical model of the robot. Consequently, precision and repeatability cannot be improved once the robot has been built: the mechanical design

of the robot must thus be meticulously handled. Conversely, accuracy can be drastically improved by a calibration process, which aims at optimising the model of the robot by taking into account the error sources acting on it. This thesis will not study this aspect: a powerful calibration procedure dedicated to high precision applications, which compensates for temperature effects and deformations due to forces generated by the task the robot has to accomplish, has been developed in [54].

Finally, the distinction between high precision and ultra-high precision, often used in this thesis to qualify robots and mechanisms, needs to be clearly specified:

- **High precision** refers to robots and mechanisms which present precisions between 0.1 and 10  $\mu\text{m}$ .
- **Ultra-high precision** refers to robots and mechanisms which present precisions better than 0.1  $\mu\text{m}$  (100 nm).

In this thesis, the approach that has been selected to design robots and mechanisms which achieve the required ultra-high precision consists in making use of a parallel kinematics and of a dedicated mechanical design resorting to flexure hinges [6, 36, 69]. These two key features are detailed in the next paragraphs.

### 1.2.3 Parallel robots

A **parallel robot** is a robot composed of at least two bodies which are linked together by more than one kinematic chain [22]. A well-known example is the Delta robot, which is illustrated in figure 1.2. When the tasks that have to be accomplished by the machine require a submicrometric precision, the use of parallel kinematics presents crucial advantages over serial arrangements:

- **Lower inertia** thanks to the actuators which are fixed to the robot frame. Moreover, as the mass which has to be set in motion is lower the dynamical behaviour of parallel robots surpasses the performances of serial manipulators by achieving higher accelerations.
- **Higher stiffness**: as more than one kinematic chain link the robot end-effector to the fixed part, the stiffness is increased, exactly as several springs arranged in parallel are stiffer than one single spring. Consequently, parallel robots also present higher eigenfrequencies than serial manipulators.
- **Higher precision**, because the kinematic loops average the machining and assembly errors instead of adding them, which is the case in serial manipulators.

In addition, the location of the motors, which are fixed to the robot frame, presents another crucial advantage for high and ultra-high precision applications: indeed, the actuators consist in the main heat source acting on the machine. Consequently, their thermal isolation allows to limit the heat conduction throughout the robot structure, thus its thermal

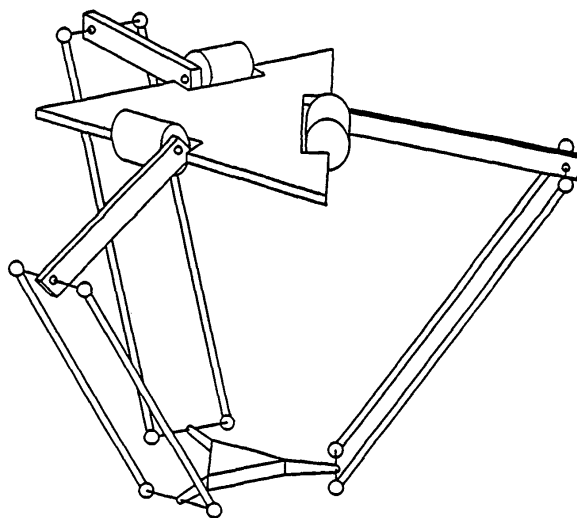


Figure 1.2: Sketch of the classical Delta kinematics, presenting 3 kinematic chains which link the end-effector (lower triangle) to the fixed frame of the robot, to which the 3 motors are attached (upper triangle). [22]

expansion. For instance, [69] proposes a system that covers the robot actuators, thus limiting both convection and conduction to the mechanical parts: the robot is thus isolated from the temperature variations of both its environment (ambient air) and its actuators.

As for the drawbacks of parallel robots, namely their limited workspace, the presence of singularities resulting in uncontrolled degrees of freedom and the complex geometric models, they can be easily overcome by a smart design and an appropriate control strategy.

Finally, a 'left hand right-hand' robot configuration also consists in an advantageous solution, which uses two robots working together like two human hands. The use of two identical parallel robots, which collaborate, following the same principle as in [75] for machine-tools, could be an interesting alternative for high precision applications: each of the machines would require a lower number of degrees of freedom than a single robot, which would consequently decrease the design complexity. However, the main drawback of the left-hand right-hand configuration lies in its laborious calibration; some research directions to solve this problem are presented in [54].

#### 1.2.4 Flexure hinges

The achievement of ultra-high precision structures requires a dedicated mechanical design, making use of flexure hinges<sup>1</sup>. This type of bearings is based on the elasticity of the material itself and thus does not suffer from the precision limitations of solid friction: the latter is typical of plain or rolling bearings, which are commonly integrated in mechanical designs. The main advantages of flexure hinges are their absence of friction, backlash and wear: they can thus be integrated in a wide range of environments, from space devices working in vacuum

---

<sup>1</sup>The content of this paragraph on flexure hinges is mainly derived from the work presented in [36].



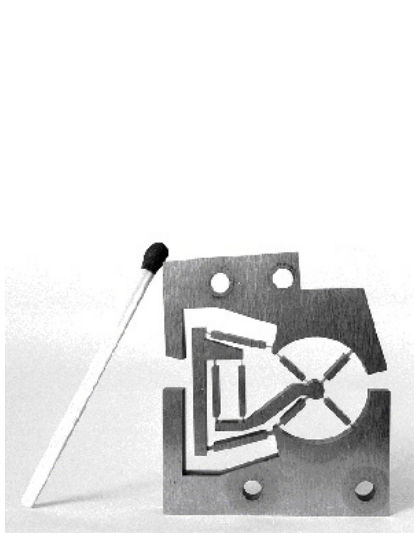


Figure 1.3: Flexure-based pivot presenting high angular strokes ( $\pm 15^\circ$ ), which is composed of two serially arranged single pivots linked with a slaving system [36].

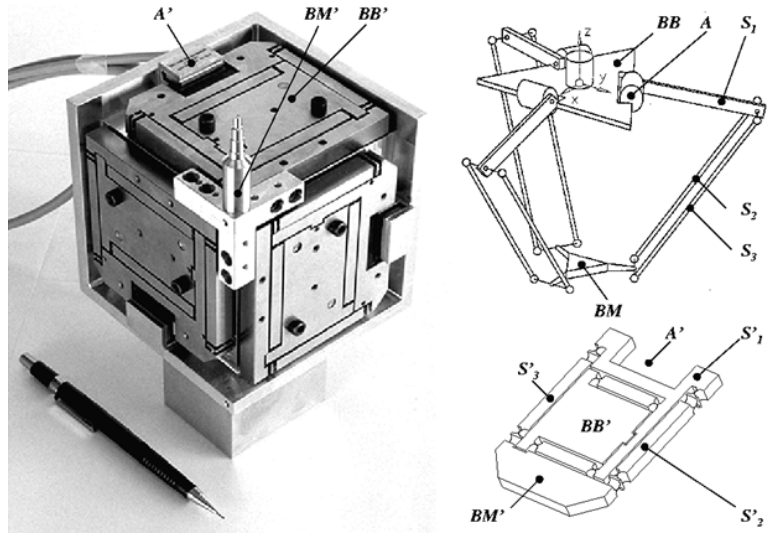


Figure 1.4: The Delta<sup>3</sup> I robot, which adapts the kinematics of the classical Delta (top right) to high precision thanks to a flexure-based structure (bottom right) [36].

to cleanrooms. Figure 1.3 presents an example of a flexure-based pivot, whereas figure 1.4 introduces the Delta<sup>3</sup> I robot, which is a flexure-based adaptation of the Delta kinematics [5, 13, 36].

However, the main limitation of flexure hinges is their low strokes, as the material has to stay within its elastic domain on the whole motion range: this condition must also be fulfilled after a high number of cycles. Only materials which present high elastic relative deformations (strains) and good fatigue behaviour should be selected. High strength alloys such as maraging steels, aluminum alloys (Avional, Perunal, Anticorrodal, ...) and titanium alloys are some examples of commonly used materials [36].

As for their manufacturing, flexure hinges are mostly machined by Wire Electro-Discharge Machining (W-EDM). This process requires the material to be conductive: the removal of the material is caused by electric discharges between an electrode, which consists in a wire whose diameter is comprised between 30 and 300  $\mu\text{m}$ , and the machined part. This manufacturing process is especially suited for flexures thanks to its high precision, to the low forces which are applied to the part during the process and to its capability of machining very hard materials after thermal treatment with an excellent surface quality. Flexure-based mechanisms can thus be machined monolithically, *i.e.* within only one block of material. Moreover, as no special tool is needed for each part, a large variety of structures can be achieved. In particular, considering the relative configuration of the wire and the part, complex features presenting 'ruled surfaces' can be machined. Planar and cylindrical designs are thus nowadays preferred, even if some W-EDM machines currently in development tend to allow the wire to be inclined of  $\pm 40^\circ$  relatively to the part, leading to new design possibilities.



Although all flexure-based structures presented in this thesis will be made of metals and designed for W-EDM machining, the use of Shape Memory Alloys [9, 10], as well as of non-conductive materials, such as fused silica glass and single crystals (silicon), is also possible. For instance, [39] introduces a sugar-cube Delta robot made of silicon. However, this field has not been extensively investigated yet: the necessary manufacturing processes are thus not directly applicable in the industrial context.

### 1.2.5 Modularity of industrial robots

Although *modularity* or *reconfigurability* of industrial robots is being widely explored, no strict and unique definition of this notion can be highlighted. Nonetheless, the extensive review of the topic literature performed in [77] has allowed to underline commonly shared features of modular robots, such as the use of standard modules to build different products and the notion of interface, which relates to the possibility of connecting the modules to the assembly. Moreover, modularity in industrial robotics mostly refers to the possibility of increasing the dynamic performances of the manipulators by modifying their structures [77].

In this thesis, *modularity of parallel industrial robots* specifically refers to the following characteristics:

- *Simplified synthesis of the robot kinematics*, thanks to the use of standardised conceptual building bricks and solution catalogues
- *Straightforward modification of the robot degrees of freedom*, at any step of the design process
- *Possibility of increasing the performances of the robot*, particularly by adjusting the location of the rotation centres

Lastly, the study conducted in [77] notably highlights the limited impact of modularisation in the industrial field, which is explained by the complexity of the reconfiguration steps. Consequently, design methodologies which allow to easily and rapidly modify parallel manipulators consist in a crucial need to enable the breakthrough of modularity in industrial robotics.

## 1.3 Objectives

The chief objective of this thesis is to drastically reduce the time-to-market of ultra-high precision robots, which is achieved by remediating to the twofold development complexity of such machines: first, the synthesis of their parallel kinematics must be facilitated; simultaneously, modularity and flexibility are aimed for in order to allow for easy modifications of the kinematics during the development process. Then, the mechanical design of the robots, making use of flexure hinges, must be improved and simplified. The specific objectives for these aspects are the following:

- Develop a concept of modular kinematics which aims at simplifying the synthesis of parallel kinematics thanks to solution catalogues. This concept will be similar to a robotic Lego, where a finite number of building bricks allows to rapidly design an ultra-high precision machine. Moreover, modifications of the kinematics to meet changes in the industrial specifications during the synthesis process are highly facilitated thanks to the modularity of the concept.
- Propose efficient flexure-based mechanical designs of the building bricks adapted to ultra-high precision, which present increased ratios between their working ranges and their overall size. The resulting set of solutions includes original structures, as well as well-known mechanisms. The aim for this aspect is to group interesting brick designs as a tool for the engineer rather than to propose a thorough catalogue of off-the-shelf mechanical solutions.
- Apply the developed methodology to a case study, which consists in a highly challenging 5-DOF micromanipulation and microassembly robot.

## 1.4 Postulate

This thesis aims at demonstrating the following hypothesis:

*'The time-to-market of ultra-high precision robots can be considerably reduced thanks to a modular design methodology; the latter allows to rapidly build and modify parallel machines with the help of a finite number of building bricks. Moreover, the robots resulting from this design procedure present similar or even improved performances in comparison with more traditionally developed robots.'*

## 1.5 Main contributions

This thesis notably includes the following originalities:

- A modular concept of kinematics which facilitates the synthesis of parallel robots
- An exhaustive conceptual solution catalogue which groups all 3175 possible kinematics generated by the combination of the 38 conceptual building bricks. This catalogue is independent from any mechanical design and can be used to develop the kinematics of a large variety of robots, from machine-tools to micro-scale robots.
- A reduced conceptual solution catalogue for ultra-high precision applications, which, thanks to criteria based on the mechanical design and machining of flexure-based mechanisms, diminishes the total amount of kinematic solutions by more than 55 %. The practical use of the concept is thus highly facilitated.
- Original flexure-based designs of the building bricks, notably including a 2-DOF actuated brick making use of a Remote Centre of Motion (RCM) and a new design of the space parallelogram featured in the Delta kinematics

- A unified actuation solution, common to all motorised bricks, which is composed of a guiding mechanism, an actuator and a position sensor
- A 5-DOF ultra-high precision robot, Legolas 5, achieving resolutions and repeatability of 50 nm in translation and 1.9  $\mu$ rad in rotation (limited by the sensors resolution).
- A new family of ultra-high precision robots, the Legolas family, which notably includes the orthogonal version of the Delta kinematics. With only 6 building bricks, one robot is proposed for each of the 19 possible end-effector mobilities.

## 1.6 Structure of the thesis report

This thesis report is organised as follows:

- *Chapter 2* reviews the *state of the art* of high precision and ultra-high precision flexure-based robots and mechanisms, as well as methodologies for the synthesis and design of parallel robots.
- *Chapter 3* introduces the *concept of modular kinematics*: the bases and notations of the methodology are detailed, as well as the establishment of the exhaustive conceptual solution catalogue.
- *Chapter 4* presents the *reduced solution catalogue for ultra-high precision applications*, as well as the selection criteria linked with the design and machining of flexure-based mechanisms which have allowed its establishment .
- *Chapter 5* details the *mechanical design of the building bricks*: original flexure-based designs, as well as common and innovative uses of well-known mechanisms, are proposed as mechanical solutions for each building brick.
- *Chapter 6* illustrates the practical use of the methodology thanks to the *case study of a 5-DOF ultra-high precision robot, Legolas 5*. The selection of an adapted kinematics in the solution catalogue and the development of the Legolas 5 prototype are presented; the results of its characterisation and a discussion conclude this section. This chapter also introduces the Legolas family, a new family of ultra-high precision parallel robots which has been generated by this case study.
- *Chapter 7* finally concludes this thesis by presenting a *summary of the originalities stemming from this work*, and by outlining some research perspectives on modular ultra-high precision robots.



# Chapter 2

## State of the art

This chapter reviews the state of the art of three key aspects of modular ultra-high precision robots, namely design methodologies of modular machines, flexure-based mechanisms, as well as existing academic and commercial ultra-high precision and high precision robots.

### 2.1 Modular design methodologies

This section presents an overview of the literature on methodologies to synthesise modular robots. As an introduction, a brief outline of methods to solve the challenging problem of parallel kinematics design is presented; the synthesis of serial structures, being straightforward, has not been included in this review. Then, this section focuses on approaches to design modular robots: after shortly depicting the simple case of serial modular manipulators, methodologies to solve the problem of parallel modular robots synthesis are detailed.

#### 2.1.1 Design methodologies of parallel robots

The kinematic synthesis of parallel robots has been a widely explored issue for several decades, which has allowed to highlight some efficient methods, such as screw theory and Lie groups approaches; [34] presents an extensive review of the literature on this topic. However, the suitability of these methodologies for modular robots design is limited, as modularity cannot be depicted in mathematical terms. Consequently, the integration of this characteristic within the synthesis process requires a more intuitive approach, where the robot designer is able to explicitly select the kinematic solutions which allow for the modularity. Two procedures can notably be underlined:

- [34] introduces a method which creatively generates kinematic solutions stemming from the elementary kinematic function which the robot has to perform, *i.e.* its desired end-effector mobility. A set of operations, such as reorientation, rearrangement, serial or parallel division, and transformation of torques into differential forces, permits the establishment of kinematic variants. Modular solutions can thus be generated, such as the 6-DOF Sigma 6 robot (see paragraph 2.3.2), which features three identical kinematic chains.

- The procedure introduced in [74] allows to generate flexure-based parallel robots: its first step consists in the synthesis of parallel kinematics thanks to the classical screw theory method. Then, solutions which are adapted to flexure-based mechanical design are selected on the basis of symmetry, manufacturability and condition of monolithic structure criteria. These requirements for example eliminate kinematics including universal joints, spherical joints or passive prismatic joints. Finally, the flexure-based robot is designed, thus generating a set of mechanical joints: in this work, the modules consequently consist of mechanically designed structures rather than in purely kinematic elements. The case study of a 6-DOF manipulator with three RPPPRR limbs, comprising each a rotational and a translational actuator, is detailed and the resulting robot is illustrated in figures 2.1 to 2.3.

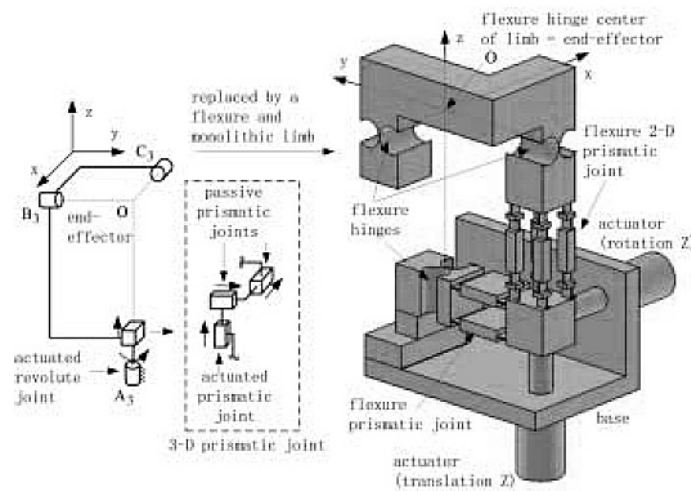


Figure 2.1: Kinematic chain of the flexure-based 6-DOF manipulator, which includes a translational and a rotational actuator [74]

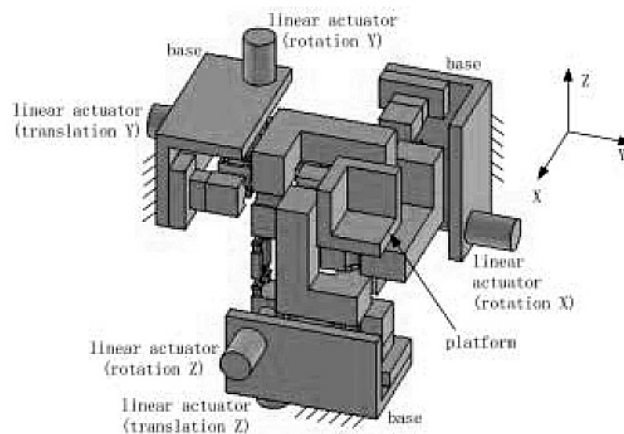


Figure 2.2: Flexure-based design of the 6-DOF manipulator, which is composed of three occurrences of the kinematic chain illustrated in figure 2.1 [74]

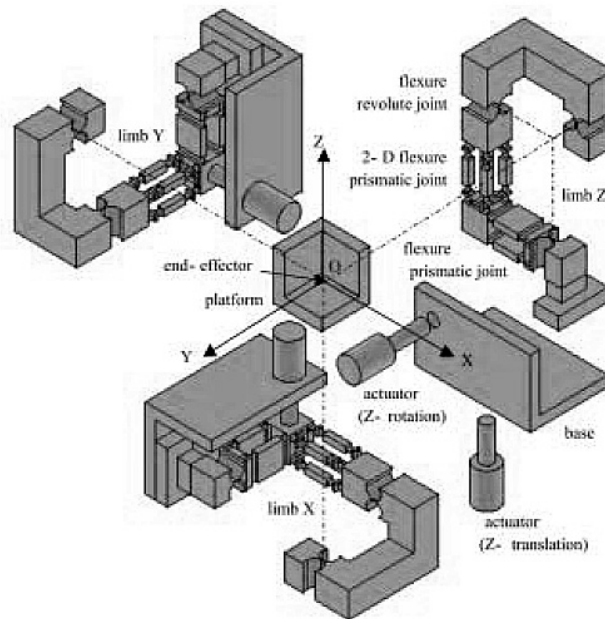


Figure 2.3: Exploded view of the 6-DOF manipulator [74]

## 2.1.2 Concepts of serial modular robots

As the kinematic synthesis of serial modular robots is straightforward, the main challenge lies in the mechanical design of the modules. These generally consist in actuated modules (usually called joints) and non-actuated modules (links, limbs), as for instance in [11, 12] or [1]. Moreover, the mechanical and electrical connectivity between modules is crucial: [78] presents a concept which allows to modify the robot mobility during its use in industry, thus quickly responding to changes in the robot task.

## 2.1.3 Concepts of parallel modular robots

The key challenge of parallel modular robots design consists in their kinematic synthesis. The works from the literature that have examined this problem can notably be divided into two categories: the first comprises the methodologies that derive from the Stewart platform, whereas the second includes concepts based on libraries of modules.

### 2.1.3.1 Methodologies based on the Stewart platform

The principle of these methods is to modify the Stewart platform to change either the mobility of its end-effector or its performances, for instance its workspace. Three works epitomise this category of parallel modular robots design methodologies:

- [62] first proposes to change both the dynamic performances of the Stewart platform and its workspace by modifying the positions of the limb attachments on the fixed



frame (see figure 2.4). To achieve this goal, the best solution relative to the specific robot requirements is determined thanks to an optimisation algorithm.

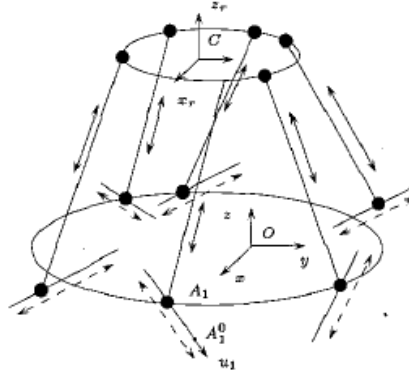


Figure 2.4: *Stewart platform structure and possible positions of the limb attachments on the fixed frame (dashed lines) [62]*

- The concept presented in [28] allows to change the mobility of the Stewart platform to 4 or 5 degrees of freedom, making use of identical limbs only. The classical screw theory is first employed to exhaustively generate the limbs, which are divided into two groups: the F-limbs, which provide a force constraint, and the C-limbs, which provide a torque constraint. Then, the screw theory also allows to transform this set of limbs into a kinematics structure, based on the hypothesis that a 4-DOF platform is obtained by connecting four identical limbs, and a 5-DOF platform by using five equivalent limbs. This procedure thus establishes a comprehensive list of possibilities: figure 2.5 illustrates two of them, namely a 4-DOF platform with four RUC C-limbs (composed of a revolute, a universal and a cylindrical joint), as well as a 5-DOF manipulator with five RRRRR F-limbs (composed of five revolute joints).
- Finally, [64] introduces a concept which allows to design derivatives of the Stewart platform with flexure-based mechanisms. The principle of this method straightforwardly consists in adding a constraining leg to the classical platform to reduce the end-effector mobility (see figure 2.6). Moreover, the leg must present the same mobility as the desired output. Figure 2.7 illustrates the exhaustive list of the possible constraining legs. Although the kinematic synthesis of the robot is highly simplified with this methodology, the mechanical complexity of the resulting machine questions its efficiency. Furthermore, the exhaustiveness of the chart presented in figure 2.7 is doubtful, as it does not take into account the relative orientation of the degrees of freedom: for instance, only one constraining leg is presented for the mobility performing a translation and a rotation, allowing to restrict only a cylindrical mobility. The constraint of a rotation and a translation along two different axes is consequently unclear.



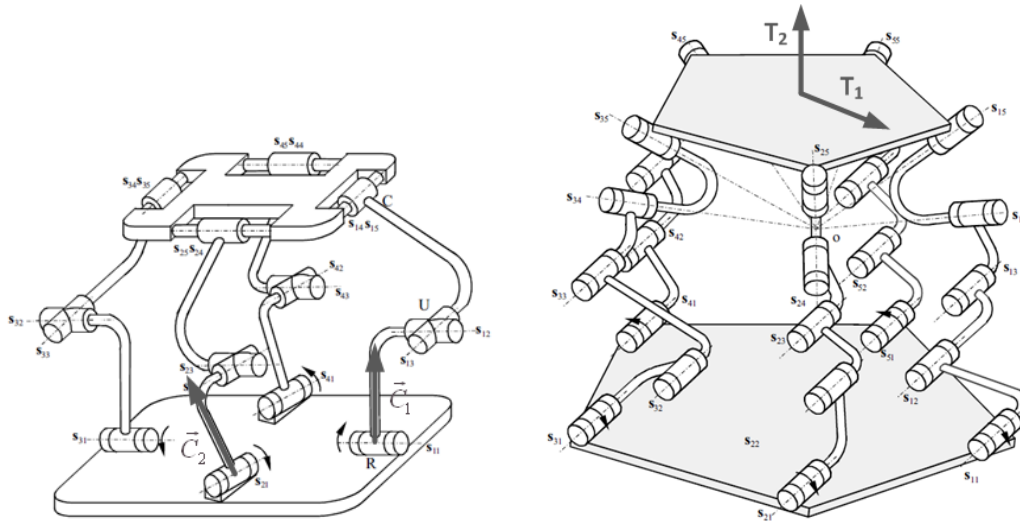


Figure 2.5: Left: 4-DOF Stewart platform based manipulator making use of 4 identical RUC limbs. This kinematics performs three translations and a rotation along an axis which is parallel to  $\vec{C}_1 \times \vec{C}_2$ , and is overconstrained. Two limbs are inclined relatively to the robot frame to avoid a singularity. Right: 5-DOF platform composed of 5 equal RRRRR limbs; this kinematics performs three rotations around the point O and two translations along the directions  $T_1$  and  $T_2$ , and is also overconstrained. [28]

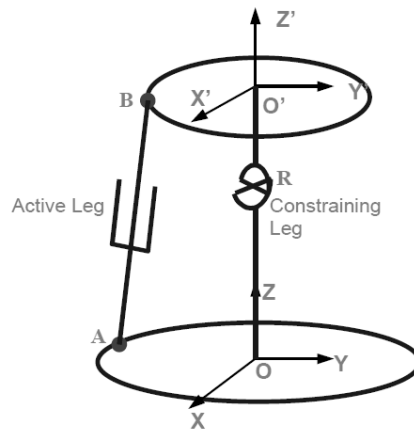


Figure 2.6: Principle of the method presented in [64] to modify the mobility of the Stewart platform

In summary, the methodologies which generate modular parallel robots by modifying the mobility or the performances of the Stewart platform present the advantage of stemming from a well-known and efficient robot structure, which considerably simplifies the design process. Nonetheless, the limitation to this particular arrangement may result in complex structures with questionable efficiency, especially for low end-effector mobility, such as in [64].

Translation \ Rotation	0	1	2	3
0				
1				
2				
3				

Figure 2.7: List of possible constraining legs [64]

### 2.1.3.2 Methodologies based on libraries of modules

The methodologies which are based on libraries of modules (or building bricks) all share a common procedure, which is the following:

1. **Establishment of a library of modules:** this library can include well-known mechanisms, manually designed building bricks or modules which have been generated by a classical synthesis method.
2. **Enumeration of robot kinematic solutions:** this list can be established by hand, with a classical synthesis method or with a genetic algorithm. In this last case, the catalogue

may be implicit, *i.e.* the robot designer does not have access to the complete set of solutions.

3. **Determination of the optimal solution for a specific problem:** this step, although not always implemented, can either be performed by an optimisation algorithm, in which case the solution is claimed to be a global optimum, or by an intuitive method, which takes advantage of the robot designer experience to select an efficient solution fulfilling the application requirements.

The following methodologies include this procedure to design modular parallel robots:

- [96] proposes a concept where the library of modules includes limb elements which are divided into two categories: the fixed-dimension modules, which are mechanically designed and consist in actuator, passive joint and end-effector modules, and the variable-dimension modules, which include rigid links, connectors and mobile platforms. This library is established by hand. Then, the generation of the kinematic solutions is illustrated with the case study of a 6-DOF non-redundant robot, whose general arrangement is first determined on the basis of symmetry and interference criteria: a configuration comprising three legs, each of them actuating two degrees of freedom, is selected. Then, the thorough list of leg possibilities is established by hand and finally includes 13 possibilities: figure 2.8 illustrates the legs composed of revolute joints only (left), and those including a prismatic joint (right). This approach, although simple, lacks flexibility: as the modules are mechanically designed, the possibility of applying the method to high precision robots would necessitate to redesign the whole library.

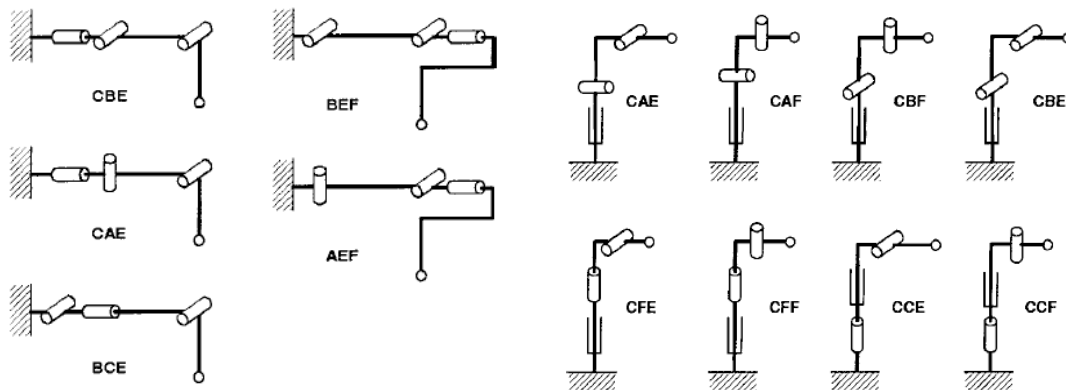


Figure 2.8: Exhaustive list of legs actuating two degrees of freedom, which include revolute joints only (left) and one prismatic joint (right). Each limb is terminated by a spherical joint, which potentially generates an internal degree of freedom on the robot end-effector [96]

- The methodology presented in [58, 59, 95] first establishes a library of mechanisms performing an exhaustive set of motions, which are called primitive generators; although this set is generated with a Lie group synthesis method, the library simply consists of a collection of known mechanisms performing these motions. Then, the robot

kinematic solutions are also generated with a Lie group algorithm, whereas the optimisation step is not implemented in this work. This methodology generates unusual robot structures, as the efficiency of the kinematics is not evaluated. Moreover, the list of robot solutions is exhaustive relatively to the chosen primitive generators; as these consist in a non-thorough gathering of known mechanisms, adding or removing a generator modifies the robot kinematics catalogue. Furthermore, the criteria for their inclusion or dismissal are unclear.

- In [51], the library of modules includes both priorly known mechanisms and modules which are designed by hand. Then, the generation of the robot kinematic solutions is performed by a genetic algorithm, whereas a Simulated Annealing optimisation process allows to select the optimal kinematics for a specific problem. The initial population of the genetic algorithm is randomly established by varying the mobility of the robot, the number of its kinematic chains and their mobility, as well as the number of modules. Moreover, the optimisation criteria are based on symmetry considerations and on the specific task requirements. The efficiency of the method can even be increased by coupling these two algorithms: the solutions selected by the optimisation algorithm are mutated and added into the genetic algorithm population to achieve a more global optimum. However, this method suffers from the drawback of being a black-box approach, where the robot designer has no access to the list of the generated robot solutions, but only to the kinematics which the algorithm has highlighted as optimal.
- The concept which is detailed in [31] also makes use of a genetic algorithm: in this case, its function is to generate the modules, which consist in kinematic robot limbs. The resulting library classifies the modules according to their mobility and comprises a tremendous number of solutions. Then, the robot kinematics solutions are established by an intuitive method, which consists in modifying a straightforward possibility by adding idle degrees of freedom to fulfill the redundancy and overconstraints requirements. Nonetheless, this methodology proposes neither optimisation process nor a selection procedure to help the robot designer to choose the most suited kinematics for his/her application. Figure 2.9 (left) illustrates some of the solutions which are genetically generated for 5-DOF limbs presenting three translations and two rotations. Moreover, some robot configurations for a three-translation manipulator are included in figure 2.9 (right).

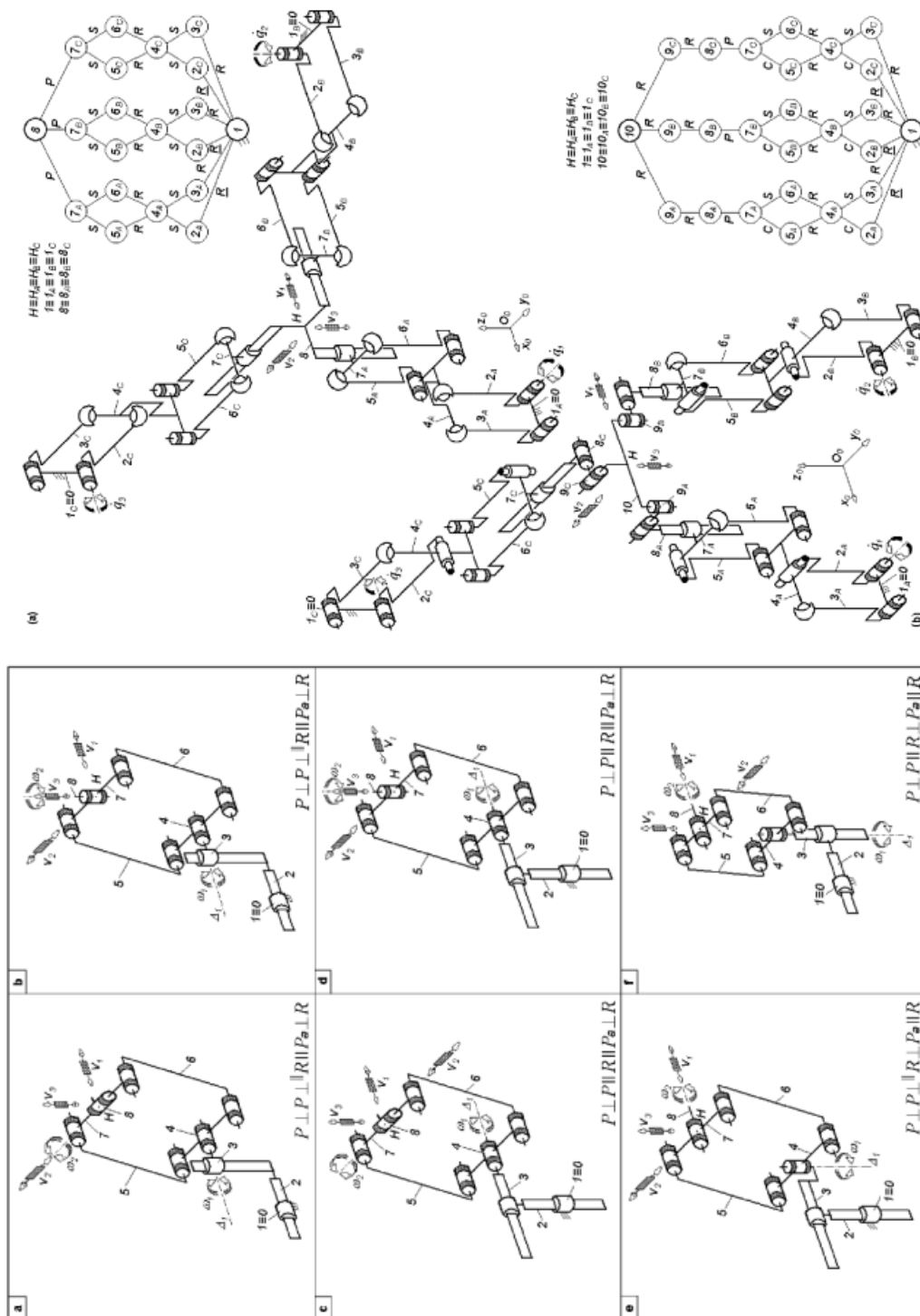


Figure 2.9: Illustration of some limb solutions generated by the genetic algorithm for limbs presenting three translations and two rotations (left) and two robot kinematics examples for a three-translation parallel manipulator [31]

- The last methodology presented here is dedicated to the generation of parallel machine-tools [90]: a library of four key modules is first established by hand and is illustrated in figure 2.10. Then, an intuitive approach, called cube method, allows to generate the exhaustive list of robot kinematics solutions. This procedure takes as an input a 6-DOF cubic robot, and consists in using the modules to constrain the degrees of freedom which are not desired on the machine output. Then, symmetry properties are sought in order to select the most efficient kinematics. Figure 2.11 illustrates the thorough list of kinematic solutions for a 4-DOF ( $T_x, T_y, T_z, R_y$ ) machine-tool, before the application of the symmetry filter. Although this methodology presents the advantages of being straightforward and of including a very low number of modules, its adaptation to high precision modular robots would necessitate to reconsider the choice of the base modules and their mechanical design. Moreover, as the number of modules is low, the list of kinematic solutions may not include an efficient solution for any specific robot task.

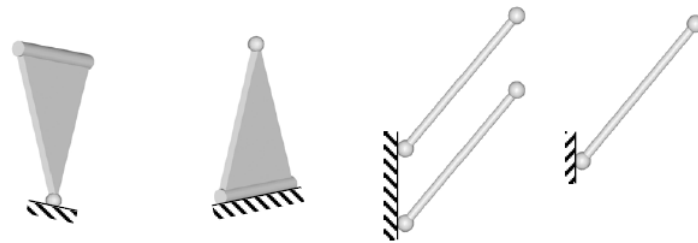


Figure 2.10: *Library of base modules [90]*

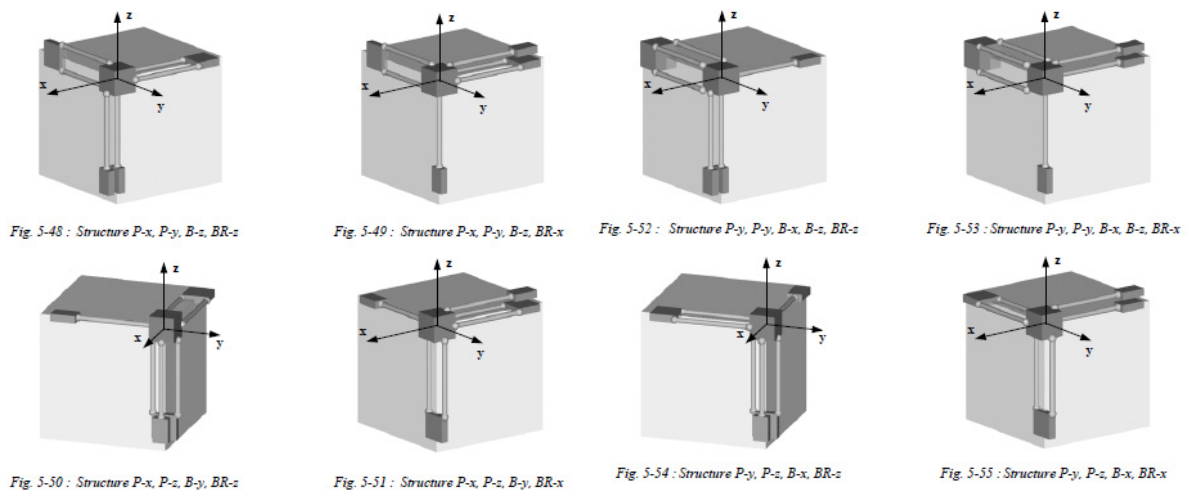


Figure 2.11: *Exhaustive list of solutions generated by the methodology for a  $T_x, T_y, T_z, R_y$  mobility, before applying the symmetry filter [90]*



## 2.2 Flexure-based mechanisms

The design of flexure-based mechanisms consists in the second key aspect of modular ultra-high precision robots; the aim of this section is thus to highlight interesting works providing synthesis, analysis and modelisation tools, as well as efficient flexure-based structures. A more extensive review of the literature on this topic can be found in [35].

The principle of inserting flexible elements in mechanical structures has been investigated for several decades: in 1954, a textbook of precision mechanics [85] was already introducing a flexure crossed pivot, whereas in 1985, a Ph. D. Thesis [26] presented numerous flexure-based structures which are now widely employed, such as translation tables and torsion pivots. Nonetheless, the extensive study of this domain has only started in the 2000s, when miniaturisation of industrial products has created the need for bearings which are capable of achieving a micrometric or submicrometric precision. The work presented in [36] can notably be underlined: it indeed provides useful tools for the designer to synthesise and analyse efficient flexure-based mechanisms, thanks to:

- ***a kinematic synthesis method***: based on the analogy with rigid articulated structures, it allows to analyse the mobility of existing systems, as well as to verify the degrees of freedom and the overconstraints of newly designed mechanisms. Figure 2.12 illustrates the mobility analysis of some common flexure-based structures.
- ***simplified mathematical models of usual flexure-based structures***, which allow for effective and rapid dimensioning
- ***efficient flexure-based designs***, such as the Delta<sup>3</sup> I robot or the compound high stroke pivot (see chapter 1, figures 1.4 and 1.3)

The following sections will detail other noticeable works which relate to these three tools to design and analyse flexure-based mechanisms.

### 2.2.1 Design methodologies

Albeit formal and systematic design methodologies for flexure-based mechanisms are infrequent in the literature, [44, 45] propose a concept to synthesise transmission flexures by using the classical screw theory. Nonetheless, this procedure leads to complex structures and may not turn out to be the most efficient approach to rapidly design a whole flexure-based ultra-high precision robot.

### 2.2.2 Modelisation

Two main methods are used to model and analyse the behaviour of flexure-based mechanisms, namely approximated mathematical models and Finite Element Analysis (FEM). [46] illustrates the first approach by introducing the notion of pseudo-rigid models: these consist in describing the behaviour of distributed compliance structures, *i.e.* whose entire bodies are deformable, by rigid links which are articulated by revolute joints. The positions of

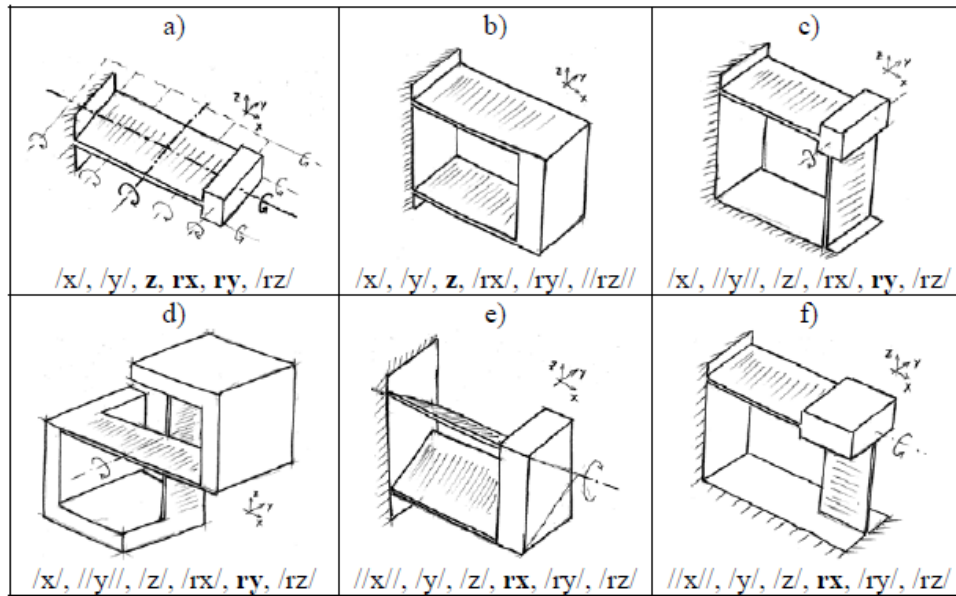


Figure 2.12: Mobility analysis of some well-known flexure-based mechanisms: bold characters stand for free motions, while blocked degrees of freedom are indicated by slashes; two slashes indicate an overconstraint motion [38]

the latter are estimated thanks to the developed model. This procedure straightforwardly applies to mechanisms making use of leaf springs; nonetheless, structures which are composed of classical necked-down flexure hinges cannot be modeled with this approach. As for mathematical description of the dynamic performances, [88] proposes eigenfrequencies and damping models of flexure-based mechanisms.

In comparison with mathematical descriptions, Finite Element Analysis allows to model complex structures, composed of any type of flexible elements (leaf springs or flexure hinges). [52] for instance introduces methods to statically and dynamically analyse flexure-based mechanisms, making use of FEM. However, this approach becomes inefficient for large aspect ratios of the flexures, returning results which present higher stiffnesses and stresses than the real structures. Albeit this problem is widely known in the domain, the solution is not straightforward to implement, and consists in developing a FEM solver which is dedicated to this kind of mechanical structures [7]. Nonetheless, not only most commercial FEM software do not permit the modification of the computing algorithm implementation, but the dedicated models are also complex to solve, thus time consuming. Some works, such as [81], investigate approaches to significantly reduce the intricacy of the analysis.

### 2.2.3 Examples of flexure-based designs

Several interesting and efficient flexure-based designs, which respond to typical issues the ultra-high precision robot designer faces, are highlighted in this section.

- The first design challenge consists in increasing the achievable stroke of flexure-based



mechanisms, especially those which perform rotational motions. [20] for instance proposes an original shape of leaf spring called serpentine, which allows to achieve higher angles than a classical leaf spring (see figure 2.13, left). Moreover, this same work introduces mechanisms which combine flexible and rolling elements, such as the CORE pivot (for Compliant Rolling-Contact Element), which is illustrated in figure 2.13. Furthermore, this figure also shows the extension of this concept to an epicyclic bearing, which can be monolithically machined and advantageously presents a restoring torque.

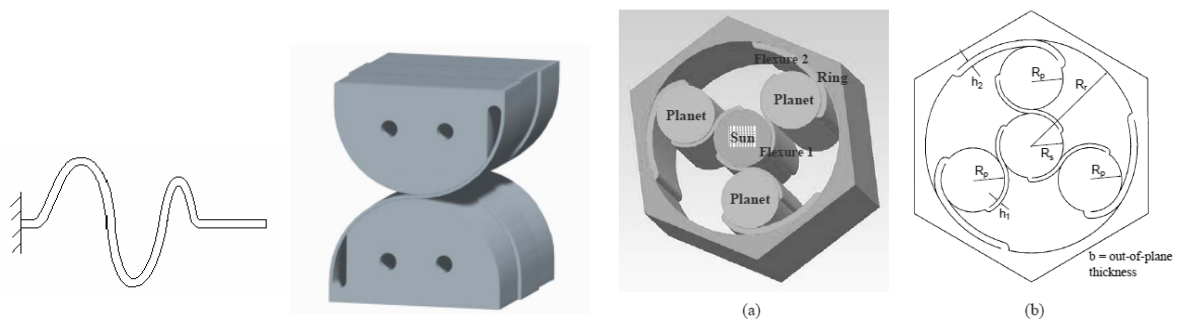


Figure 2.13: Principles of the serpentine (left), of the CORE (Compliant Rolling-Contact Element) pivot (middle) and of the CORE epicyclic bearing (right) [20]

- In ultra-high precision robots, gravity effects must be compensated for, since they generate non-negligible displacements of the flexures; to achieve this aim, one solution consists in adding a spring whose restoring force is constant along its whole stroke, *i.e.* its stiffness must be close to zero. [50] proposes a solution composed of two leaf springs, which is illustrated in figure 2.14. If the breadth of the leaf springs is constant, the force value is zero, whereas a triangular shape, such as the one presented in figure 2.14, allows for a constant and non-zero force along the entire stroke.

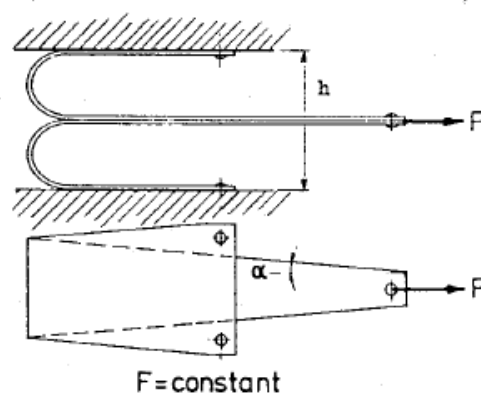


Figure 2.14: Principle of a constant-force mechanism [50]

- Some existing mechanisms, such as the Tx-Ty table proposed in [50] (see figure 2.15), can be used to mechanically design the building bricks of the modular concept.

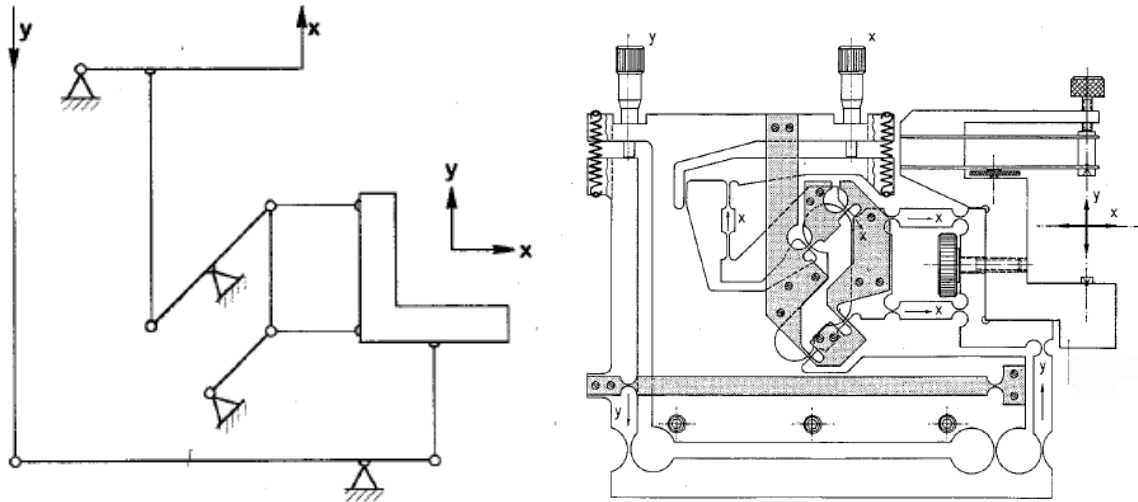


Figure 2.15: *Kinematics (left) and design (right) of a Tx, Ty table with collinear actuators [50]*

Lastly, some works introduce the use of less common materials to machine flexure-based mechanisms, such as Shape Memory Alloys (SMA) [10] or monocrystalline silicon: [39] presents a sugar cube Delta robot made of this material, which has been machined by DRIE (Deep Reactive Ion Etching); the prototype is illustrated in figure 2.16. Finally, [14] extensively details design rules for compliant MEMS. Although the use of these materials is nowadays scarce in the industrial domain, especially because the machining processes have not yet been adapted to batch production, these works prefigure the evolution of the flexure-based mechanisms domain.

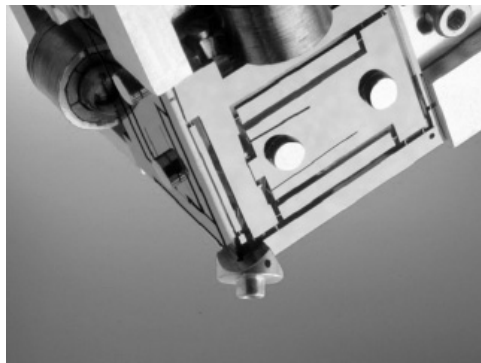


Figure 2.16: *Sugar cube Delta kinematics made of monocrystalline silicon and machined by DRIE (Deep Reactive Ion Etching) [39]*

## 2.3 High precision and ultra-high precision robots

This last section illustrates interesting examples of academic and commercial ultra-high precision and high precision robots.

### 2.3.1 Delta<sup>3</sup> robots family

The design principle of the Delta<sup>3</sup> robots family is to adapt the classical three-translation Delta kinematics (see figure 1.2) to ultra-high precision, in particular to the  $\mu$ -EDM (Electro Discharge Machining) manufacturing process. The Delta<sup>3</sup> I [5, 13, 36] converts the ternary structure into a cubic kinematics, which is illustrated in figure 1.4: this robot achieves linear strokes of  $\pm 1$  mm with a 50 nm resolution and a 100 nm repeatability. The global volume of the machine reaches 1.33 dm<sup>3</sup>, thus corresponding to a cube with edges of 110 mm. Furthermore, this robot lays the foundations of modular structures, as the three kinematic chains are designed as identical planar mechanisms. Nonetheless, the main limitation of this first prototype is the presence of a low transverse eigenfrequency, which creates an out of plane motion of the three planar structures composing the robot. Consequently, the dynamic performances are highly limited.

In the second prototype, the Delta<sup>3</sup> II [5, 6, 13, 69], the cubic geometry is replaced by an orthogonal arrangement of the kinematic chains; this robot is illustrated in figure 2.17 and achieves strokes of  $\pm 2$  mm with a 5 nm resolution and a 10 nm repeatability. In comparison with the first version, the strokes have been doubled, whereas the lowest eigenfrequency has been increased to 450 Hz. Nonetheless, the total volume of the machine has been multiplied by a factor 6, reaching 8 dm<sup>3</sup>.

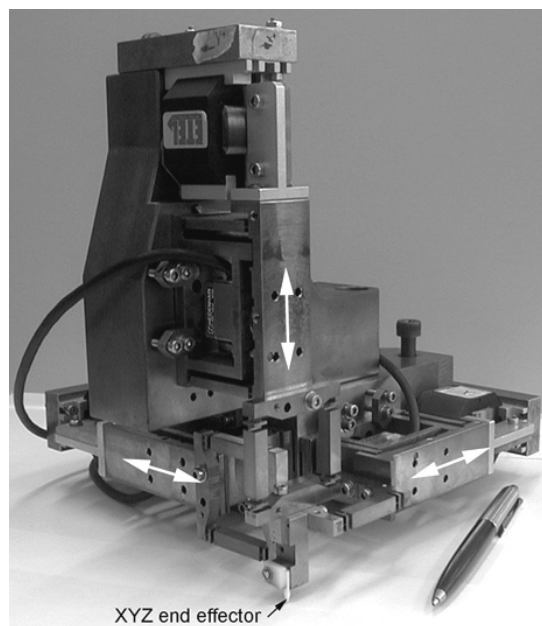


Figure 2.17: Delta<sup>3</sup> II prototype [5]

A more industrialised prototype of this Delta version, the Delta<sup>3</sup> III [57, 48] (see figure 2.18), allows to achieve even higher strokes ( $\pm 4$  mm) for a total robot volume of  $13 \text{ dm}^3$  ( $240 \times 240 \times 240 \text{ mm}^3$ ). Moreover, this version includes three identical kinematic chains designs, whereas the Delta<sup>3</sup> II prototype is composed of two different orientations of the same mechanisms.

Lastly, the Delta<sup>3</sup> IV robot, also called Agietron Micro-Nano, has been developed in collaboration with GF AgieCharmilles and Mecartex [3, 57] as a tool for a classical high-stroke EDM system, thus increasing the achievable machining precision (see figure 2.18). This version adopts the original ternary symmetry and includes three identical kinematic chain designs. Strokes of  $\pm 3$  mm are achieved with 20 nm resolution, for a total robot volume of  $200 \times 200 \times 250 \text{ mm}^3$ .

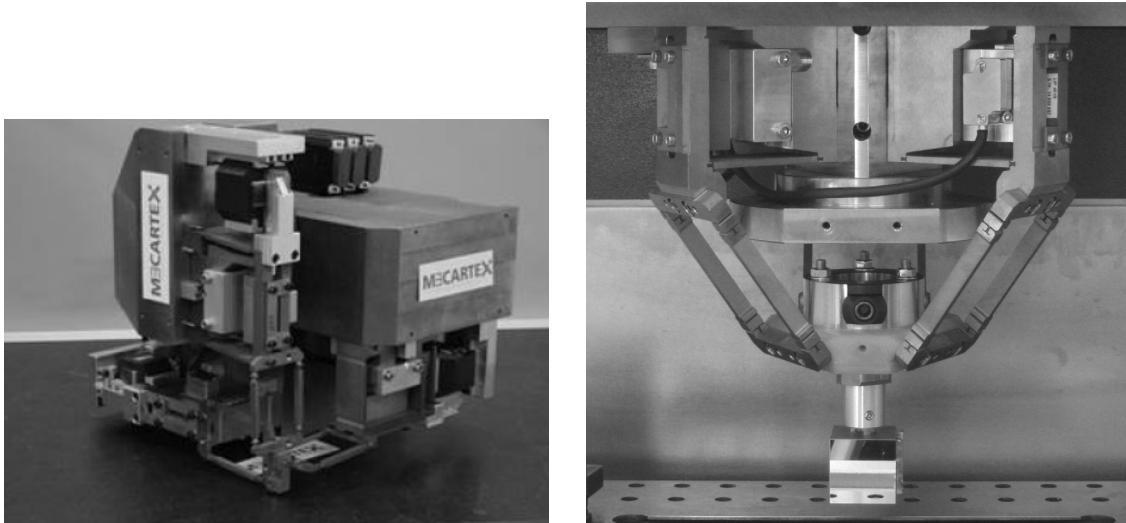


Figure 2.18: Delta<sup>3</sup> III [48] and Delta<sup>3</sup> IV (Agietron Micro-Nano) [54] prototypes

### 2.3.2 Sigma 6 robot

This 6-DOF ultra-high precision robot [33, 34] presenting high dynamical performances has been developed for the active alignment of optical fibers (see figure 2.19). This machine is composed of three kinematic chains, which share the same mechanical design: each of them is composed of two actuators and two arms whose role is to transmit the motions to the robot end-effector. Figure 2.20 illustrates the design of a kinematic chain, whereas figure 2.21 details the flexure-based structure of the transmission arms. As for the Sigma 6 performances, strokes of  $\pm 4$  mm and  $\pm 4^\circ$  can be achieved; nonetheless, the maximal angle can only be reached if the translations do not exceed 1 mm. Moreover, the resolution and repeatabilities of the motions achieve 10 nm and  $0.5 \mu\text{rad}$ . Finally, the total volume of the Sigma 6 reaches  $6.15 \text{ dm}^3$  ( $164 \times 147 \times 225 \text{ mm}^3$ ).

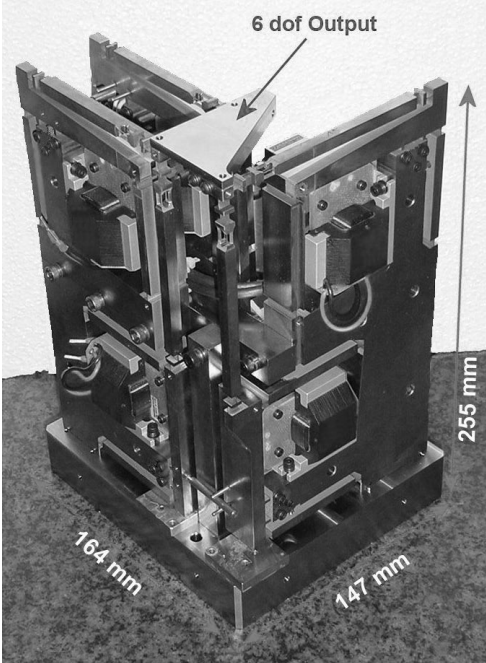


Figure 2.19: Sigma 6 prototype [34]

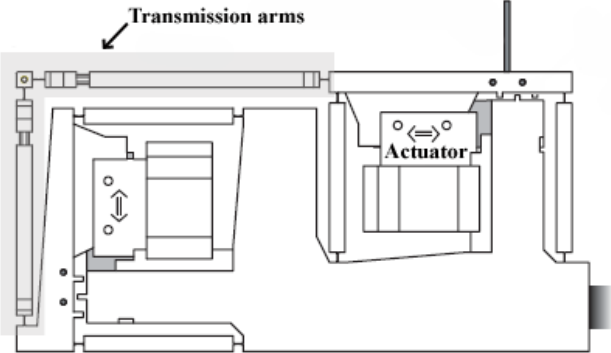


Figure 2.20: Mechanical design of a Sigma 6 kinematic chain [34]

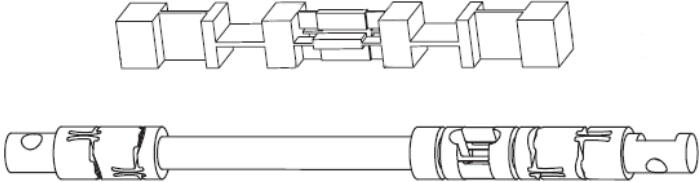


Figure 2.21: Flexure-based design of the Sigma 6 transmission arms [34]



### 2.3.3 Academic high precision robots

The Tribias 6-DOF robot [73] has been developed for the assembly of optical components, achieving strokes of  $\pm 5$  mm and  $\pm 2.5^\circ$  and resolutions of  $0.1 \mu\text{m}$  and  $8 \mu\text{rad}$ . This academic prototype, whose total volume reaches  $800 \times 800 \times 300 \text{ mm}^3$ , includes both the flexure high-stroke compound pivot (see section 1.2.4) and an interesting motion converter, which allows to achieve a submicrometric translational resolution with a ball screw transmission. Figure 2.22 illustrates the principle and the prototype of the Tribias robot.

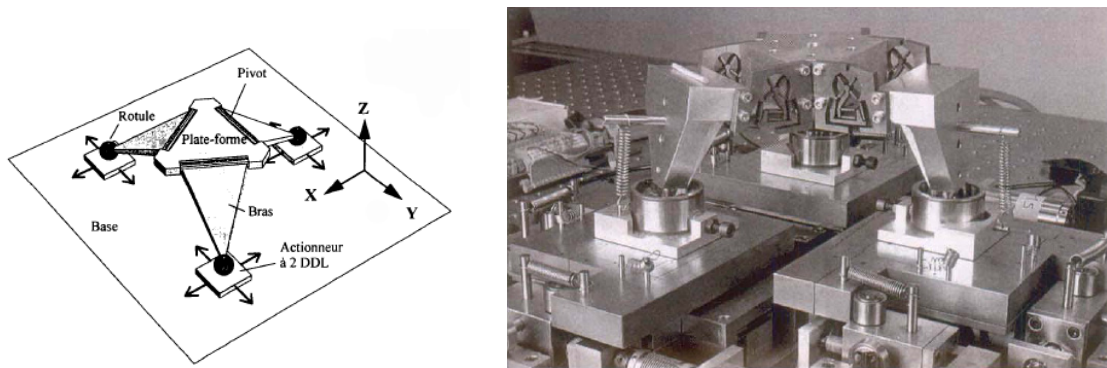


Figure 2.22: Principle (left) and prototype (right) of the Tribias 6-DOF robot [73]

Two robots which have been developed by the Technische Universität Braunschweig convert known parallel arrangements to high precision applications: the 3-translation Triglides<sup>s</sup> [41, 79] (figure 2.23, left) adapts the Delta kinematics with flexible elements and linear rolling bearings. This prototype achieves a workspace of  $112 \times 112 \times 122 \text{ mm}^3$  with a resolution of  $0.125 \mu\text{m}$  and a repeatability of  $3 \mu\text{m}$ ; its footprint reaches  $1280 \times 980 \text{ mm}^2$ . Although this prototype achieves higher strokes than most high precision robots, its bulky volume questions the efficiency of its use for the production of small devices. As for the Micabo<sup>hs</sup> [40, 84] (figure 2.23, right), this 6-DOF robot reaches a workspace of  $40 \times 40 \times 18 \text{ mm}^3$  for a footprint of  $270 \times 240 \text{ mm}^2$ ; the resolution of the output reaches  $0.1 \mu\text{m}$  and its repeatability  $0.3 \mu\text{m}$ .

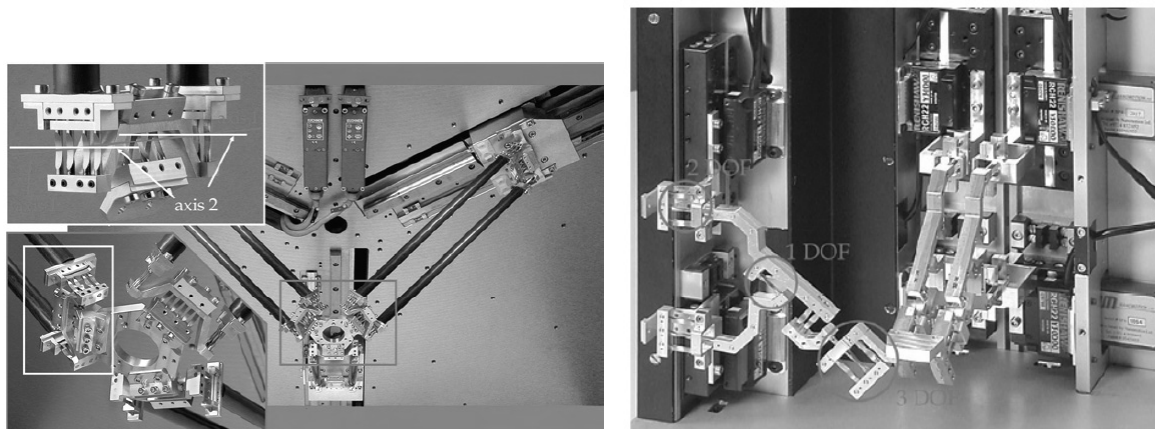


Figure 2.23: 3-DOF Triglides<sup>s</sup> (left) and 6-DOF Micabo<sup>hs</sup> (right) prototypes [84]

Finally, the MiniPaR robot [16, 17], which has been developed by DIMEC University of Genoa, is a decoupled Cartesian three-translation parallel robot which is composed of stacked super-elastic foils, performing high precision planar joints, and of linear actuators including rolling bearings (see figure 2.24). The machined prototype presents a workspace of  $30 \times 30 \times 30 \text{ mm}^3$  for a total volume of  $480 \times 195 \times 295 \text{ mm}^3$ , and a motion accuracy of  $1 \mu\text{m}$ .

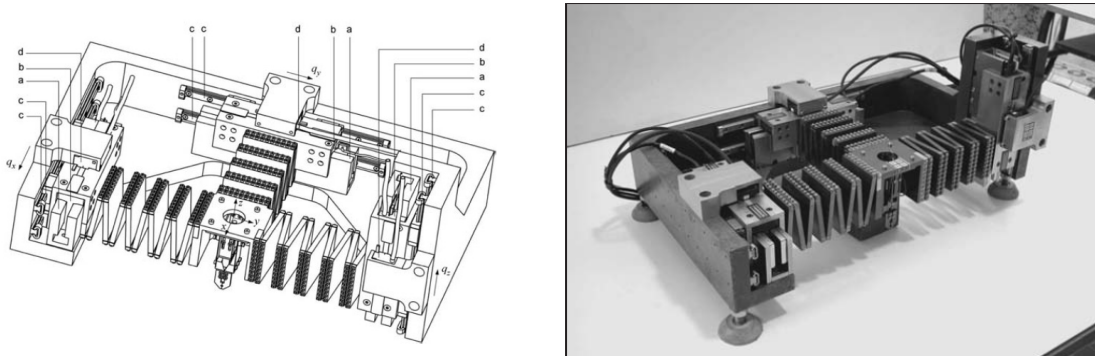


Figure 2.24: *Three-translation MiniPaR robot design principle (left) and machined prototype (right) [17]*

### 2.3.4 Commercial high precision and ultra-high precision robots

Most commercial high precision and ultra-high precision robots present a Stewart platform arrangement, which is often called Hexapod: for instance, PI miCos [63] proposes a whole range of such products, which includes the HP-550 model ( $100 \times 100 \times 100 \text{ mm}^3$  workspace, rotation angles of  $40^\circ$  for Rx and Ry and  $60^\circ$  for Rz, with a pivot point which can be set by the customer, resolutions of  $0.5 \mu\text{m}$  and  $10 \mu\text{rad}$ , total volume of  $78 \text{ dm}^3$ ) and the more compact HP-300 ( $30 \times 30 \times 15 \text{ mm}^3$  workspace, rotation angles of  $20^\circ$ , resolutions of  $0.5 \mu\text{m}$  and  $10 \mu\text{rad}$ , total volume of  $12.5 \text{ dm}^3$ ).

Furthermore, this company proposes an interesting alternative to the Stewart platform, which consists in SpaceFab 6-DOF robots: these present the same kinematics as the afore-described Tribias, including three identical chains composed of two linear actuators, a passive revolute joint and a passive spherical joint (see figure 2.25). For instance, the SpaceFab 3000 BS model achieves a workspace of  $50 \times 12.7 \times 100 \text{ mm}^3$  and angles of  $10^\circ$  with  $0.5 \mu\text{m}$  and  $20 \mu\text{rad}$  resolutions. Nonetheless, the total size of this product ( $600 \times 444 \times 209 \text{ mm}^3$ ) remains highly bulky for the achieved strokes; figure 2.25 highlights the size of the stacked actuated linear tables compared to the robot kinematics volume. Moreover, the replacement of these by a more effective design performing two translations could easily increase the achieved precision of this robot.

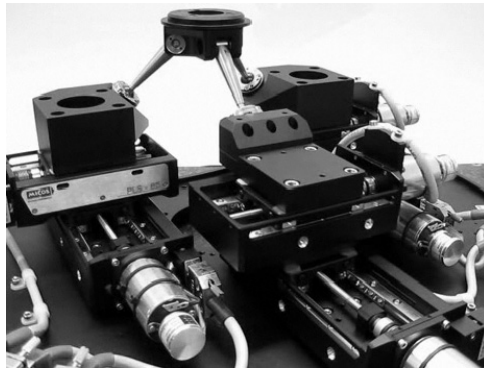


Figure 2.25: 6-DOF SpaceFab robot design [63]

## 2.4 Conclusion

This chapter has presented an overview of the state of the art in the domain of modular ultra-high precision robots; the emphasis has specifically been placed on three key aspects, namely modular synthesis methodologies, flexure-based mechanisms design and existing high precision and ultra-high precision robots. The review of the most interesting works on these topics *has underlined the lack of a global approach, i.e. which would examine and propose solutions for both the kinematic synthesis and the mechanical design of the robot, for any end-effector mobility.*

In comparison with the previous works on modular ultra-high precision parallel robots, this thesis aims at developing a concept featuring the following attributes:

- *three levels of modularity*
  - the *conceptual building bricks*, which will be strictly independent from any mechanical design. Consequently, the kinematic part of the methodology will allow the synthesis of a large variety of machines, from machine-tools to micro-scale robots.
  - the *mechanical design of the building bricks*: the concept will propose a gathering of efficient flexure-based mechanisms for ultra-high precision applications. Furthermore, the effectiveness of this second modularity level will lie in the possibility of replacing the mechanical design of only one building brick without influencing the other parts of the robot.
  - *elements of the bricks mechanical design*, which will especially include the possibility of adjusting the position of rotation centres thanks to Remote Centres of Motion (RCM).
- *a powerful and complete design methodology*, which will not only provide a general kinematic synthesis method appropriate for any type of parallel orthogonal robots, but will also propose a complete procedure for the selection of the kinematic arrangement



and mechanical design of the robot building bricks, depending on the specific application requirements. This thorough procedure will be illustrated with the development of an ultra-high precision 5-Degree of Freedom robot.

Finally, these features will allow the modular concept for the synthesis of ultra-high precision robots to be considered as a *design tree*: thanks to the explicit statement of hypotheses at each step of the methodology, the user will indeed be able to enter the concept at any level and to adapt the selection criteria to his/her own design problem.



# Chapter 3

## Concept of modular kinematics

This chapter introduces the fundamentals of the design methodology, which consist in the conceptual aspects leading to the kinematic synthesis of the modular parallel robots. After stating the bases of the concept and the notations, the obtention of the exhaustive conceptual solution catalogue is detailed. As the aspects presented in this chapter are purely conceptual, *i.e.* totally independent from any mechanical design, this part of the methodology can be applied to design the kinematics of a large variety of robots, from machine-tools to microscale robots.

### 3.1 Modular parallel robot and building bricks

This methodology consists in designing a modular parallel robot composed of one to three kinematic chains, which are orthogonally arranged. This robot is symbolised by a cube: each kinematic chain is disposed along a different face, whereas the end-effector is located on one of its corners (see figure 3.1, left). Its kinematic synthesis makes use of a finite number of conceptual building bricks, which can be either active or passive (see figure 3.1, right). Each kinematic chain of the modular robot consists in the serial arrangement of an active brick with a passive one.

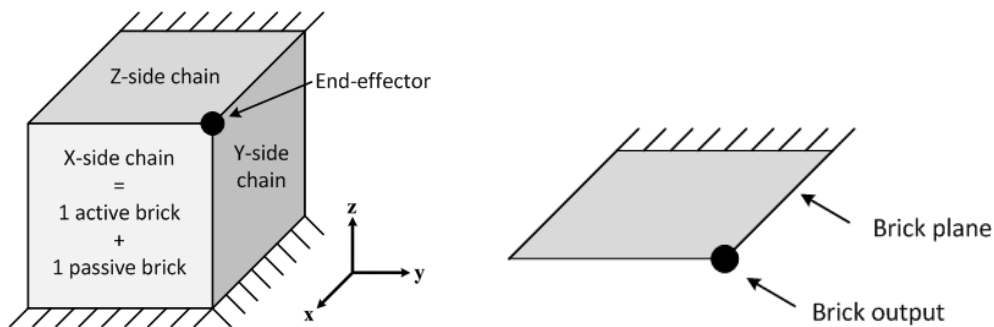


Figure 3.1: Symbolism of the parallel robot designed with the modular concept (left) and of the building bricks (right)

The modular methodology takes as an input the desired robot mobility: only the pres-

ence or absence of the 6 possible end-effector degrees of freedom is considered at this step of the procedure. This global requirement is then transformed into a thorough list of all possible combinations of active and passive bricks fulfilling it, thanks to the exhaustive conceptual solution catalogue, which will be detailed in section 3.2. Finally, a kinematics is selected depending on the robot specific requirements, as well as on mechanical design considerations.

The effectiveness of this concept to respond to changes in the industrial specifications during the design process lies in its modularity: a minimal number of bricks, in most cases only one, needs to be modified to add or remove a degree of freedom. Moreover, the active bricks composing a robot being kinematically uncoupled, even its geometric model and its control algorithm require only minor changes to fulfill the new specifications.

### 3.1.1 Conceptual building bricks

The modular methodology makes thus use of a finite number of conceptual building bricks, which can be either active or passive:

- The role of the **active bricks** is to actuate from one to three degrees of freedom; the other motions are blocked.
- The **passive bricks** link the output of the active bricks to the end-effector of the robot, thus performing a transmission of the actuated motions. Their degrees of freedom are either passive, *i.e.* free to move but not actuated, or blocked.

A generic notation uniformly represents the conceptual building bricks by symbolising their two main features:

- **The free degrees of freedom of the brick, *i.e.* the active or passive motions, are represented by the letters**, namely T for translations and R for rotations. Uppercase letters (T, R) stand for actuated motions, whereas lowercase letters (t, r) symbolise passive degrees of freedom, which allows to discriminate both types of building bricks.
- **The subscripts indicate the direction of the motions relatively to the face of the cube on which the brick is positioned.** Regarding the orthogonal coordinate system presented in figure 3.1, three directions are possible:  $\perp$  indicates that the considered motion is along an axis which is orthogonal to the face plane, whereas  $\parallel$  stands for a degree of freedom which is along one of the two directions that belong to that plane (see figure 3.2). Moreover, the additional subscripts 1 and 2 explicitly express the directions of several degrees of freedom along both possible axes of the plane. Figure 3.3 illustrates an example where this discrimination is mandatory.
- The order of the motions in the brick notation has arbitrarily been set to the following:  $T_{\parallel}$ ,  $T_{\perp}$ ,  $R_{\parallel}$ , and  $R_{\perp}$  for the active bricks, and the corresponding  $t_{\parallel}$ ,  $t_{\perp}$ ,  $r_{\parallel}$ , and  $r_{\perp}$  for the passive bricks.

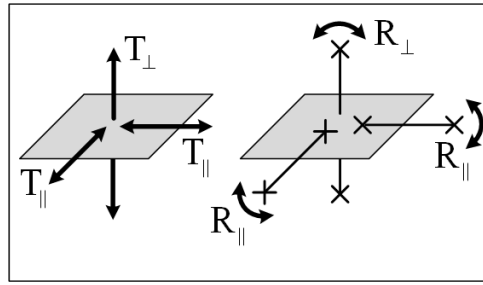


Figure 3.2: Possible directions of the brick degrees of freedom relative to the face plane

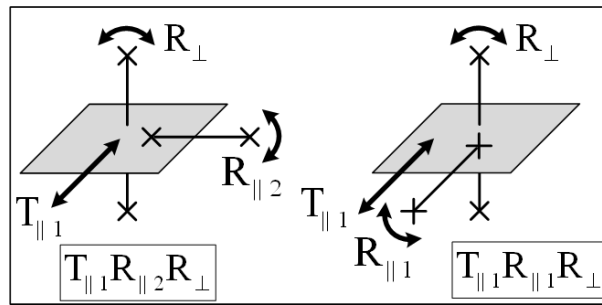


Figure 3.3: Example of two active bricks to illustrate the use of the additional 1 and 2 subscripts

Following these guidelines, the exhaustive set of conceptual building bricks is established. The active bricks, which actuate from one to three motions, perform the 12 possible output mobilities: their total number is 25, as several bricks can present the same degrees of freedom with different orientations relatively to the face of the cube on which they are located. The choice to limit the number of actuated degrees of freedom to three is related to the aim of the design methodology, which consists in simplifying the kinematic synthesis of parallel robots: designing bricks which actuate a higher mobility than three is as complex as directly building an equivalent robot. Thus, their inclusion in the concept does not help decreasing the intricacy of the synthesis.

Furthermore, 38 passive bricks are featured in the methodology, including the passive version of the 25 active bricks and the 13 bricks performing the 4- and 5-DOF motions. Note that the 6-DOF passive brick has been discarded as it cannot perform the transmission of any motion, all its degrees of freedom being free. Moreover, the 0-DOF brick, whose motions are all blocked, has also been relinquished for its uselessness. All other mobilities have been included in the concept, as the design of 4- or 5-DOF passive bricks is easier to achieve than the corresponding actuated mechanisms. Both the 4-DOF space parallelogram which is included in the classical Delta kinematics (see figure 1.2) and in its flexure-based adaptation (figure 1.4, 2.17), and the Sigma 6 robot arms (figure 2.21) epitomise this observation.

The exhaustive list of the conceptual building bricks, including their notation and their graphical representation, is illustrated in figures 3.4 to 3.8. The alternation of grey and white backgrounds groups subsequent bricks which share the same degrees of freedom with different orientations relatively to the cube face.

<b>ACTIVE BRICKS</b>							
$R_{\parallel}$		$T_{\parallel}$		$T_{\parallel}T_{\parallel 2}$		$T_{\parallel}T_{\perp}$	
$R_{\perp}$		$T_{\perp}$		$T_{\perp}R_{\parallel}$		$T_{\perp}R_{\perp}$	
$T_{\parallel}R_{\parallel 1}$		$T_{\parallel}R_{\perp}$		$T_{\perp}R_{\perp}$		$T_{\parallel}R_{\parallel 2}$	
$R_{\parallel}R_{\perp}$		$T_{\parallel}T_{\perp}T_{\perp}$		$T_{\parallel}T_{\parallel 2}T_{\perp}$		$T_{\parallel}T_{\perp}R_{\parallel 2}$	

Figure 3.4: List of the conceptual active bricks (1/2). The bold line groups the bricks which share the same mobility

ACTIVE BRICKS, continued				
$T_{\parallel 1} T_{\parallel 2} R_{\perp}$	$T_{\perp} R_{\parallel 1} R_{\parallel 2}$	$T_{\parallel 1} R_{\parallel 2} R_{\perp}$	$T_{\perp} R_{\parallel 1} R_{\perp}$	$T_{\parallel 1} R_{\parallel 1} R_{\perp}$
$T_{\parallel 1} R_{\parallel 1} R_{\parallel 2}$		$R_{\parallel 1} R_{\parallel 2} R_{\perp}$		

Figure 3.5: List of the conceptual active bricks (2/2)

<b>PASSIVE BRICKS</b>					
$I_{\parallel}$	$I_{\perp}$	$t_{\parallel}$	$t_{\perp}$	$t_{\parallel}t_{\parallel 2}$	$t_{\parallel}t_{\perp}$
$t_{\parallel}I_{\parallel 1}$	$t_{\perp}I_{\perp}$	$t_{\parallel}I_{\perp}$	$t_{\perp}I_{\parallel}$	$t_{\parallel 1}I_{\parallel 2}$	$I_{\parallel}I_{\parallel 2}$
$I_{\perp}I_{\perp}$	$t_{\parallel 1}t_{\parallel 2}$	$t_{\parallel 1}I_{\perp}$	$t_{\parallel 1}t_{\perp}I_{\parallel 1}$	$t_{\parallel 1}t_{\parallel 2}I_{\parallel 1}$	$t_{\parallel 1}t_{\perp}I_{\parallel 2}$

Figure 3.6: List of the conceptual passive bricks (1/3)



**PASSIVE BRICKS, continued**

$t_{\parallel 1} t_{\parallel 2} r_{\perp}$		$t_{\perp} r_{\parallel 1} r_{\parallel 2}$		$t_{\perp} r_{\parallel 1} r_{\perp}$	
$t_{\parallel 1} r_{\parallel 1} r_{\parallel 2}$		$t_{\parallel 1} t_{\parallel 2} r_{\perp}$		$t_{\parallel 1} t_{\perp} r_{\parallel 1} r_{\perp}$	
$t_{\parallel 1} r_{\parallel 1} r_{\perp}$		$r_{\parallel 1} r_{\parallel 2} r_{\perp}$		$t_{\parallel 1} t_{\perp} r_{\parallel 1} r_{\perp}$	
$t_{\parallel 1} t_{\perp} r_{\parallel 1} r_{\parallel 2}$		$t_{\parallel 1} t_{\parallel 2} r_{\perp} r_{\parallel 1}$		$t_{\perp} r_{\parallel 1} r_{\parallel 2} r_{\perp}$	
$t_{\parallel 1} t_{\perp} r_{\parallel 1} r_{\perp}$		$t_{\parallel 1} t_{\perp} r_{\parallel 1} r_{\parallel 2}$		$t_{\perp} r_{\parallel 1} r_{\parallel 2} r_{\perp}$	

Figure 3.7: List of the conceptual passive bricks (2/3); the double line separates the passive version of the 25 active bricks, presenting one to three DOF, from the passive bricks performing four and five DOF

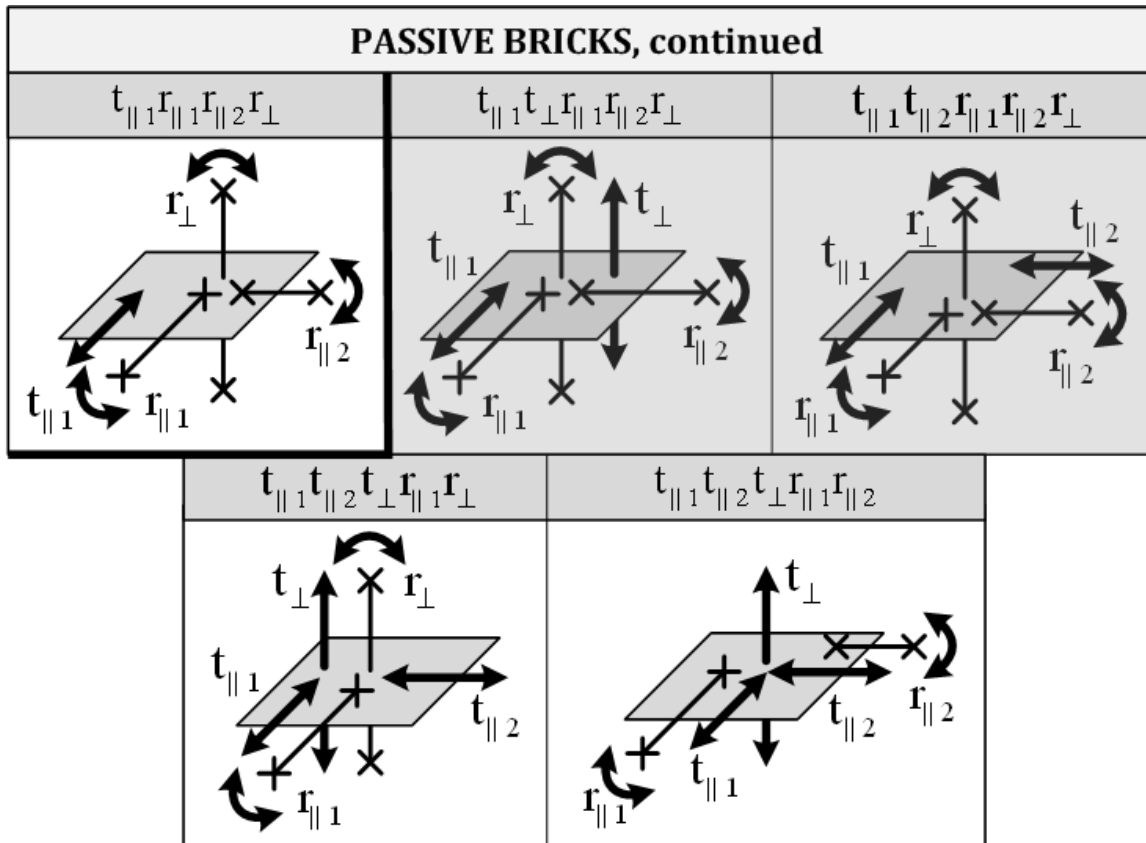


Figure 3.8: List of the conceptual passive bricks (3/3)

### 3.2 Generation of the exhaustive conceptual solution catalogue

The exhaustive conceptual solution catalogue consists in the core of the modular methodology, as it allows to significantly reduce the time necessary to synthesise the robot kinematics. All possible kinematics stemming from the concept are indeed listed in this catalogue, in which the robot designer has only to select the most suited solution for his/her specific requirements.

This thorough catalogue needs to be generated only once. This process includes two main steps: first, the exhaustive list of all active bricks arrangements actuating the desired robot degrees of freedom is established for each of the 19 possible robot mobilities. Then, for each of these arrangements, all combinations of passive bricks performing the transmission of these motions without overconstraints are itemised. The next paragraphs detail both of these steps.

In this thesis, the solution catalogue has been generated by an intuitive approach, which is first presented to allow the reader to understand the method; then, the same catalogue has been automatically created, which has proven its thoroughness.

### 3.2.1 Active bricks arrangements

The generation of the catalogue first consists in listing all possibilities of arranging one to three active bricks on the cube so that they actuate the degrees of freedom which the robot has to perform. As six permutations of two and three bricks on the cube (only three for a unique brick) lead to the same kinematic solution, the latter is itemised only once (see figure 3.9).

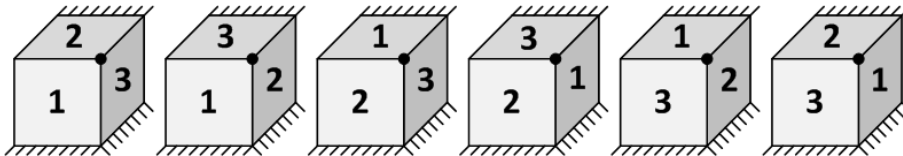


Figure 3.9: List of the six possible permutations leading to the same kinematic solution

The procedure to generate the list of the active bricks arrangements for each possible robot mobility is the following:

1. **Establish the different families of solutions which actuate the required degrees of freedom:** these are characterised by the number of kinematic chains (one to three), and by the qualitative motions which each chain has to actuate (translation, rotation).
2. **For each of these families, combine all building bricks which actuate the required motions:** each kinematic chain described in a family is now replaced by an active building brick; each substitution leads to several possibilities, as one or more brick can be selected to actuate the desired motions. Knowing the number of potential bricks for each chain, a simple combinatory computation returns the maximal number of arrangements for this family. This step consists in establishing the list of these possibilities.
3. **Verify the consistency of these arrangements with the concept definition:** the second step of the procedure indeed generates solutions which are not compatible with the methodology theory, for example arrangements where two active bricks should be located on the same face of the cube. This last step thus consists in removing these spurious solutions.

Two examples are now detailed: the first consists in a planar joint, which illustrates the use of the procedure on a simple case, whereas the second highlights the quick growth of the number of active bricks arrangements for high-DOF robot mobilities.

#### 3.2.1.1 First example: planar joint mobility

The planar joint mobility includes three degrees of freedom, two translations and one rotation, whose directions are along three orthogonal axes. Figure 3.10 illustrates this mobility with the symbolism of the modular concept. The directions of the motions have been arbitrarily set to  $T_x$ ,  $T_y$  and  $R_z$ : this choice does not influence the progress of the procedure, as a simple rotation of the robot cube allows to reorient the mobility along the desired axes.

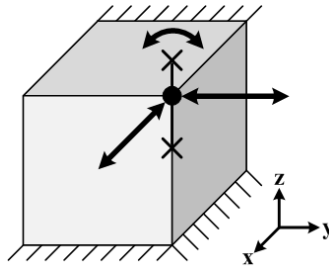


Figure 3.10: Graphical representation of the robot presenting the planar joint mobility

First, the families of solutions which actuate the required degrees of freedom are the following:

1. *1 kinematic chain*, actuating 2 translations and 1 rotation.
2. *2 kinematic chains*: the first actuates 2 translations, the second actuates 1 rotation.
3. *2 kinematic chains*: the first actuates 1 translation and 1 rotation, the second actuates 1 translation.
4. *3 kinematic chains*: two of them actuate 1 translation, the third actuates 1 rotation.

The second step of the procedure consists in replacing the kinematic chains by active bricks which perform the desired motions. For instance, the second family of the previous list accepts the following building bricks:

- $T_{\parallel}T_{\perp}$  and  $T_{\parallel 1}T_{\parallel 2}$  to substitute for the first kinematic chain, thus performing 2 translations
- $R_{\parallel}$  and  $R_{\perp}$  to substitute for the second kinematic chain, thus performing 1 rotation

The total amount of combinations of these four bricks is thus  $2 \cdot 2 = 4$ , which are the following:

- $T_{\parallel}T_{\perp}$  and  $R_{\perp}$
- $T_{\parallel}T_{\perp}$  and  $R_{\parallel}$
- $T_{\parallel 1}T_{\parallel 2}$  and  $R_{\perp}$
- $T_{\parallel 1}T_{\parallel 2}$  and  $R_{\parallel}$

The last step of the procedure consists in verifying the consistency of these solutions with the concept, which is straightforward when the arrangements are graphically represented, as in figure 3.11: if the first kinematic chain is replaced by the  $T_{\parallel}T_{\perp}$  active brick (represented by the hatched face), the remaining rotation (symbolised by the dashed line) can be performed either by the  $R_{\perp}$  or the  $R_{\parallel}$  brick. Nonetheless, when the  $T_{\parallel 1}T_{\parallel 2}$  brick actuates the two translations, the  $R_{\perp}$  brick cannot perform the remaining rotation, as it would necessitate that both bricks are located on the same face of the cube.

After applying the same reasoning to the other solution families, the planar joint mobility accepts 14 different active bricks arrangements.

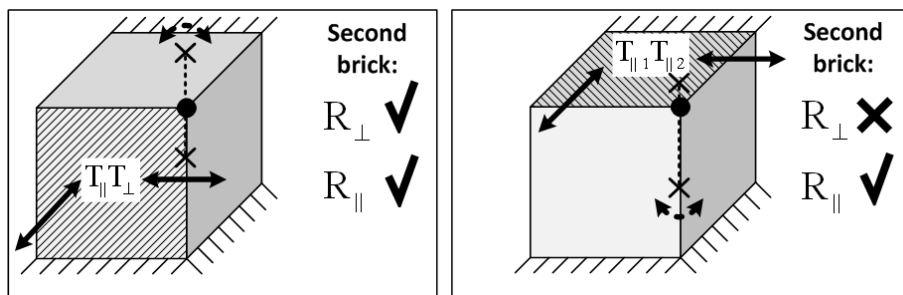


Figure 3.11: Graphical representation to check the consistency of the solutions

### 3.2.1.2 Second example: 4-DOF mobility

The 4-DOF mobility studied in this second example has only an additional degree of freedom in comparison with the planar joint mobility: it indeed performs two translations and two rotations, whose axes are oriented as represented in figure 3.12. Note that the directions of the motions along the  $x$ ,  $y$  and  $z$  axes have arbitrarily been set, as in the previous example.

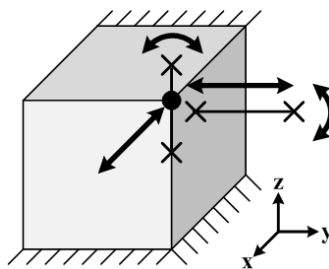


Figure 3.12: Graphical representation of the robot presenting the considered 4-DOF mobility

The families of solutions for this mobility are the following:

1. 2 kinematic chains: the first actuates 2 translations, the second 2 rotations.
2. 2 kinematic chains, both of them actuating 1 translation and 1 rotation.
3. 2 kinematic chains: the first actuates 2 translations and 1 rotation, the second 1 rotation.
4. 2 kinematic chains: the first actuates 2 rotations and 1 translation, the second 1 translation.
5. 3 kinematic chains: the first actuates 2 translations, the two remaining actuate 1 rotation.
6. 3 kinematic chains: the first actuates 2 rotations, the two remaining actuate 1 translation.
7. 3 kinematic chains: the first actuates 1 translation and 1 rotation, the second 1 translation, the third 1 rotation.

Not only the number of solution families is notably higher than for the planar joint mobility, but also the number of combinatory possibilities explodes: the second family accepts for example 25 of them (5 active bricks are possible for each chain, thus  $5 \cdot 5 = 25$ ), among which 11 solutions are compatible with the concept.

This mobility can finally be performed by 59 different arrangements of active building bricks: in comparison with the planar mobility, only one degree of freedom has been added, which has led to a total number of solutions which has more than tripled.

### 3.2.2 Passive bricks arrangements

Once the exhaustive list of the active bricks arrangements achieving each of the 19 possible robot mobilities has been established, the combinations of passive bricks performing the transmission of the actuated motions without overconstraints have to be itemised.

For each of the active bricks arrangements, the procedure to obtain the list of the corresponding passive bricks is the following:

1. For each kinematic chain, the passive brick has to block the degrees of freedom which are actuated by the serially arranged active brick.
2. For each kinematic chain, the degrees of freedom which correspond to the motions actuated by the active bricks of the other kinematic chains are set as passive.
3. The remaining degrees of freedom correspond to the blocked motions of the robot end-effector; the role of the passive brick is thus to avoid overconstraints, *i.e.* to ensure that the position of the degrees of freedom are imposed by one and only one passive brick. In other words, the motions must be blocked in one passive brick and free in the others. This condition leads to several possibilities for each active bricks arrangement: their total number is computed as follows:

$$\#solutions = (n_{DOF})^{m_{chains}}$$

where:

- $\#solutions$  is the number of passive bricks arrangements
- $n_{DOF}$  is the number of blocked motions of the robot end-effector
- $m_{chains}$  is the number of kinematic chains (one to three)

If the robot is composed of several identical active bricks, this number is decreased as some passive bricks arrangements become equivalent.

This procedure can be applied to the planar joint mobility detailed in paragraph 3.2.1.1: figure 3.13 graphically presents the reasoning on one of the active bricks arrangements. The crossed out degrees of freedom first correspond to the motions which are actuated by the active brick of the chain: they are thus blocked. Then, the circled motions are set to passive, as they are actuated by the other kinematic chain. Lastly, 3 degrees of freedom remain, which leads to  $3^2 = 9$  passive bricks arrangements: figure 3.13 presents one of the possibilities.

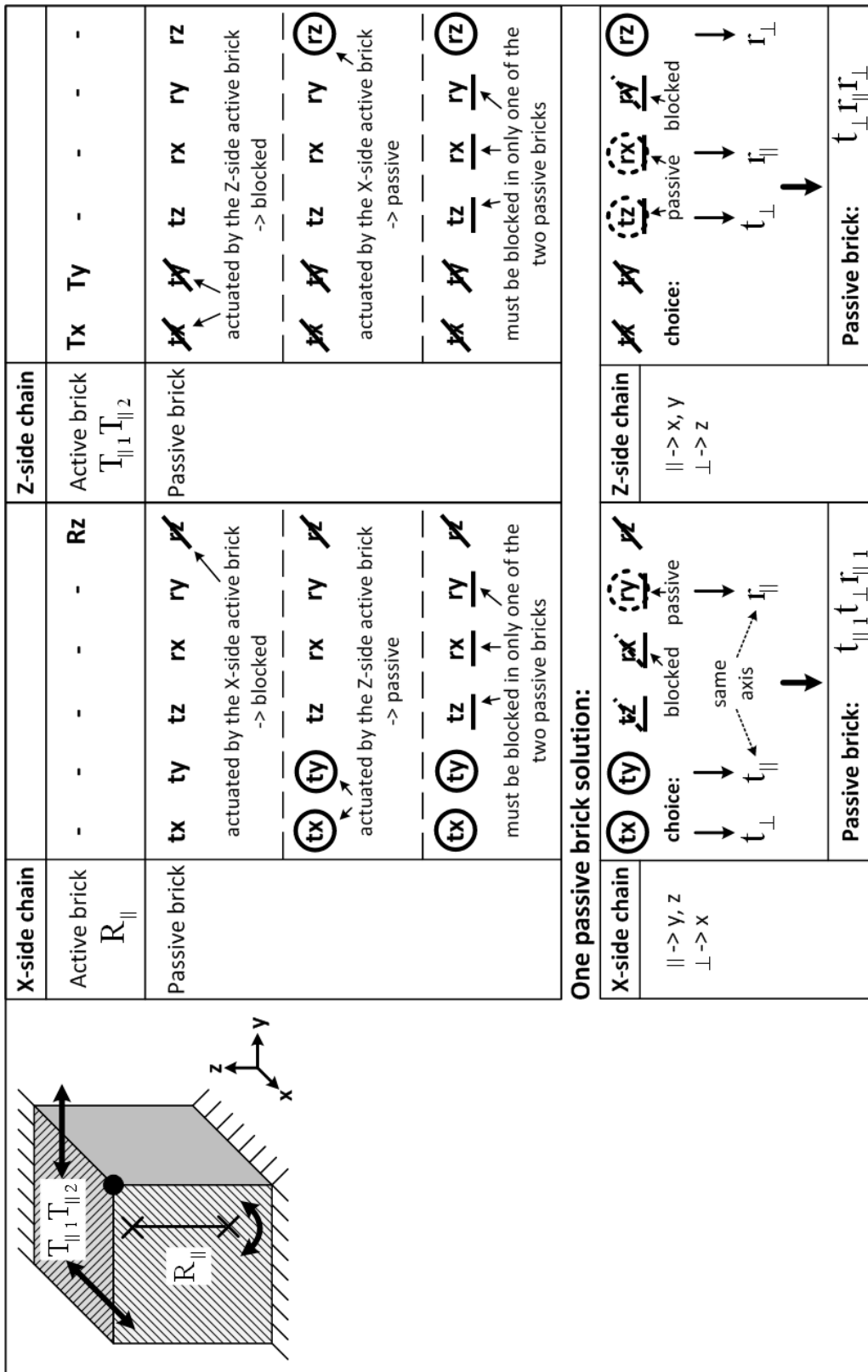


Figure 3.13: Graphical representation of the procedure to obtain the thorough list of passive bricks corresponding to the active bricks arrangement; the crossed out DOF are blocked, the circled motions are set as passive, and the remaining displacements must be blocked in only one passive brick to avoid overconstraints



Moreover, this example allows to highlight the following observation: the same active bricks solution can lead to different sets of corresponding passive bricks, depending on the relative orientation of the actuated motions on the robot cube. Figure 3.14 illustrates this situation: both of the sketched cubes make use of the same active bricks to perform the same degrees of freedom; however, these possibilities do not consist in permutations of the same kinematics, as they are not differentiated by only a simple reorientation of the cube. Two distinctive sets of passive bricks are thus generated: a possibility from each set is presented in figure 3.14. Some passive bricks arrangements may be included in both sets; they are however counted as two distinct solutions, as the final kinematics of the robot is not equivalent.

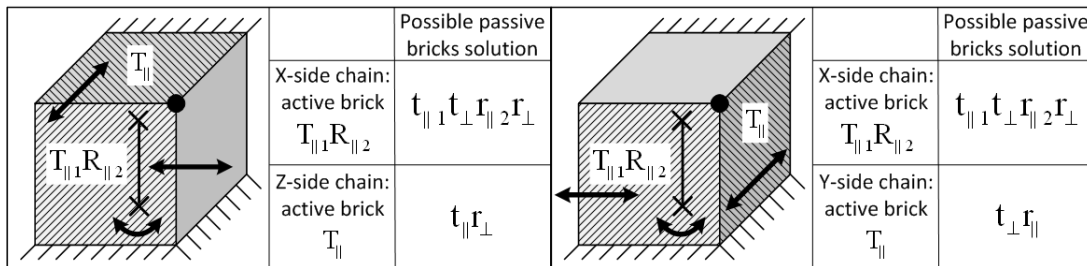


Figure 3.14: Illustration of the different passive bricks sets generated by the same active bricks solution

In the end, the enumeration of all passive bricks arrangements generates 158 kinematic solutions for the planar joint mobility, whereas for the 4-DOF example presented in paragraph 3.2.1.2, 492 possibilities perform the desired robot mobility.

**After applying the aforesaid procedure to each of the 19 possible robot mobilities, the exhaustive conceptual solution catalogue features a total of 3175 kinematic solutions, including 547 different active bricks arrangements.** All these possibilities are graphically represented in appendix B.

### 3.2.3 Automatic generation of the conceptual solution catalogue

The intuitive approach which has been detailed in the last paragraphs has allowed to establish the conceptual solution catalogue; moreover, a second method has been developed to automatically generate the active bricks solutions, making use of combinatory algorithms to produce the arrangements. Briefly, four main steps are implemented:

1. A list of all brick combinations is established, based on simple combinatory algorithms.
2. A first dismissal test suppresses the solutions which actuate more than once the same end-effector degree of freedom. For example, an arrangement where two bricks actuate the translation along the x axis would be removed at this step.
3. A second test deletes the combinations which are inconsistent with the concept, for instance the ones where two bricks should be located on the same face of the cube.



4. The last test suppresses the permutations of the same active bricks arrangement (see figure 3.9).

This algorithm has been implemented in MATLAB and has proven the exhaustiveness of the active bricks arrangements list established by hand. As for the passive bricks solutions, the formula presented in 3.2.2 allows to thoroughly itemise them. More details on the algorithm generating the active bricks solutions and some outlines of a program which automatically lists the corresponding passive bricks are to be found in appendix A.

In conclusion, the objective of the methodology, which consists in decreasing the complexity of the kinematic design of parallel robots, is chiefly achieved: instead of having to synthesise a robot from scratch, the designer has only to select the most suited kinematics for a specific application. At this point of the methodology, both the building bricks and the kinematic solutions are independent from any mechanical design; they thus allow to synthesise a large variety of robots, from machine-tools to microscale robots. Figure 3.15 summaries the hypotheses which have led to the establishment of the exhaustive conceptual solution catalogue.

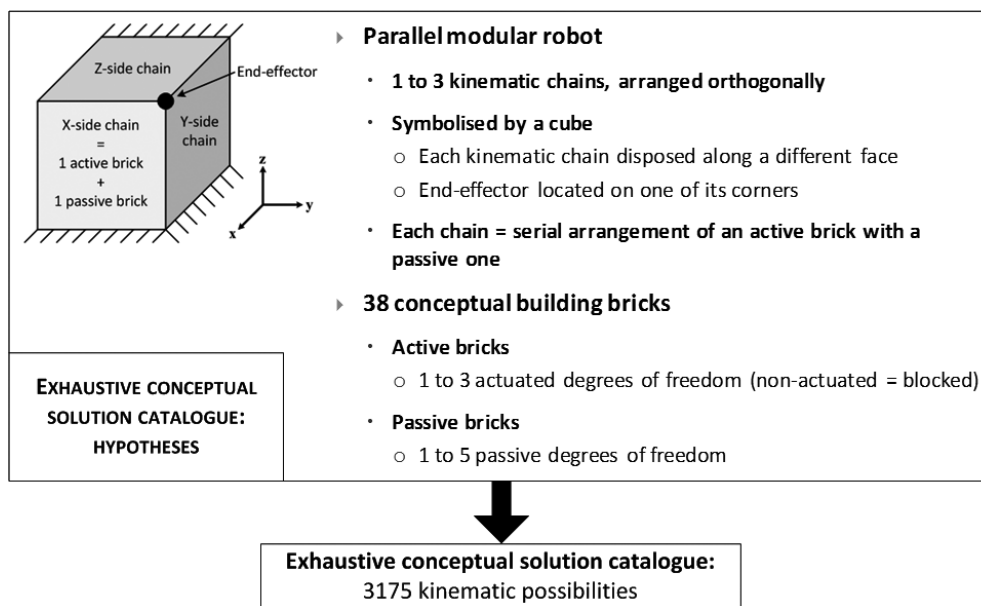


Figure 3.15: Summary of the hypotheses which have led to the establishment of the exhaustive conceptual solution catalogue

Moreover, a reduction of the solution catalogue can be performed to improve the convenience of the methodology by diminishing the number of possible bricks arrangements. Although no building brick or kinematic solution from the list is a priori unsuited regardless the purpose of the robot, selection criteria linked with the application domain can be formulated. As this thesis focuses on ultra-high precision, hypotheses linked with the mechanical design and the machining of flexure-based structures are presented in the following chapter: they will allow to establish a reduced and thus more functional conceptual solution catalogue.



# Chapter 4

## Reduced solution catalogue for ultra-high precision

This chapter introduces the selection criteria linked with the design and machining of flexure-based mechanisms which have been used in this thesis to determine which building bricks can be smartly designed with flexure hinges. Consequently, only the kinematic solutions which are suited to ultra-high precision applications are retained to establish the reduced conceptual solution catalogue.

### 4.1 Hypotheses for ultra-high precision

High-performance flexure-based mechanisms can only be achieved if their design is shrewdly performed and if the machining of the structures is carefully examined from the beginning of the mechanical synthesis. As seen in section 1.2.4, all flexure-based mechanisms which are designed in this thesis are *made of metals and intended for monolithical machining by Wire Electro-Discharge Machining (W-EDM)*. These considerations lead to three main hypotheses: only the building bricks that meet these requirements are retained for ultra-high precision applications.

- *The building bricks for ultra-high precision are designed as planar mechanisms, or as structures presenting a rotational symmetry*: this criterion arises from the monolithic machining of flexure-based mechanisms by Wire Electro-Discharge Machining (W-EDM). As detailed in section 1.2.4, the relative configuration of the wire and the part only allows to machine ruled surfaces. Moreover, the planarity hypothesis represents a crucial advantage for the design of these structures. The differentiation between a blocked and a free degree of freedom of a mechanism indeed lies in its stiffness along the considered motion: the stiffness of the blocked displacement should be at least 100 times higher than the one of a free motion [36]. Practically, a factor of around 1000 is recommended to avoid low transverse eigenfrequencies. For a prismatic hinge or a leaf spring, the stiffnesses of the natural degrees of freedom are proportional to  $I_y = \frac{bh^3}{12}$ , whereas for the transverse blocked motions, they are proportional to  $I_x = \frac{b^3h}{12}$ ,

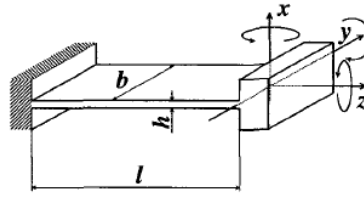


Figure 4.1: Prismatic hinge or leaf spring [36]

where  $b$ ,  $h$ , and the  $x$ ,  $y$  axes are defined in figure 4.1 [36]. If  $b$  is the thickness of the planar structure, increasing this parameter by a factor of 10 allows to multiply the transverse stiffness by 1000; albeit the natural stiffness is simultaneously increased by the same factor of 10, the admissible natural stroke is not influenced by this modification. This consideration is particularly significant for the active building bricks, as they are by definition located further from the robot end-effector than the passive bricks: the stiffnesses along their blocked degrees of freedom must be maximised to limit parasitic displacements resulting from the application of forces and moments on the robot end-effector.

- **The active degrees of freedom are performed by linear actuators only:** the lack of standard ultra-high precision rotary sensors and actuators on the market imposes the use of linear devices only. Consequently, rotations are achieved by differential actuation of two motors, or of one motor and the robot frame. By hypothesis, this differential motion takes place solely within the active bricks, *i.e.* no differential actuation is performed between two kinematic chains of the robot.

These hypotheses stem from design and machining considerations of flexure-based structures made of metals and machined with Wire Electro-Discharge Machining. Consequently, if these prerequisites are not fulfilled, these criteria must be revised.

## 4.2 Building bricks for ultra-high precision

### 4.2.1 Active bricks

Following the aforementioned hypotheses, an active building brick is suited for ultra-high precision applications only if an efficient mechanical design fulfilling both the planarity and the linear actuation criteria exists. Figure 4.2 summaries the conceptual active bricks which are retained for ultra-high precision.

ACTIVE BRICKS FOR ULTRA-HIGH PRECISION			
$R_{\parallel}$	$R_{\perp}$	$T_{\parallel}$	$T_{\perp}$
$T_{\parallel 1} T_{\parallel 2}$	$T_{\parallel} T_{\perp}$	$T_{\parallel} R_{\perp}$	$T_{\perp} R_{\parallel}$
$T_{\parallel 1} R_{\parallel 2}$	$T_{\parallel 1} T_{\perp} R_{\parallel 2}$		$T_{\parallel 1} T_{\parallel 2} R_{\perp}$

Figure 4.2: Active building bricks for ultra-high precision applications

Comparatively to the exhaustive list of building bricks, the following ones have been discarded:

- The bricks which actuate more than one rotation:** figure 4.3 illustrates a rigid body which is symbolised by a cube. This body is linked to a fixed frame with a ball joint, which is located on the desired centre of rotation (represented by the grey sphere); two rotations, around both x and y axes, have to be performed. The linear actuation hypothesis imposes that these rotations are created by the application of two forces: the black arrows represent the possible force directions to rotate around x, whereas the dashed arrows stand for the force directions to rotate around y. This graphical representation highlights the fact that the directions of both forces and the rotation centre cannot be included in the same plane. Consequently, the bricks actuating two

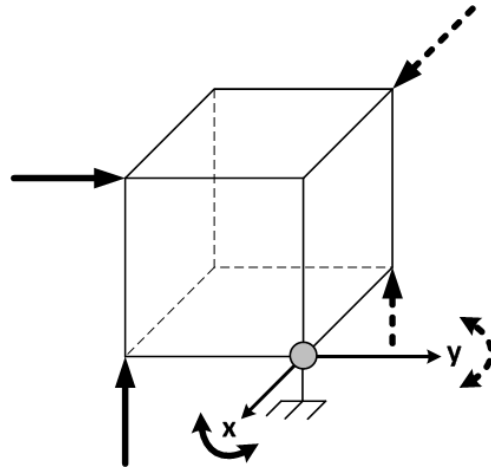


Figure 4.3: Sketch of a rigid body which can rotate around both  $x$  and  $y$  axes, with a common rotation centre. The arrows stand for the direction of the actuating forces (black to rotate around  $x$  and dashed to rotate around  $y$ )

or three rotations are discarded, as they cannot be designed as planar structures.

- **The bricks which include a cylindrical joint:** as no efficient design fulfilling both the planarity and the linear actuation criteria has been obtained, a kinematic chain including this joint is replaced by two kinematic chains including one brick performing the rotation and one performing the translation. Figure 4.4 illustrates the case of the cylindrical joint brick and one possible substitution. The thorough list of replacements can be found in the exhaustive conceptual solution catalogue in appendix B.

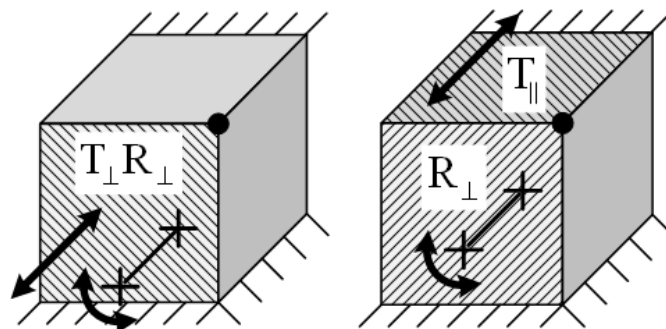


Figure 4.4: Example of the cylindrical joint brick, which can for instance be replaced by the 2-chain configuration on the right

- **The brick which actuates three translations,** which cannot be straightforwardly achieved by a purely planar structure.

### 4.2.2 Passive bricks

The passive bricks which are relevant for ultra-high precision applications are selected on the basis of the hypotheses stated in paragraph 4.1: the bricks are thus retained only if one or more flexure-based designs fulfilling the planarity or the rotational symmetry criterion exist. Comparatively to the exhaustive list, only three types of bricks are discarded: these consist in the brick performing three translations ( $t_{\parallel}t_{\perp}t_{\perp}$ ), the one presenting three rotations ( $r_{\parallel}r_{\perp}r_{\perp}$ ), as well as both bricks performing three translations and one rotation ( $t_{\parallel}t_{\perp}t_{\perp}r_{\perp}$  and  $t_{\parallel}t_{\perp}t_{\perp}r_{\parallel}$ ). Nonetheless, these mobilities may be efficiently achieved by flexure-based structures which require other machining methods: figure 4.5 shows two possible flexure-based designs performing a spherical joint, excerpted from [36]. Figures 4.6 to 4.8 summary the selected conceptual passive bricks for ultra-high precision.

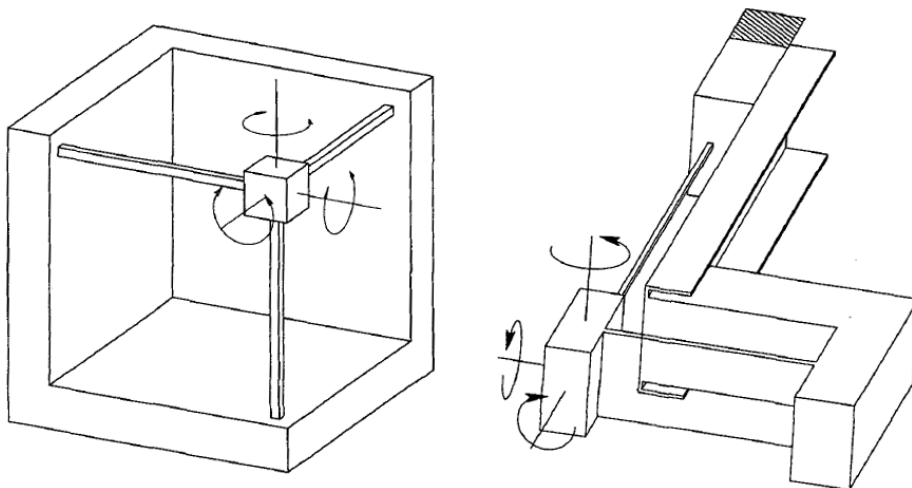


Figure 4.5: Sketch of two possible flexure-based structures performing a spherical joint [36]

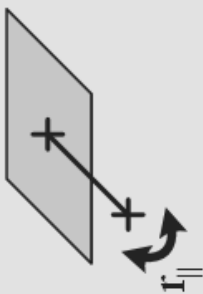
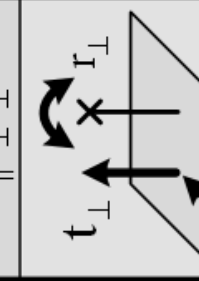
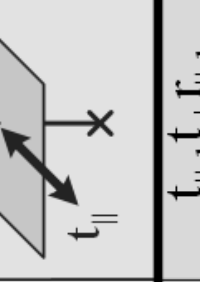
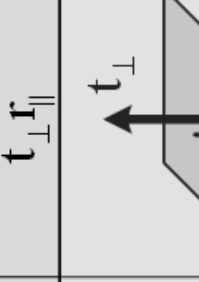
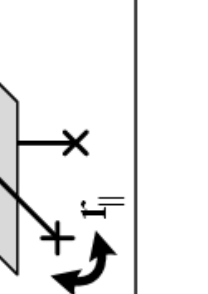
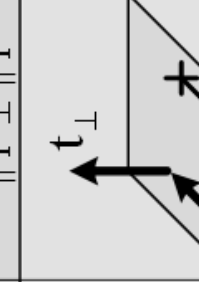
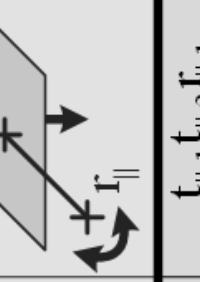
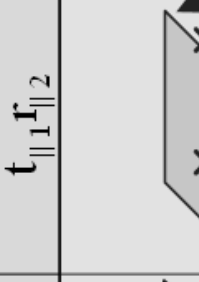
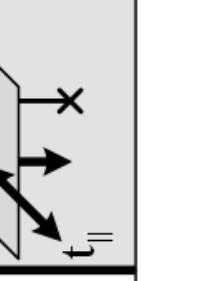
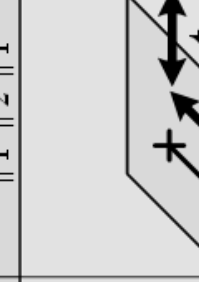
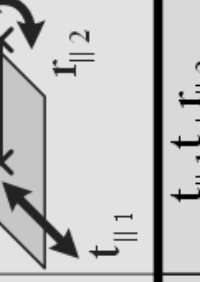
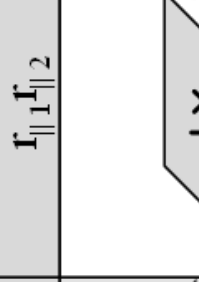
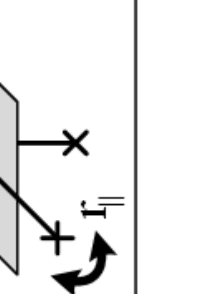
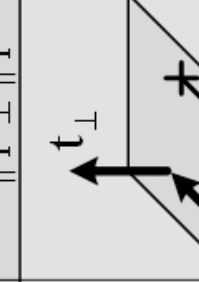
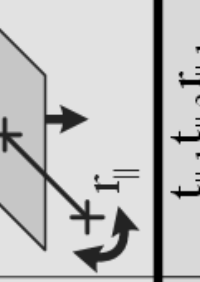
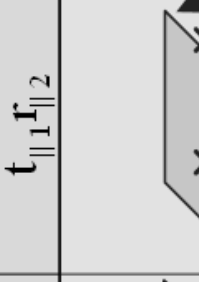
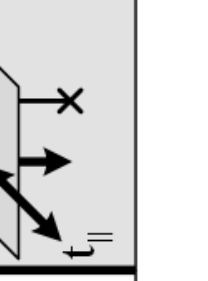
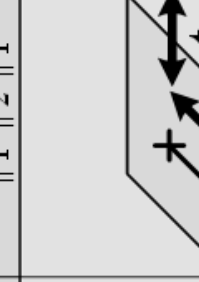
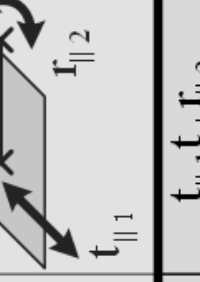
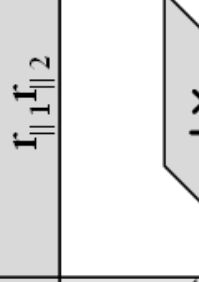
PASSIVE BRICKS FOR ULTRA-HIGH PRECISION							
$f_{\parallel}$		$f_{\perp}$		$t_{\parallel}$		$t_{\perp}$	
$f_{\parallel} f_{\perp}$		$t_{\parallel} f_{\perp}$		$t_{\parallel} f_{\parallel}$		$t_{\perp} f_{\parallel}$	
$f_{\parallel} f_{\perp} t_{\parallel}$		$t_{\parallel} f_{\perp} t_{\perp}$		$t_{\parallel} f_{\parallel} t_{\perp}$		$t_{\perp} f_{\parallel} t_{\perp}$	
$f_{\parallel} f_{\perp} t_{\perp}$		$t_{\parallel} f_{\perp} f_{\parallel}$		$t_{\parallel} f_{\parallel} f_{\perp}$		$t_{\perp} f_{\perp} f_{\parallel}$	
$f_{\parallel} f_{\perp} t_{\parallel} t_{\perp}$		$t_{\parallel} f_{\perp} f_{\parallel} t_{\perp}$		$t_{\parallel} f_{\parallel} f_{\perp} t_{\perp}$		$t_{\perp} f_{\perp} f_{\parallel} t_{\perp}$	

Figure 4.6: Passive building bricks for ultra-high precision applications (1/3)



<b>PASSIVE BRICKS FOR ULTRA-HIGH PRECISION, continued</b>							
$t_{\perp} r_{\parallel 1} r_{\parallel 2}$		$t_{\parallel 1} r_{\parallel 2} r_{\perp}$		$t_{\parallel 1} r_{\parallel 1} r_{\perp}$		$t_{\parallel 1} r_{\parallel 1} r_{\parallel 2}$	
$t_{\parallel 1} t_{\perp} r_{\parallel 2} r_{\perp}$		$t_{\parallel 1} t_{\parallel 2} r_{\parallel 1} r_{\perp}$		$t_{\parallel 1} t_{\perp} r_{\parallel 1} r_{\perp}$		$t_{\parallel 1} t_{\parallel 2} r_{\parallel 1} r_{\parallel 2}$	
$t_{\perp} r_{\parallel 1} r_{\parallel 2} r_{\perp}$		$t_{\parallel 1} r_{\parallel 1} r_{\parallel 2} r_{\perp}$		$t_{\parallel 1} t_{\perp} r_{\parallel 1} r_{\parallel 2} r_{\perp}$		$t_{\parallel 1} t_{\parallel 2} t_{\perp} r_{\parallel 1} r_{\perp}$	

Figure 4.7: Passive building bricks for ultra-high precision applications (2/3)

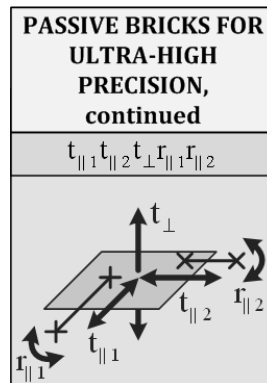


Figure 4.8: *Passive building bricks for ultra-high precision applications (3/3)*

### 4.3 Reduced conceptual solution catalogue

Finally, the reduced conceptual solution catalogue is obtained by retaining only the kinematic solutions which are exclusively composed of the bricks illustrated in figures 4.2 and 4.6 to 4.8.

*This catalogue includes 1429 possibilities, based on 193 active bricks arrangements, which thus consists in a reduction of more than 55% of the amount of solutions. The graphical representation of the solutions can be found in appendix C.*

Moreover, the hypotheses for ultra-high precision have considerably contributed to decrease the complexity of the robot synthesis: they have indeed transformed this 3-D design problem into several 2-D ones. Whereas the flexure-based structures resulting from the 3-D synthesis are complex and scarcely flexible, the 2-D solutions are simpler, well-mastered and easier to machine monolithically. Figure 4.9 illustrates this observation, whereas figure 4.10 summaries the hypotheses which have led to the establishment of the reduced conceptual solution catalogue.

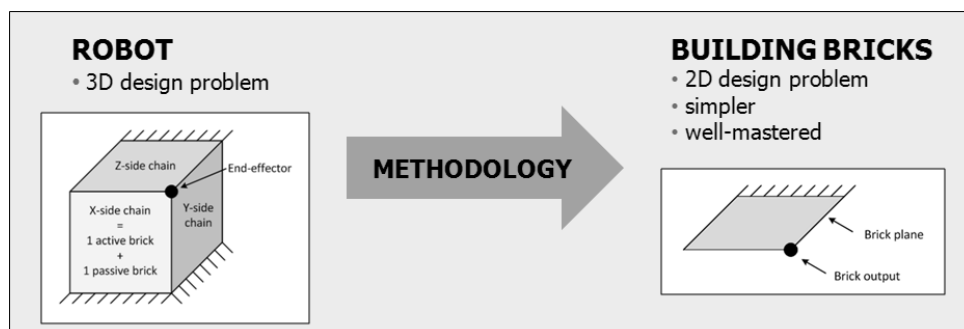


Figure 4.9: *Graphical representation of the methodology*

Since the list of all conceptual building bricks suited for ultra-high precision has been established, the next step consists in examining their mechanical design. Consequently, the

next chapter extensively studies this aspect and proposes one or more efficient flexure-based structures fulfilling the aforescribed hypotheses for each building brick.

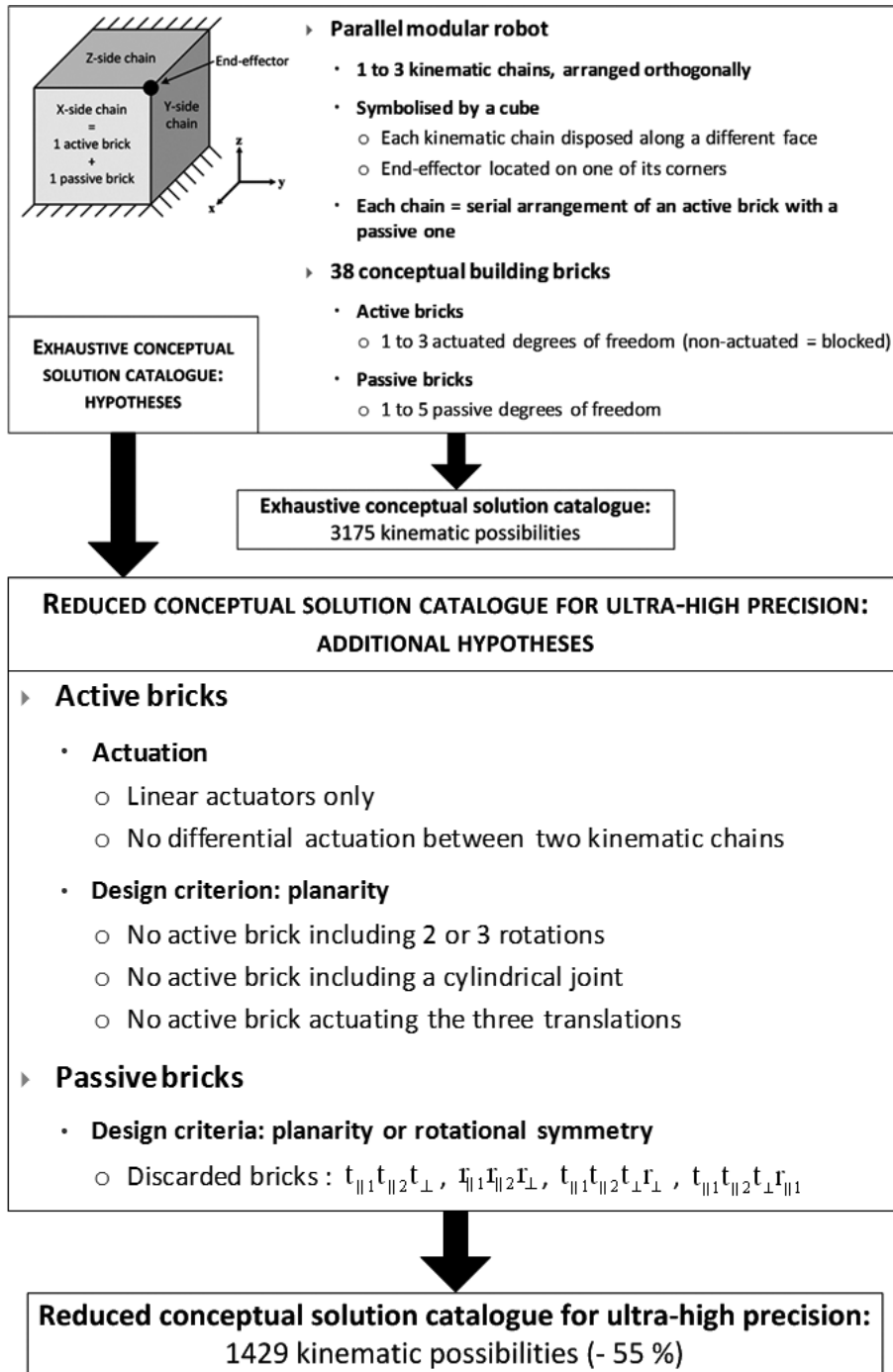


Figure 4.10: Summary of the successive hypotheses which have led to the establishment of the reduced conceptual solution catalogue for ultra-high precision



# Chapter 5

## Mechanical design of the building bricks

The flexure-based design of the building bricks dedicated to ultra-high precision is detailed in this chapter. An efficient mechanical solution is proposed for each active brick, which includes a standardised actuation sub-brick, thus adding a new level to the modularity to the concept. As for the passive bricks, one or several possible designs are presented, comprising original structures, as well as common and innovative uses of well-known mechanisms. Moreover, it is crucial to highlight the aim of this chapter, which is to group interesting brick designs as a tool for the robot designer rather than to propose a thorough catalogue of off-the-shelf mechanical solutions.

### 5.1 Challenges in flexure-based brick design

As the trend to miniaturise industrial products goes hand in hand with the miniaturisation of the production lines, the main challenge of industrial high precision robots design consists in minimising their volume while maximising their workspace. Consequently, a key objective of this thesis is the ***maximisation of the ratio between the translational strokes and the characteristic dimension of the robot***. The latter is defined as the largest dimension of the prism enclosing its mechanical parts (see equation 5.1).

$$R_s = \frac{\text{total linear stroke [mm]}}{\text{characteristic dimension [mm]}} \quad (5.1)$$

Currently, the ultra-high precision robots which present the highest  $R_s$  ratio are the Delta<sup>3</sup> II ( $R_s = 0.02$ ,  $\pm 2$  mm stroke for a characteristic dimension of 200 mm, total volume: 3 dm<sup>3</sup>, see section 2.3 and figure 2.17) and the Sigma 6 ( $R_s = 0.031$ ,  $\pm 4$  mm stroke for a characteristic dimension of 255 mm, total volume: 6 dm<sup>3</sup>). Nonetheless, the achievement of the  $R_s$  maximisation is highly challenging as the ratio between the strokes of flexure-based mechanisms and their volume are limited by the admissible stress in the material.

Moreover, numerous high-precision robots and mechanisms performing both rotational and translational motions ***suffer from the same limitation: the maximum angle and the maximum translation cannot be achieved at the same time***. This situation is first caused by

the strokes of the actuators, which are not sufficient to allow the combined motions. Then, the second cause of this phenomenon is illustrated in figure 5.1: if the centre of rotation does not coincide with the robot output, high translational compensatory motions are necessary to keep its position constant during the rotation. For instance, a distance of 10 mm between the system output and the rotation centre necessitates a compensatory displacement of 1.75 mm when a rotation of  $10^\circ$  is performed. A significant part of the robot translational range is thus necessary to compensate for this motion, which limits the functional translation which can be simultaneously achieved. The Sigma 6 robot epitomises this observation: its maximal angle of  $4^\circ$  can indeed be obtained only with a translation inferior to 1 mm.

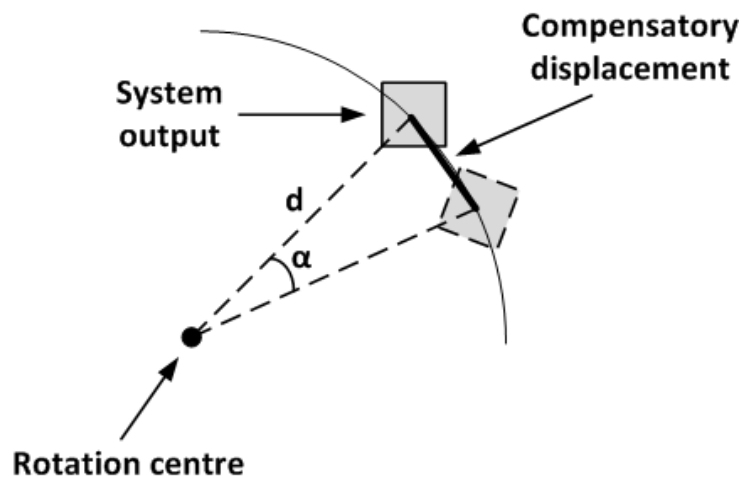


Figure 5.1: Sketch of the parasitic displacement generated by the rotation around a centre which does not coincide with the system output

*A smart design making use of a Remote Centre of Motion (RCM) can overcome this problem* by virtually locating the rotation centre at the system output, without adding any mechanical part at this point. All active bricks which perform rotational motions include this astute solution: detailed descriptions of its implementation with flexure hinges are found in sections 5.2.2.1, 5.2.2.4 and 5.2.2.5.

## 5.2 Mechanical design of the active bricks for ultra-high precision

This section introduces the standardised actuation sub-brick and possible flexure-based designs of each active brick for ultra-high precision.

### 5.2.1 Actuation sub-brick

As stated in chapter 4, the actuation of the building bricks for ultra-high precision is performed by linear actuators only. Moreover, the guiding of the actuator moving part has to be

performed without friction to fulfill the required submicrometric precision: a flexure-based structure is thus necessary to substitute for classical rolling or plain bearings. Consequently, each active brick comprises the same actuation system, which includes three components: a linear actuator, a guiding system for the actuator moving part and a position sensor. This subset forms the *actuation sub-brick*, which adds a new level of modularity to the methodology. Each active brick indeed includes an actuation sub-brick for each of its degrees of freedom; the flexure-based mechanisms which transform the linear motions of the actuators into the desired mobility are then attached to them. The following paragraphs detail some efficient solutions for each component of the actuation sub-brick.

### 5.2.1.1 Linear flexure-based guiding mechanism

A simple and efficient flexure-based mechanism performing a translational motion consists in the *4-hinge table* [36], which is illustrated in figure 5.2. Either elliptic, prismatic or truncated circular hinges are conceivable; however, the radius of both circular and elliptic joints necessary to achieve a high stroke in comparison with the space requirement of the mechanism are enormous, thus amounting to a nearly prismatic hinge.

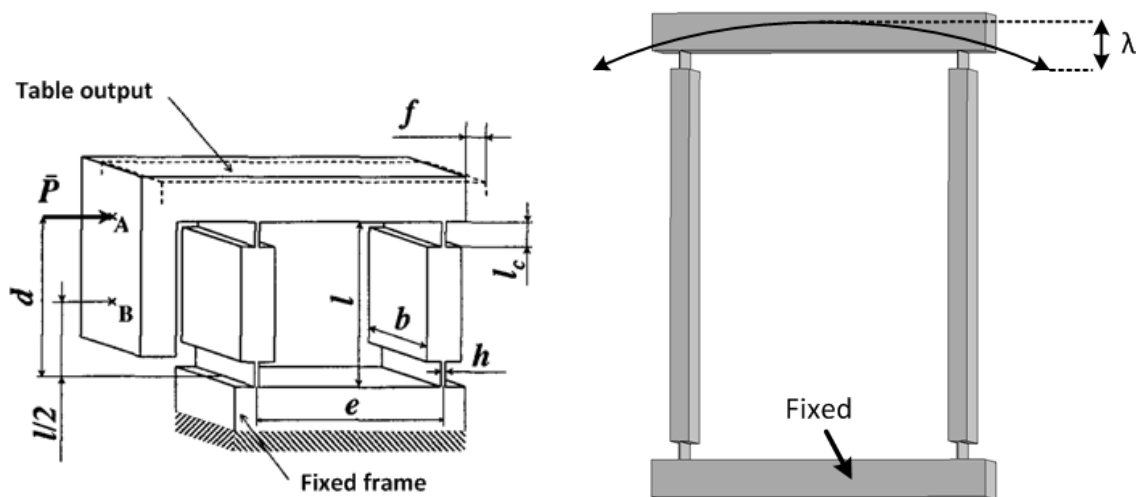


Figure 5.2: Sketch of the 4-prismatic hinge table with geometric parameters (left, [36]) and its quasi parabolic trajectory (right)

As depicted on figure 5.2, the movement performed by the 4-hinge table is not rectilinear, but consists in a translation along a quasi parabolic trajectory: the parasitic translation  $\lambda$  is maximal at both ends of the strokes. The behaviour of the 4-prismatic hinge table is described with equations 5.2 to 5.7, excerpted from [36]. Note that these provide useful estimates of the structure performances even if they are valid only when no traction or compression forces act on the mechanism; more complete models can be found in [36].

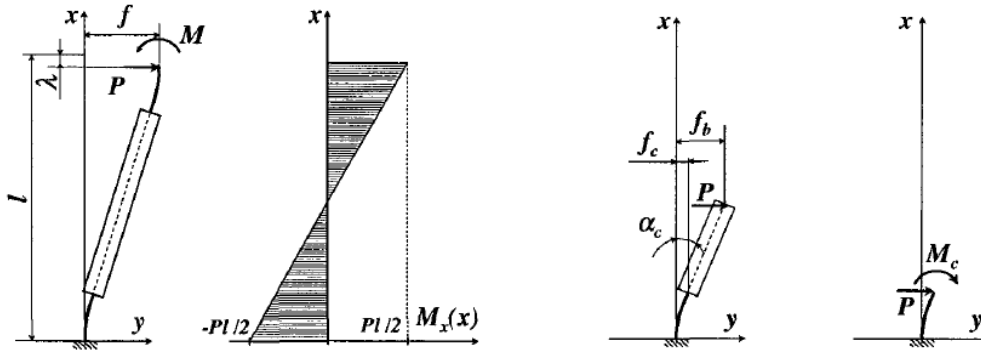


Figure 5.3: Model used to compute the translation stiffness and maximal parasitic displacement  $\lambda$  of the 4-prismatic hinge table (with no traction/compression force) [36]

The maximum stroke of the 4-hinge table is evaluated as:

$$f_{adm} = \frac{\xi \cdot (3 - 3\xi + \xi^2) \cdot l^2 \cdot \sigma_{adm}}{3 \cdot E \cdot h} \text{ [m]} \quad (5.2)$$

where  $l$  is the length of the table arms (see figures 5.2 and 5.3),  $h$  is the thickness of the prismatic hinges, and  $E$  is the Young's modulus of the material. Furthermore,  $\sigma_{adm}$  stands for the admissible stress, which is defined as the endurance limit divided by a safety factor [36]. Last,  $\xi = \frac{2 \cdot l_c}{l}$  is a parameter which describes the ratio between the hinge length ( $l_c$ ) and the arm length.

Then, the natural stiffness of the table is computed as follows:

$$K = \frac{2 \cdot b \cdot h^3 \cdot E}{\xi \cdot (3 - 3\xi + \xi^2) \cdot l^3} \left[ \frac{N}{m} \right] \quad (5.3)$$

where  $b$  is the depth of the table arms (see figure 5.2).

Finally, the maximal parasitic translation of the 4-hinge table is estimated by equation 5.4: the first term of this equation represents the effect of the rotation of the rigid segment of the arm, whereas the second stands for the shortening of the deflected flexure hinges [36].

$$\lambda \approx l \cdot (1 - \xi) \cdot (1 - \cos(\arctan(y'(l_c)))) + 2 \int_0^{l_c} (y'(x))^2 dx \text{ [m]} \quad (5.4)$$

The derivative of the hinge deflection curve at maximal deflection  $f_{adm}$  is described by the following equation, derived from the model illustrated in figure 5.3:

$$y'(l_c) = \frac{(M_c + P \cdot l_c)}{EI} \cdot l_c - \frac{P}{2EI} \cdot l_c^2 \quad (5.5)$$

where:

$$P = \frac{K \cdot f_{adm}}{2} \quad (5.6)$$



and

$$M_c = \frac{P \cdot l \cdot (1 - \xi)}{2} \quad (5.7)$$

The chief disadvantage of the integration of the 4-hinge table in the actuation sub-brick consists in its parasitic displacement  $\lambda$ : this issue can be overcome by choosing an actuation principle which accepts a parasitic translation of its moving part. This aspect will be detailed in section 5.2.1.2.

Moreover, if the robot specifications impose a rectilinear motion, a **13-hinge compound table** can be used [36]: it consists of two 4-hinge tables which are serially arranged and coupled by a slaving mechanism to suppress the internal degree of freedom. Figure 5.4 illustrates this mechanism; note that in this figure, as in most works including the 13-hinge compound table, the geometric parameters of the coupling lever do not maximise the rectilinearity of the motion; the optimal design is described in [23]. Furthermore, the integration of this solution in the actuation sub-brick is only necessary when the robot includes a sole translation, or when the parasitic motions of the robot translations cannot be actively compensated for by the control algorithm.

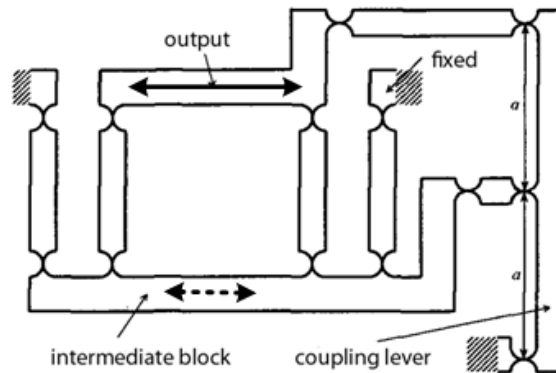


Figure 5.4: Sketch of the 13-hinge compound table [36]

### 5.2.1.2 Linear actuator

As the robots designed with this modular methodology are intended for industrial use, **electromagnetic actuators** are preferred over piezo-electric or ultrasonic actuators for their high repeatability. Likewise, the moving coil / static magnet configuration is advantageous as it minimises both the moving mass and the hysteresis created by the magnets. As for the actuator force requirements, ultra-high precision micromanipulation and microassembly tasks typically necessitate a continuous force of 10 N. Moreover, as high dynamical performances are a crucial benefit in terms of production rates, the actuator peak force value must be sufficient to set the robot in motion with the desired acceleration: it thus directly depends on the robot moving mass. Hence, no generic value can be enunciated. Following these criteria, two main types of actuators are conceivable:

- **The voice coil actuator:** frequently encountered in loudspeakers, the most widespread design on the market consists in a cylindrical arrangement of the moving coil and the static magnets. Like the classical DC (direct current) motors, its control is straightforward: the actuation force is directly proportional to the coil current. However, if the 4-hinge table is selected as guiding system of the coil, its parasitic motion can be problematic: its value is indeed generally higher than the actuator air gap between the coil and the magnets. Nonetheless, a simple solution consists in taking advantage of the symmetric behaviour of the parasitic motion: the same maximal value is achieved at both ends of the strokes, whereas the minimum is reached at the table equilibrium point. The solution thus consists in eccentrically mounting the coil at zero stroke to optimise the use of the available air gap (see figure 5.5).

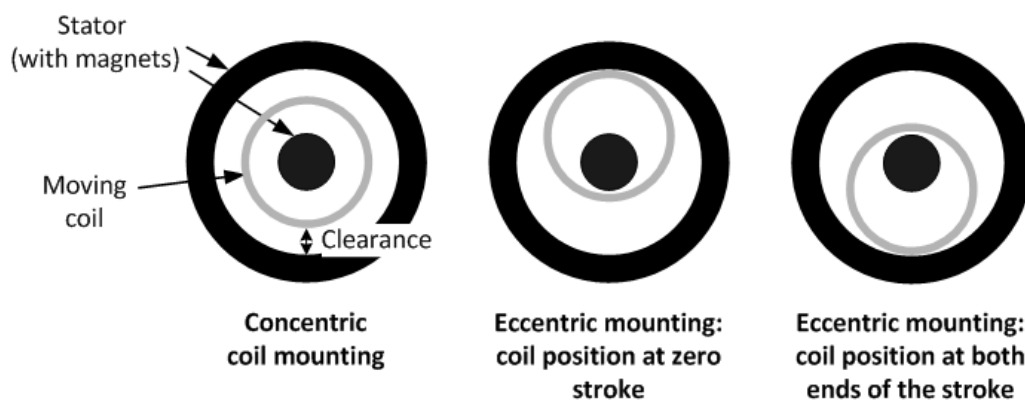


Figure 5.5: Principle of the eccentric voice coil mounting (the actuation direction is orthogonal to the section)

- **The ironless EC (electronic commutation) actuator,** which is composed of a U-shape frame with fixed magnets and a prismatic moving coil (see figure 5.6): similarly to brushless DC motors, this 2-phase or 3-phase actuator needs an integrated Hall sensor and a dedicated electronics to manage the phase commutation, which complexifies its control. Nonetheless, this solution presents two noteworthy advantages, the first being its direct compatibility with the parasitic motion of the 4-hinge table (see figure 5.6). Then, its design allows to integrate it between both arms of the 4-hinge table, leading to a more compact solution.

Finally, the selection of voice coil or ironless EC actuators highly depends on the availability of standard products on the market which fulfill the robot force and stroke requirements. As these are specific to each application, no preferred solution emerges at this point of the methodology.

### 5.2.1.3 Linear position sensor

The last component of the actuation sub-brick is the linear position sensor; at the present time, optic incremental linear encoders and Linear Variable Differential Transformers (LVDT)

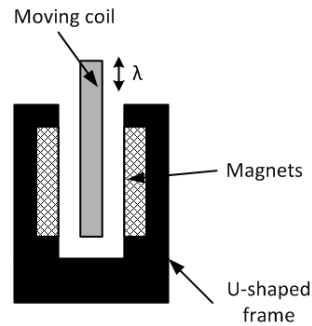


Figure 5.6: *Transverse section of the EC actuator (the actuation direction is orthogonal to the section)*

are the only standard products available on the market which allow to achieve the required submicrometric precision. Nonetheless, the LVDT solution presents the same drawback as the voice coil actuation: the parasitic motion of the 4-hinge table may indeed be problematic if the design of the sensor does not allow an eccentric mounting. Furthermore, as the measurement of the actuation sub-brick guiding system determines the resolution of the whole robot and thus limits its repeatability and accuracy, the resolution of the sensor must be carefully chosen regarding the specifications of the industrial application.

## 5.2.2 Active bricks design

The mechanical design of the active bricks including the aforescribed actuation sub-brick is now detailed. As stated in chapter 4, the bricks must be designed as planar flexure-based mechanisms. Moreover, the physical plane including the flexure-based structure is not necessarily coincident with the plane of the brick on the conceptual cube (see figure 5.7). Consequently, bricks which share the same mobility can be identically designed, regardless the orientation of the motions relatively to the cube face plane. In the following sections, the bricks are thus grouped according to their mobility: one efficient flexure-based design is proposed for each of them. Note that in this section, only sketches of the design principles are presented; the mechanical solutions of the  $T_{\parallel}$  and the  $T_{\parallel}R_{\perp}$  active bricks will be thoroughly examined in chapter 6.

### 5.2.2.1 $R_{\parallel}$ and $R_{\perp}$ bricks

The mechanical flexure-based design of these bricks, which perform a single rotation, includes a Remote Centre of Motion (RCM) to ensure that the position of the robot end-effector is kept constant during the rotation without performing compensatory translations (see section 5.1). Figure 5.8 illustrates the design principle of these bricks, where two functional subsets can be highlighted:

- ***The position of the rotation centre is defined by the virtual intersection of both hinges which link the brick output to the fixed frame.*** The optimal angle between these two hinges is  $90^{\circ}$ , which maximises the transverse stiffness of the mechanism.

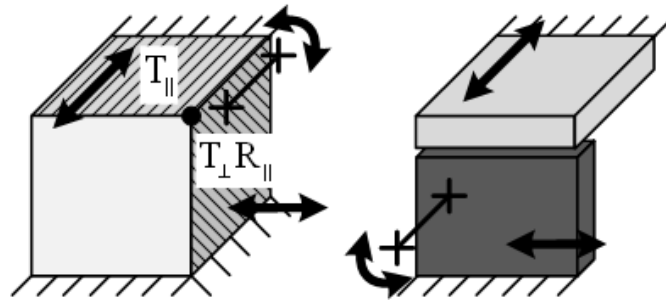


Figure 5.7: The conceptual kinematic arrangement (left) is built with two planar flexure-based mechanisms (right): for the brick performing the translation, the cube face plane is coincident with the plane of the mechanism, whereas for the second brick, the plane of the flexure-based structure is orthogonal to the face of the concept cube.

- **The linear motion of the actuation sub-brick performs the rotation:** through the vertical hinge, the force produced by the actuator is transformed into a moment, which causes the output to rotate. Moreover, the classical lever law  $M = F \cdot d$  can be applied, where  $M$  is the moment,  $F$  is the actuation force and  $d$  is the orthogonal distance between the force and the rotation centre (see figure 5.8).

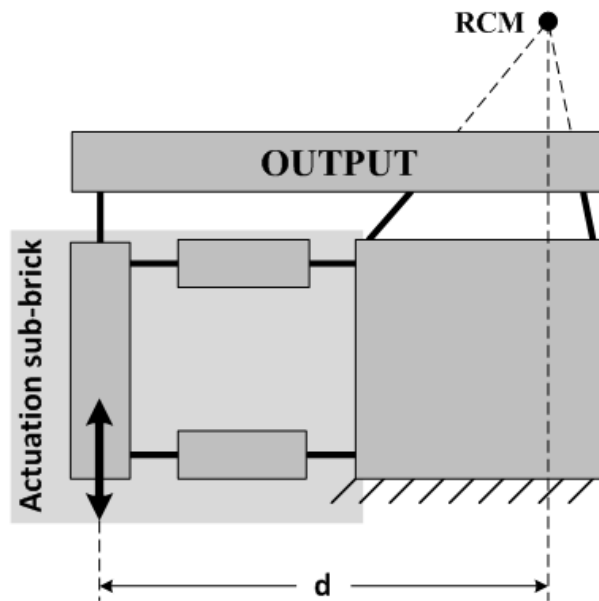


Figure 5.8: Sketch of the  $R_{\parallel}$  and  $R_{\perp}$  bricks design principle, including the actuation sub-brick and a Remote Centre of Motion. The proposed solution actuates a rotation which is orthogonal to the mechanism plane, and must be reoriented relatively to the concept cube to perform a  $R_{\parallel}$  brick.

This flexure-based mechanism notably allows to freely choose the position of the rotation axis: the latter must be located on the end-effector of the robot, which is in most cases not coincident with the brick output, as in figure 5.8. Its position must thus be carefully chosen regarding the robot kinematics and specifications.

Moreover, the choice of the distance between the actuator and the rotation centre ( $d$  on figure 5.8) influences the performances of the structure:

- The angular resolution is improved as this distance is increased.
- The actuation force which is necessary to rotate the output of a given angle decreases as the distance increases.
- The actuator linear stroke which is needed to perform this same angle conversely increases as the distance increases.

Consequently, the distance between the actuator and the Remote Centre of Motion should be optimised with respect to the robot specifications, as well as to the actuator performances.

Lastly, the actuation sub-brick consisting in a simple 4-hinge table is highly efficient within these bricks, as its role is only to apply a force to the flexure-based structure; the parasitic translation described in section 5.2.1.1 does not influence the behaviour of the brick output.

### 5.2.2.2 $T_{\parallel}$ and $T_{\perp}$ bricks

As for the bricks which only perform a translation, their mechanical design simply consists in the actuation sub-brick described in section 5.2.1 (see figure 5.9).

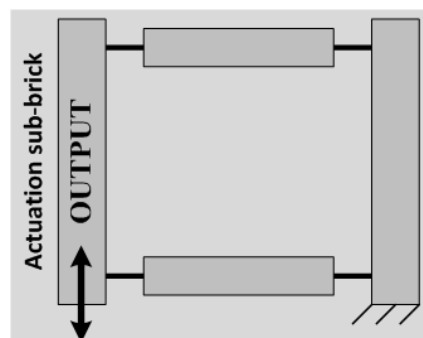


Figure 5.9: Mechanical design of the  $T_{\parallel}$  and  $T_{\perp}$  bricks; the proposed solution actuates a translation which is parallel to the mechanism plane, and must be reoriented relatively to the concept cube to perform a  $T_{\perp}$  brick.

### 5.2.2.3 $T_{\parallel 1}T_{\parallel 2}$ and $T_{\parallel}T_{\perp}$ bricks

These active bricks, which perform two translations, admit two efficient designs, illustrated in figures 5.10 and 5.11. The first solution, excerpted from [43], includes two actuators which are oriented along the same direction. An inclined lever transforms these collinear motions into two orthogonal translations (see figure 5.10). This configuration presents the significant advantages of allowing a compact integration, as well as simplified electrical connections. However, the output working range is limited by the admissible stroke of the sole hinge achieving the lever function.

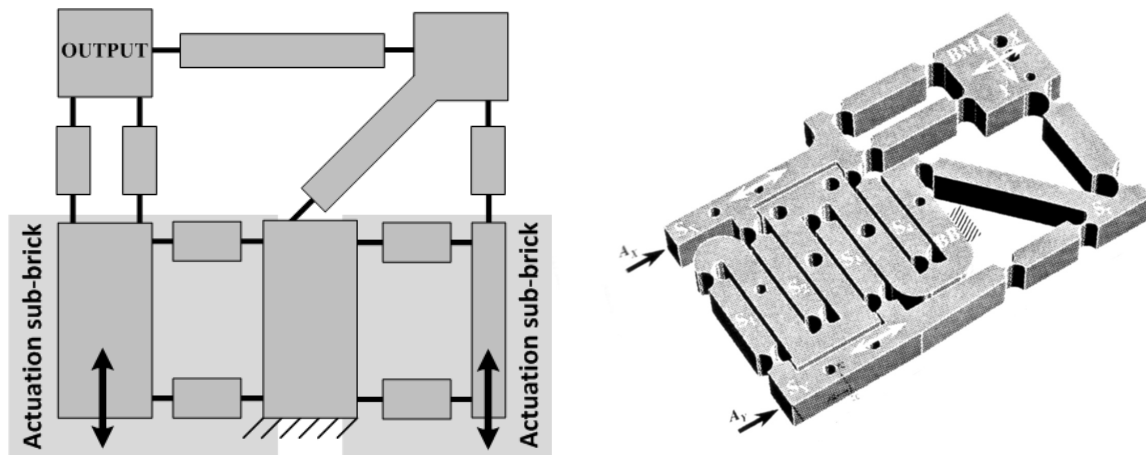


Figure 5.10: Sketch of the  $T_{||1} T_{||2}$  and  $T_{||} T_{\perp}$  bricks first design principle, including two actuators oriented in the same direction (left) and illustration of the flexure-based mechanism developed in [43] (right). The proposed solution actuates two translations which are parallel to the mechanism plane, and must be reoriented relatively to the concept cube to perform a  $T_{||} T_{\perp}$  brick.

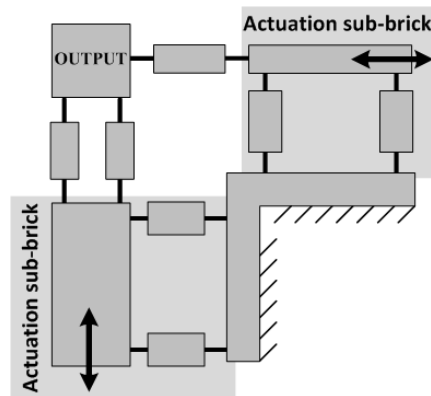


Figure 5.11: Sketch of the  $T_{||1} T_{||2}$  and  $T_{||} T_{\perp}$  bricks second design principle

Consequently, if the robot specifications impose high translational strokes, the second solution, which includes two actuators oriented along orthogonal directions, consists in an advantageous alternative (see figure 5.11). Furthermore, both designs allow for an active compensation of the parasitic translations of the 4-hinge tables. Note that the solution proposed by [50], which also makes use of two collinear actuators and a lever system to transform the direction of the motion (see figure 2.15), could also be adapted to alternatively perform this active brick.

#### 5.2.2.4 $T_{||} R_{\perp}$ , $T_{\perp} R_{||}$ and $T_{||1} R_{||2}$ bricks

Performing a translation and a rotation which are oriented along two different directions, these three active bricks include a Remote Centre of Motion and a differential actuation. Figure 5.12 illustrates their design principle, as well as a mock-up with assembled leaf springs

proving the soundness of this solution. In this mechanism, the translation is achieved by the synchronous motion of both actuators. As for the rotation, the position of the actuator linked with the hinges defining the rotation centre is kept constant, whereas the movement of the second linear actuator performs the rotation. As described in paragraph 5.2.2.1, the distance between this last actuator and the rotation centre must be carefully chosen.

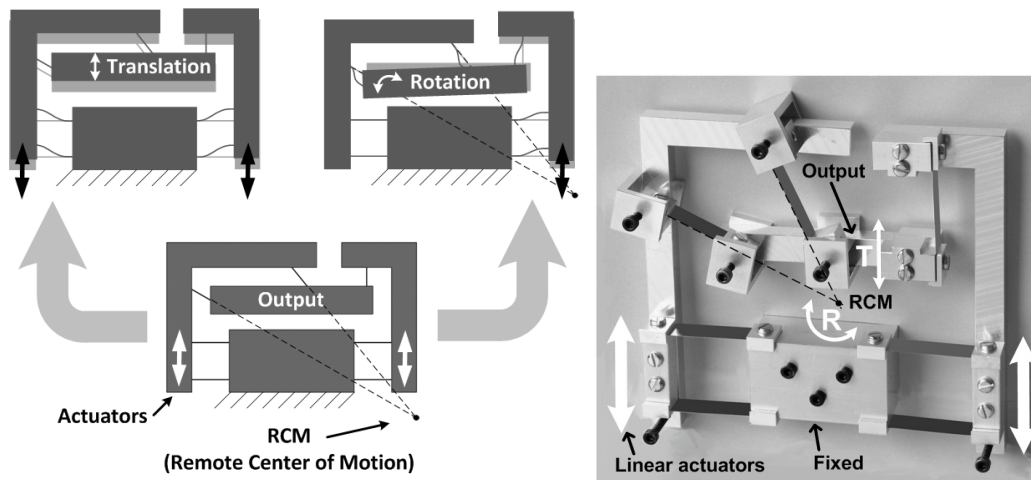


Figure 5.12: Sketch of the  $T_{\parallel}R_{\perp}$ ,  $T_{\perp}R_{\parallel}$  and  $T_{\parallel}R_{\parallel}$  bricks design principle, including a RCM (left), and mock-up of the flexure-based structure (right)

### 5.2.2.5 $T_{\parallel}T_{\parallel}R_{\perp}$ and $T_{\parallel}T_{\perp}R_{\parallel}$ bricks

Finally, these two bricks performing a planar joint mobility include the design principles of all aforesaid active bricks: to simplify the understanding of the mechanism, figure 5.13, top, first shows a solution without the Remote Centre of Motion. The first translation (along the vertical axis on figure 5.13, top) is achieved by the synchronous motion of the two actuators on the right. Then, the movement of the far left actuator performs the second translation. Last, solely displacing the actuator on the far right allows for the rotation along an axis which is orthogonal to the structure. Including a Remote Centre of Motion is now straightforward, as it only consists in inclining two arms of the structure (see figure 5.13, bottom).



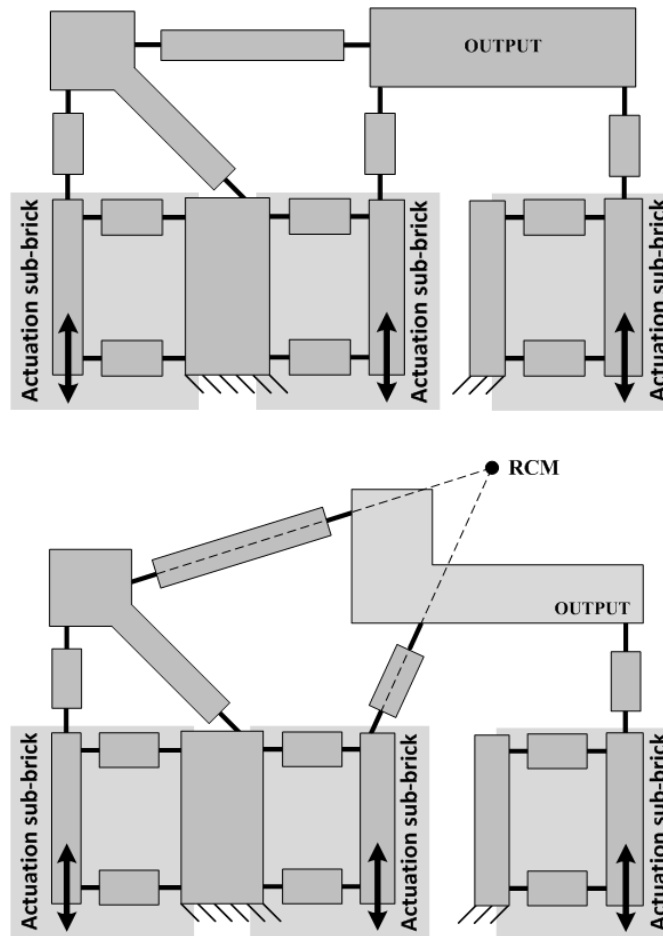


Figure 5.13: Sketch of the  $T_{||1} T_{||2} R_{\perp}$  and  $T_{||1} T_{\perp} R_{||2}$  bricks design principle: without RCM (top) and with RCM (bottom). The proposed solution actuates two translations which are parallel to the mechanism plane, and a rotation which is orthogonal to this plane. Consequently, it must be reoriented relatively to the concept cube to perform a  $T_{||1} T_{\perp} R_{||2}$  brick.

### 5.3 Mechanical design of the passive bricks for ultra-high precision

This section details the design principles of the methodology passive bricks for ultra-high precision. As stated in chapter 4, these must be planar flexure-based structures, or flexure-based mechanisms presenting a rotational symmetry to fulfill the synthesis and machining criteria. Consequently, one or several possible designs are presented, comprising original structures, as well as common and innovative uses of well-known mechanisms. Moreover, it is crucial to highlight that the aim of this section is to group interesting brick designs as a tool for the robot designer rather than to propose a thorough catalogue of off-the shelf mechanical solutions. Note that only sketches of the solution principles are presented; the  $t_{||1} t_{\perp} r_{||1} r_{||2}$  passive brick design will be comprehensively studied in chapter 6.



### 5.3.1 $r_{\parallel}$ and $r_{\perp}$ bricks

These passive bricks, which perform a revolute joint, admit five flexure-based designs, which are the following:

- **The crossed-blades pivot [36]**, which is illustrated in figure 5.14, can include either unseparated or separated blades: whereas the unseparated cylindrical joint is easier to machine, the separated solution allows to achieve a higher rotation angle with a lower joint stiffness. Moreover, this option can also be performed with necked-down hinges rather than with leaf springs (see figure 5.14, right): this structure, although not straightforward to manufacture, is more adapted to Wire Electro-Discharge Machining. More details about the stroke, stiffness and parasitic shift of the rotation centre of these cylindrical joints can be found in [36].

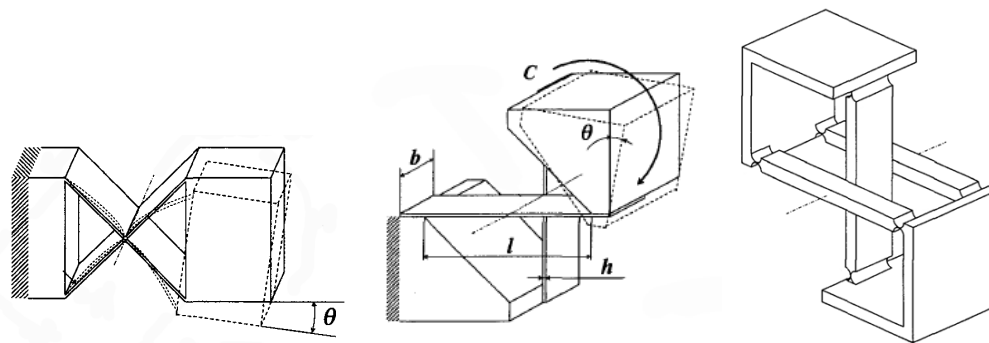


Figure 5.14: Sketches of the unseparated cross spring pivot (left) and of the separated cross pivot, with leaf springs (middle) and with flexure hinges (right) [36]

- **Planar high-stroke revolute joints**, which notably include the Butterfly pivot [37] and the redundant high-stroke pivot [36]: these consist in several serially arranged revolute joints (four in the Butterfly pivot and two in the redundant high-stroke pivot), which are linked by a slaving mechanism whose role is to suppress one of the internal degrees of freedom. The advantages of these designs notably include the high achievable strokes ( $\pm 15^\circ$ ), as well as the significant decrease in the parasitic shift of the rotation centre compared to other flexure-based revolute joints. Figure 5.15 illustrates both designs.
- **Torsion pivots**, which can admit several designs: the first one is based on a squirrel cage structure and is composed of four leaf springs arranged in a quaternary symmetry (see figure 5.16, left). Nonetheless, the admissible angle of this design is highly limited by the internal stresses in the leaf springs because of the intrinsic overconstraints. [32] proposes a solution to reduce these stresses, which is illustrated in figure 5.16, right: it consists in arranging only four leaf springs in a quaternary symmetry and to modify the clamping shape from a straight line to a parabola. This design indeed allows to optimise the stress concentration in the blades, but lacks in flexibility: only one parabola

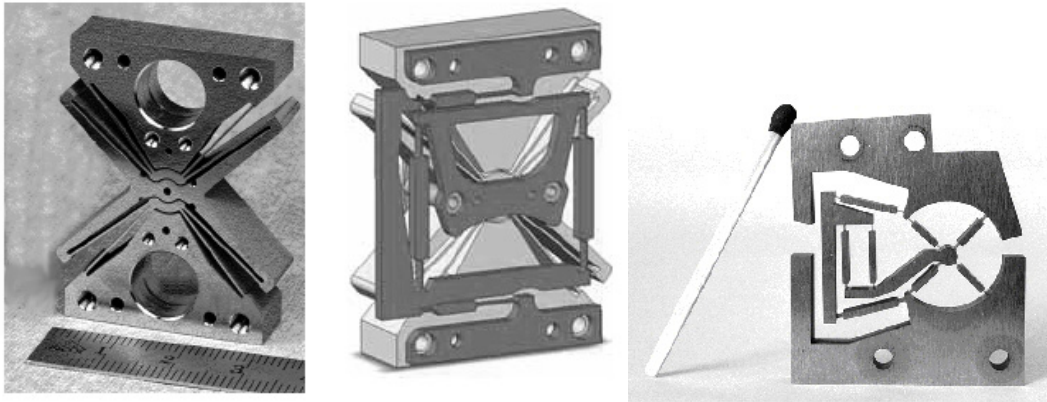


Figure 5.15: High-stroke Butterfly pivot without (left) and with slaving mechanism (middle) [37] and redundant high-stroke pivot (right, [36])

exists for each set of parameters  $a$  and  $r$  (length of the leaf spring and external radius of the pivot). Moreover, a significant drawback of the torsion pivots consists in the parasitic shift of the rotation centre, which is caused by the shortening of the leaf springs during their combined torsion and bending.

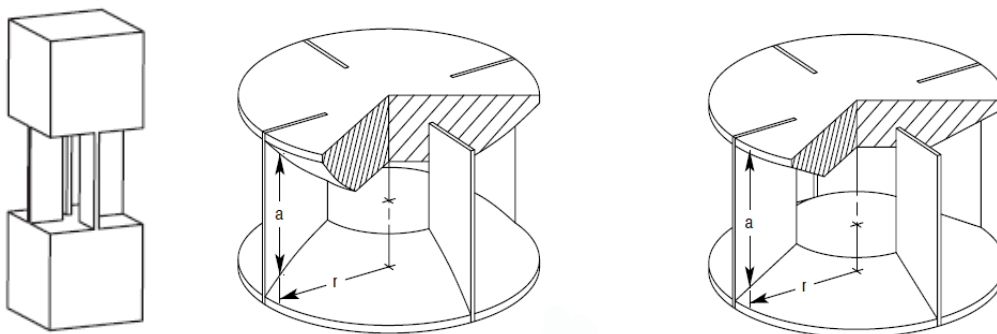


Figure 5.16: Sketch of a squirrel cage torsion pivot (left, [34]) and of optimised variants to minimise the stresses in the leaf springs (right, [32])

- Furthermore, **a design combining the concepts of the torsion pivots and of the 13-hinge compound table (see figure 5.4) has been developed** in the frame of this thesis: its principle consists in serially arranging two torsion pivots linked with a slaving mechanism which suppresses the internal degree of freedom. The crucial advantages of this design are first the increase of the stroke, which is equal to twice the rotation angle of a single torsion pivot. Then, the stress concentration in the leaf springs has been optimised by modifying the shape of the spring itself. Last, the compound design allows to suppress the parasitic shift of the rotation centre. Figure 5.17 shows the cylindrical joint principle, the optimal shape of the leaf springs, as well as a scaled W-EDM machined prototype of a single pivot stage. More details on this joint design can be found in [80].

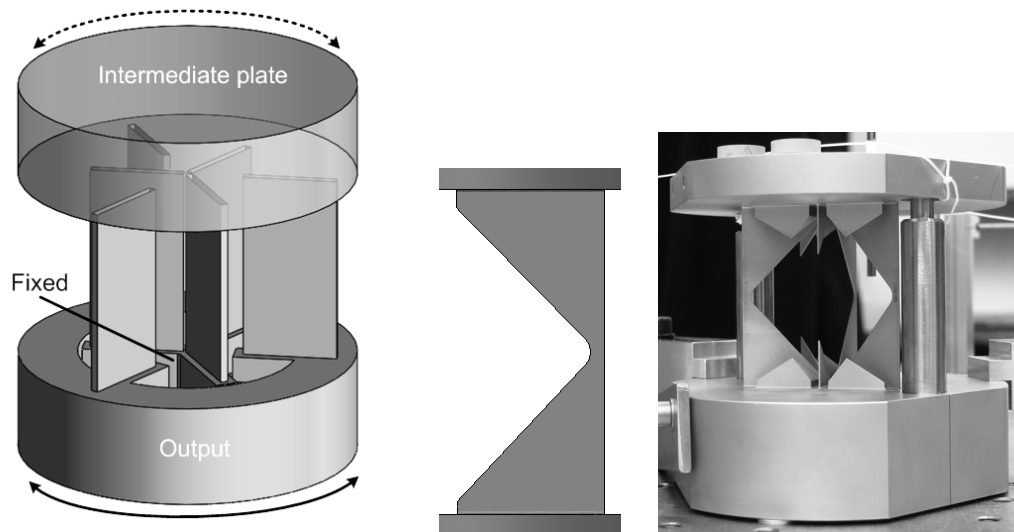


Figure 5.17: Sketch of the compound torsion pivot principle without its slaving mechanism (left), optimised leaf spring shape (middle) and scaled W-EDM machined prototype of a single pivot stage (right)

- Lastly, the *same flexure-based design as the active brick* performing a cylindrical joint can be used (see figure 5.8).

### 5.3.2 $t_{\parallel}$ and $t_{\perp}$ bricks

A simple, easily machined and efficient flexure-based design performing a single translation consists in the structure which has been proposed in paragraph 5.2.2.2 for the corresponding active bricks.

### 5.3.3 $t_{\parallel 1} t_{\parallel 2}$ and $t_{\parallel} t_{\perp}$ bricks

These bricks, which perform two translations, accept an efficient design which simply consists in two serially arranged 4-hinge tables. Figure 5.18 shows a possible compact arrangement of this flexure-based structure.

### 5.3.4 $t_{\parallel 1} r_{\parallel 1}$ and $t_{\perp} r_{\perp}$ bricks

The cylindrical joint is a challenging mobility to design with flexure hinges; nonetheless, the principle which consists in a 4-hinge table serially arranged with a torsion pivot fulfills the design criteria (see figure 5.19). The machining of this structure by W-EDM, although possible, is excessively complex; these passive bricks should then only be scarcely featured in the synthesised ultra-high precision robots.

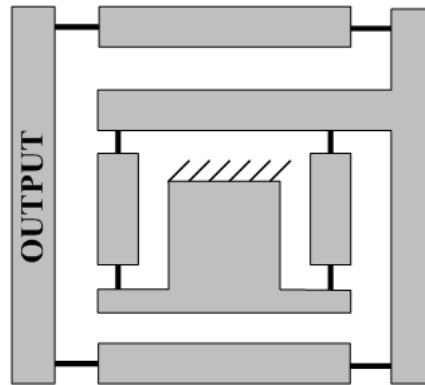


Figure 5.18: Sketch of a  $t_{||1}t_{||2}$  and  $t_{||}t_{\perp}$  bricks design principle including two 4-hinge tables which are serially arranged

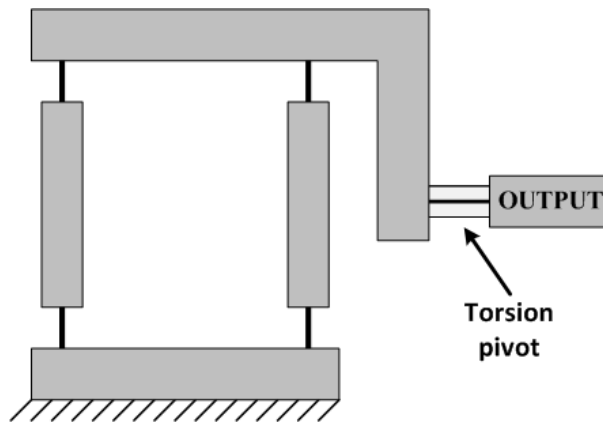


Figure 5.19: Sketch of the  $t_{||1}r_{||1}$  and  $t_{\perp}r_{\perp}$  bricks design principle

### 5.3.5 $t_{||}r_{\perp}$ , $t_{\perp}r_{||}$ and $t_{||1}r_{||2}$ bricks

A simple solution to design the  $t_{||}r_{\perp}$ ,  $t_{\perp}r_{||}$  and  $t_{||1}r_{||2}$  bricks consists in the flexure-based structure illustrated in figure 5.20: although the machining of the two separated crossed-blades pivots is not straightforward, it can be performed by W-EDM, leading to an elegant, high-stroke and efficient design.

### 5.3.6 $r_{||1}r_{||2}$ and $r_{||}r_{\perp}$ bricks

These bricks, which perform a universal joint, admit the design principle which is illustrated in figure 5.21. Note that the strokes of this structure are limited by the admissible bending and torsion angles of the leaf springs, which leads to rotation angles which hardly reach  $10^{\circ}$ .

### 5.3.7 $t_{||}t_{\perp}r_{\perp}$ , $t_{||1}t_{\perp}r_{||1}$ and $t_{||1}t_{||2}r_{||1}$ bricks

The design of the  $t_{||}t_{\perp}r_{\perp}$ ,  $t_{||1}t_{\perp}r_{||1}$  and  $t_{||1}t_{||2}r_{||1}$  bricks derives from the structures performing two translations, which are composed of two 4-hinge tables (see section 5.3.3): a torsion rev-



Figure 5.20: Sketch of a  $t_{\parallel}r_{\perp}$ ,  $t_{\perp}r_{\parallel}$  and  $t_{\parallel 1}r_{\parallel 2}$  bricks design solution, featuring two separated crossed-blades pivots

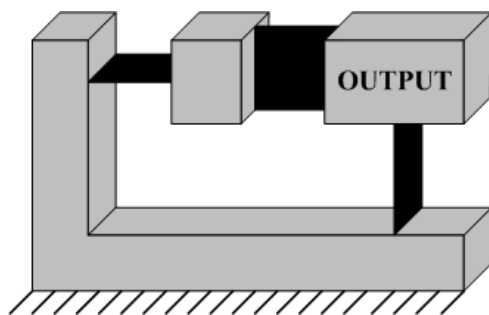


Figure 5.21: Sketch of the  $r_{\parallel 1}r_{\parallel 2}$  and  $r_{\parallel}r_{\perp}$  bricks design principle

olute joint is simply serially added to the mechanism (see figure 5.22). Note that the relative order of the three joints which compose this solution can be modified. As the machining of these bricks are not straightforward, their integration in ultra-high precision robots should be minimised.

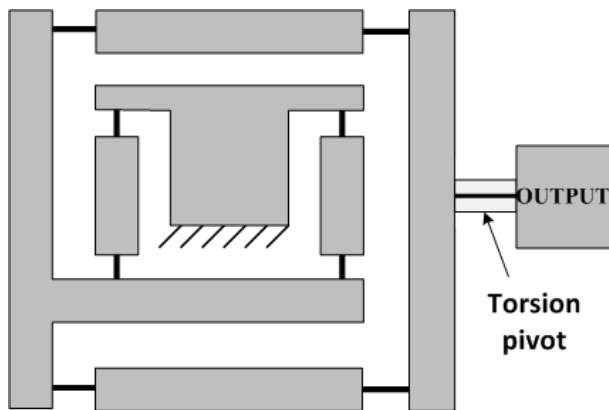


Figure 5.22: Sketch of the  $t_{\parallel}t_{\perp}r_{\perp}$ ,  $t_{\parallel 1}t_{\perp}r_{\parallel 1}$  and  $t_{\parallel 1}t_{\parallel 2}r_{\parallel 1}$  bricks design principle

### 5.3.8 $t_{\parallel 1} t_{\perp} r_{\parallel 2}$ and $t_{\parallel 1} t_{\parallel 2} r_{\perp}$ bricks

These bricks can efficiently be designed with a similar flexure-based structure as developed for the active brick performing two translations (see figure 5.11): the second arm which links the output to the 4-hinge table is simply removed, allowing the rotation of the output along an axis which is orthogonal to the brick plane (see figure 5.23).

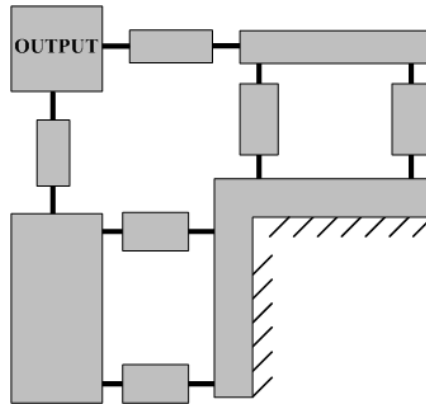


Figure 5.23: Sketch of the  $t_{\parallel 1} t_{\perp} r_{\parallel 2}$  and  $t_{\parallel 1} t_{\parallel 2} r_{\perp}$  bricks design principle

### 5.3.9 $t_{\perp} r_{\parallel 1} r_{\parallel 2}$ and $t_{\parallel 1} r_{\parallel 2} r_{\perp}$ bricks

A well-known flexure-based mechanism can efficiently perform the  $t_{\perp} r_{\parallel 1} r_{\parallel 2}$  and  $t_{\parallel 1} r_{\parallel 2} r_{\perp}$  bricks: it simply consists in a leaf spring, which can be designed with or without reinforcements, depending on the stroke and stiffness specifications (see figure 5.24).

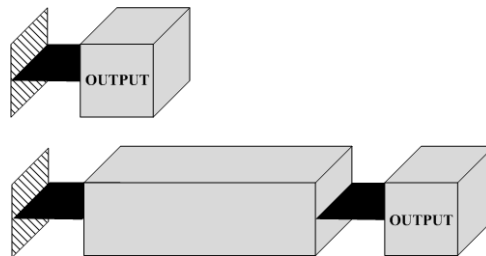


Figure 5.24: Sketch of the  $t_{\perp} r_{\parallel 1} r_{\parallel 2}$  and  $t_{\parallel 1} r_{\parallel 2} r_{\perp}$  bricks design principle, which simply consists in a leaf spring

### 5.3.10 $t_{\perp} r_{\parallel} r_{\perp}$ , $t_{\parallel 1} r_{\parallel 1} r_{\perp}$ and $t_{\parallel 1} r_{\parallel 1} r_{\parallel 2}$ bricks

The  $t_{\perp} r_{\parallel} r_{\perp}$ ,  $t_{\parallel 1} r_{\parallel 1} r_{\perp}$  and  $t_{\parallel 1} r_{\parallel 1} r_{\parallel 2}$  bricks can be designed as illustrated in figure 5.25; note that the torsion axis of the horizontal arm should be coincident with the bending axis of the vertical arm to reduce parasitic displacements during the rotation around the dashed line: figure 5.25 exemplifies the ideal arrangement of this mechanism.

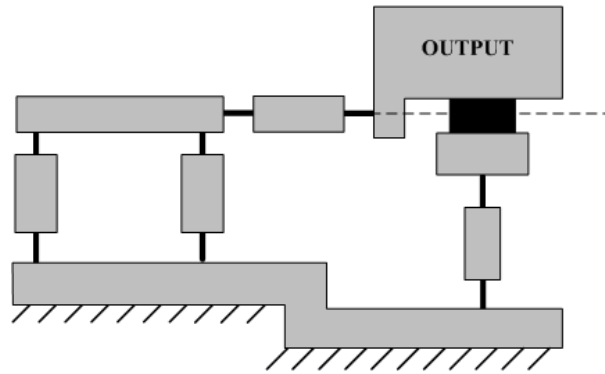


Figure 5.25: Sketch of the  $t_{\perp}r_{\parallel}r_{\perp}$ ,  $t_{\parallel}r_{\parallel}r_{\perp}$  and  $t_{\parallel}r_{\parallel}r_{\parallel}$  bricks design principle

### 5.3.11 $t_{\parallel}t_{\perp}r_{\parallel}r_{\perp}$ , $t_{\parallel}t_{\perp}r_{\parallel}r_{\parallel}$ and $t_{\parallel}t_{\parallel}r_{\parallel}r_{\perp}$ bricks

The design of the  $t_{\parallel}t_{\perp}r_{\parallel}r_{\perp}$ ,  $t_{\parallel}t_{\perp}r_{\parallel}r_{\parallel}$  and  $t_{\parallel}t_{\parallel}r_{\parallel}r_{\perp}$  bricks admits two solutions: the first one is the well known space parallelogram mechanism (see figure 5.26), which is featured in all flexure-based versions of the Delta kinematics (see figures 1.4 and 2.17). A second design, which consists of the serial arrangement of a 4-hinge table and a leaf spring, is illustrated in figure 5.27: although the machining of the final structure (figure 5.27, right) is not straightforward, this solution allows to minimise the traction and compression stresses in the hinges by applying the translation force at mid-length of the arms (see figure 5.2).

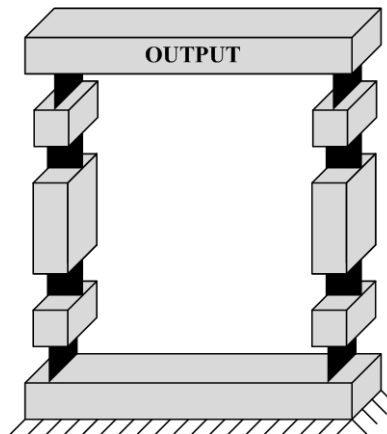


Figure 5.26: Sketch of the  $t_{\parallel}t_{\perp}r_{\parallel}r_{\perp}$ ,  $t_{\parallel}t_{\perp}r_{\parallel}r_{\parallel}$  and  $t_{\parallel}t_{\parallel}r_{\parallel}r_{\perp}$  bricks design called space parallelogram, which is featured in the flexure-based versions of the Delta kinematics (see figures 1.4 and 2.17)

### 5.3.12 $t_{\parallel}t_{\perp}r_{\parallel}r_{\perp}$ and $t_{\parallel}t_{\parallel}r_{\parallel}r_{\parallel}$ bricks

The design of these bricks derives from the mechanism proposed in section 5.3.7: it consists in the serial arrangement of two 4-hinge tables and two torsion pivots (see figure 5.28). Note that the relative order of the four joints which compose this solution can be modified. As

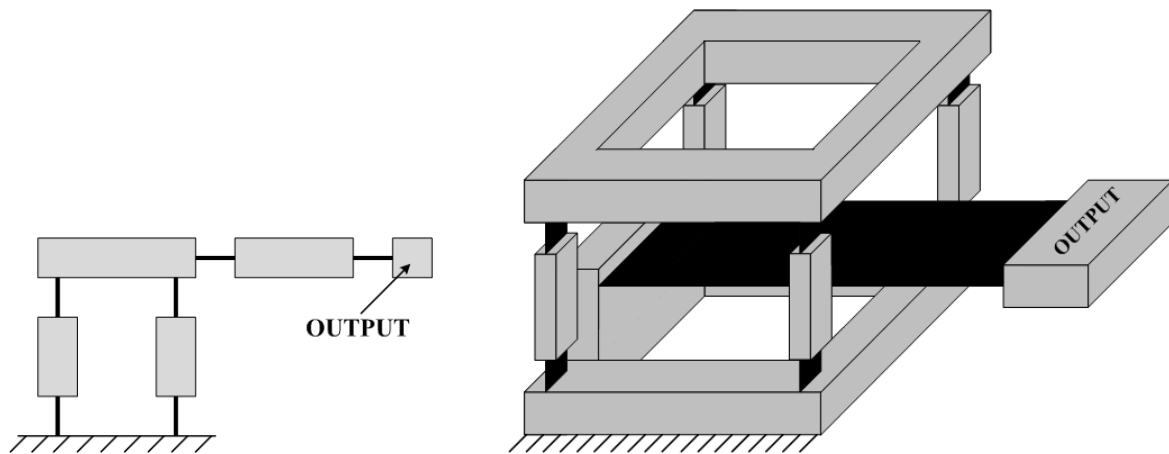


Figure 5.27: Sketches of the second  $t_{\parallel 1} t_{\perp} r_{\parallel 2} r_{\perp}$ ,  $t_{\parallel 1} t_{\perp} r_{\parallel 1} r_{\parallel 2}$  and  $t_{\parallel 1} t_{\parallel 2} r_{\parallel 1} r_{\perp}$  bricks design: principle (left) and final structure (right)

stated in section 5.3.7, the integration of these structures in an ultra-high precision robot should be minimised because of the excessive complexity of their machining.

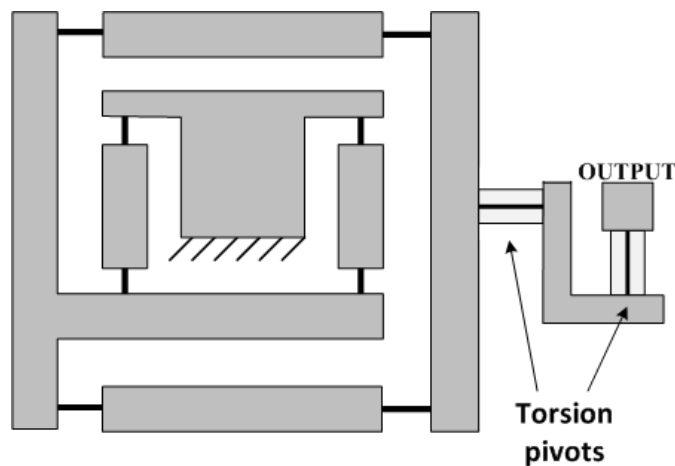


Figure 5.28: Sketch of the  $t_{\parallel 1} t_{\perp} r_{\parallel 1} r_{\perp}$  and  $t_{\parallel 1} t_{\parallel 2} r_{\parallel 1} r_{\parallel 2}$  bricks design principle

### 5.3.13 $t_{\perp} r_{\parallel 1} r_{\parallel 2} r_{\perp}$ and $t_{\parallel 1} r_{\parallel 1} r_{\parallel 2} r_{\perp}$ bricks

The  $t_{\perp} r_{\parallel 1} r_{\parallel 2} r_{\perp}$  and  $t_{\parallel 1} r_{\parallel 1} r_{\parallel 2} r_{\perp}$  bricks are performed by a design making use of a separated crossed-pivot, which is illustrated in figure 5.29. Although complex to machine, this solution is advantageous when the robot specifications require only one high-stroke rotation, which is then performed by the crossed-blades pivot.



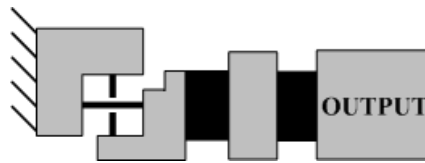


Figure 5.29: Sketch of the  $t_{\perp} r_{\parallel 1} r_{\parallel 2} r_{\perp}$  and  $t_{\parallel 1} r_{\parallel 1} r_{\parallel 2} r_{\perp}$  bricks design principle

### 5.3.14 $t_{\parallel 1} t_{\perp} r_{\parallel 1} r_{\parallel 2} r_{\perp}$ and $t_{\parallel 1} t_{\parallel 2} r_{\parallel 1} r_{\parallel 2} r_{\perp}$ bricks

This mobility, which only blocks one translation, can be efficiently achieved by an L-shaped leaf spring, or corner-blade, which is illustrated in figure 5.30. Furthermore, the Sigma 6 arms design [34], which is illustrated in figure 5.31, can also be used to perform this passive brick. The squirrel cage torsion pivot, although optional, allows to increase the angle of the arm torsion. This design is equivalent to a classical rod and only precludes the translation along the arm axis.

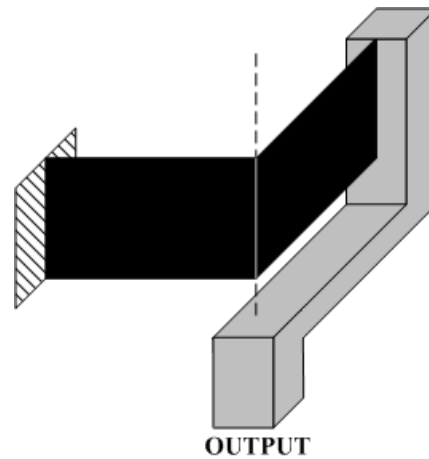


Figure 5.30: Use of a corner-blade as passive  $t_{\parallel 1} t_{\perp} r_{\parallel 1} r_{\parallel 2} r_{\perp}$  and  $t_{\parallel 1} t_{\parallel 2} r_{\parallel 1} r_{\parallel 2} r_{\perp}$  bricks. The output of the brick must be aligned with the blade corner to correctly block the translation along the vertical axis. Note that the illustrated solution facilitates the understanding of the design principle and can easily be adapted to strictly fulfill the planarity hypothesis.

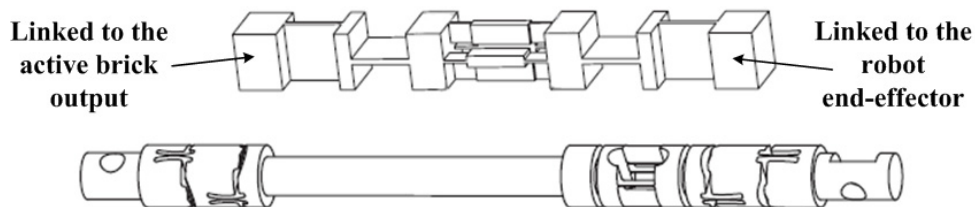


Figure 5.31: Use of the Sigma 6 robot arms [34] as passive  $t_{\parallel 1} t_{\perp} r_{\parallel 1} r_{\parallel 2} r_{\perp}$  and  $t_{\parallel 1} t_{\parallel 2} r_{\parallel 1} r_{\parallel 2} r_{\perp}$  bricks

### 5.3.15 $t_{\parallel 1} t_{\parallel 2} t_{\perp} r_{\parallel 1} r_{\perp}$ and $t_{\parallel 1} t_{\parallel 2} t_{\perp} r_{\parallel 1} r_{\parallel 2}$ bricks

The passive  $t_{\parallel 1} t_{\parallel 2} t_{\perp} r_{\parallel 1} r_{\perp}$  and  $t_{\parallel 1} t_{\parallel 2} t_{\perp} r_{\parallel 1} r_{\parallel 2}$  bricks can efficiently be designed as illustrated in figure 5.32: this structure, which stems from the planar space parallelogram design, only blocks the rotation along the axis which is orthogonal to the mechanism plane.

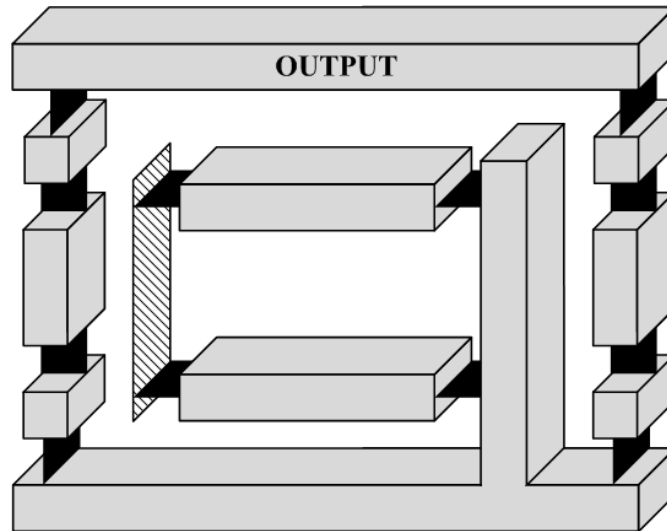


Figure 5.32: Sketch of the  $t_{\parallel 1} t_{\parallel 2} t_{\perp} r_{\parallel 1} r_{\perp}$  and  $t_{\parallel 1} t_{\parallel 2} t_{\perp} r_{\parallel 1} r_{\parallel 2}$  bricks design principle

## 5.4 Discussion

The active and passive bricks designs which have been introduced in this chapter have been developed to fulfill the ultra-high precision criteria stated in chapter 4: ***the active bricks must be planar and linearly actuated mechanisms, whereas the passive bricks are planar structures or mechanisms presenting a rotational symmetry.*** These hypotheses have been specified on the basis of the chosen manufacturing method, namely Wire Electro-Discharge Machining, and of the standard actuation solutions available on the market. Nonetheless, efficient flexure-based structures which do not satisfy these criteria can be achieved, for example making use of other machining means, such as the spherical joints presented in figure 4.5.

Furthermore, the aim of this chapter has explicitly been to provide and group interesting brick designs as a tool for the engineer rather than to propose a thorough catalogue of off-the-shelf mechanical solutions. Two simple considerations allow to highlight the crucial role of the designer who will use this methodology and mechanical solution catalogue:

- First, ***two functions can be performed by the passive bricks degrees of freedom: they can either fulfill a functional need, which is to allow an end-effector motion, or to avoid overconstraints. The first role requires that the passive displacement presents***

*the same high stroke as the end-effector degree of freedom, whereas the second demands a much lower motion range.* The robot designer has thus to carefully determine the role of each degree of freedom of the considered passive brick in order to set its stroke specifications: this may lead the engineer to design his/her own brick to fulfill the specific requirements of the application.

- Then, *the conceptual frame of the methodology necessitates the active and passive bricks of a kinematic chain to be serially arranged. Nonetheless, this does not imply that both bricks should be separately designed and assembled afterwards: a more global approach can be highly advantageous.* Indeed, at this stage of the methodology, one or several robot kinematics have already been selected in the conceptual solution catalogue: the active and passive bricks composing each kinematic chain are thus known. Consequently, the choice of the mechanical solutions to perform these bricks can and must take into account their combination within the kinematic chain and the arrangement of the chains within the robot. This global approach may for example lead to the design of a single monolithic mechanism performing the function of both active and passive bricks.

Consequently, the role of the robot designer is crucial when the modular methodology presented in this thesis is practically applied to an industrial robot synthesis. The next chapter, which details the case study of a 5-degree of freedom robot, will allow to illustrate the complementarity of the methodology potentialities and the added value of the creative designer work to achieve a high-performance ultra-high precision robot.



# Chapter 6

## Case study: 5-DOF ultra-high precision robot

The application of the modular methodology is now illustrated with the study of a 5-degree of freedom ultra-high precision industrial robot. This chapter consequently details the kinematic synthesis and the mechanical design which have led to the manufacturing of the Legolas 5 prototype. First, a kinematic solution is selected in the reduced solution catalogue for ultra-high precision, on the basis of the robot specifications. Then, the mechanical design of the necessary active and passive bricks is thoroughly examined, as well as some crucial aspects of the prototype finalisation, such as assembly, force alignment and gravity compensation. Finally, the characterisation of the Legolas 5 is presented and a discussion of the obtained results concludes this chapter.

### 6.1 Robot specifications

The choice of the 5-degree of freedom mobility to illustrate the use of the methodology has been motivated by a typical task an ultra-high precision industrial robot has to perform, namely micromanipulation. This often requires three translations ( $T_x$ ,  $T_y$  and  $T_z$ ) and two tip-tilt rotations ( $R_x$  and  $R_y$ ). This kinematics is complex to design and manufacture, which explains the scarcity of prototypes, especially in the industrial context. The specifications for this 5-DOF robot are the following:

- **Strokes:**  $\pm 5$  mm and  $\pm 10^\circ$ , maximum translation and angle simultaneously achievable
- **Resolutions:** 50 nm for the translations and  $2 \mu\text{rad}$  [ $0.4^\circ$ ] for the rotations. Note that as mentioned in section 1.2.2, the robot accuracy will not be studied in this thesis
- **Total robot volume:** minimised
- **Easily modifiable** into a 4-DOF or a 6-DOF robot
- **Minimal number of different bricks**
- **High eigenfrequencies**

## 6.2 Kinematics synthesis

The first step of the methodology consists in the synthesis of the robot kinematics, which is selected in the reduced solution catalogue for ultra-high precision on the basis of the previously stated robot requirements.

### 6.2.1 Active bricks arrangements

The reduced solution catalogue for ultra-high precision lists 27 possible active bricks arrangements for the considered Tx, Ty, Tz, Rx, Ry mobility (see pages 227 to 229). These can be grouped in four categories:

- 2 *kinematic chains*, including a planar joint brick and a brick actuating a translation and a rotation along different axes (solutions 1 to 5)
- 3 *kinematic chains*, including a planar joint brick, a rotation brick and a brick actuating a translation (solutions 6 to 10)
- 3 *kinematic chains*, including a brick actuating two translations, a rotation brick and a brick actuating a translation and a rotation along different axes (solutions 11 to 19)
- 3 *kinematic chains*, including two bricks actuating a translation and a rotation along different axes, and a translation brick (solutions 20 to 27)

The conceptual active bricks are now replaced by sketches of their mechanical design, whose planes are oriented to perform the required mobility. As stated in chapter 5, although the bricks are designed as planar mechanisms, the physical plane including the flexure-based structure is not necessarily coincident with the plane of the brick on the conceptual cube (see figure 5.7). Bricks which share the same mobility are thus identically designed, regardless the orientation of the motions relatively to the cube face plane. Figure 6.1 illustrates the replacement of the conceptual bricks by their mechanical design principles for the first kinematic category (solutions 1 to 5): the resulting arrangements are notably reorientations of the same mechanical solution. This observation is the direct consequence of the hypothesis stated in chapter 5: indeed, if bricks which share the same mobility are differently designed depending on the orientation of their degrees of freedom relatively to the conceptual cube face, this observation becomes irrelevant.

Once the conceptual active bricks have been replaced by their flexure-based planar designs, as in figure 6.1, the possibilities from each kinematic category eventually amount to the same mechanical solution. Consequently, the corresponding passive bricks are also equivalent: only one active brick arrangement for each family can thus be retained for the next step of the methodology. This solution can be arbitrarily selected: in this example, the chosen active bricks possibility only includes bricks whose conceptual and physical planes are coincident. For instance, the selected active bricks arrangement of the first family is the first solution (far left on figure 6.1). Figure 6.2 illustrates the four remaining active bricks solutions for the considered 5-DOF robot.

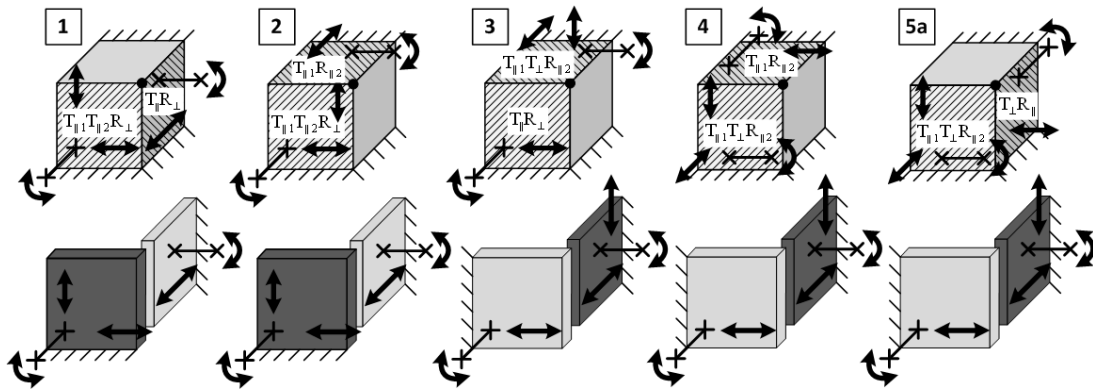


Figure 6.1: Conceptual active bricks solutions from the first category (top) and corresponding arrangements of their bricks mechanical designs (dark grey stands for the planar joint brick, whereas light gray stands for the 2-DOF brick)

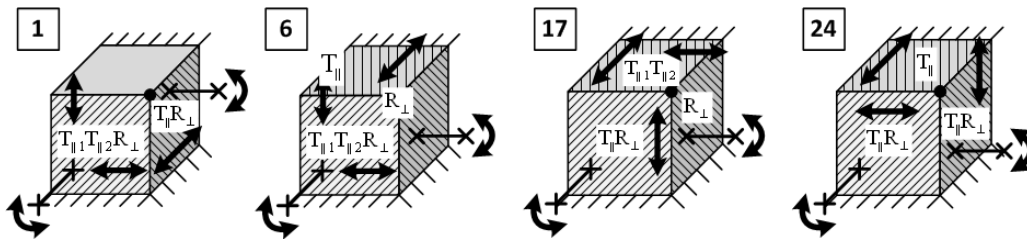


Figure 6.2: Sketches of the four remaining active bricks arrangements for the  $T_x$ ,  $T_y$ ,  $T_z$ ,  $R_x$ ,  $R_y$  mobility

## 6.2.2 Passive bricks arrangements

The next step of the methodology consists in examining the possible passive bricks for each of the four remaining active bricks arrangements: these are excerpted from the reduced solution catalogue for ultra-high precision and illustrated in figure 6.3. The aim of this step is to first discard the solutions which do not lead to an efficient and compact robot kinematics: the two following criteria are thus valid regardless the specific requirements of the machine and can be applied on the synthesis of any ultra-high precision robot.

The **first dismissing criterion, based on force alignment observations**, aims at limiting parasitic displacements along the blocked degrees of the bricks, which result from the application of forces and moments on the robot end-effector. This is achieved by minimising the orthogonal distance between the robot output and the brick, which should ideally be aligned. In other words, the active and passive brick of a kinematic chain must fulfill the following criterion: if the passive brick is planar, its plane must be parallel (ideally coincident) with the active brick plane, whereas if the passive brick presents a rotational symmetry, its axis must belong to a plane which is parallel to the active brick. In the case of the 5-DOF mobility, this assumption allows to dismiss the first passive bricks arrangement of solution 1, as well as the third arrangement of solution 24 (see figure 6.3): in both cases, the  $t_{\parallel 1} t_{\perp 1} r_{\parallel 2}$  brick is inevitably orthogonal to the active brick plane.

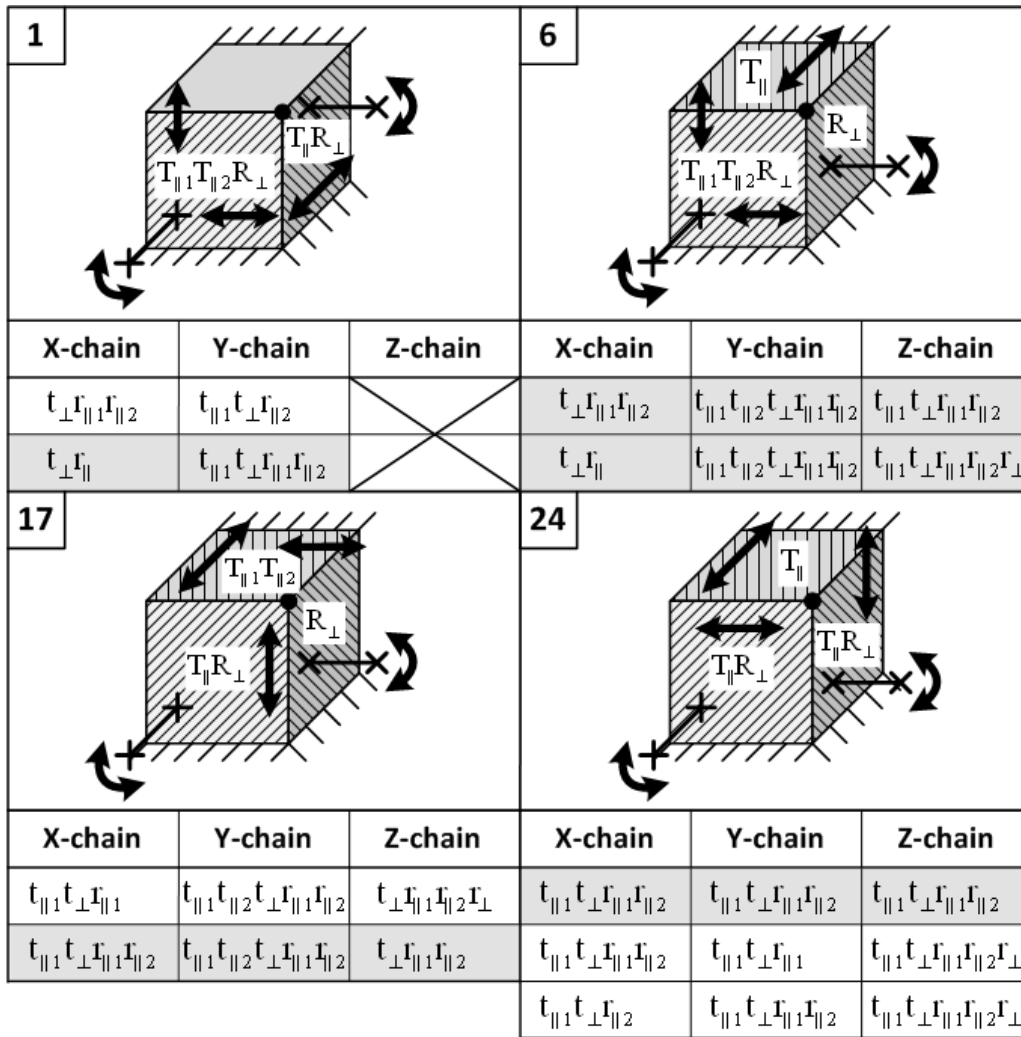


Figure 6.3: *Passive bricks solutions for the four remaining active bricks arrangements. The grey backgrounds indicate the solutions which are retained after the passive bricks arrangements selection.*

Then, ***the possibilities which include passive bricks which are excessively complex to machine must be examined***: the solution is retained only if the active and passive brick of the considered kinematic chain can be designed as one efficient flexure-based mechanism. As stated in chapter 5, the involved passive bricks are the following:  $t_{||1}r_{||1}$  and  $t_{\perp}r_{\perp}$ ,  $t_{||}t_{\perp}r_{\perp}$ ,  $t_{||1}t_{\perp}r_{||1}$  and  $t_{||1}t_{||2}r_{||1}$ , as well as  $t_{||1}t_{\perp}r_{||1}r_{\perp}$  and  $t_{||1}t_{||2}r_{||1}r_{||2}$ . In the case of the 5-DOF mobility, the  $t_{||1}t_{\perp}r_{||1}$  brick is included in solutions 17 and 24 (see figure 6.3) and serially arranged with a  $T_{||}R_{\perp}$  active brick. Performing these two bricks with a single mechanism would amount to the design of a  $t_{||1}t_{||2}t_{\perp}r_{||1}r_{\perp}$  brick, where  $t_{||2}$  and  $r_{\perp}$  should be actuated: both motorisations are nonetheless not straightforward in the brick design proposed in paragraph 5.3.15. Consequently, the use of a single mechanism to perform both bricks would not be efficient, and both passive bricks solutions which include this configuration are dismissed.



The kinematic solutions which remain after the application of these two criteria are highlighted with grey backgrounds in figure 6.3. Then, the specific robot requirements are used to select the most suited kinematics for the application. In the case considered here, two kinematic specifications have not been exploited yet, namely the minimal number of different building bricks and the simple transformation into another mobility. The number of different building bricks of the remaining solutions is thus computed:

- *Active bricks arrangement #1* (see figure 6.3): 4 building bricks
- *Active bricks arrangement #6*: 6 bricks for both solutions
- *Active bricks arrangement #17*: 6 bricks
- *Active bricks arrangement #24*: 3 bricks

The active brick arrangement #24 and the remaining passive brick solution thus consists in the optimal solution for the minimal number of building bricks criterion: this kinematic is recalled in figure 6.4. Furthermore, the transformation into another mobility is straightforwardly performed: a 6-DOF robot is obtained by replacing the  $T_{\parallel}$  by a third  $T_{\parallel}R_{\perp}$  brick, thus presenting only two different building bricks. Moreover, a 4-DOF robot is simply achieved by replacing one of the  $T_{\parallel}R_{\perp}$  bricks by a  $T_{\parallel}$  or a  $R_{\perp}$  one, depending on the degrees of freedom which are required (three translations and one rotation, or two translations and two rotations).

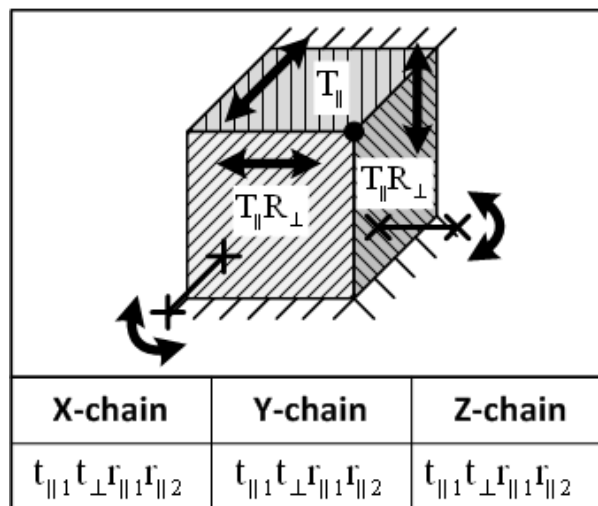


Figure 6.4: *Final kinematic solution of the 5-DOF ultra-high precision robot*

Figure 6.5 presents the kinematic solution with sketches of the design principles, whereas figure 6.6 illustrates a scaled mock-up including assembled leaf springs and hand-actuation. The details of the bricks mechanical design will be presented in section 6.3.

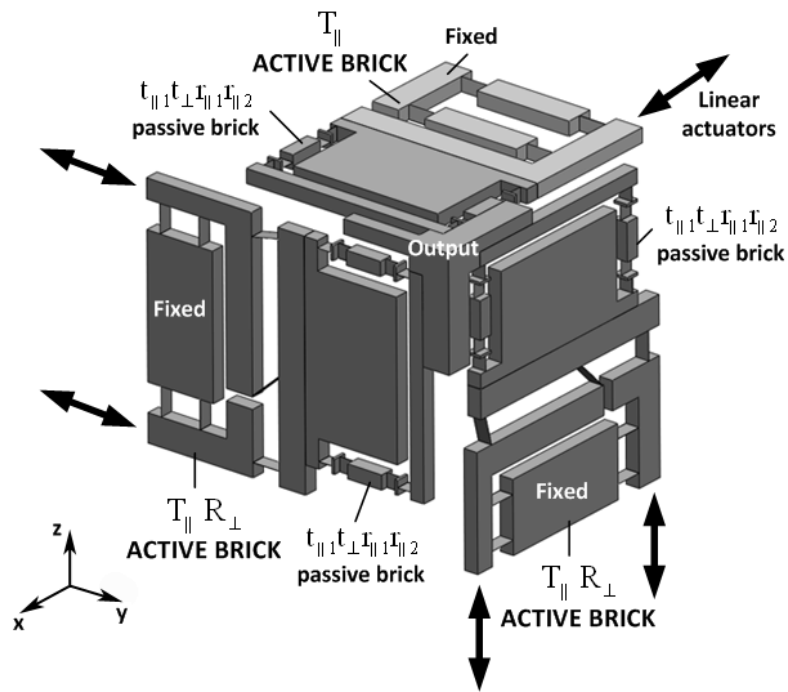


Figure 6.5: Sketch of the kinematic solution with the bricks design principles

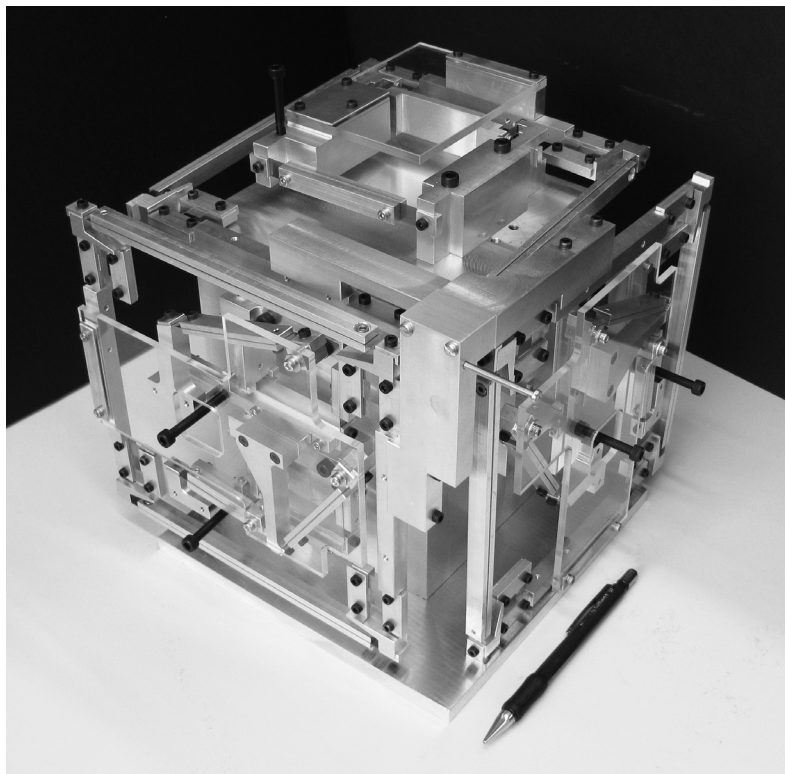


Figure 6.6: Scaled mock-up with assembled leaf springs and hand-actuation

### 6.2.3 Legolas, ultra-high precision parallel robots family

The application of the methodology on the synthesis of robots presenting the same specifications as this 5-DOF case but different degrees of freedom has allowed to generate a new kinematic family, named Legolas family. The latter presents a kinematic solution for each of the 19 possible end-effector mobilities, making use of only 6 different building bricks, which are the following:

- **Active bricks:**  $T_{\parallel}$ ,  $R_{\perp}$ ,  $T_{\parallel}R_{\perp}$
- **Passive bricks:**  $t_{\parallel}r_{\perp}$ ,  $t_{\perp}r_{\parallel}$ ,  $t_{\parallel 1}t_{\perp 1}r_{\parallel 1}r_{\parallel 2}$

<b>2 (2)</b> 	<b>1 (1)</b> 	<b>3a (3a)</b> 						
X-chain	Y-chain	Z-chain	X-chain	Y-chain	Z-chain	X-chain	Y-chain	Z-chain
						$t_{\parallel 1}t_{\perp 1}r_{\parallel 1}r_{\parallel 2}$	$t_{\perp}r_{\parallel}$	
<b>1 (3)</b> 	<b>1 (1)</b> 	<b>2 (4)</b> 						
$t_{\perp}r_{\parallel}$	$t_{\parallel 1}t_{\perp 1}r_{\parallel 1}r_{\parallel 2}$		$t_{\parallel 1}t_{\perp 1}r_{\parallel 1}r_{\parallel 2}$	$t_{\perp}r_{\parallel}$				
<b>5 (6)</b> 	<b>10 (17)</b> 	<b>9 (9)</b> 						
$t_{\parallel 1}t_{\perp 1}r_{\parallel 1}r_{\parallel 2}$	$t_{\parallel 1}t_{\perp 1}r_{\parallel 1}r_{\parallel 2}$	$t_{\parallel 1}t_{\perp 1}r_{\parallel 1}r_{\parallel 2}$	$t_{\parallel 1}t_{\perp 1}r_{\parallel 1}r_{\parallel 2}$	$t_{\parallel 1}t_{\perp 1}r_{\parallel 1}r_{\parallel 2}$	$t_{\parallel 1}t_{\perp 1}r_{\parallel 1}r_{\parallel 2}$	$t_{\parallel}r_{\perp}$		$t_{\parallel 1}t_{\perp 1}r_{\parallel 1}r_{\parallel 2}$
<b>1 (6)</b> 	<b>6 (17)</b> 	<b>1 (5)</b> 						
$t_{\perp}r_{\parallel}$	$t_{\parallel 1}t_{\perp 1}r_{\parallel 1}r_{\parallel 2}$		$t_{\parallel 1}t_{\perp 1}r_{\parallel 1}r_{\parallel 2}$	$t_{\parallel 1}t_{\perp 1}r_{\parallel 1}r_{\parallel 2}$	$t_{\parallel 1}t_{\perp 1}r_{\parallel 1}r_{\parallel 2}$	$t_{\parallel 1}t_{\perp 1}r_{\parallel 1}r_{\parallel 2}$	$t_{\parallel 1}t_{\perp 1}r_{\parallel 1}r_{\parallel 2}$	$t_{\parallel 1}t_{\perp 1}r_{\parallel 1}r_{\parallel 2}$

Figure 6.7: Active and passive bricks arrangements for each of the 19 possible mobilities of the Legolas family (1/2); the numbers refer to the position of the solutions in the reduced (plain) and exhaustive (in parentheses) solution catalogues

Figures 6.7 and 6.8 illustrate the active and passive bricks solutions for each robot mobility. Then, the arrangement and mechanical design of each robot of this family will be outlined and illustrated in appendix E on the basis of the mechanical solutions and assembly considerations which will be presented in the next section.

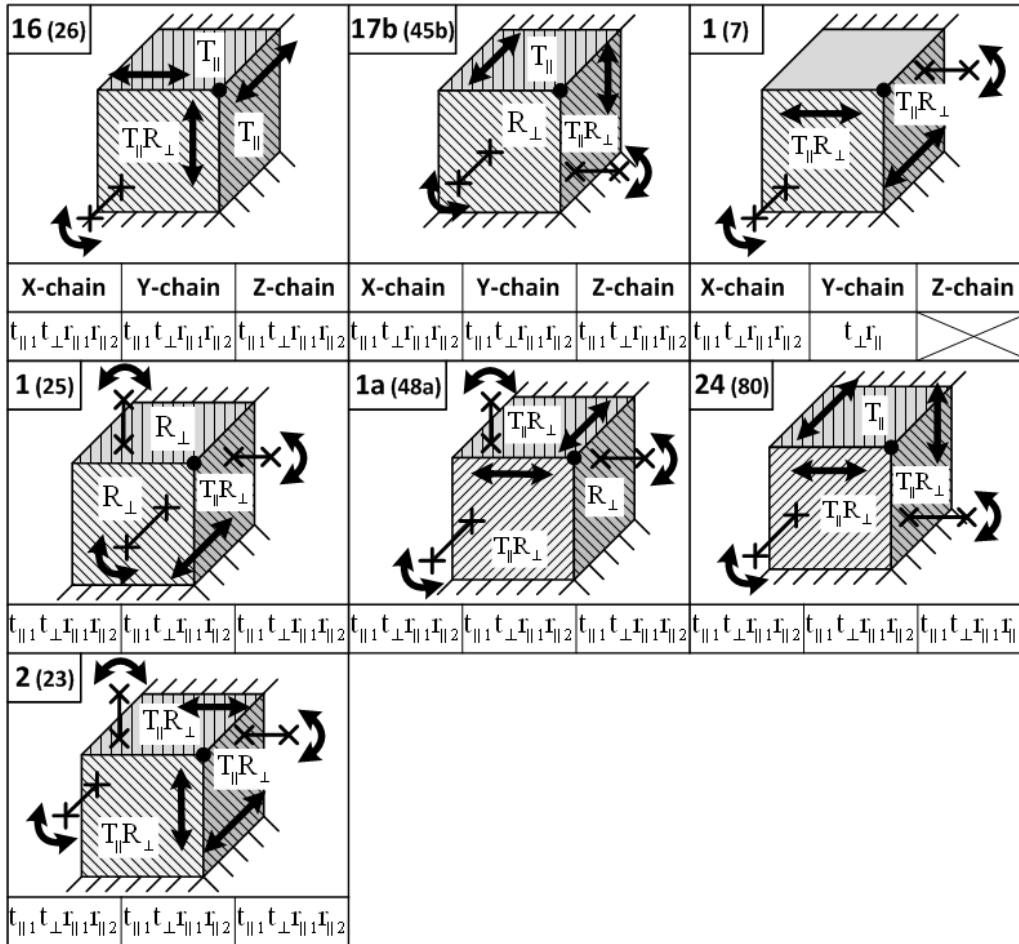


Figure 6.8: Active and passive bricks arrangements for each of the 19 possible mobilities of the Legolas family (2/2)

## 6.3 Mechanical design

This section is dedicated to the mechanical design of the Legolas 5 prototype: first, the selected solutions to perform the three necessary building bricks is detailed, notably including the actuation sub-brick development. Then, key design and assembly subtleties are underlined, such as precise mounting of leaf springs, alignment of forces and gravity compensation.

### 6.3.1 Active bricks design

The development of the actuation sub-brick, which is featured in both robot active bricks, is the first step of the design process: it notably includes the choice of the sensors and actuators, as well as the dimensioning of the 4-prismatic hinge table, whose role is to guide the actuator moving part (see section 6.3.1.1). The mechanical design of both the  $T_{\parallel}$  and  $T_{\parallel}R_{\perp}$  bricks is then presented. Note that appendix E completes this section by detailing solutions for all active bricks which have been retained for ultra-high precision applications.

#### 6.3.1.1 Actuation sub-brick

As the Legolas 5 robot includes the  $T_{\parallel}R_{\perp}$  active brick, two versions of the actuation sub-brick must be developed: the first actuates only the translation, while the second performs both the translation and the rotation. The latter must then present a higher stroke in order to simultaneously achieve the maximal displacement and angle (see section 5.2.2.4). The choice of the sub-brick first component, namely the sensor, is straightforward, as it only depends on the desired robot resolution and strokes: the sensor which will be included in the actuation sub-brick is the optical incremental linear encoder LIK-41 from Numerik Jena [71], which presents a resolution of 50 nm and a customer set measuring length. On the other hand, the design of the 4-hinge table and the selection of the actuator are tightly coupled. The requirements of the guiding system are indeed the following:

- **4-prismatic hinge table**
  - *Strokes:*
    - \*  $\pm 5 \text{ mm}$  for the table which actuates only a translation
    - \*  $\pm (5 \text{ mm} + \vartheta \cdot d)$  for the table which simultaneously performs a translation and a rotation, where  $\vartheta$  is the desired angle in radians ( $\pm 0.175 \text{ rad}$ ) and  $d$  is the orthogonal distance between the actuation force and the rotation centre. As this parameter is crucial for the efficiency of the brick (see section 5.2.2.1) the achievable stroke of both the table and the actuator must thus be carefully chosen.
  - *Parasitic displacement*  $\lambda$  (see section 5.2.1.1):
    - \* *insignificant* if an ironless EC actuator is selected

- \* *minimised* if a voice coil actuator is selected; its maximal admissible value then depends on the air gap between the coil and the magnet (see section 5.2.1.2)
- *Total volume: minimised*; the mechanism should ideally be included in a  $100\text{ mm} \times 100\text{ mm}$  surface

Note that the last two criteria cannot be minimised simultaneously, as decreasing the parasitic displacement causes the length of the table arms to increase (see section 5.2.1.1); an acceptable compromise must thus be found.

As for the actuator selection, albeit an ironless EC actuator would have allowed for a more compact robot design, the scarcity of standard products fulfilling the Legolas 5 specifications has not permitted to find a suitable solution. Consequently, a cylindrical voice coil from BEI Kimco [8] has been selected, whose main characteristics are detailed in table 6.1. This actuator will be integrated in both versions of the actuation sub-brick.

Model	Stroke	Force constant	Continuous force	Peak force	Clearance
LA15-26-000A	$\pm 12.7\text{ mm}$	8.81 N/A	11.57 N	44.48 N	0.38 mm

Table 6.1: Selected BEI Kimco voice coil characteristics

The actuator characteristics determine the maximum value of the parasitic displacement  $\lambda$ , which is equal to twice the clearance between the coil and the magnet (see figure 5.5), namely  $0.76\text{ mm}$ . The design of both 4-hinge tables can consequently be performed, making use of the formulas detailed in section 5.2.1.1; as the material of the flexures is steel, generic values of 210 GPa for the Young's modulus and of 500 MPa for the maximal admissible stress have been used to evaluate the model. Table 6.2 summarises the main features of the resulting designs (see figure 6.9 for the geometric parameters definition).

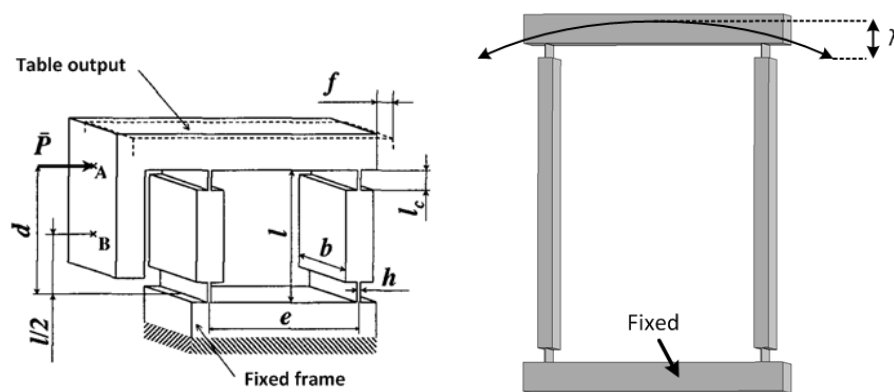


Figure 6.9: Sketch of the 4-prismatic hinge table with geometric parameters (left, [36]) and its parabolic trajectory (right)



	Stroke ( $f$ )	$h$	$l_c$	$l$	$\lambda$	$b$	Natural stiffness
T table	$\pm 5$ mm	200 $\mu\text{m}$	5 mm	80 mm	169.9 $\mu\text{m}$	20 mm	365 N/m
T + R table	$\pm 10$ mm	200 $\mu\text{m}$	5 mm	100 mm	531.5 $\mu\text{m}$	20 mm	228 N/m

Table 6.2: Design summary of the translation (above) and the combined translation and rotation (below) 4-hinge tables

The mechanism which allows the adjustment of the actuator stator and coil relative positioning will be detailed in section 6.3.3.2. Furthermore, the mechanical linkage between the coil and the steel guiding system is performed by parts made of POM (polyoxymethylene): this material, which presents a low thermal conductivity, limits the conduction of the heat generated by the actuator into the flexure-based mechanism.

Nonetheless, the moving mass of the whole actuation sub-brick which performs the simultaneous translation and rotation reaches 0.6 kg when including a monolithic steel 4-hinge table, which highly limits its dynamical performances. Consequently, it must be drastically decreased, which is achieved by designing *the Legolas 5 prototype with aluminum parts and assembled steel leaf springs*. The total moving mass of the aforementioned actuation sub-brick is thus decreased by a factor of 3.7, which multiplies the theoretical maximum acceleration by the same value.

The development of the Legolas 5 prototype *will thus additionally allow to prove that robots which are composed of assembled leaf springs can achieve precisions below 0.1  $\mu\text{m}$ , and present high dynamic performances thanks to their lower moving mass*. Indeed, to the knowledge of the author, all ultra-high precision robots of the literature present monolithic structures, while assembly of flexures has only been performed for high precision machines, such as the Micabo<sup>hs</sup> and the Triglides<sup>s</sup> (see section 2.3.3).

The following paragraphs present the design of the active and passive bricks with assembled leaf springs, whereas section 6.3.3.1 will detail the flexures alignment and mounting method. Note that the mechanical solutions have still been selected in chapter 5, albeit the planarity and rotational symmetry criteria are less significant when the flexures are assembled.

### 6.3.1.2 $T_{\parallel}$ active brick

The mechanical design of the  $T_{\parallel}$  active brick simply consists in the low-stroke actuation sub-brick, which only motorises the translation. Figure 6.10, left, presents the sub-brick 4-hinge table, including an integrated mechanical stop; the assembly of the leaf springs will be detailed in section 6.3.3.1. Furthermore, figure 6.10, right, shows the complete  $T_{\parallel}$  active brick, where a key feature can be highlighted: the leaf springs present a non-constant breadth, which allows to increase the transverse stiffness and eigenfrequency of the guiding system [6]; this subtlety will be detailed in the force alignment section (6.3.4.1).

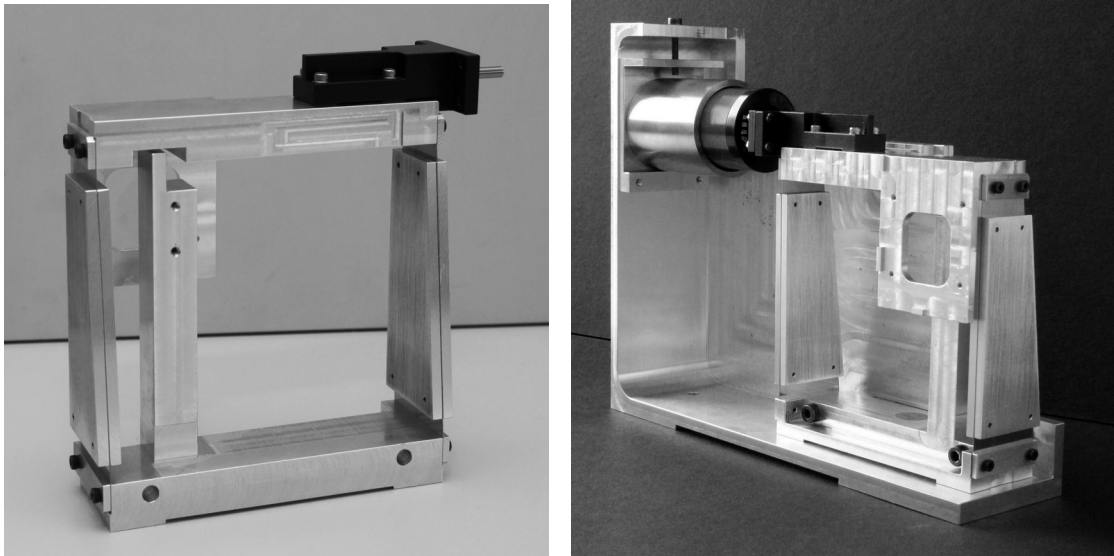


Figure 6.10: Assembled leaf springs 4-prismatic hinge table actuating the translation (left) and complete  $T_{\parallel}$  active brick (right)

### 6.3.1.3 $T_{\parallel}R_{\perp}$ active brick

The detailed mechanical design of the  $T_{\parallel}R_{\perp}$  active brick, which is based on the principle described in section 5.2.2.4, is illustrated in figure 6.11, left: the synchronous actuation of both sub-bricks perform the translation, whereas the rotation is obtained by the sole motion of the high-stroke sub-brick, thus allowing to simultaneously achieve the maximal translational stroke and angle. As in the case of the  $T_{\parallel}$  active brick, the 4-hinge tables leaf springs present a non-constant breadth to increase the transverse stiffness. Furthermore, figure 6.12, left, shows both actuation sub-bricks, without the mechanism transforming the linear motion into a rotation. The latter is composed of two parts (see section 5.2.2.1): first, two leaf springs, illustrated in figure 6.12, right, define the position of the Remote Centre of Motion; they are assembled to the sub-brick which only actuates the translation (see figure 6.11, right). Then, a single leaf spring, whose role is to transform the actuator force into a moment, is linked to the high-stroke sub-brick (see figure 6.11, left). The orthogonal distance between this leaf spring and the rotation centre,  $d$ , is determined by the maximal rotation angle and the actuator stroke, as discussed in section 6.3.1.1.

Note that the design of this active brick is not strictly planar, but rather consists of three planes which are arranged in parallel (see figure 6.11, left): two of them include the actuation sub-bricks, whereas the third encompasses both parts of the RCM mechanism. This configuration leads to a more compact design, and also allows to align the RCM mechanism with the robot end-effector, thus limiting the effect of parasitic forces and moments. Furthermore, as illustrated in figure 6.11, left, all three RCM leaf springs will be assembled to the passive brick, which intrinsically causes overconstraints; to limit their effect, the position of the passive brick is set by both broad leaf springs defining the rotation centre, whereas the narrow leaf spring applying the force can easily adapt to this position by deforming itself. If



necessary, an additional necked-down hinge can be performed in the latter to suppress the overconstraint.

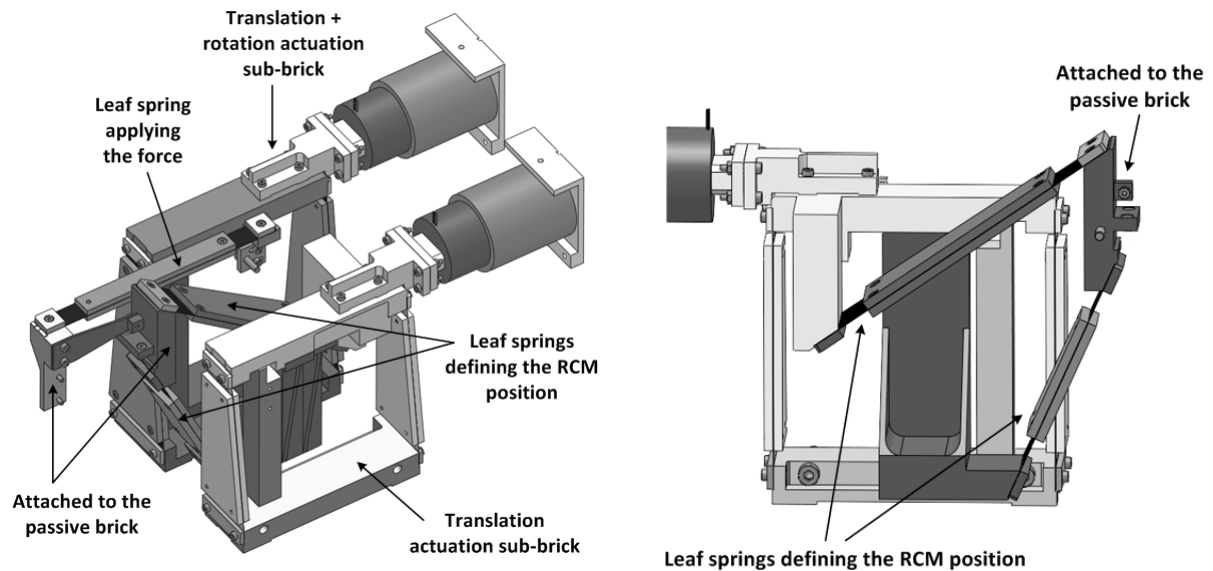


Figure 6.11: Detailed design principle of the  $T_{\parallel}R_{\perp}$  active brick (left) and detail of the translation actuation sub-brick including the leaf springs defining the RCM position (right)

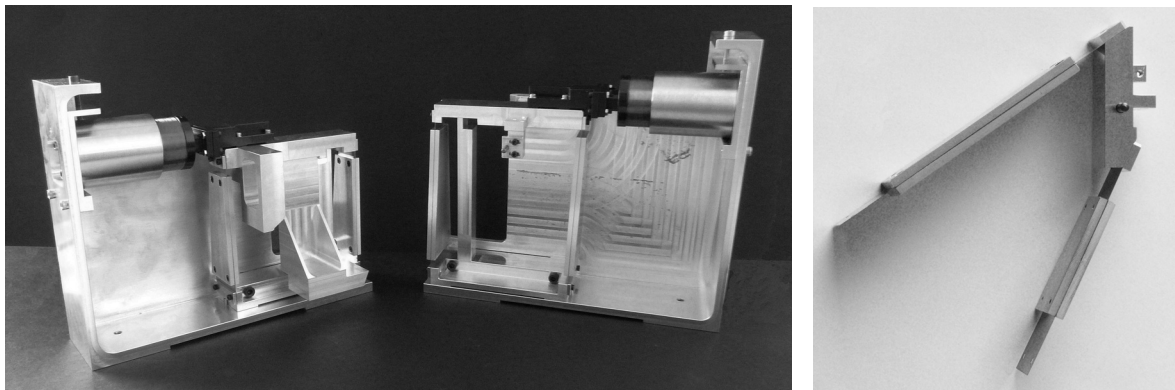


Figure 6.12: Picture of both actuation sub-bricks, without the RCM mechanism (left) and sub-assembly of the leaf springs defining the RCM position (right)

### 6.3.2 $t_{\parallel}t_{\perp}r_{\parallel}r_{\parallel 2}$ passive brick design

The mechanical solution which has been retained for the three  $t_{\parallel}t_{\perp}r_{\parallel}r_{\parallel 2}$  passive bricks of the Legolas 5 is composed of a 4-hinge table and of a 3-DOF serially arranged leaf spring (see figure 5.27 and section 5.3.11). This design notably presents the advantage of allowing to align the forces of both the table and the leaf spring with the end-effector, thus limiting parasitic deformations of the mechanical structure. The main criterion for the design of the 4-hinge table consists in the minimisation of the volume requirement. As for the leaf spring,

its torsion axis must be aligned with the rotation axis of the robot, whereas its shape must allow for high-stroke combined torsion and flexion motions. Figure 6.13 illustrates the three passive bricks of the Legolas 5 robot: the first one, which corresponds to the X-side kinematic chain, features a broad leaf spring with a central hole, allowing both the compactness of the design and the limitation of the intrinsic overconstraints in a broad plate subject to torsion. On the other hand, the Y-side and Z-side bricks present a tensile specimen-like shape, which is also efficient to reduce stresses in the leaf spring during simultaneous torsion and flexion. Note that the parasitic deformations of the 4-hinge table are expected to be higher in the case of the Z-side design, as the leaf spring position does not coincide with the middle of the table arms.

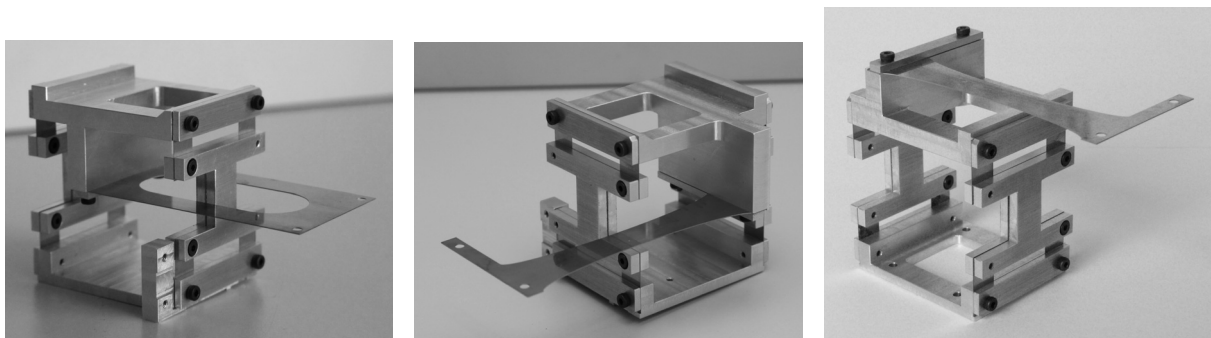


Figure 6.13: *Detailed design of the X-side (left), Y-side (middle) and Z-side (right) passive bricks*

### 6.3.3 Design and assembly subtleties

#### 6.3.3.1 Leaf spring assembly

The alignment and assembly of the leaf springs must be carefully performed in order to limit the parasitic deformations of the flexure mechanisms; in the Legolas 5 prototype, each leaf spring is assembled with screws and clamped between a support and a prismatic washer. The precise relative positioning of these three parts is achieved as illustrated in figure 6.14, top: the vertical alignment, as well as the parallelism between the parts, are set by two protrusions on the support. Furthermore, the use of a precision gauge block during the assembly process allows to laterally align the support, the leaf spring and the washer. Figure 6.14, bottom, presents a detail of a resulting leaf spring mounting. Note that in the case of 4-hinge tables, only three of the four clampings must present the alignment protrusions to avoid overconstraining the mechanism during the assembly. Lastly, the machining geometric tolerances, which are presented on figure 6.14, top, allow to minimise parasitic displacements of the 4-hinge tables.

#### 6.3.3.2 Actuators adjustment

As detailed in section 5.2.1.2, the use of cylindrical voice-coil actuators necessitates to fine-tune the relative position of the moving coil and the stator, thus preventing the parabolic

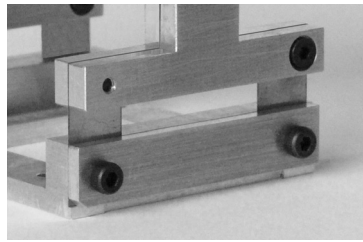
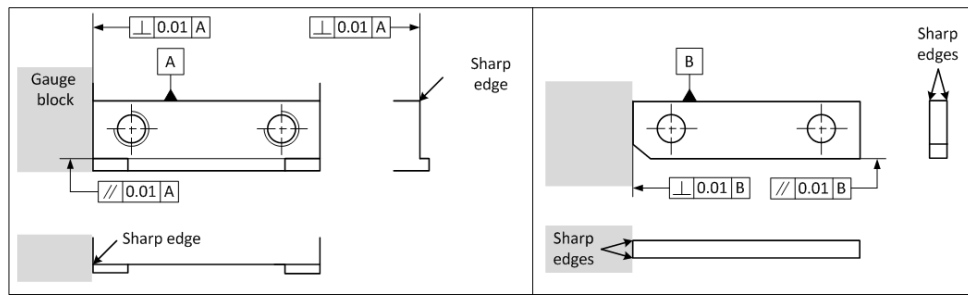


Figure 6.14: Assembly principle and geometric tolerances of the clamping parts: support (top left) and prismatic washer (top right); the chamfered edge of the washer solely consists in an assembly point of reference. Bottom: detail of a 4-hinge table leaf spring assembly

trajectory of the 4-hinge table from causing friction between these parts. The solution which has been retained for the prototype is to use the coil as a reference by assembling it to the guiding table, and to adjust the relative position of the stator. The latter is screwed to a plate which can translate vertically relative to the brick fixed frame thanks to two pins which slide in a slot; an adjustment screw allows to precisely modify its position. Once in place, the plate is rigidly linked to the brick frame with fixation screws. This adjustment mechanism is illustrated in figure 6.15. Lastly, note that this procedure must be performed when the bricks are mounted on the robot base: this indeed allows to include in the fine-tuning the effects of gravity and of the bending of the bricks frames, which occurs when these are screwed into the robot support.

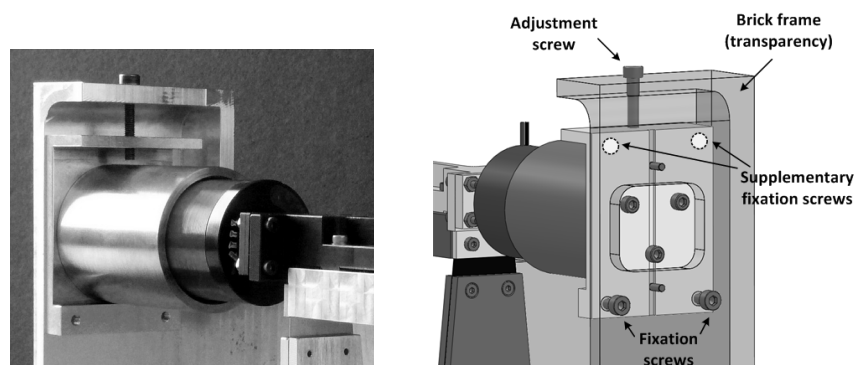


Figure 6.15: Illustrations of the mechanism for the actuator adjustment; note that supplementary fixation screws could be added at the specified location to limit the efforts acting on the screws and to prevent the plate from oscillating when the actuator performs high accelerations

### 6.3.3.3 Gravity compensation

The compensation of gravity, or static balancing, is mandatory to avoid that the own weight of the robot mobile parts plastically deforms the leaf springs; in the Legolas 5 prototype, the solution which has been retained to counterbalance the gravity effects consists in acting at two levels:

- *at the level of the actuation sub-bricks which present a vertical translation:* the gravitational force acting on the sub-brick mobile parts is counterbalanced by adding a traction spring in parallel with the 4-hinge table (see figure 6.16, left). The equilibrium point of the system corresponds to the middle of the table stroke. In the Legolas 5 prototype, this solution is included in both actuation sub-bricks of the Y-side kinematic chain.
- *at the end-effector level:* the moment generated by gravity acting on the passive brick and RCM mechanism mobile parts is counterbalanced by adding a traction spring which links the output of the actuation sub-brick to the passive brick (see figure 6.16, right). As previously, the equilibrium point of the system corresponds to the zero-stroke of the output. Moreover, the stiffness of the spring should be minimised to limit the effect of the force variation due to the end-effector displacements. Lastly, as the spring must withstand a rotation of  $\pm 10^\circ$  between its extremities, increasing its length consists in a noteworthy advantage. Both X-side and Y-side kinematic chains of the Legolas 5 include this solution.

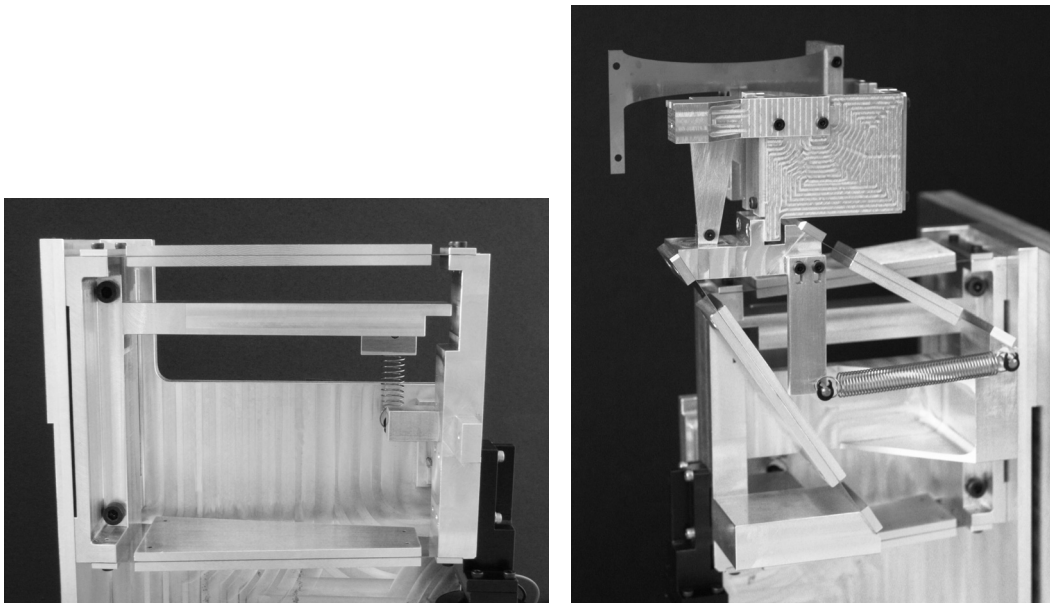


Figure 6.16: *Left: Gravity compensation of an actuation sub-brick presenting a vertical translation / Right: Gravity compensation at the level of the end-effector*



### 6.3.4 Legolas 5 prototype

Figures 6.17 and 6.18 illustrate the resulting Legolas 5 prototype, presenting a general view, as well as a detail of the end-effector and passive bricks. Furthermore, the  $R_s$  ratio of this robot (see section 5.1) can now be evaluated:

- Volume of the prism enclosing the robot mechanical parts:  $339 \times 397 \times 269 \text{ mm}^3$
- Characteristic dimension: 397 mm
- Total linear stroke: 10 mm
- $R_s$  ratio: 0.025

Although this value is already satisfactory as it equates the highest  $R_s$  ratios of the existing ultra-high precision robots (see section 5.1), further directions to improve the prototype compactness will be outlined in the discussion which closes this chapter (section 6.5).

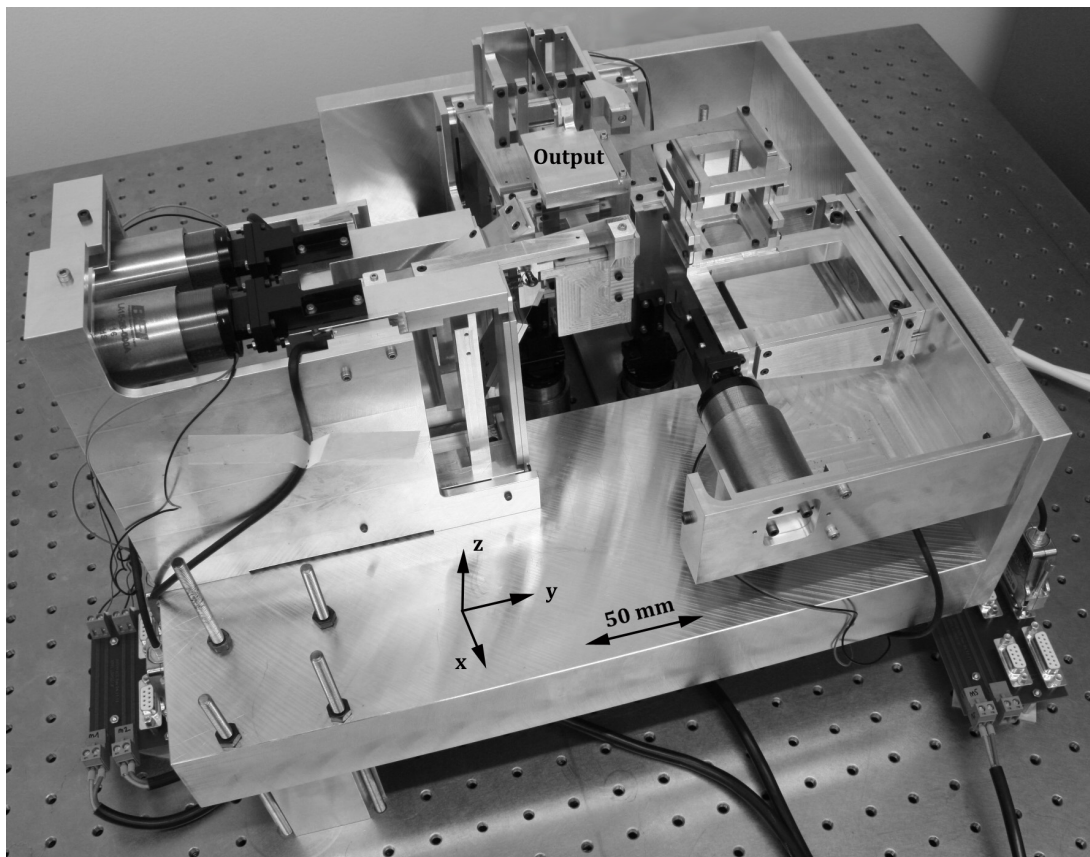


Figure 6.17: *Legolas 5 prototype*

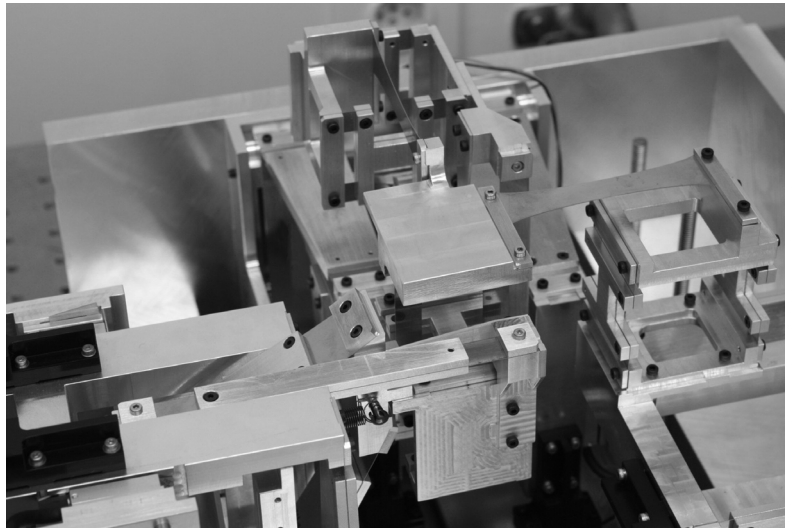


Figure 6.18: Detailed view of the Legolas 5 end-effector and passive bricks

#### 6.3.4.1 Force alignment

Force alignment consists in a crucial aspect of the robot prototype development, which aims at minimising parasitic deformations of the flexure-based mechanisms when forces or moments are applied to the end-effector. These can either be external, *i.e.* occur when the robot is performing a task, or result from the actuation of the degrees of freedom. Moreover, as compactness and design efficiency requirements do generally not permit to align all force lines, a thorough analysis must be performed to identify the mechanisms which are the most sensitive to parasitic effects. In the case of the Legolas 5 prototype, these consist in the passive bricks, which consequently need to be carefully aligned, whereas the active bricks design and arrangement must minimise the amplitude of the parasitic movements. This aim is achieved by taking this problematic into account during both the design and assembly processes:

- **Passive bricks:**

- *Assembly:* the torsion axis of the brick leaf spring is aligned with the rotation axis of the robot, which is defined by the RCM of the corresponding active brick (see figures 6.19 and 6.20). Note that if the function of the leaf spring torsion is to remove an overconstraint, the position of the axis can be freely chosen; this situation occurs in the X-side kinematic chain of the prototype. On the other hand, the flexion of the passive brick leaf spring being less sensitive to misalignments, the position of its axis does not need to be coincident with the end-effector rotation axis.
- *Design:* the position of the passive brick leaf spring is selected to avoid parasitic moments on the 4-hinge table: consequently, its clamping is located at middle-length of the table arms [35] (see figure 6.9). This situation is included in both

Y-side (figure 6.19) and X-side chains (figure 6.20). Note that this optimisation has not been performed in the Z-side chain passive brick due to compactness limitations.

- **Active bricks:** as detailed in section 6.3.1.3, the  $T_{\parallel}R_{\perp}$  active brick design principle is composed of three planes which are arranged in parallel; the middle plane, which includes the RCM mechanism, is the most sensitive to force misalignment. Indeed, the whole robot performances are deteriorated if the rotation axis position is inaccurately defined because of parasitic displacements. Consequently, the following solutions are implemented:
  - *Assembly:* minimise the orthogonal distance between the end-effector and the RCM mechanism to limit the effect of parasitic forces and moments
  - *Design:* expand the breadth of the actuation 4-hinge tables leaf springs in order to increase the transverse stiffness of these mechanisms [6]

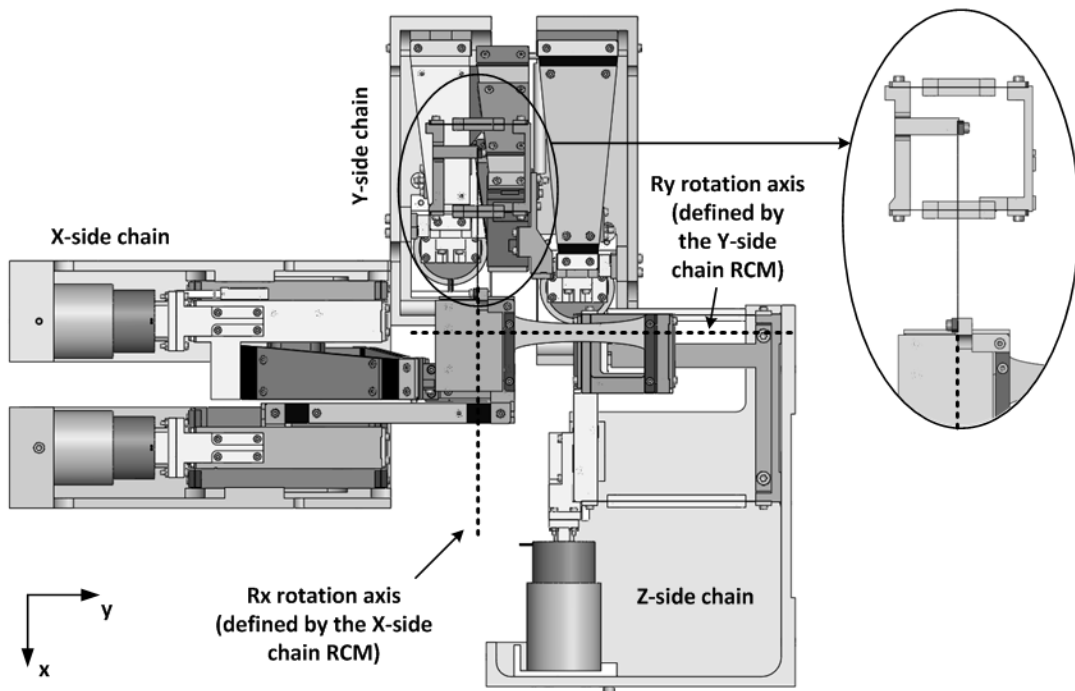


Figure 6.19: Top view of the Legolas 5 prototype, highlighting the forces alignment of the bricks

## 6.4 Characterisation and results

This section details the measurements performed on the Legolas 5 prototype: first, the individual characterisation of the actuation sub-bricks is presented, allowing to estimate the

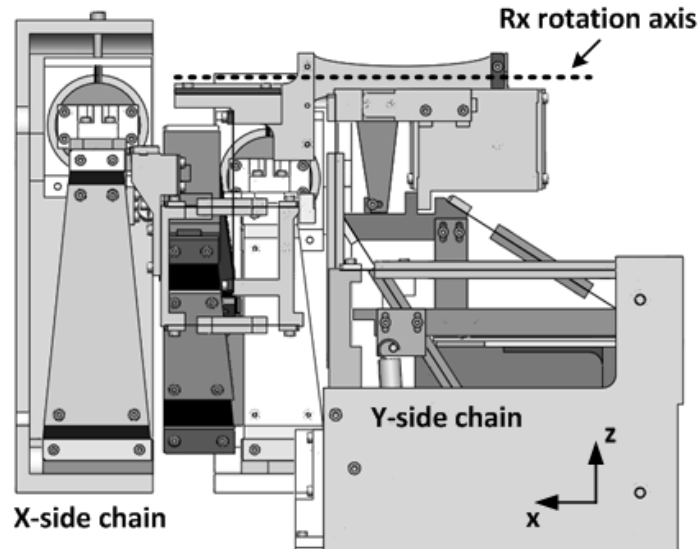


Figure 6.20: Right view of the Legolas 5 prototype; the Z-side chain has been removed for clarity purposes

accuracy of the theoretical model which has been used for their design. Then, crucial performances of the Legolas 5, such as workspace, resolution, repeatability and eigenfrequencies, are evaluated.

#### 6.4.1 Actuation sub-bricks

The aim of the actuation sub-bricks characterisation is to evaluate the efficiency of the simplified theoretical model presented in section 5.2.1.1 to design these flexure-based mechanisms. To achieve this goal, each sub-brick is individually assembled in its final position on the robot main frame, thus allowing the following measurements:

- **4-hinge table stiffness:** the sub-brick sensor allows to read the position of the guiding system while a force is exerted by the actuator; the value of the latter is obtained by monitoring the current injected in the coil.
- **4-hinge table maximum parasitic displacement  $\lambda$ :** this parameter is quantified thanks to a SIOS® SP-2000 laser interferometer (resolution: 1.24 nm, wavelength: 633 nm, stroke: 2 m) [86] and a mirror cube (material: Zerodur®, volume: 30 x 30 x 30 mm<sup>3</sup>, weight: 68 g); the resolution of the measurement, which is limited by the flatness of the mirror surface, is approximately 30 nm. Furthermore, as the mechanical design of all single translation and combined translation and rotation tables are respectively identical, this parameter has only been quantified on one of each type of 4-hinge tables. Figure 6.21 illustrates the measurement setup.

Lastly, note that for these measurements, the zero-stroke of the guiding systems corresponds to the mechanical stop which causes the maximal insertion of the actuator coil.



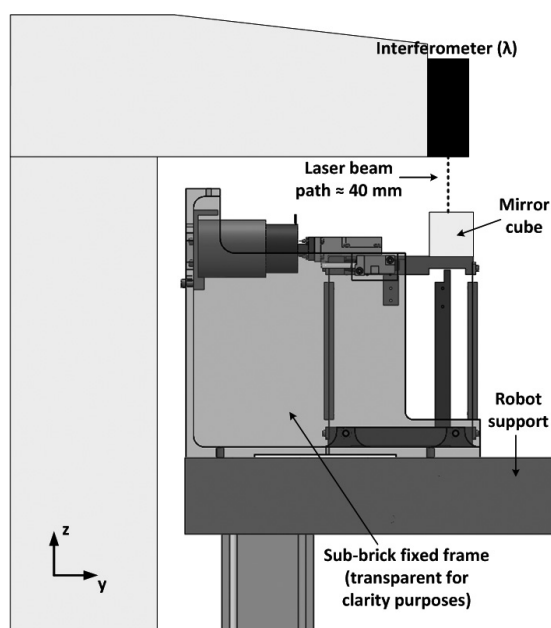


Figure 6.21: Measurement setup for the quantification of the parasitic displacement  $\lambda$  of the combined translation and rotation actuation table

#### 6.4.1.1 Single translation actuation sub-bricks

As a reminder, the simplified model which has been used to design these mechanisms predicts a **stiffness of 365 N/m** and a **maximum parasitic displacement  $\lambda$  of 169.9  $\mu\text{m}$**  (see table 6.2).

- ***Tx actuation table (Z-side kinematic chain)***: the measured stiffness of this 4-hinge table presented in figure 6.22 confirms the linearity of the relation between the guiding system position and the applied force.

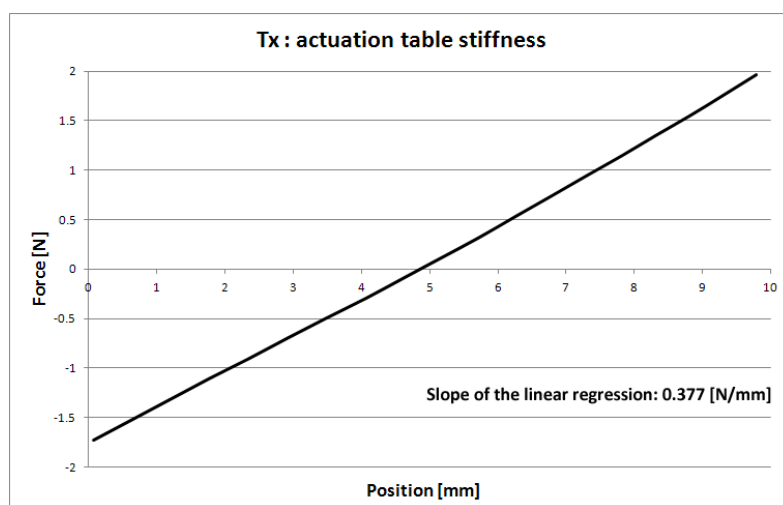


Figure 6.22: Measured stiffness of the Tx actuation sub-brick table (Z-side chain)

Furthermore, the linear regression performed on these measurements accepts a slope value of 377 N/m; the theoretical and real values of the table stiffness thus present a discrepancy of only 3%. As for the maximal parasitic displacement  $\lambda$ , the measured value of 170  $\mu\text{m}$  fits the model with an error of less than 1%.

- ***T<sub>y</sub> actuation table (X-side kinematic chain):*** in the case of this 4-hinge table, gravity acting on the mechanism mobile parts creates a compression force on the leaf springs; the stiffness of the table is expected to be lower to the model estimation, which is valid only if no traction/compression force is applied to the table. Furthermore, [35] demonstrates that the guiding system stiffness varies approximately linearly with this external force: performing a measurement with gravity creating a traction force on the same sub-brick and computing the average stiffness value of the two situations should allow to match the model estimation. Figure 6.23 presents the quantified stiffness of the table in the robot normal position (gravity in compression), differing of 11.5% with the theoretical value, whereas figure 6.24 illustrates the second measurement (gravity in traction) force/position graph. The averaged stiffness is thus equal to 352.5 N/m, presenting a discrepancy of 3% with the model estimation. Lastly, the table stiffness has been evaluated in a position where gravity does not create any traction / compression force in the leaf springs: the obtained value is 367 N/m, which differs of less than 1% with the theoretical value.

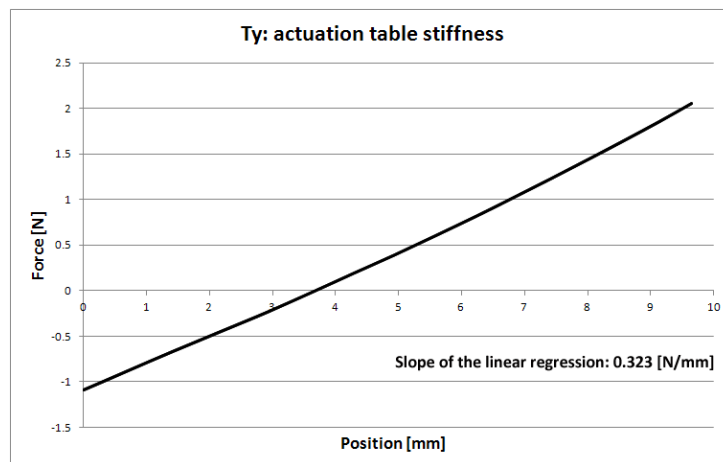


Figure 6.23: Measured stiffness of the  $T_y$  actuation sub-brick table (X-side chain)

- ***T<sub>z</sub> actuation table (Y-side kinematic chain):*** as this sub-brick actuates a vertical translation, a traction spring, presenting a stiffness of 254 N/m, counterbalances the effect of gravity by acting in parallel with the 4-hinge table. Figure 6.25 illustrates the measured force/position ratio of the whole mechanism: the latter matches the theoretical value, obtained by adding the stiffnesses of the spring and of the table, with an error of 9%.

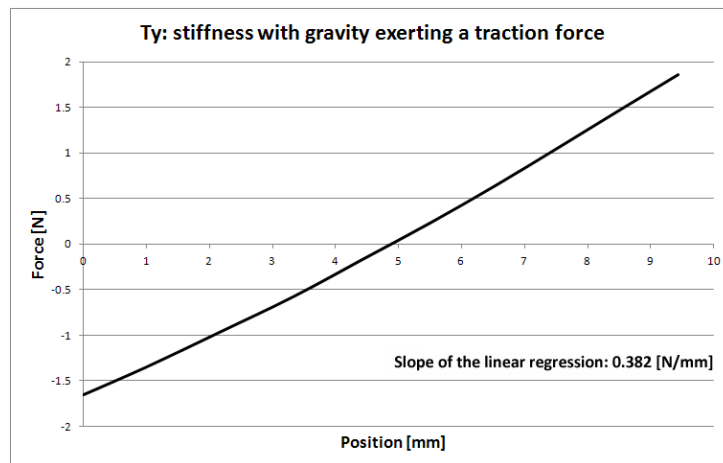


Figure 6.24: Measured stiffness of the Ty actuation table with gravity exerting a traction force

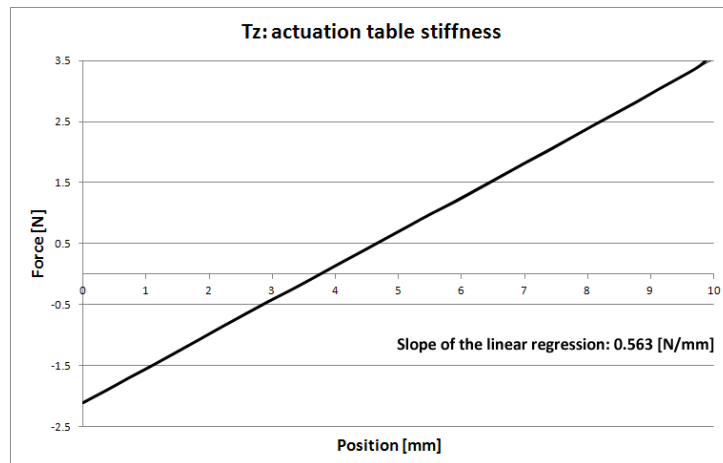


Figure 6.25: Measured stiffness of the Tz actuation sub-brick table (Y-side chain)

### 6.4.1.2 Translation and rotation actuation sub-bricks

As a reminder, the simplified model which has been used to design these mechanisms predicts a **stiffness of 228 N/m** and a **maximum parasitic displacement  $\lambda$  of 531.5  $\mu\text{m}$**  (see table 6.2).

- ***Ty/Rx actuation table (X-side kinematic chain):*** The measured stiffness of this sub-brick, illustrated in figure 6.26, presents a non-linearity which is more pronounced than in the case of the single translation sub-bricks.

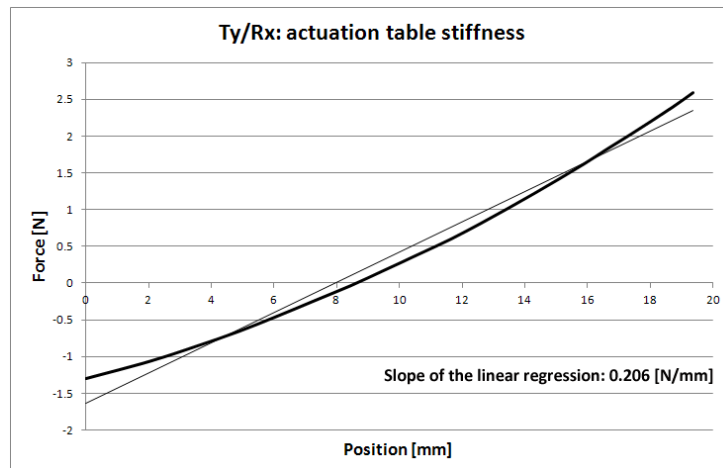


Figure 6.26: Measured stiffness of the Ty/Rx actuation sub-brick table (X-side chain): linear regression on the full stroke

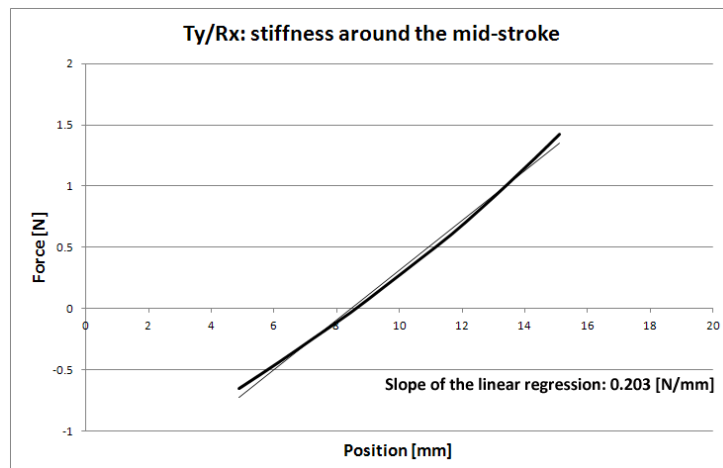


Figure 6.27: Measured stiffness of the Ty/Rx actuation sub-brick: linear regression around the mid-stroke

Consequently, the stiffness of the mechanism is evaluated by computing a linear regression around the mid-stroke point (see figure 6.27). In the case of this Ty/Rx table,

the resulting stiffness value is 203 N/m, which consists in a 11% error compared to the model estimation. The gravity acting on the table, thus exerting a compression force on the leaf springs, can account for this difference. Furthermore, a second stiffness measurement has been performed without the actuator, the force being applied on the mechanism with successive weights of 20 g each. The obtained force/position characteristics is linear, which shows that the simplified model is adequate to estimate the stiffness of the 4-hinge table. The non-linearity thus results from the actuation, potentially because of a force constant which varies with the actuator stroke. Nonetheless, as in the Legolas 5 prototype, the closed-loop will control the position of the actuation sub-brick, this effect will be considered within the control algorithm. Lastly, the measured value of the maximal parasitic displacement  $\lambda$ , namely 533  $\mu\text{m}$ , fits the model with an error of less than 1%.

- ***Tz/Ry actuation table (Y-side kinematic chain):***

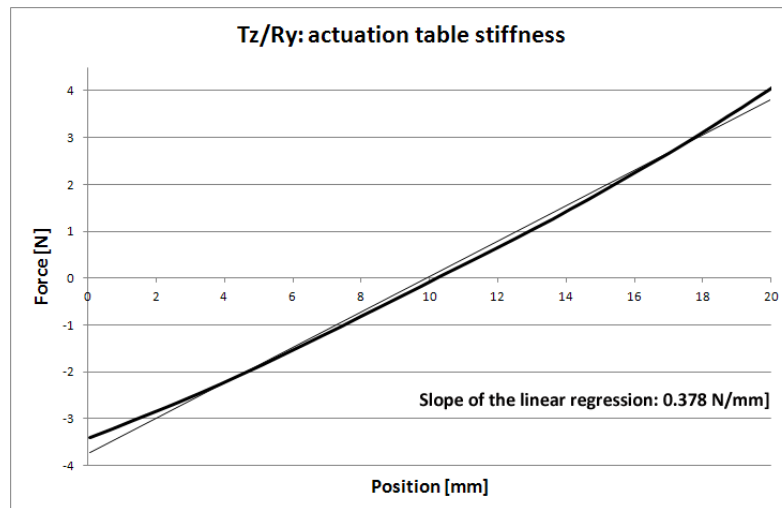


Figure 6.28: Measured stiffness of the Tz/Ry actuation sub-brick table (Y-side chain): linear regression on the full stroke

As this sub-brick actuates a vertical translation, a traction spring, presenting a stiffness of 140 N/m, counterbalances the effect of gravity by acting in parallel with the 4-hinge table. Figures 6.28 and 6.29 illustrate the measured force/position ratio of the whole mechanism: the latter matches the theoretical value, which is obtained by adding the stiffnesses of the spring and of the table, with an error of 1%.

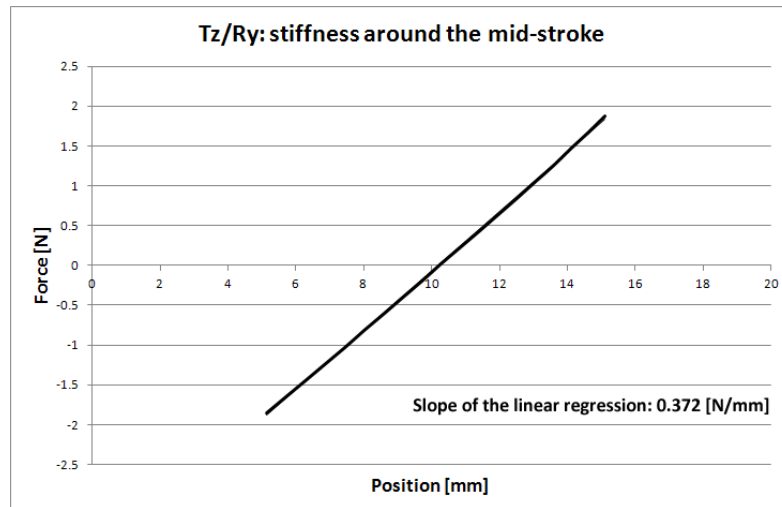


Figure 6.29: Measured stiffness of the  $T_z/R_y$  actuation sub-brick table ( $Y$ -side chain): linear regression around the mid-stroke

In conclusion of this section, the characterisation of the actuation sub-bricks experimentally validates the applicability of the simplified model to design the flexure-based 4-hinge tables. Indeed, both the stiffness and the maximal parasitic displacement present differences of less than 11% between the measured and theoretical values. This discrepancy is even lower when no traction/compression force due to gravity is exerted on the 4-hinge tables leaf springs. Consequently, the simplified theoretical model presented 5.2.1.1 is proven to be a useful tool for the design of the actuation sub-bricks.

### 6.4.1.3 Eigenfrequencies

Lastly, the eigenfrequency characterisation of the actuation sub-bricks is performed to allow for a correct analysis of the whole Legolas 5 prototype dynamic performances. The two lowest, and consequently most detrimental vibration modes of 4-hinge tables consist in transverse flexion and torsion (see figure 6.30); the selected design of the leaf spring geometry, as detailed in section 6.3.4.1, is highly advantageous as it simultaneously increases the transverse stiffnesses and eigenfrequencies.

The vibration measurement system is composed of an impact hammer (Brüel & Kjær, Type 8206-002) and a unidirectional accelerometer (Brüel & Kjær, DeltaTron<sup>®</sup> Accelerometer 4507, weight: 4.8 g), which is fixed to the output of the actuation sub-brick; the acquisition software then provides the amplitude of the mechanism response in a frequency bandwidth of 2 kHz. Table 6.3 summarises the results obtained for the five actuation sub-bricks. Note that the slight variations in the values of the three single translation tables, as well as of both combined translation and rotation tables, are caused by differences in the output design, which increase or decrease the moving mass of the mechanisms.

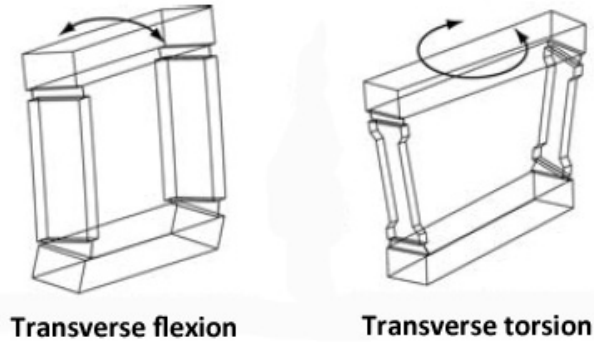


Figure 6.30: Two lowest vibration modes of the 4-hinge table [6]

Actuation table	Transverse flexion frequency	Transverse torsion frequency
Tx	140 Hz	270 Hz
Ty	135 Hz	252.5 Hz
Tz	147.5 Hz	302.5 Hz
Ty/Rx	160 Hz	300 Hz
Tz/Ry	137.5 Hz	292.5 Hz

Table 6.3: Two lowest eigenfrequencies of each actuation sub-brick

## 6.4.2 Legolas 5 prototype

The closed-loop characterisation of the full Legolas 5 prototype is now performed, allowing to measure its workspace, resolution, repeatability, and eigenfrequencies. The position of each robot actuator is controlled with a PID (proportional-integral-derivative) algorithm presenting a sampling period of 500  $\mu$ s. Note that the zero-position of the robot is defined as the middle of its workspace, which corresponds to the middle-stroke of each of its actuators.

### 6.4.2.1 Workspace

As the Legolas 5 robot includes three theoretically decoupled kinematic chains and no singularity in its workspace, this characterisation can be performed for each chain separately. Furthermore, the translations are measured at the level of the actuators, as their motion is directly transmitted to the end-effector, whereas the rotations are evaluated thanks to a Schae-vitz Sensors Accustar inclinometer (Measurement Specialities<sup>TM</sup> [56],  $\pm 20^\circ$  stroke,  $0.01^\circ$  resolution, figure 6.31), which is glued on the robot end-effector and allows to cover the whole range of these displacements.

- ***X-side kinematic chain: Ty, Rx motions:***

The workspace of this kinematic chain is estimated by varying the positions of both



Figure 6.31: Schaevitz Sensors AccuStar inclinometer (Measurement Specialities<sup>TM</sup> [56],  $\pm 20^\circ$  stroke,  $0.01^\circ$  resolution); the mounting including three spheres allows to precisely position the measurement device on the robot output. [54]

actuators and by measuring the resulting  $T_y$  translation and  $R_x$  rotation: figure 6.32 shows the obtained results. Note that the translation is set by the position of the low-stroke sub-brick, whereas the rotation angle is determined by the difference between the position of both actuators. In the Legolas 5 prototype, the maximal value of this difference has been set to 5 mm, allowing to fulfill the specifications by simultaneously achieving a 5 mm translation and a  $10^\circ$  rotation. This workspace is represented in dark grey on figure 6.32, right. Nonetheless, without this limitation, all combinations of actuator positions are achievable (area in light grey on figure 6.32, right). Furthermore, the maximal angles (white dots on this figure) can be achieved without mechanical interference and have been estimated to  $-16.5^\circ$  and  $17^\circ$  respectively. Note that the linearity of the relation between the actuators position difference and the rotation angle is not valid anymore at those points: the high constraints in the leaf springs, which have not been designed to achieve such angles, can first account for this observation. Furthermore, the deformation of the leaf spring which creates the moment (see figure 6.11, left) does not allow an efficient transmission of the actuation force anymore at these extreme positions. Consequently, the rotation angles of the Legolas 5 prototype will be limited to  $\pm 10^\circ$  for further use.

- ***Y-side kinematic chain:  $T_z$ ,  $R_y$  motions:***

Figure 6.33 illustrates the  $T_z$  translation and  $R_y$  rotation strokes resulting from the variation of the actuators positions. As in the previous case, the maximal achievable angles reach  $\pm 15^\circ$ , but will be limited to  $\pm 10^\circ$  (dark grey area on figure 6.33, right) to guarantee the elasticity of the leaf springs deformations.

- ***Z-side kinematic chain:  $T_x$  motion:***

The stroke of the  $T_x$  translation can be straightforwardly evaluated by measuring the extent of the motion at the level of the actuation sub-brick, which consists in a 9.998 mm stroke, limited by the machining tolerances of the mechanical stop.



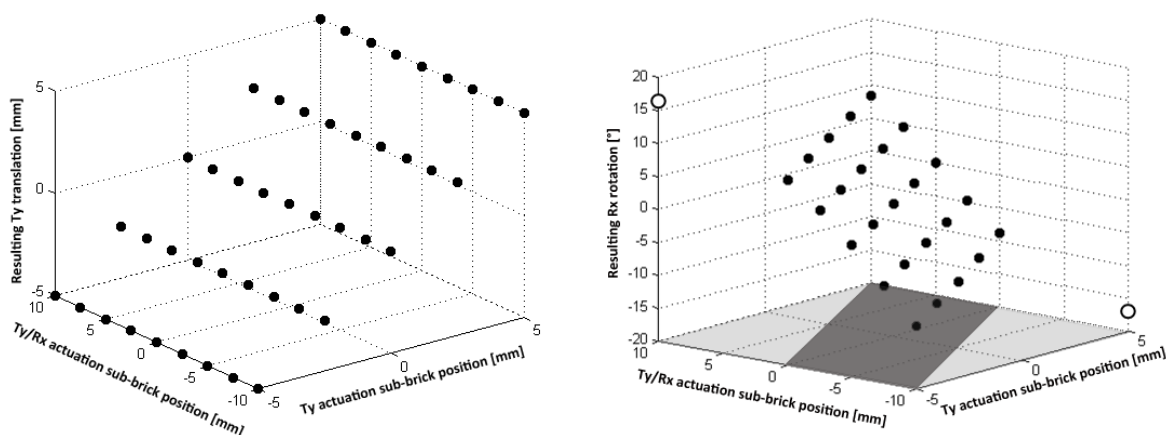


Figure 6.32: *Ty translation (left) and Rx rotation (right) as a function of the relative displacements of the two brick actuators*

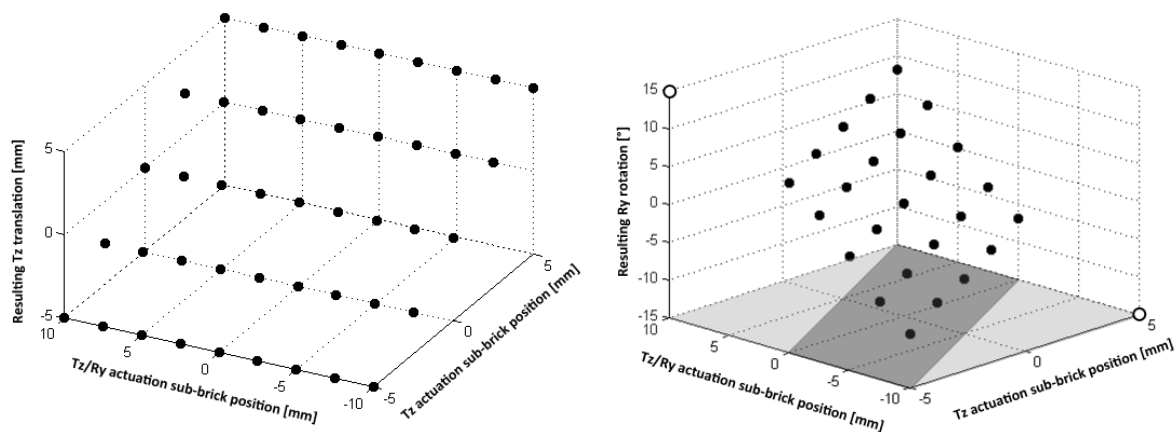


Figure 6.33: *Tz translation (left) and Ry rotation (right) as a function of the relative displacements of the two brick actuators*

In conclusion, the workspace characterisation of the Legolas 5 prototype shows that the requirements are fulfilled, as combined strokes of  $\pm 5$  mm for the translations and  $\pm 10^\circ$  for the rotations can be achieved. Furthermore, the real maximal strokes values simultaneously reach  $\pm 15^\circ$  and  $\pm 5$  mm without mechanical interference; nonetheless, these positions cause high stresses in the leaf springs, which have not been designed to achieve such high angles, and will not be allowed in this Legolas 5 prototype.

### 6.4.2.2 Resolution and repeatability

This section is dedicated to the quantification of the resolution and repeatability of each of the Legolas 5 degrees of freedom, which is performed by applying a desired position profile to the actuators and by measuring the resulting motion on the robot end-effector. Note that the minimal achievable values are limited by the proprioceptive sensor resolution, which is 50 nm for the Legolas 5 (see section 1.2.2).

The measurement system is composed of the interferometer and mirror cube described in section 6.4.1 for the translations, whereas a Newport LDS-1000 autocollimator ([67], 0.02" resolution,  $\pm 400''$  stroke) is used to quantify the rotations (see figures 6.34 and 6.35). Note that the interferometer includes a moving average algorithm which filters the measurement noise: in consequence, the graphs presented in the following paragraphs illustrate the average position of the end-effector.

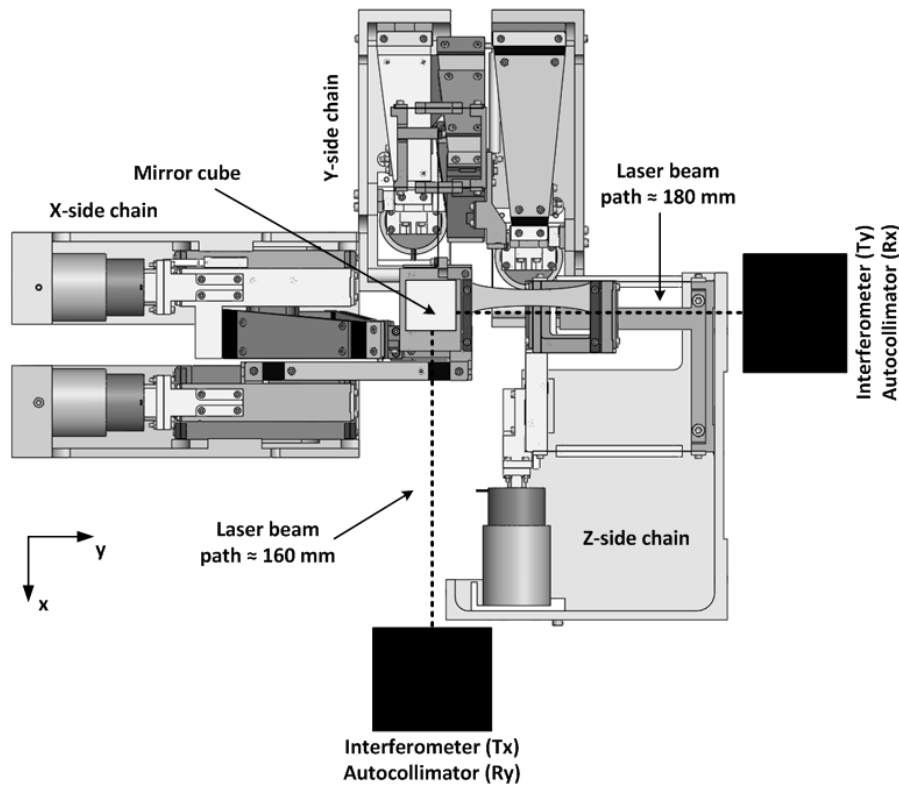


Figure 6.34: Measurement setup for the quantification of the resolution and repeatability of  $T_x$ ,  $T_y$ ,  $R_x$  and  $R_y$

Furthermore, the resolution is evaluated by applying steps of 50 nm around a central position to the actuation system; varying the latter allows to verify that the degree of freedom resolution is constant on its whole stroke. The control algorithm ensures that the position of the actuation sub-brick oscillates between  $\pm 50$  nm (with punctual higher peaks), with a mean value which is always lower than the sensor resolution. As for the repeatability, its evaluation consists in alternating between two actuation sub-brick positions distant of 2 mm,

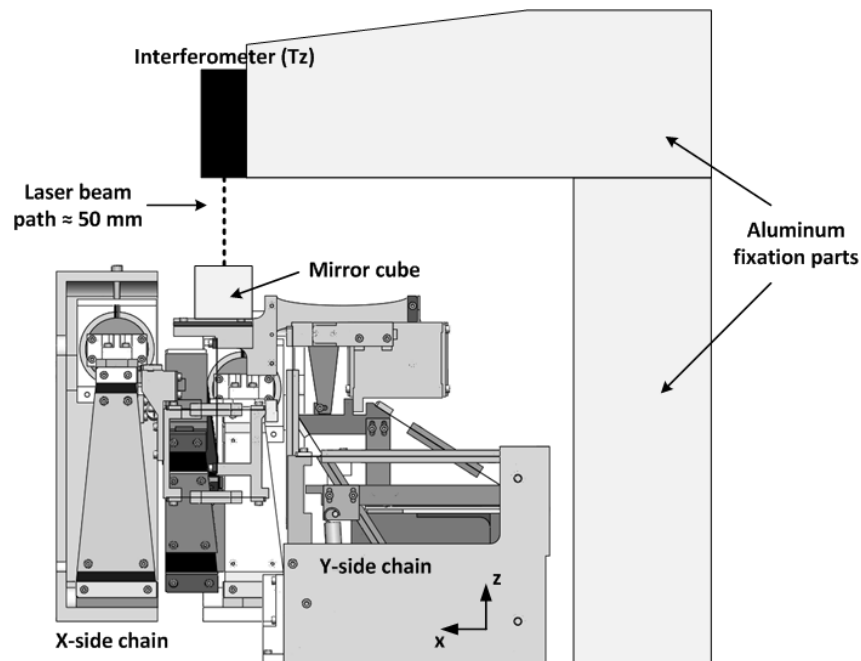


Figure 6.35: Measurement setup for the quantification of the resolution and repeatability of  $T_z$

which corresponds to an end-effector displacement of around 2 mm and  $4^\circ$  (see figure 6.36, middle). As in the case of the resolution, the central position can be changed to check the constancy of the repeatability over the whole motion stroke.

- ***T<sub>x</sub> translation:***

Figure 6.36 illustrates the obtained results for the  $T_x$  translation: the resolution graph (top) shows that steps of 50 nm can clearly be distinguished at the level of the robot end-effector, whereas the repeatability graph (centre and bottom) presents values which are below the sensor resolution. Note that the oscillations on the constant position areas, which represent the mean position error, present values which are below the sensor resolution and similar to the mean position error evaluated at the level of the actuation. Finally, these measurements have been performed at five different positions of the  $T_x$  translation motion and exhibit similar results, thus proving that both the resolution and the repeatability are constant over the whole stroke.

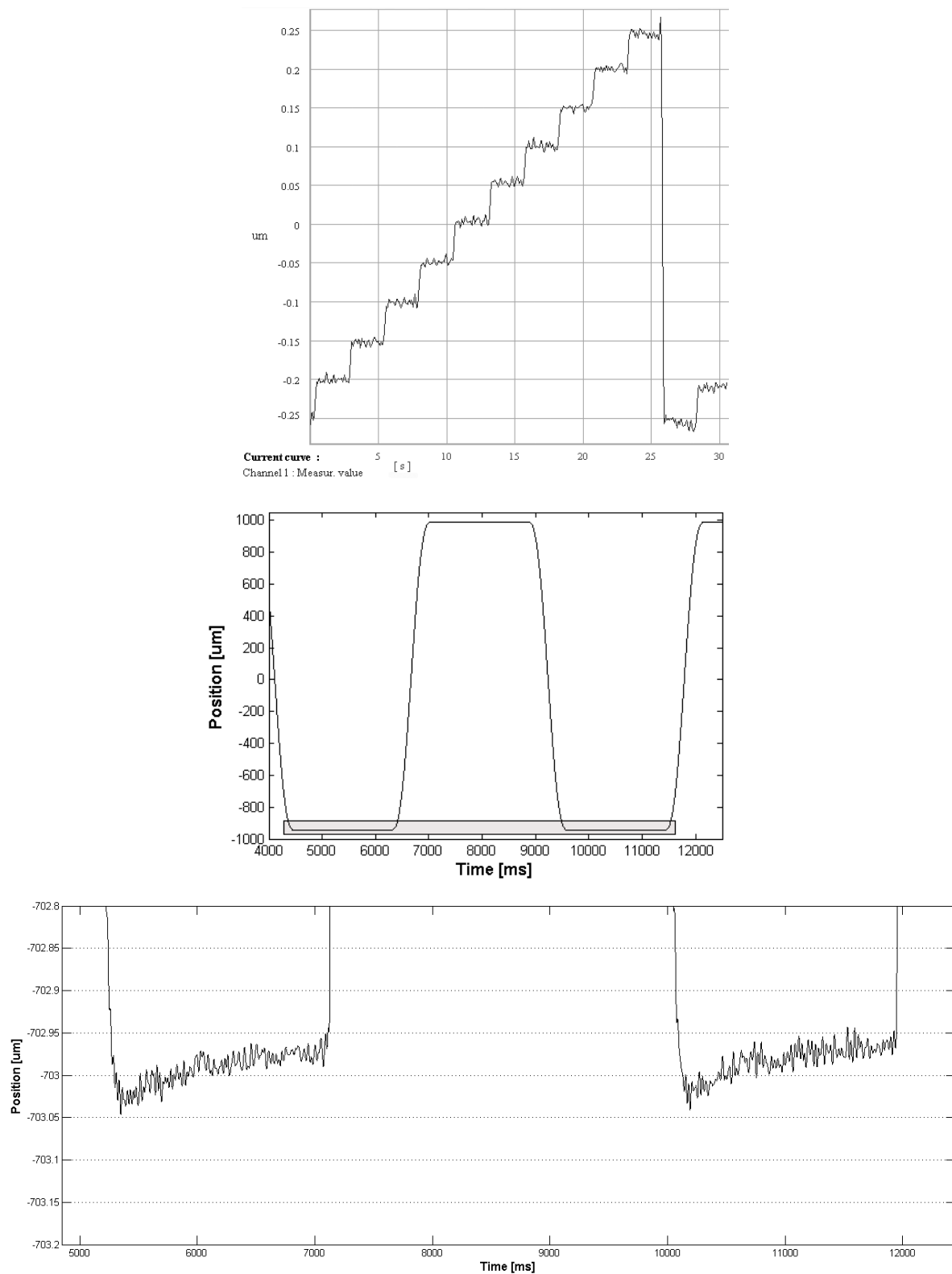


Figure 6.36: *Top: resolution evaluation of the Tx translation; middle: position profile of the repeatability measurement; bottom: detailed view of two consecutive steps, allowing to evaluate the repeatability of the Tx translation. Note that the position drift mainly results from the increase of the air temperature on the laser beam path, which is caused by the Tx actuation (see figure 6.34)*

- ***Ty translation:***

Figure 6.37 illustrates the obtained results for the Ty translation, which are similar to the previously detailed Tx translation measurements.

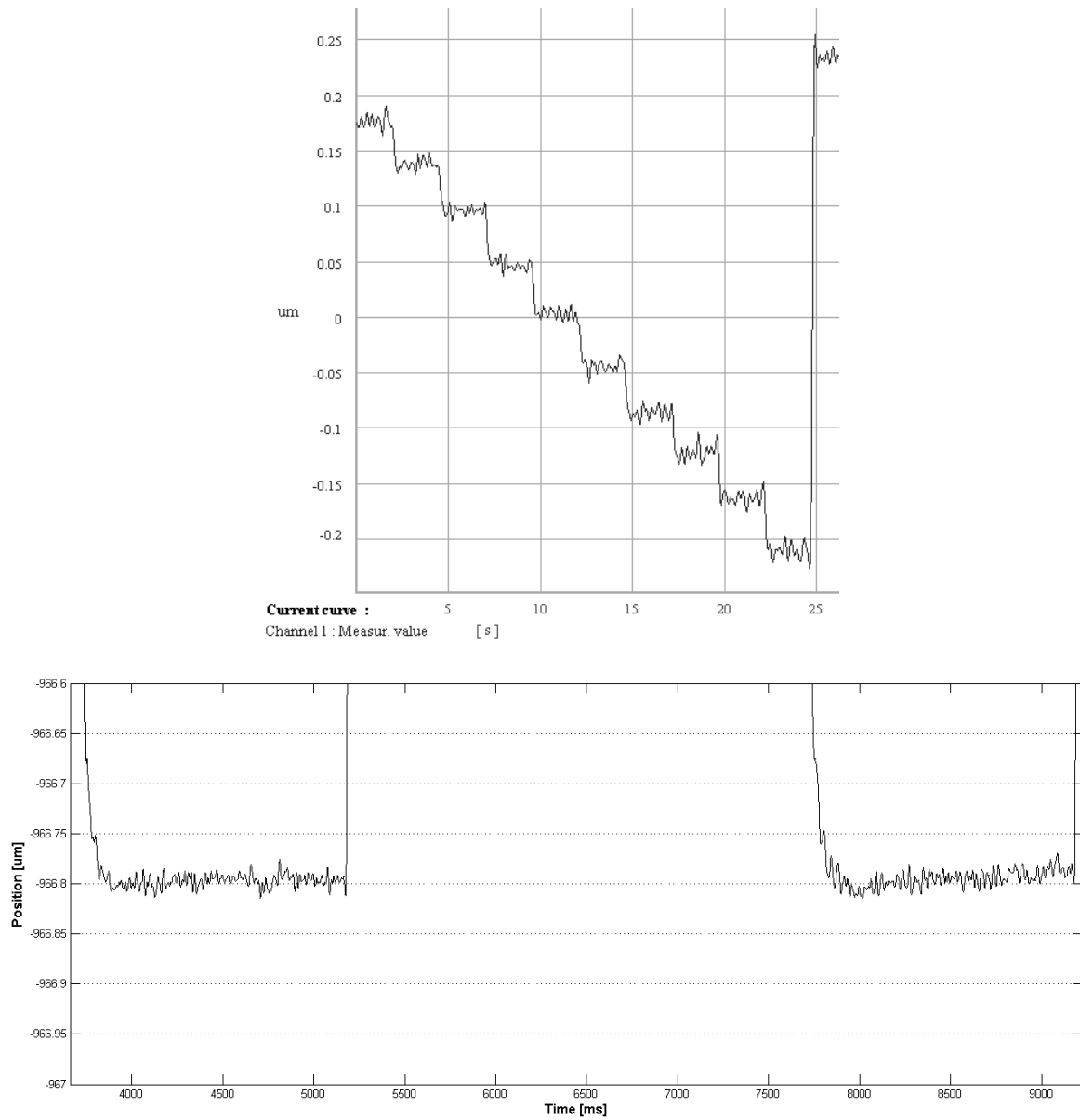


Figure 6.37: Resolution (top) and repeatability (bottom) evaluations of the Ty translation

- ***Tz translation:***

Figure 6.38 illustrates the obtained results for the Tz translation, which are similar to the other translations measurements.

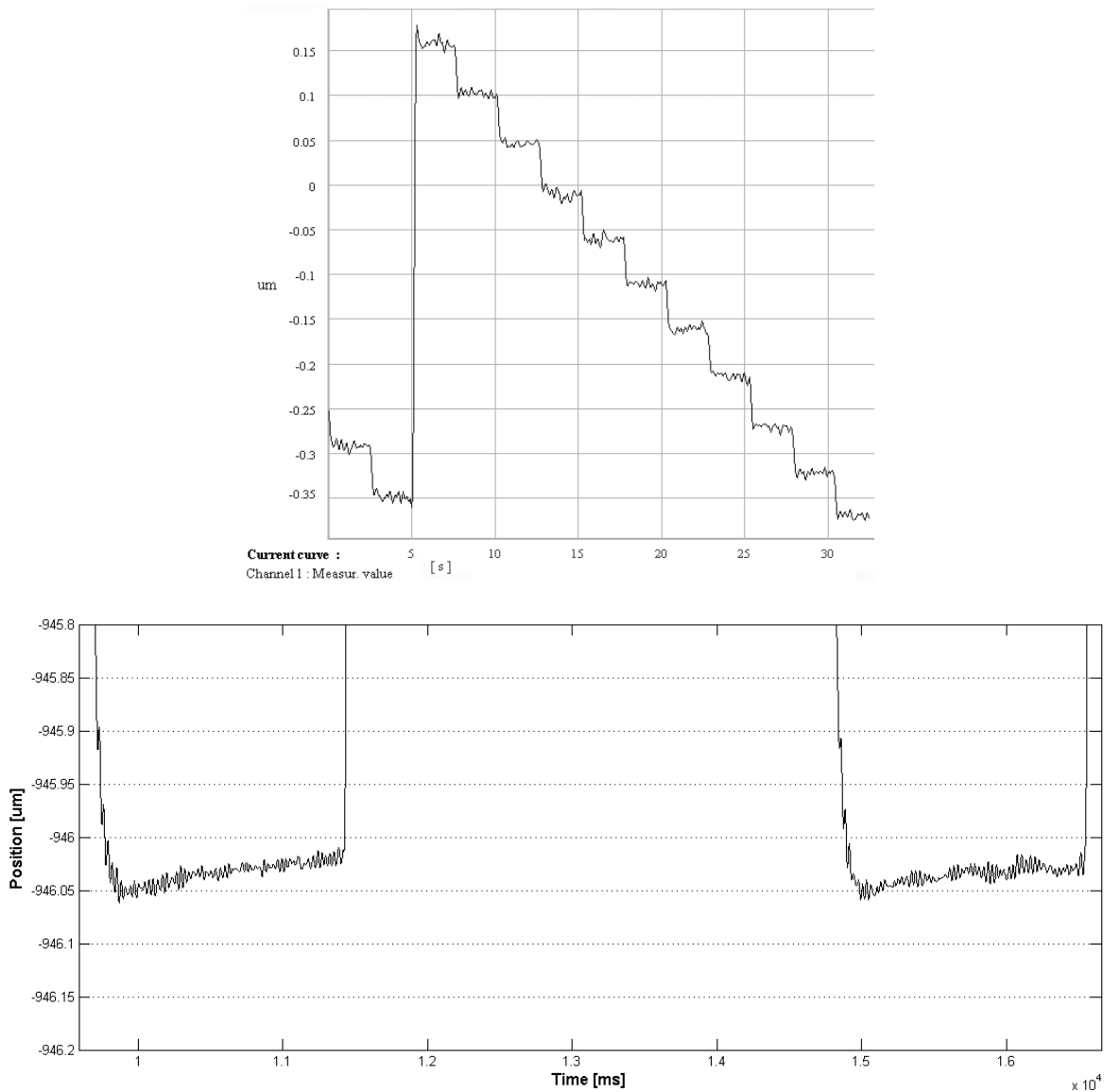


Figure 6.38: Resolution (top) and repeatability (bottom) evaluations of the  $T_z$  translation

- ***R<sub>x</sub> rotation:***

Figure 6.39 illustrates the raw measurements of the  $R_x$  rotation resolution, whereas figure 6.40 presents the same data, which have been filtered by means of a moving average algorithm: steps of 50 nm at the level of the actuator result in rotations of  $0.35''$  ( $1.7 \mu\text{rad}$ ) on the end-effector, thus defining the resolution of this  $R_x$  motion. Furthermore, the graph of the non-filtered data allows to highlight the real end-effector position, which oscillates with amplitudes lower than  $\pm 0.35''$ : these correspond to the  $\pm 50$  nm (with punctual higher peaks) position error caused by the sensor resolution.

As for the repeatability of the Rx rotation, figure 6.41 illustrates the raw and filtered measurements: this allows to underline that both the amplitude of the non-filtered oscillations and the repeatability of the motion stay below the estimated resolution.

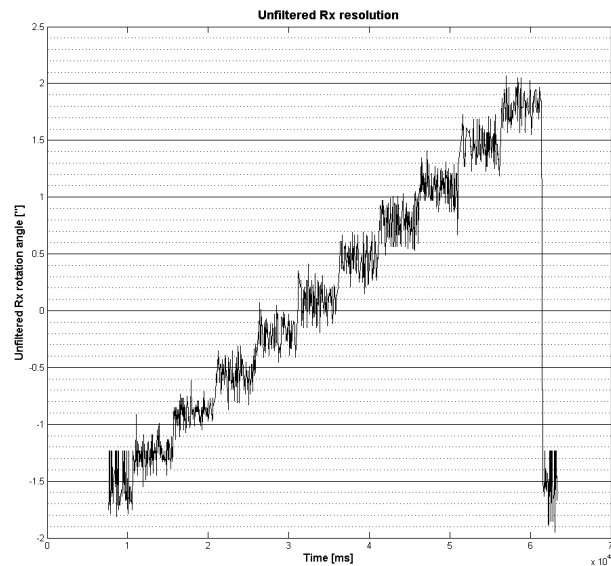


Figure 6.39: *Unfiltered resolution of the Rx rotation*

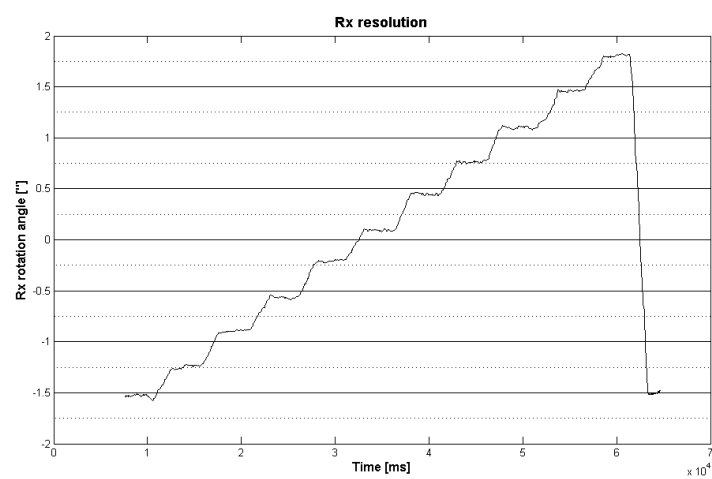


Figure 6.40: *Filtered (moving average algorithm) resolution of the Rx rotation*

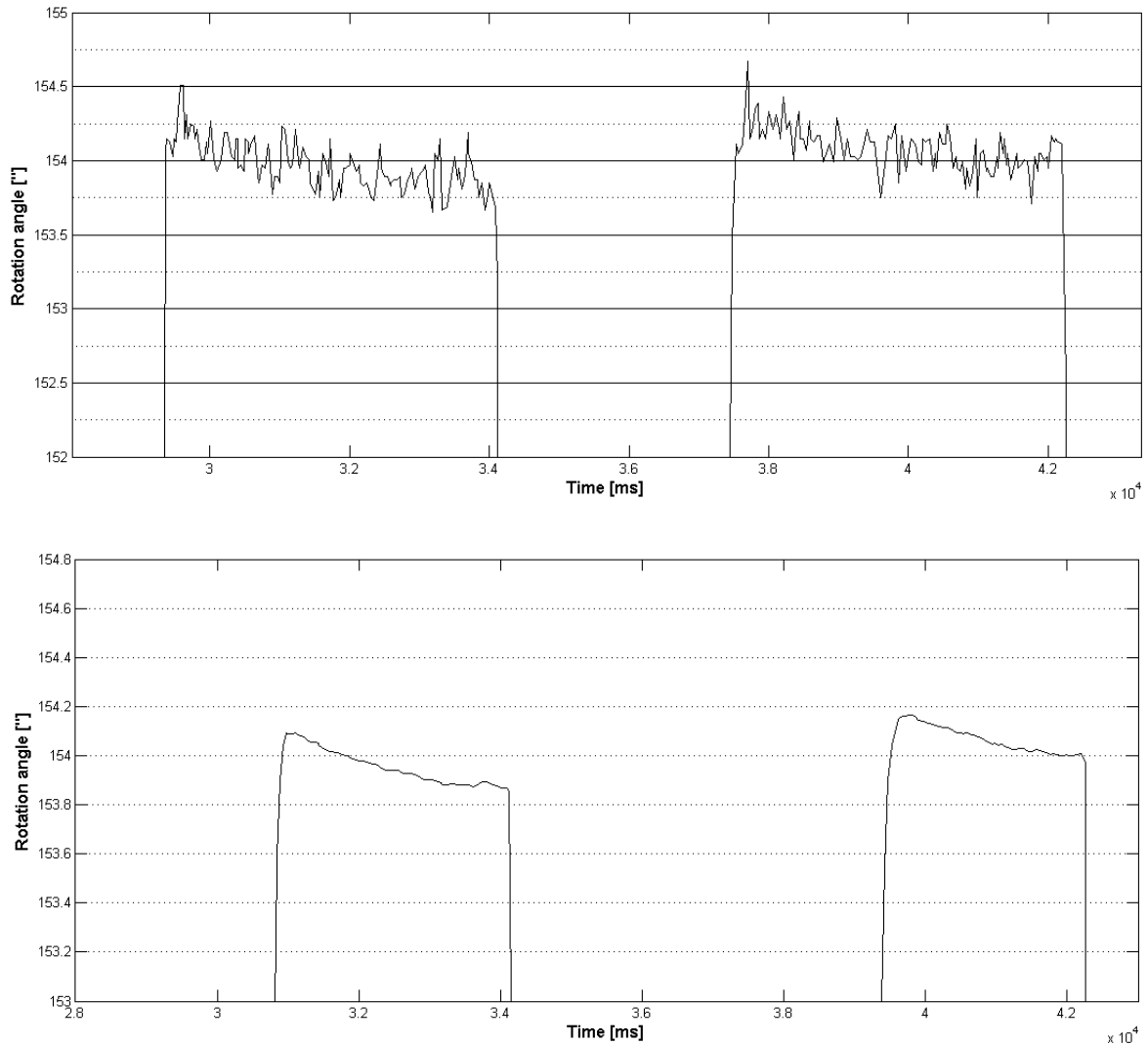


Figure 6.41: *Unfiltered (top) and filtered (bottom) repeatability of the Rx rotation*

- ***Ry rotation:***

The quantification of the Ry resolution and repeatability exhibit similar results as the previously detailed motion. Figures 6.42 and 6.43 present the graphs of the raw and averaged measurements, allowing to estimate the resolution of this rotation to  $0.39''$  ( $1.9 \mu\text{rad}$ ) and to prove that the repeatability stays below this value.

In conclusion, the characterisation of the resolution and repeatability of each motion of the Legolas 5 prototype proves that the requirements are fulfilled: these quantities achieve values of 50 nm and  $1.9 \mu\text{rad}$ , which correspond to the sensor resolution.



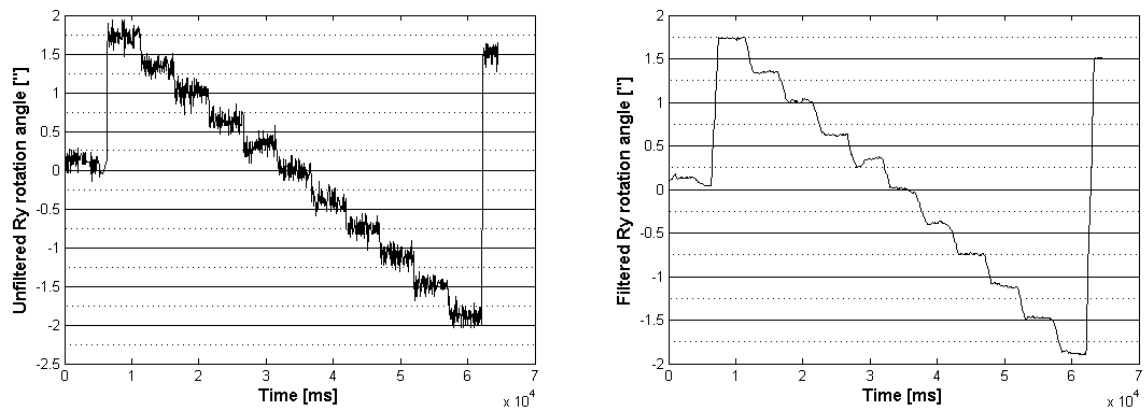


Figure 6.42: Raw (left) and averaged (right) measurements of the Ry rotation resolution

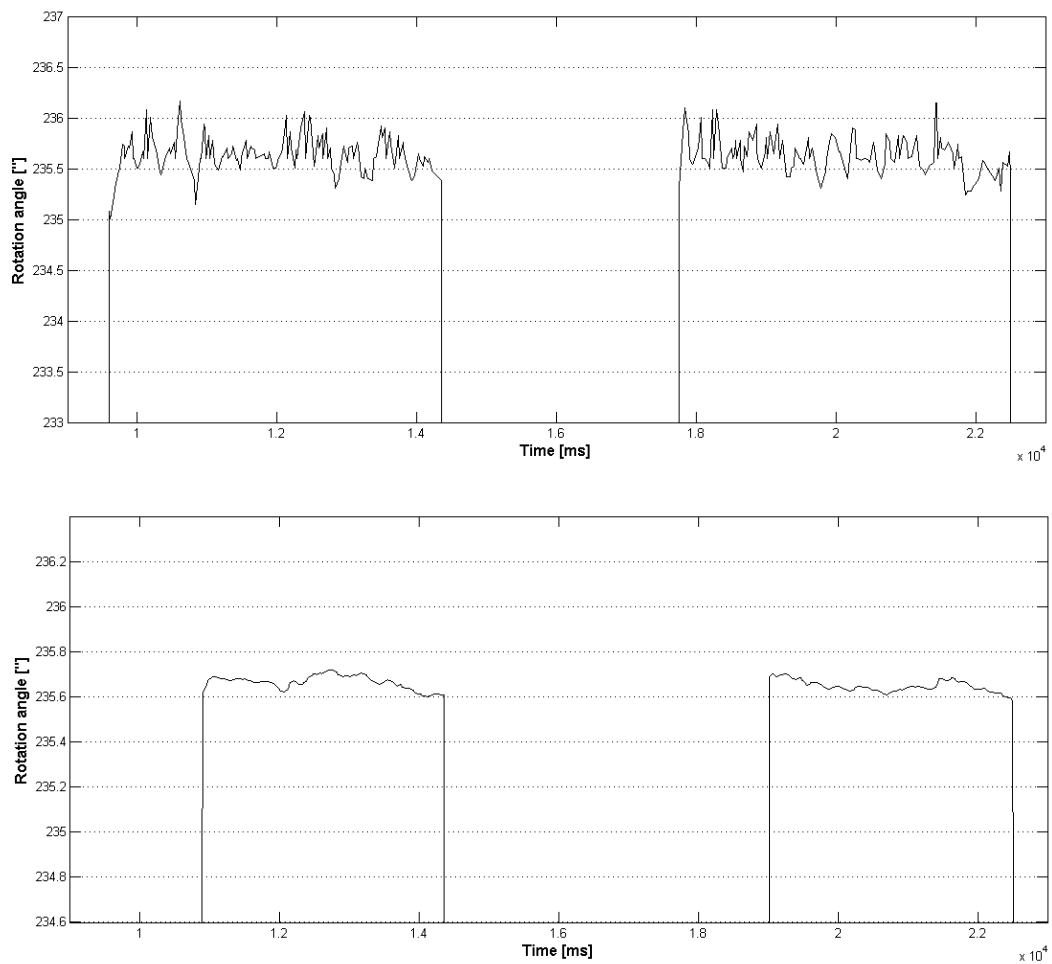


Figure 6.43: Raw (top) and averaged (bottom) measurements of the Ry rotation repeatability

### 6.4.2.3 Eigenfrequencies

The quantification of the Legolas 5 eigenfrequencies allows to estimate its dynamical performances and to detect potential weaknesses in the mechanical design. The latter are liable to generate low vibration modes, thus deteriorating the behaviour of the robot at high accelerations. The same measurement system as described in section 6.4.1.3 is used, with the accelerometer fixed to the Legolas 5 end-effector. Figures 6.44 to 6.46 illustrate the obtained results. Furthermore, the analysis of these graphs in the light of the previous actuation sub-bricks dynamic characterisation allows to identify the sources of the lowest vibration modes:

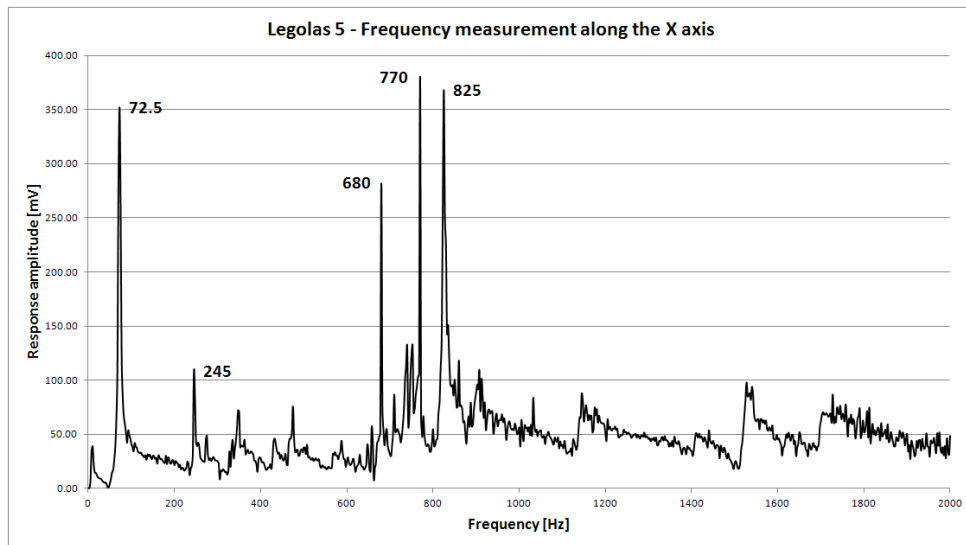


Figure 6.44: Frequency measurement of the Legolas 5 prototype along the X axis

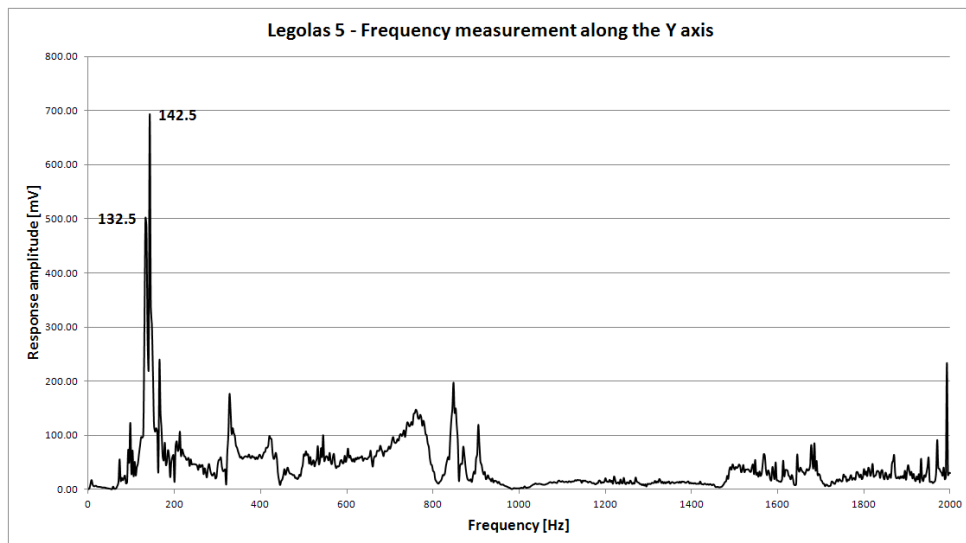


Figure 6.45: Frequency measurement of the Legolas 5 prototype along the Y axis

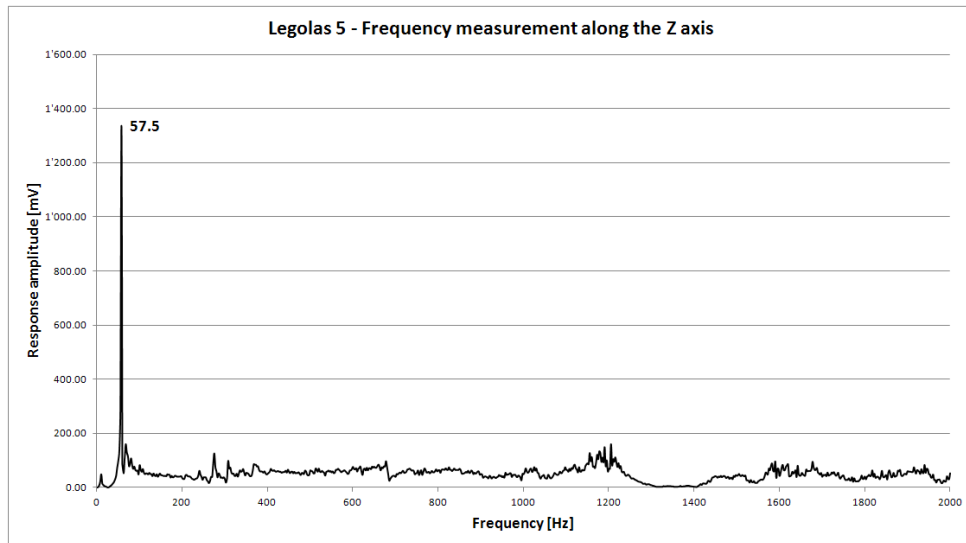


Figure 6.46: Frequency measurement of the Legolas 5 prototype along the Z axis

- **Lowest eigenfrequencies along the X axis:**
  - 72 Hz: transverse flexion of the Z-side passive brick leaf spring
  - 245 Hz: transverse flexion of the X-side active brick
- **Lowest eigenfrequencies along the Y axis:**
  - 132.5 Hz and 142.5 Hz: transverse flexion of both Y-side actuation sub-brick tables
- **Lowest eigenfrequency along the Z axis:**
  - 57.5 Hz: transverse flexion of the Y-side passive brick leaf spring

Consequently, this analysis highlights a first source of low vibration modes, which consists in the transverse flexion of the passive bricks leaf spring. As detailed in section 6.3.2, two different designs are included in the Legolas 5 prototype: the tensile specimen-like solution, as featured in the Y-side and Z-side passive bricks, generates an eigenfrequency which is lower than 100 Hz, as opposed to the broad leaf spring with a central hole option, which is included in the X-side passive brick. Consequently, a straightforward design improvement consists in adopting this last solution for all passive bricks. A simplified model, illustrated in figure 6.47, allows to compute the increase in the leaf spring transverse stiffness and eigenfrequency:

- **Tensile specimen-like shape, approximated by a prismatic leaf spring:** the transverse flexion stiffness of this design is directly proportional to the moment of inertia of the leaf spring, given by  $I_1 = \frac{b^3 h}{12}$  [36]. The numeric application of this formula for both X-side and Z-side passive bricks results in a moment of inertia of  $1.5 \cdot 10^{-11} \text{ [m}^4\text{]}$ .

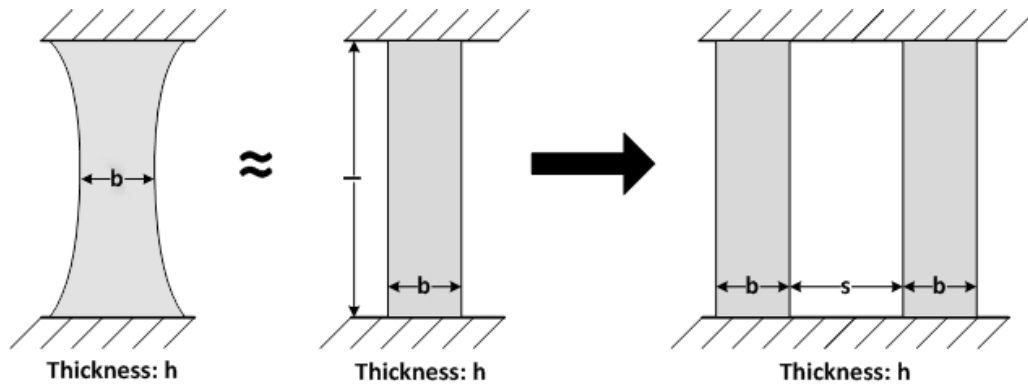


Figure 6.47: Simplified model of the solution proposed to improve the passive brick leaf spring transverse stiffness and eigenfrequency

- *Broad leaf spring with a central hole option:* a simple computation allows to derive the moment of inertia of this configuration:  $I_2 = \frac{2b^3h}{3} + b^2sh + \frac{bs^2h}{2}$ . The X-side leaf spring thus presents a transverse moment of inertia of  $9.8 \cdot 10^{-10} \text{ [m}^4\text{]}$ .

Consequently, this simple design improvement allows to multiply the transverse stiffness of the leaf spring by 65. Furthermore, as the eigenfrequency value is proportional to the square root of the stiffness, the vibration mode is multiplied by a factor 8. The new expected frequencies are thus 580 Hz along the X axis and 460 Hz along the Z axis, which are highly satisfactory.

Furthermore, performing accelerations of around  $10 \text{ m/s}^2$  with the Legolas 5 prototype has highlighted a second source of low eigenfrequencies, which consists in the low transverse stiffness of the leaf springs which define the position of the RCM in both X-side and Y-side active bricks. In addition, a buckling phenomenon occurs when a force is applied on the passive brick, as illustrated in figure 6.48 for the X-side active brick. The resulting transverse force and moment charge one half of the leaf springs in traction and the other half in compression, which generates buckling. Figure 6.49 illustrates this behaviour on the lower leaf spring of the X-side chain. This buckling phenomenon is even worsened by the presence of warping, which results from the torsion moment created by the force applied on the passive brick. Moreover, the consequent low eigenfrequency cannot be detected at the level of the end-effector, as the passive brick leaf spring acts as a filter. Nonetheless, a measurement with the accelerometer fixed on the passive brick allows to estimate this mode, which oscillates at 62.5 Hz for the X-side and 85 Hz for the Y-side chains.

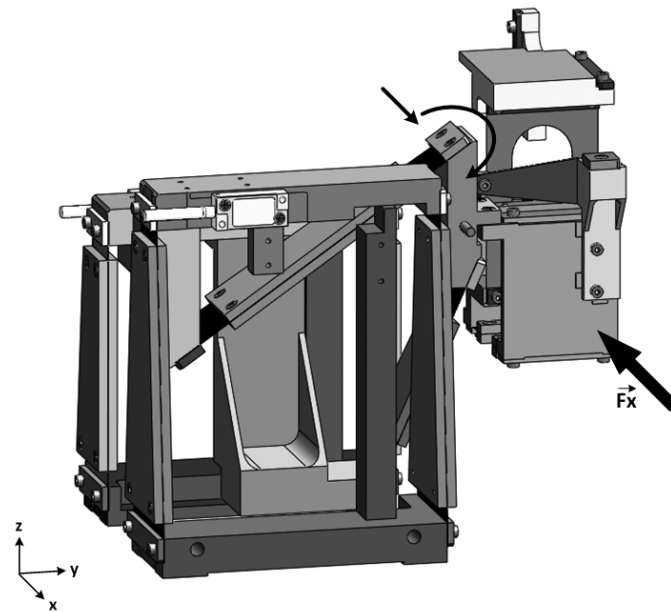


Figure 6.48: Situation which highlights the buckling of the leaf springs defining the position of the RCM

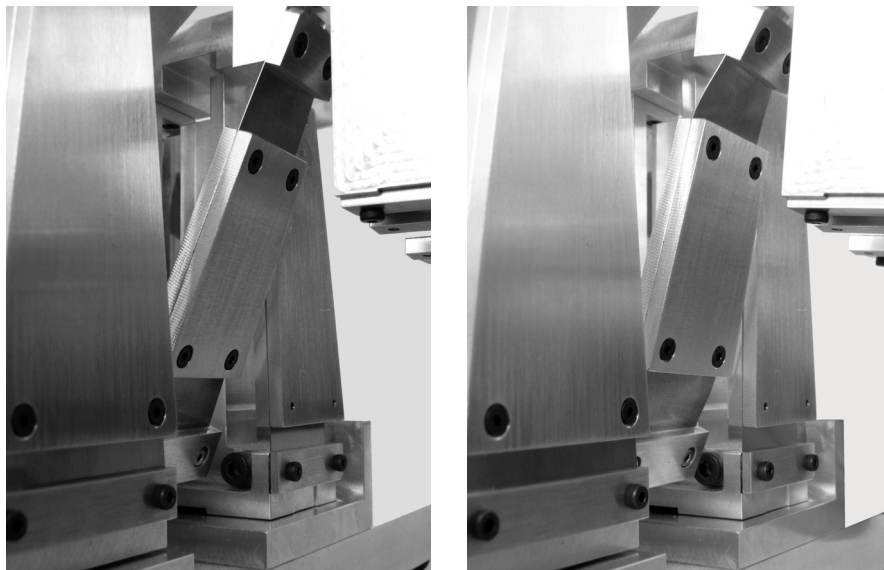


Figure 6.49: Pictures of the unloaded (left) and loaded (right) lower leaf spring defining the RCM position, highlighting the buckling phenomenon

This mechanism must hence be improved in order to increase the critical buckling load of the leaf springs: a key aspect consists in reducing the length of the prismatic hinges, as the critical buckling load is inversely proportional to the square of this parameter [36]. Furthermore, the current design includes four hinges sharing the same length, which is adapted to the flexure which undergoes the highest deformation. Straightforwardly, the model can

be refined by separately designing each of the four hinges and by reducing the safety factor which defines the admissible stress in the flexures. The resulting optimised mechanism is illustrated in figure 6.50. This improvement has been practically implemented in the Legolas 5 X-side chain and has allowed to increase the corresponding eigenfrequency to 102.5 Hz (+ 64 %).

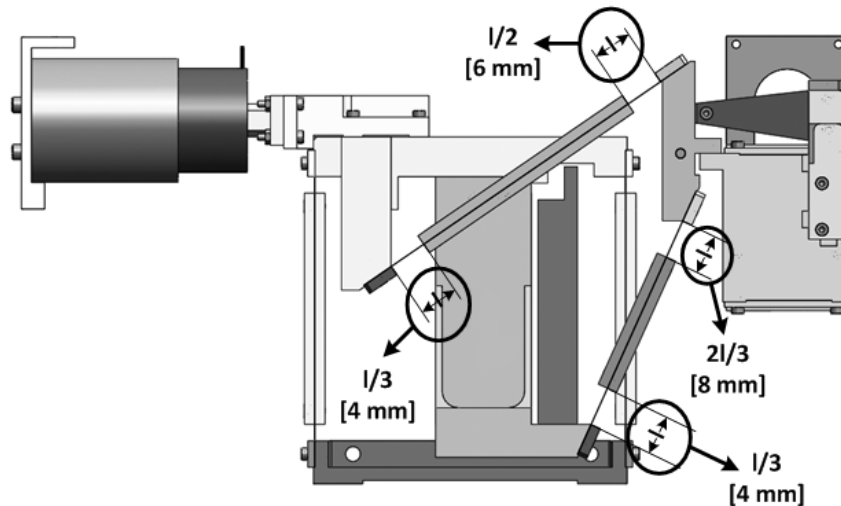


Figure 6.50: *Length optimisation of the leaf spring hinges*

Nonetheless, optimising the length of the prismatic hinges is neither sufficient to entirely suppress the buckling phenomenon nor to increase the corresponding eigenfrequency to a value which is not detrimental to the robot dynamic behaviour. Subsequently, a further improvement, illustrated in figure 6.51, is advocated: it consists in modifying the positions of the RCC mechanism flexure hinges to form a trapezium. Figure 6.51, bottom, shows two possibilities to achieve this desideratum: if the upper leaf spring is modified (bottom left), its length is inevitably decreased, which may be detrimental to the rotational stroke. Thus, the solution proposed in figure 6.51 (bottom right), although more challenging to integrate in the current prototype, should be preferred.

Lastly, the four RCC mechanism prismatic hinges could also be replaced by separated leaf spring cross pivots (see figure 5.14, middle). These mechanisms achieve the same stroke as prismatic hinges with an increased transverse stiffness, which allows to augment the value of the corresponding eigenfrequency. Note that the natural stiffness is also increased, which will thus necessitate a higher actuation force to achieve the same rotation of  $\pm 10^\circ$  on the robot end-effector.

To conclude, this section has presented the characterisation of the Legolas 5 dynamical performances by estimating the eigenfrequencies of this robot. This has allowed to detect two design weaknesses, which are generating low vibration modes. Simple and efficient improvements have been proposed to overcome this issue. Note that robot specifications which require high rotation angles inevitably lead to mechanisms which are more liable to

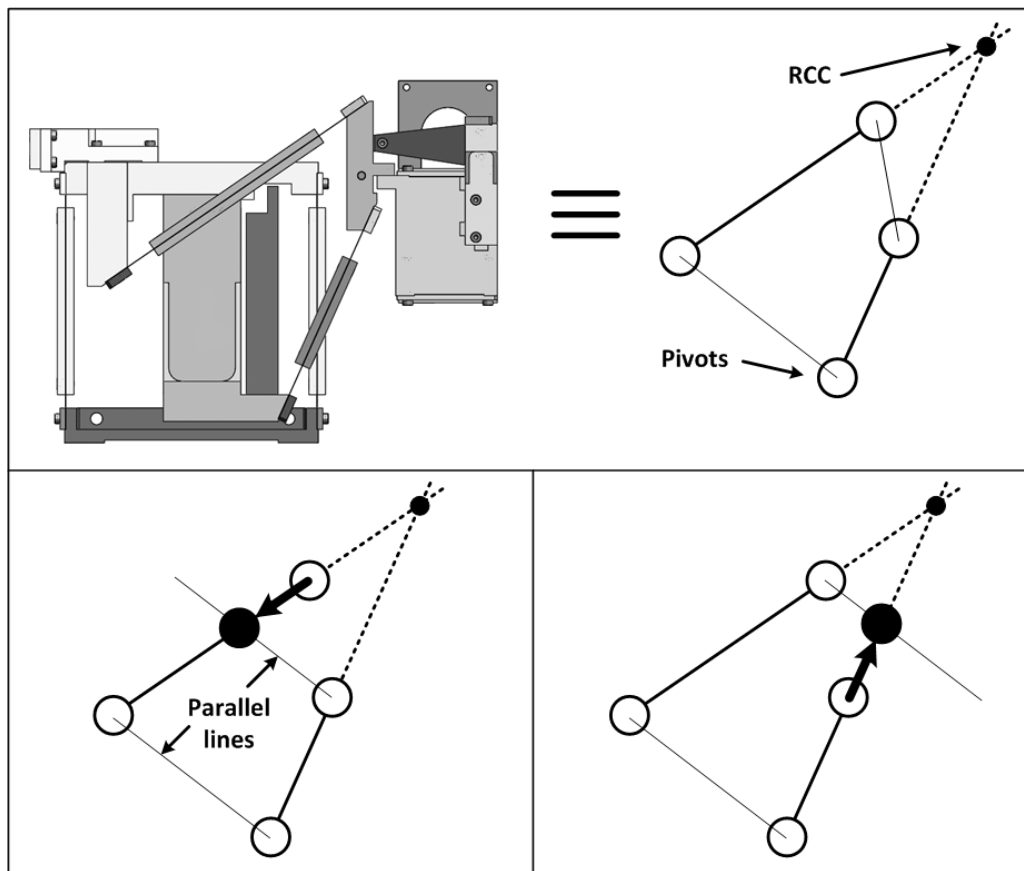


Figure 6.51: *Top: modelisation of the current RCC mechanism with ideal pivots; bottom: two solutions to improve of the mechanism by displacing the pivots to form a trapezium; the left solution is detrimental to the rotation stroke, as it shortens the length of the upper leaf spring*

undergo the previously described buckling phenomenon. Indeed, fulfilling this need inevitably implies the three following concessions to allow for such high deformation angles:

- increased length of the prismatic hinges
- increased length of the leaf springs defining the RCC
- increased distance between the end-effector and the fixation of the RCC leaf springs, because of their increased length

The mechanical design of the active bricks including rotational degrees of freedom with high strokes must thus be given particular attention to guarantee high static and dynamic performances.

## 6.5 Discussion

This chapter has detailed the application of the modular design methodology to a practical example, consisting in an ultra-high precision 5-degree of freedom robot. This has first allowed to illustrate the use of the conceptual solution catalogues by detailing the procedure which selects a kinematics regarding the specific application requirements. Then, the mechanical design of the necessary active and passive bricks has been thoroughly examined, leading to the Legolas 5 prototype. Furthermore, ***this case study has highlighted the creative design process which has to be accomplished to transform a kinematics and mechanical principle into a real and efficient robot***: first, albeit the modular concept symbolises the robot with a cube, the final arrangement of the Legolas 5 only retains the orthogonal arrangement of the kinematic chains. Then, the detailed design of the Legolas 5 building bricks has illustrated the evolution of the flexure-based mechanisms, from the principles proposed in the mechanical solution catalogue to the final arrangement of the bricks. Finally, the shrewd assembly of the building bricks in the Legolas 5 prototype has underlined some design subtleties, such as force alignment and gravity compensation.

Subsequently, ***the characterisation of the Legolas 5 prototype has allowed to prove that the requirements of the robot are fulfilled***: the workspace estimation has first highlighted that simultaneous translations of 5 mm and rotations of  $10^\circ$  are achieved; furthermore, angles of  $15^\circ$  can be reached without mechanical interference, even though they cause high stresses in the leaf springs, which have not been designed for such high strokes. Then, further measurements have shown that the resolution and repeatability of the motions attain 50 nm and  $1.9 \mu\text{rad}$  and are limited by the selected sensor resolution only. As for the dynamic performances, the estimation of the robot eigenfrequencies has highlighted two chief weaknesses, and has thus allowed to propose simple solutions to improve the design efficiency. Note that the evaluation of the stiffness of the prototype will be performed in a second time. *These noteworthy results verify that the Legolas 5 prototype, and more generally robots which are synthesised with the modular design methodology and composed of assembled leaf springs, can achieve ultra-high precision.*

Besides, the following further improvements are advocated in consideration of the industrial Legolas 5 version development:

- ***Replace the voice-coil actuation by EC actuators*** (see figure 5.6), which enables their integration between both arms of the 4-hinge tables, such as illustrated in figure 6.52. This would necessitate the development of custom-made actuators, as none of the devices which are currently available on the market fulfill the Legolas 5 requirements. As a consequence, the compactness of the robot is increased and leads to a new Rs ratio of 0.033 (+ 30%): this value outstrips the highest Rs ratio of the existing ultra-high precision machines (see section 5.1). As for the total robot volume, it is decreased by a factor of 2.7.
  - New volume of the prism enclosing the robot mechanical parts:  $248 \times 307 \times 178 \text{ mm}^3$



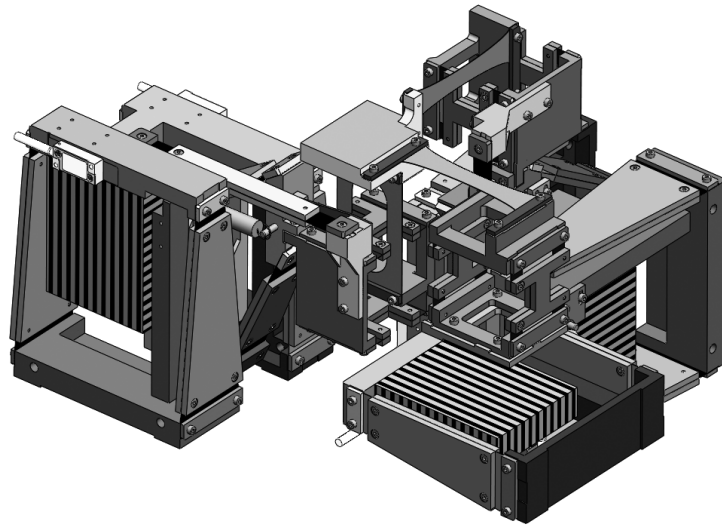


Figure 6.52: CAD view of the Legolas 5 prototype with integrated EC actuators, symbolised by hatched solids (the fixed frames have been hidden for clarity purposes)

- Characteristic dimension: 307 mm
  - Total linear stroke: 10 mm
  - $R_s$  ratio: 0.033
- **Select sensors presenting a higher resolution**, thus increasing the achievable resolution of the robot, as it has been proven to be only limited by this characteristics.

Lastly, the remarkable performances of the Legolas 5 prototype enhances the potentialities of the whole Legolas family, whose 19 possible kinematics have been introduced in section 6.2.3: with only 6 different building bricks, three of them being featured in the Legolas 5 prototype, one robot solution is proposed for each of the 19 possible end-effector mobilities. Appendix E presents the detailed mechanical design of each family member. As an example, the Legolas robot which performs three translations is included in figure 6.53: the orthogonal version of the Delta kinematics, as featured in the Delta<sup>3</sup> I, II and III (see section 2.3.1), can be recognised, additionally comprising the original design of the space parallelogram mechanism detailed in section 6.3.2.

*Furthermore, as the development of each Legolas robot stems from the same considerations which have led to the Legolas 5 prototype, such as force alignment and gravity compensation, the performances of each family member are expected to be as satisfactory as the results of the Legolas 5 characterisation. Consequently, this case study has not only generated one ultra-high precision 5-DOF robot, but a whole family of 19 high-performance machines.*

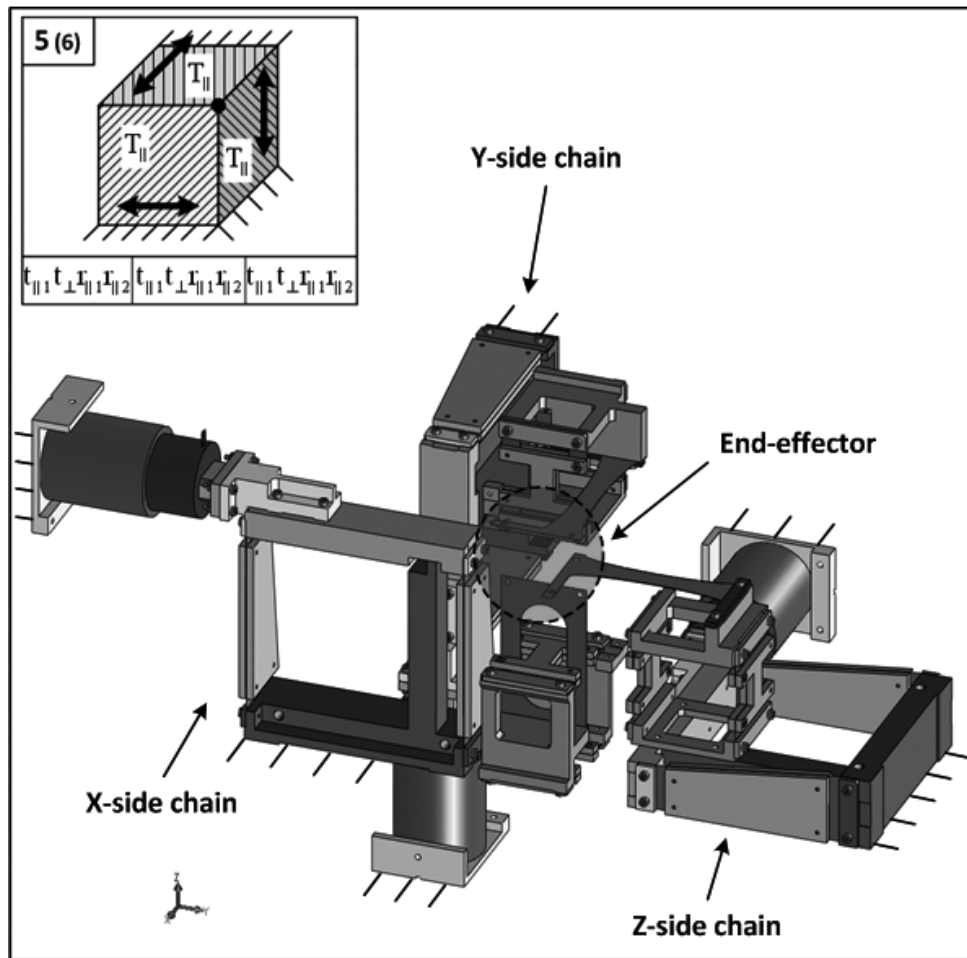


Figure 6.53: 3-DOF ( $T_x$ ,  $T_y$ ,  $T_z$ ) Legolas robot, including three times the same kinematic chain

# Chapter 7

## Conclusion

### 7.1 General conclusion

This thesis responds to the growing need for industrial production tools capable of manipulating and assembling devices with a submicrometric precision: the current miniaturisation trend indeed tends to decrease the size of both the products and the production lines, thus demanding compact ultra-high precision robots to perform these tasks. Nonetheless, their development is still highly costly, both in time and money, and results in scarcely flexible machines: if the customer specifications change during the design process, the latter has to be restarted, often from the very beginning, thus consisting in a significant waste of resources.

Furthermore, the state of the art of this thesis has highlighted the lack of a global approach which examines and proposes solutions for both the parallel kinematics synthesis and the flexure-based mechanical design of these robots, which consist in two crucial and interdependent aspects. Besides, some degrees of freedom arrangements, such as the 5-DOF mobility, are scarcely studied, as both their kinematics and their mechanical design are highly challenging to synthesise.

Consequently, this thesis overcomes these issues by proposing a modular design methodology, which can be paralleled to a robotic Lego: a finite number of conceptual building bricks allow to quickly design and modify parallel robots. The core of this concept lies in the exhaustive conceptual solution catalogue which, for each possible end-effector mobility, lists all combinations of building bricks performing the desired motions. Furthermore, this work focuses on ultra-high precision machines: it thus proposes a reduced conceptual solution catalogue, which is based on design and machining considerations, along with original flexure-based solutions for the mechanical design of the building bricks. Finally, the case of an ultra-high precision 5-DOF robot has been studied to illustrate the practical use of the methodology and to enhance the creative process which leads to the achievement of a high-performance machine.

## 7.2 Original contributions

The research which has been performed in the frame of this thesis has led to the following original contributions:

- ***A modular design methodology***, which not only provides a general kinematic synthesis method appropriate for any type of parallel orthogonal robots, but also proposes a complete procedure for the selection of a solution adapted for a specific application and mechanical designs of the robot building bricks. In addition, this methodology remarkably includes three levels of modularity:
  - the first consists in the ***conceptual building bricks***: as these are purely kinematic, their list is exhaustive and strictly independent of any mechanical design. The kinematic part of the methodology and the conceptual exhaustive solution catalogue can thus be directly applied to the synthesis of a large variety of machines, from machine-tools to micro-scale robots; only the mechanical design of the bricks must be reviewed in order to fulfill the application specific requirements.
  - the second level is composed of the ***mechanical design of the building bricks***: a gathering of efficient flexure-based mechanisms for ultra-high precision applications is proposed, and must be regarded as a tool for the designer rather than a set of off-the-shelf solutions. Consequently, other existing or newly designed flexure-based structures can be added to this collection by the user. Furthermore, the effectiveness of this second modularity level lies in the possibility of replacing the mechanical design of only one building brick without influencing the other parts of the robot.
  - the third level of modularity consists in ***elements of the bricks mechanical design***: the presence of a standardised actuation sub-brick, which is common to all active bricks, considerably simplifies their design. Moreover, the possibility of adjusting the position of the rotation centre thanks to a Remote Centre of Motion allows to significantly improve the overall robot performances.
- ***An exhaustive conceptual solution catalogue***, which, for each of the 19 possible end-effector mobilities, itemises all combinations of building bricks actuating the desired motions.
- ***Two methods to generate this exhaustive conceptual solution catalogue***, by hand or automatically.
- ***A reduced conceptual solution catalogue*** for ultra-high precision applications, which is grounded on specific flexure-based design and machining considerations.
- ***A gathering of efficient flexure-based mechanisms for ultra-high precision applications***, in particular:

- *Original active bricks designs* for the  $R_{\parallel}$  and  $R_{\perp}$ , the  $T_{\parallel}R_{\perp}$ ,  $T_{\perp}R_{\parallel}$  and  $T_{\parallel}R_{\parallel 2}$ , as well as the  $T_{\parallel 1}T_{\parallel 2}R_{\perp}$  and  $T_{\parallel 1}T_{\perp}R_{\parallel 2}$  bricks
- *Original passive bricks designs*, among which the innovative solution for the  $t_{\parallel 1}t_{\perp}r_{\parallel 2}r_{\perp}$ ,  $t_{\parallel 1}t_{\perp}r_{\parallel 1}r_{\parallel 2}$  and  $t_{\parallel 1}t_{\parallel 2}r_{\parallel 1}r_{\perp}$  bricks can be underlined
- ***An ultra-high precision 5-degree of freedom robot with assembled leaf spring, the Legolas 5***, which features the following characteristics:
  - Detailed mechanical design with assembled leaf springs of the  $T_{\parallel}$ ,  $T_{\parallel}R_{\perp}$  and  $t_{\parallel 1}t_{\perp}r_{\parallel 1}r_{\parallel 2}$  bricks
  - Simultaneous strokes of  $\pm 5$  mm for the translations and  $\pm 10^{\circ}$  for the rotations
  - Motions resolution and repeatability of 50 nm and  $1.9 \mu\text{rad}$ , limited by the sensors resolution
- ***a thorough ultra-high precision robots family***, which, for each of the 19 possible end-effector mobilities, provides a complete robot, from the kinematics synthesis to the mechanical design, making use of only 6 different building bricks.

## 7.3 Perspectives

The establishment of the modular design methodology and the generation of the Legolas family proposed in this thesis open new research directions, which will be interesting to investigate in future work, namely:

- ***A two-fold solution catalogue software***, which not only automatically generates the solution catalogue thanks to the algorithm proposed in appendix A, but also includes a graphical representation of the kinematics, such as featured in appendices B and C. Furthermore, this software could include a list of all possible building bricks which the user could select or dismiss; the reduced solution catalogue could thus be automatically generated in real time depending on the wishes of the robot designer.
- ***The establishment of new sets of hypotheses for the mechanical design of the building bricks and the reduced solution catalogue***: for instance, the option of designing ultra-high precision robots with assembled leaf springs allows for a wider diversity of flexure-based structures, as the planarity or rotational symmetry constraints imposed for the mechanical designs of chapter 5 are no longer mandatory. Additionally, the increasing use of non-metals for flexures and the associated machining methods may require new sets of hypotheses. Whereas electro-chemical discharge machining allows to shape non-conductive materials with a similar process to classical Wire-EDM, silicon flexures necessitate cleanroom methods, such as DRIE (Deep Reactive Ion Etching): the machining and design constraints must thus be adapted in consequence. One can even imagine the use of thermosetting and thermoplastic polymers to perform flexure-based mechanisms, which would be fabricated by injection molding. Although studies on this field are still scarce, this research direction could be of high

interest for biomedical and surgery purposes: the modularity of the concept would indeed suppress the need for the machine re-sterilisation by enabling the use of low-cost and disposable flexure mechanisms.

- **The development of a Legolas 5 industrial prototype:** besides the design improvements which have been recommended in section 6.5, an interesting characterisation would consist in the estimation of the parasitic rotation around the vertical axis (Rz) caused by the actuated motions. As this displacement cannot be compensated for by calibration, it must be minimised: in addition to the careful design of the mechanisms, the effect of assembly defects must be limited, which necessitates the by-hand fine tuning of the mountings, under the monitoring of measurement devices. Furthermore, the prototype stiffness should be evaluated, as this characteristic is of crucial importance in regard with the tasks the robot will have to perform. Moreover, a dynamical model of the robot could be implemented to improve the control algorithm for high accelerations, whereas the calibration of the machine including forces and thermal effects [54] would complete the study of this robot.
- **The enhancement of the whole Legolas family,** with the practical construction of the  $t_{\parallel r_{\perp}}$  and  $t_{\perp r_{\parallel}}$  passive bricks, following the detailed mechanical design proposed in appendix E, as well as the development and characterisation of a Legolas prototype performing another end-effector mobility.

## 7.4 Final note

Finally, the flexibility and creativity allowed by the modular design methodology proposed in this thesis deserve to be highlighted: the concept can indeed be considered as a *design tree*, as the explicit statement of hypotheses at each step of the methodology permits the user to enter at any level and to adapt them to his/her specific needs (see figure 7.1). Whereas the ultra-high precision Legolas family provides fully designed robots, which only necessitate the adaptation of the mechanisms to the application requirements (strokes, position of the rotation centres, ...), a more creative user may decide to modify the mechanical design criteria, thus defining a new reduced conceptual solution catalogue. Moreover, the chapter which proposes mechanical designs for the building bricks aims at gathering interesting flexure-based principles as a tool for the engineer, rather than at proposing a thorough catalogue of off-the-shelf solutions. Lastly, this methodology allows the expert in robot kinematics synthesis to start directly from the conceptual building bricks and the thorough solution catalogue to reinterpret the procedure according to his/her specific needs.

Furthermore, neither this methodology nor solution catalogues are expected to optimally solve the challenging robot synthesis problem. No generic method is indeed capable of responding to the wide range of applications of parallel industrial robots as efficiently as an engineer, whose creativity and experience are essential and irreplaceable. Consequently, the concept proposed here provides kinematics and mechanical design suggestions, which help preventing the engineer to encounter the 'writer's block'; to conclude, Isaac Asimov went

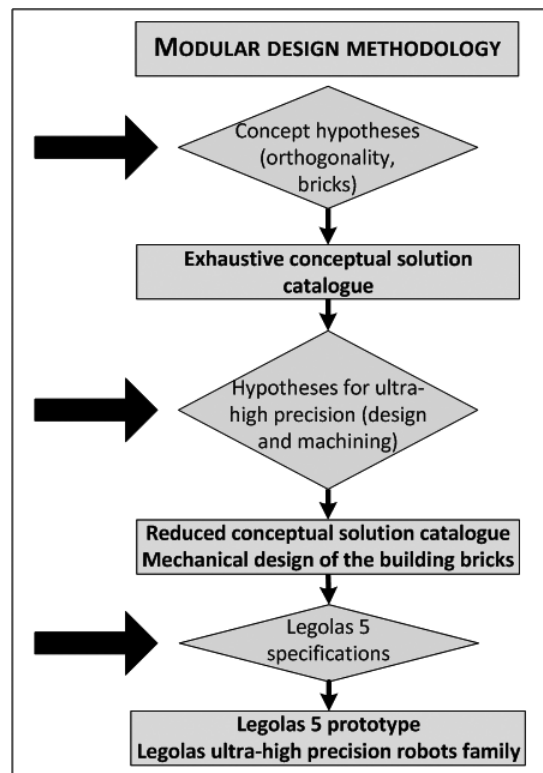


Figure 7.1: Illustration of the modular methodology as a design tree; the lateral arrows symbolise the different levels of hypotheses which the user can review to fulfill the specific needs of his / her application

further into the analogy with the artistic world as he wrote in one of his scientific essay [4] the following quote, which utterly illustrates the spirit of this thesis:

*'How often people speak of art and science as though they were two entirely different things, with no interconnection. An artist is emotional, they think, and uses only his intuition; he sees all at once and has no need of reason. A scientist is cold, they think, and uses only his reason; he argues carefully step by step, and needs no imagination. That is all wrong. The true artist is quite rational as well as imaginative and knows what he is doing; if he does not, his art suffers. The true scientist is quite imaginative as well as rational, and sometimes leaps to solutions where reason can follow only slowly; if he does not, his science suffers.'*





# Appendix A

## Automatic generation of the exhaustive conceptual solution catalogue

This appendix completes chapter 3 by detailing the automatic generation of the exhaustive conceptual solution catalogue. The presented procedure, which lists all active bricks arrangements, has been implemented in MATLAB and has allowed to check the thoroughness of the catalogue established by hand (see section 3.2). Furthermore, the method to obtain both the active bricks arrangements and the corresponding passive bricks solutions, although not implemented, is outlined as a conclusion of this appendix.

### A.1 Generation of the active bricks arrangements

The automatic generation of the active bricks arrangements first requires to introduce the notion of *mobility unit*, which defines a degree of freedom by expressing its three following characteristics:

- the main letter (T, R) symbolises the *nature of the degree of freedom*, *i.e.* translational or rotational
- the first subscript ( $\parallel$ ,  $\perp$ ) stands for the *orientation of the degree of freedom relatively to the face of the conceptual cube* (see figure 3.1)
- the second subscript (x, y, z) indicates the *direction of the degree of freedom relatively to the robot end-effector coordinate frame* (see figure 3.1)

Table A.1 presents all possible mobility units.

T $_{\parallel x}$	T $_{\parallel y}$	T $_{\parallel z}$	T $_{\perp x}$	T $_{\perp y}$	T $_{\perp z}$
R $_{\parallel x}$	R $_{\parallel y}$	R $_{\parallel z}$	R $_{\perp x}$	R $_{\perp y}$	R $_{\perp z}$

Table A.1: Exhaustive list of the mobility units

The introduction of this notion then requires to express the concept active bricks in terms of mobility units: the resulting bricks are called *active mobility bricks*.

### A.1.1 Active mobility bricks generation

The establishment of the active mobility bricks is achieved by first generating all possible combinations of mobility units. Then, three elimination algorithms are applied to retain only the solutions which are consistent with both basic mobility considerations and with the concept definitions. The implemented program accepts as an input the number of degrees of freedom of the active mobility bricks; it must thus be run three times to obtain the thorough list of 1-DOF, 2-DOF and 3-DOF active mobility bricks. Figure A.1 illustrates its flowchart.

First, a straightforward combinatory formula (see equation A.1) allows to determine the total number of solutions for 1-DOF, 2-DOF and 3-DOF bricks. Consequently, the first step of the program consists in filling a chart with all these combinatory possibilities, which includes 12 solutions for 1-DOF active bricks, 144 for 2-DOF bricks and 1728 for 3-DOF bricks.

$$\# \text{ combinatory solutions} = (\# \text{ mobility units})^{\# \text{ brick DOF}} \quad (\text{A.1})$$

Then, the following dismissal tests are applied to each solution of the chart to check its coherence:

- the first test deletes the solutions where *a degree of freedom of the end-effector is actuated more than once*
- the second dismisses the possibilities which are *inconsistent with the concept, i.e.* which present one of the following situations:
  - three parallel motions along three different axes are actuated by a brick
  - two or three orthogonal degrees of freedom along different axes are included in a brick
- the third deletes the *permutations of the same solution*

As a result, the exhaustive list of the active mobility bricks includes *12 solutions for 1-DOF bricks, 42 for 2-DOF bricks and 60 for the 3-DOF case.*

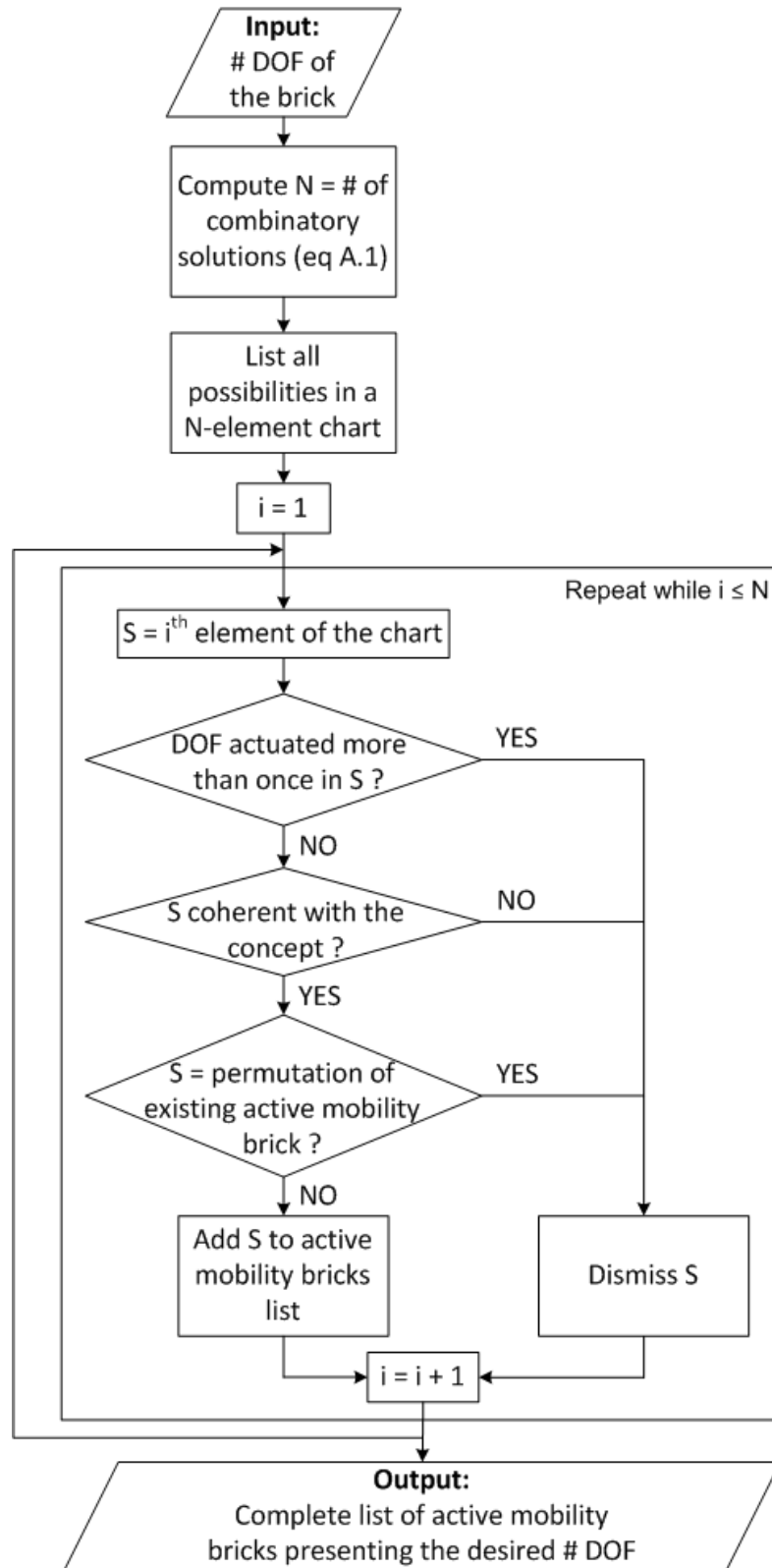


Figure A.1: Flowchart of the program generating the active mobility bricks list

### A.1.2 Establishment of the active bricks arrangements catalogue

The exhaustive active bricks arrangements catalogue is then generated by the program whose flowchart is illustrated in figure A.2. The input of this algorithm consists in the desired number of active bricks and their number of degrees of freedom. For example, the  $1 + 2$  input stands for a 2-kinematic chain configuration, where the bricks respectively actuate one and two degrees of freedom. This program must thus be run 15 times to itemise all possible active bricks arrangements (see table A.2).

First, the procedure requires to compute the total number of combinatory possibilities, which is simply given by the product of the number of active mobility bricks which are possible for each of the desired active brick. For example, the aforementioned  $1 + 2$  example accepts  $12 \cdot 42 = 504$  solutions (12 possible active mobility bricks performing one degree of freedom and 42 actuating two degrees of freedom). A chart is then filled with these combinatory possibilities.

The second step of the program then consists in applying three dismissal tests to each solution to check its coherence with both the concept and mobility considerations:

- the first test deletes the solutions where *a degree of freedom of the end-effector is actuated more than once*
- the second dismisses the possibilities which are *inconsistent with the concept*, i.e. where two bricks should be located on the same face of the conceptual cube
- the third deletes the *permutations of the same solution* (see figure 3.9), which are characterised by identical building bricks actuating the same robot end-effector mobility

Table A.2 details the number of active bricks arrangements generated for each of the 15 possible inputs.

The implementation of this program has allowed to verify the thoroughness of the solution catalogue established by hand in chapter 3 by comparing the active bricks arrangements itemised with these two different and complementary approaches.

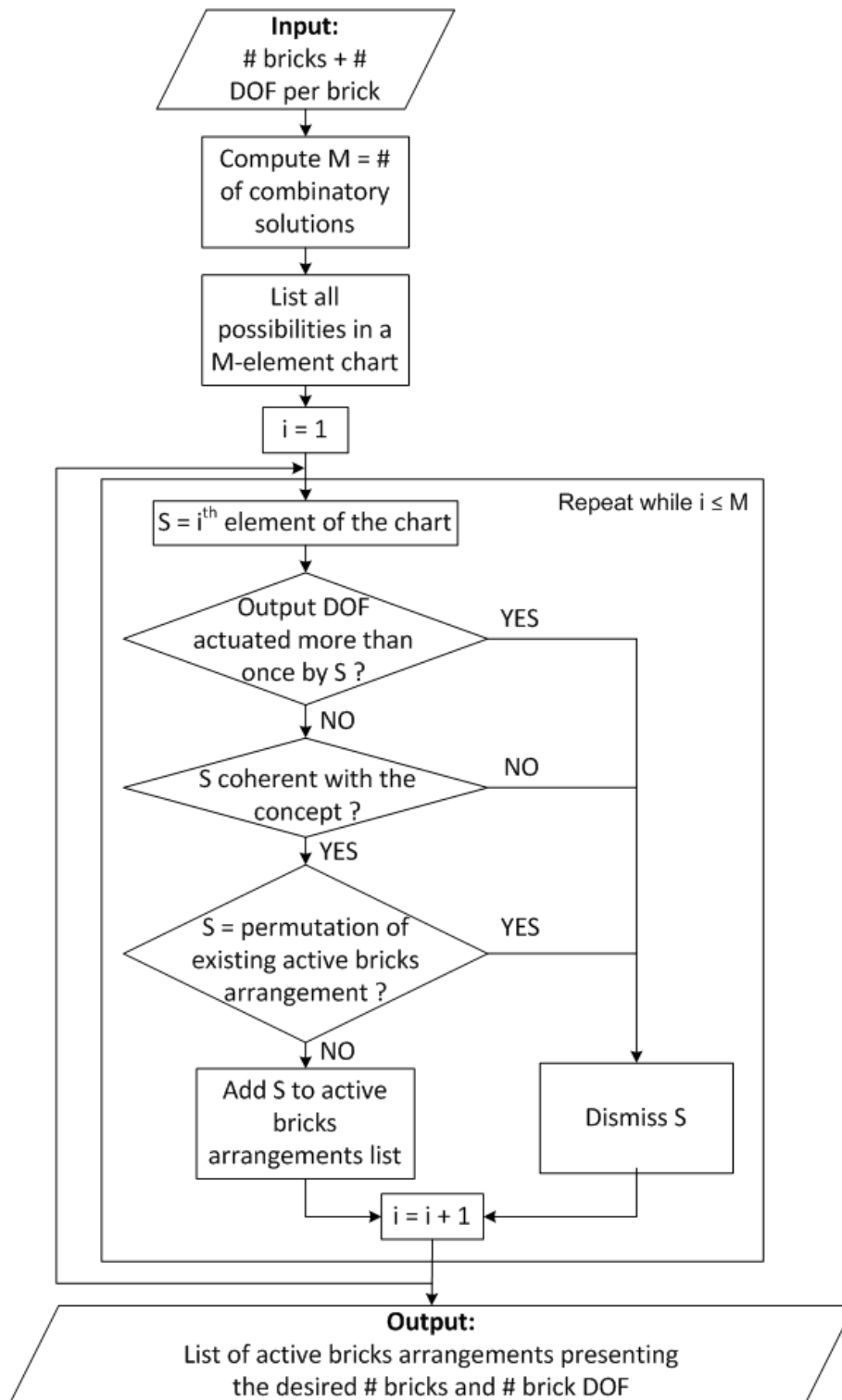


Figure A.2: Flowchart of the program generating the complete list of active bricks arrangements

Program input	Brick 1	Brick 2	Brick 3	Robot end-effector	# solutions
1	1 DOF	∅	∅	1 DOF	4
2	2 DOF	∅	∅	2 DOF	9
1 + 1	1 DOF	1 DOF	∅	2 DOF	13
3	3 DOF	∅	∅	3 DOF	12
1 + 2	1 DOF	2 DOF	∅	3 DOF	48
1 + 1 + 1	1 DOF	1 DOF	1 DOF	3 DOF	24
1 + 3	1 DOF	3 DOF	∅	4 DOF	48
1 + 1 + 2	1 DOF	1 DOF	2 DOF	4 DOF	76
2 + 2	2 DOF	2 DOF	∅	4 DOF	41
1 + 1 + 3	1 DOF	1 DOF	3 DOF	5 DOF	54
1 + 2 + 2	1 DOF	2 DOF	2 DOF	5 DOF	76
2 + 3	2 DOF	3 DOF	∅	5 DOF	52
2 + 3 + 1	2 DOF	3 DOF	1 DOF	6 DOF	60
2 + 2 + 2	2 DOF	2 DOF	2 DOF	6 DOF	20
3 + 3	3 DOF	3 DOF	∅	6 DOF	10

Table A.2: Number of active bricks arrangements for each of the 15 possible program inputs

## A.2 Generation of the passive bricks arrangements

As a conclusion of this appendix, the outline of the procedure to generate both active bricks arrangements and the corresponding passive bricks solutions is presented. Similarly to the active building bricks, a preliminary step consists in expressing the concept passive bricks in terms of mobility units, thus itemising the passive mobility bricks. The procedure to generate them is similar to the aforementioned program to generate the active mobility bricks (see section A.1.1).

Moreover, an observation which has been detailed in section 6.3 is crucial for the implementation of the program: it consists in underlining that the same active bricks arrangement may generate different sets of passive bricks, depending on the relative orientation of the actuated motions on the robot cube. Figure 3.14 is here recalled as figure A.3 to illustrate this situation: note that both solutions actuate the same end-effector degrees of freedom with identical active bricks; the algorithm described in section A.1.2 thus considers them as permutations of the same arrangement. Nonetheless, they accept two distinct sets of passive bricks.

Consequently, the algorithm generating the passive bricks solutions has to be integrated in the procedure establishing the active bricks arrangements. Figure A.4 shows the new program flowchart, whereas figure A.5 details the algorithm which itemises the passive bricks possibilities.

		Possible passive bricks solution			Possible passive bricks solution
	X-side chain: active brick $T_{\parallel 1} R_{\parallel 2}$	$t_{\parallel 1} t_{\perp} r_{\parallel 2} r_{\perp}$		X-side chain: active brick $T_{\parallel 1} R_{\parallel 2}$	$t_{\parallel 1} t_{\perp} r_{\parallel 2} r_{\perp}$
Z-side chain: active brick $T_{\parallel}$	$t_{\parallel} r_{\perp}$	Y-side chain: active brick $T_{\parallel}$	$t_{\perp} r_{\parallel}$		

Figure A.3: Illustration of the different passive bricks sets generated by the same active bricks solution

The first step of the additional procedure (see figure A.5) consists in filling a chart with all combinatory possibilities of passive bricks; the number of solutions is given by the following formula:

$$\# \text{ combinatory solutions} = (\# \text{ passive mobility bricks})^{\# \text{ kinematic chains}}$$

Then, four tests are applied to each of the chart possibility to verify its coherence:

- the first only retains the solutions where ***the passive bricks block the degrees of freedom which are actuated by their serially arranged active brick***
- the second solely keeps the possibilities where ***the passive bricks permit the degrees of freedom which are actuated by the other kinematic chains***
- the third suppresses the solutions where ***an undesired end-effector mobility is permitted by more than one passive brick***
- the fourth deletes the ***permutations of the same solution***; this step is only coherent if an active brick is included twice or three times in the arrangement

Finally, the main program algorithm which removes the permutations of the same active bricks arrangement (see figure A.4) must be modified to retain the solutions which accept several sets of passive bricks. Consequently, two active bricks arrangements are considered as permutations only if the three following criteria are fulfilled:

- the same set of active bricks is included in each solution
- the same end-effector mobility is actuated
- both solutions share the same set(s) of passive bricks

The procedure proposed in this section could be implemented to check the exhaustiveness of the conceptual solution catalogue established by hand. In this thesis, this verification has not been performed as both the manual and automatic generation methods are identical. Furthermore, the number of passive bricks solutions for each active bricks arrangement can be simply computed as presented in section 3.2.2 and allows for a straightforward verification of the completeness of the passive bricks solutions list.

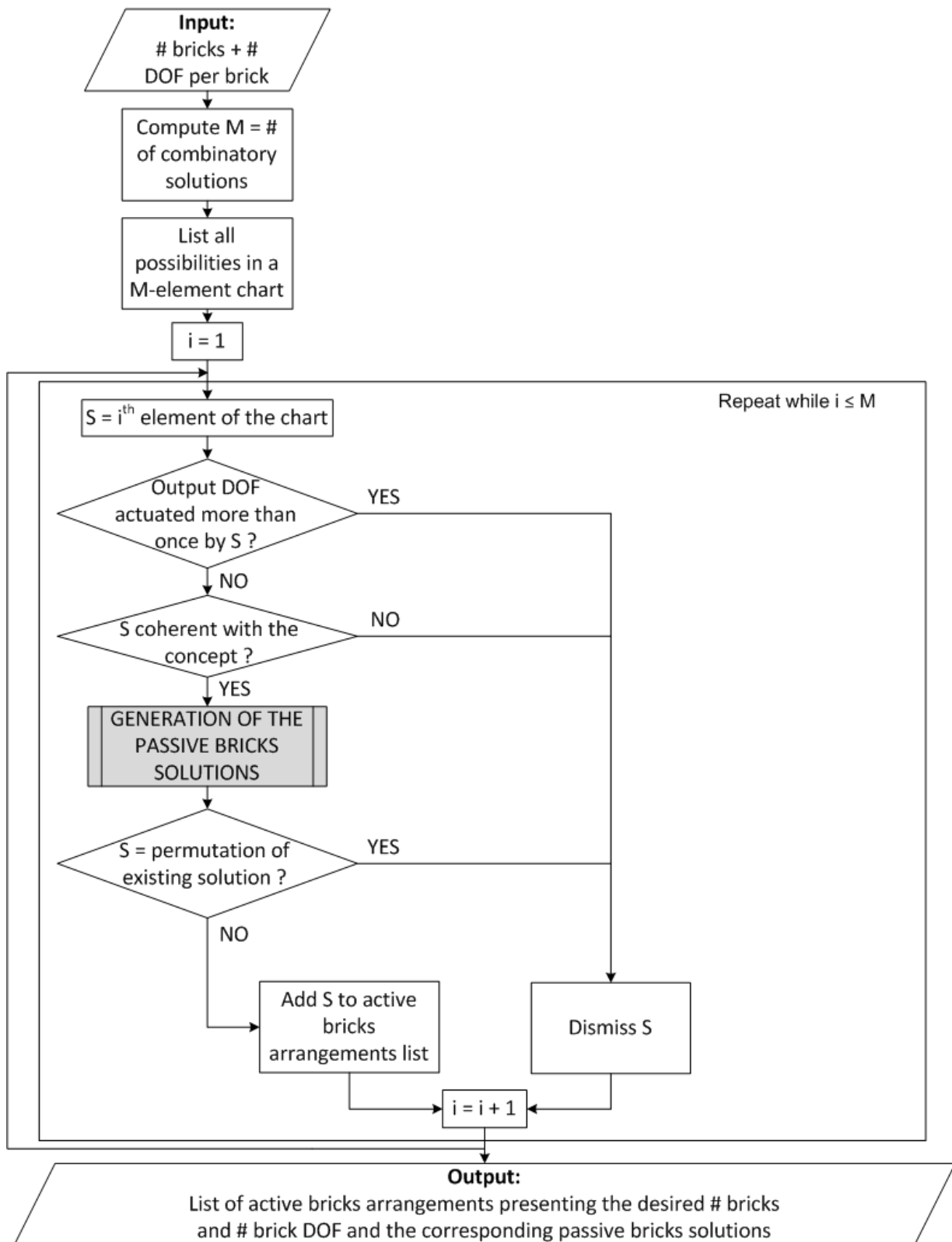


Figure A.4: Flowchart of the modified program to generate both the active bricks arrangements and their corresponding passive bricks solutions



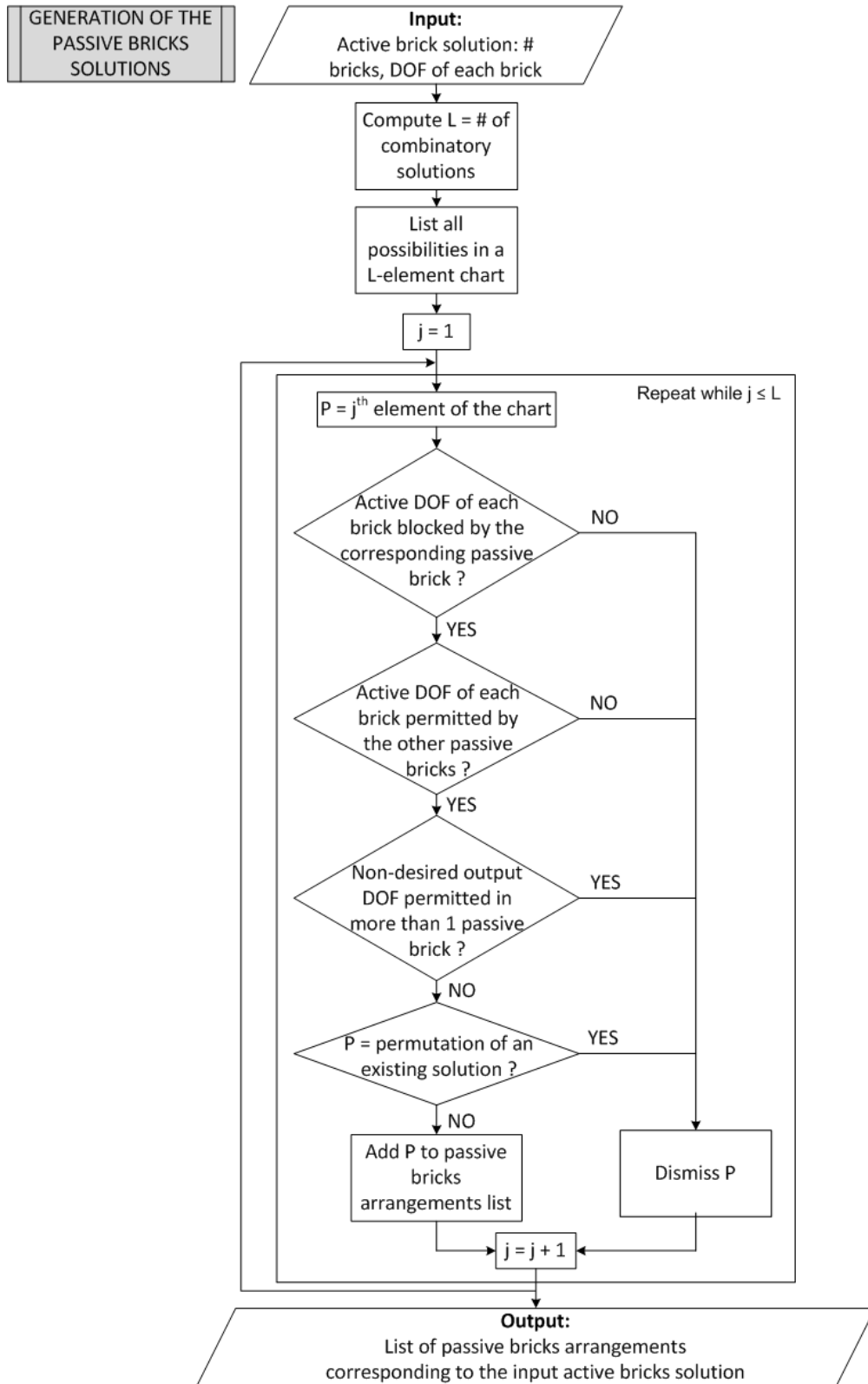


Figure A.5: Flowchart of the algorithm to generate the passive bricks arrangements for an active bricks solution



# Appendix B

## Exhaustive conceptual solution catalogue

The exhaustive conceptual solution catalogue, whose obtention has been detailed in chapter 3, is included in this appendix. The kinematic arrangements of active bricks are graphically represented and arranged according to the mobility which the robot end-effector performs, whereas the corresponding passive bricks solutions are simply listed. Note that the orientations of the motions along the x, y and z axes have been arbitrarily set: a simple rotation of the robot cube allows to reorient the mobility along the desired directions. Figure 3.1 is featured as a preamble of this appendix to recall the system coordinates and the notations of the kinematic chains.

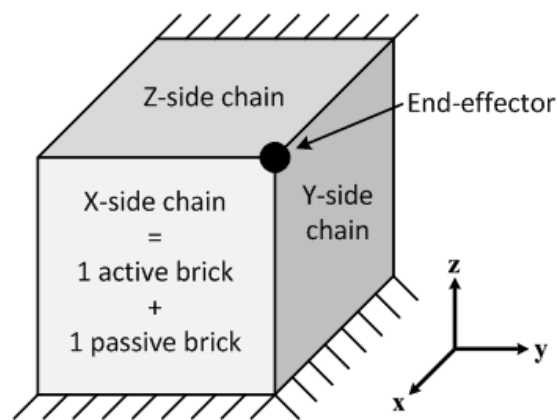
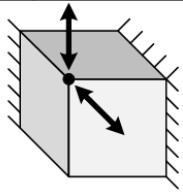
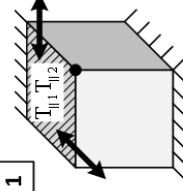
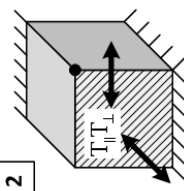
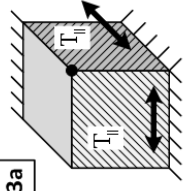
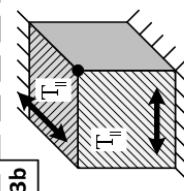
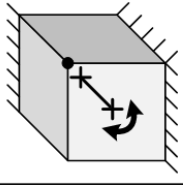
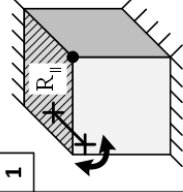
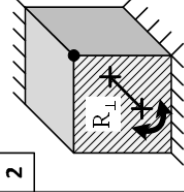
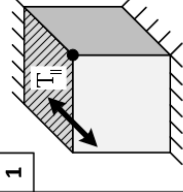
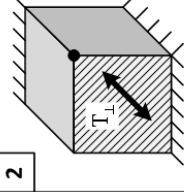
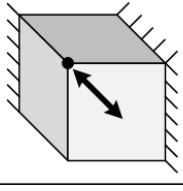


Figure B.1: Symbolism of the parallel robot designed with the modular concept

Robot mobility	Active bricks arrangement	X-chain passive brick	Y-chain passive brick	Z-chain passive brick
 <p>2 DOF 2 translations Tx, Ty</p>	<p>1</p>  <p>2</p> 	 <p>3a</p>	 <p>3b</p>	
		$t_{\perp}$ $t_{\parallel 1}$ $t_{\parallel 2}$ $t_{\perp 1}$ $t_{\perp 2}$ $t_{\parallel 1}$ $t_{\parallel 2}$ $t_{\perp 1}$ $t_{\perp 2}$ $t_{\parallel 1}$ $t_{\parallel 2}$ $t_{\perp 1}$ $t_{\perp 2}$		

Robot mobility	Active bricks arrangement	X-chain passive brick	Y-chain passive brick	Z-chain passive brick
 <p>Revolute joint 1 DOF 1 rotation: Rx</p>	<p>1</p>  <p>2</p> 	<p>1</p>  <p>2</p> 		
 <p>Prismatic joint 1 DOF 1 translation: Tx</p>				

Robot mobility	3	4		Active bricks arrangement			<p>X-chain passive brick</p> $t_{111}^1, t_{112}^1, t_{121}^1, t_{122}^1, t_{211}^1, t_{212}^1, t_{221}^1, t_{222}^1$	<p>Y-chain passive brick</p>	<p>Z-chain passive brick</p> $t_{111}^1, t_{112}^1, t_{121}^1, t_{122}^1, t_{211}^1, t_{212}^1, t_{221}^1, t_{222}^1$
----------------	---	---	--	---------------------------	--	--	---	------------------------------	---

Robot mobility	4	5	1	2	Active bricks arrangement					X-chain passive brick	Y-chain passive brick	Z-chain passive brick
		<p>Cylindrical joint 2 DOF 1 translation: Tx 1 rotation: Rx</p>										

Robot mobility	Active bricks arrangement	X-chain passive brick	Y-chain passive brick	Z-chain passive brick
4				
5				
		$t_{  }$ $t_{\perp}$ $t_{  1} t_{  2}$ $t_{  1} t_{  2} t_{\perp}$ $t_{  1} t_{  2}$ $t_{  1} t_{\perp}$ $t_{  1} t_{  2} t_{\perp}$ $t_{  1} t_{\perp}$ $t_{  1} t_{  2} t_{\perp}$ $t_{  1} t_{\perp}$ $t_{  1} t_{  2} t_{\perp}$ $t_{  1} t_{\perp}$ $t_{  1} t_{  2} t_{\perp}$ $t_{  1} t_{\perp}$		

Robot mobility	Active bricks arrangement	X-chain passive brick	Y-chain passive brick	Z-chain passive brick
5				
1				
2				
3				
2 DOF 1 translation: Tx 1 rotation: Ry				











Robot mobility	Active bricks arrangement	X-chain passive brick	Y-chain passive brick	Z-chain passive brick
	<p><b>15</b></p>			$t_{11}^1 t_{12}^1 t_{11}^2 t_{12}^2$ $t_{11}^1 t_{11}^2$ $t_{11}^1 t_{12}^2$ $t_{12}^1 t_{11}^2$ $t_{11}^1 t_{12}^1$ $t_{12}^1 t_{12}^2$ $t_{11}^2 t_{12}^1$ $t_{11}^2 t_{12}^2$
	<p><b>16a</b></p>	$t_{11}^1 t_{12}^1 t_{11}^2$ $t_{11}^1 t_{12}^2$ $t_{11}^2 t_{11}^1$ $t_{11}^2 t_{12}^1$ $t_{11}^2 t_{12}^2$ $t_{12}^1 t_{11}^1$ $t_{12}^1 t_{12}^2$ $t_{12}^2 t_{11}^1$ $t_{12}^2 t_{12}^1$		
	<p><b>16b</b></p>			
	<p><b>17</b></p>	$t_{11}^1 t_{12}^1 t_{11}^2$ $t_{11}^1 t_{12}^2$ $t_{11}^2 t_{11}^1$ $t_{11}^2 t_{12}^1$ $t_{11}^2 t_{12}^2$ $t_{12}^1 t_{11}^1$ $t_{12}^1 t_{12}^2$ $t_{12}^2 t_{11}^1$ $t_{12}^2 t_{12}^1$		

Robot mobility	Active bricks arrangement	X-chain passive brick	Y-chain passive brick	Z-chain passive brick
	<p><b>10</b></p>	$t_{11}^1 t_{12}^1 t_{11}^2$ $t_{11}^1 t_{12}^2$ $t_{11}^2 t_{11}^1$ $t_{11}^2 t_{12}^1$ $t_{11}^2 t_{12}^2$ $t_{12}^1 t_{11}^1$ $t_{12}^1 t_{12}^2$ $t_{12}^2 t_{11}^1$ $t_{12}^2 t_{12}^1$		$t_{11}^1 t_{11}^2$ $t_{11}^1 t_{12}^2$ $t_{11}^2 t_{11}^1$ $t_{11}^2 t_{12}^1$ $t_{11}^1 t_{12}^1$ $t_{11}^1 t_{12}^2$ $t_{12}^1 t_{11}^1$ $t_{12}^1 t_{12}^2$ $t_{12}^2 t_{11}^1$ $t_{12}^2 t_{12}^1$
	<p><b>11</b></p>		$t_{11}^1 t_{11}^2$ $t_{11}^1 t_{12}^2$ $t_{11}^2 t_{11}^1$ $t_{11}^2 t_{12}^1$ $t_{11}^1 t_{12}^1$ $t_{11}^1 t_{12}^2$ $t_{12}^1 t_{11}^1$ $t_{12}^1 t_{12}^2$ $t_{12}^2 t_{11}^1$ $t_{12}^2 t_{12}^1$	
	<p><b>12</b></p>			
	<p><b>13</b></p>			$t_{11}^1 t_{12}^1 t_{11}^2$ $t_{11}^1 t_{12}^2$ $t_{11}^2 t_{11}^1$ $t_{11}^2 t_{12}^1$ $t_{11}^1 t_{12}^1$ $t_{11}^1 t_{12}^2$ $t_{12}^1 t_{11}^1$ $t_{12}^1 t_{12}^2$ $t_{12}^2 t_{11}^1$ $t_{12}^2 t_{12}^1$
	<p><b>14</b></p>	$t_{11}^1 t_{12}^1 t_{11}^2$ $t_{11}^1 t_{12}^2$ $t_{11}^2 t_{11}^1$ $t_{11}^2 t_{12}^1$ $t_{11}^1 t_{12}^1$ $t_{11}^1 t_{12}^2$ $t_{12}^1 t_{11}^1$ $t_{12}^1 t_{12}^2$ $t_{12}^2 t_{11}^1$ $t_{12}^2 t_{12}^1$		





















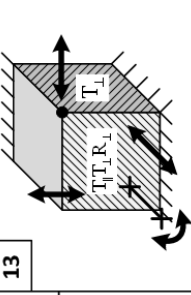
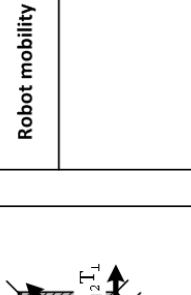
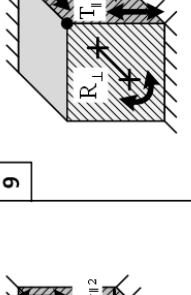
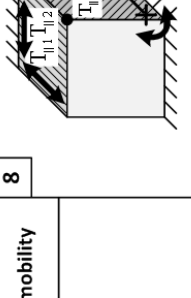
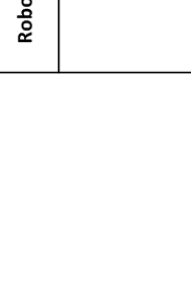











<p>Robot mobility</p>	<p>8</p> 	<p>9</p> 	<p>10a</p> 	<p>10b</p> 	<p>11a</p> 	<p>11b</p> 	<p>12</p>	<p>13</p>	<p>14</p>	<p>15</p>	<p>16</p>	<p>17</p>	<p>18</p>	
<p>X-chain</p> <p>Y-chain</p> <p>Z-chain</p>	<p>X-chain</p> <p>Y-chain</p> <p>Z-chain</p>	<p>X-chain</p> <p>Y-chain</p> <p>Z-chain</p>	<p>X-chain</p> <p>Y-chain</p> <p>Z-chain</p>	<p>X-chain</p> <p>Y-chain</p> <p>Z-chain</p>	<p>X-chain</p> <p>Y-chain</p> <p>Z-chain</p>	<p>X-chain</p> <p>Y-chain</p> <p>Z-chain</p>	<p>X-chain</p> <p>Y-chain</p> <p>Z-chain</p>	<p>X-chain</p> <p>Y-chain</p> <p>Z-chain</p>	<p>X-chain</p> <p>Y-chain</p> <p>Z-chain</p>	<p>X-chain</p> <p>Y-chain</p> <p>Z-chain</p>	<p>X-chain</p> <p>Y-chain</p> <p>Z-chain</p>	<p>X-chain</p> <p>Y-chain</p> <p>Z-chain</p>	<p>X-chain</p> <p>Y-chain</p> <p>Z-chain</p>	<p>X-chain</p> <p>Y-chain</p> <p>Z-chain</p>

























Robot mobility	54		X-chain	Y-chain	Z-chain
	55a		X-chain	Y-chain	Z-chain
	55b		X-chain	Y-chain	Z-chain
	56		X-chain	Y-chain	Z-chain

Robot mobility	53a		X-chain	Y-chain	Z-chain
	53b		X-chain	Y-chain	Z-chain
	53c		X-chain	Y-chain	Z-chain
	53d		X-chain	Y-chain	Z-chain

Robot mobility		4 DOF 2 translations 2 rotations Tx, Ty, Rx, Ry			
57					
58					
59a					
59b					
Robot mobility		4 DOF 2 translations 2 rotations Tx, Ty, Rx, Ry			
57					
58					
59a					
59b					
Robot mobility		4 DOF 2 translations 2 rotations Tx, Ty, Rx, Ry			

Robot mobility		4 DOF 2 translations 2 rotations Tx, Ty, Rx, Ry			
1					
2					
3					
3a					
4					
4a					
4b					
5					
Robot mobility		4 DOF 2 translations 2 rotations Tx, Ty, Rx, Ry			

Robot mobility	12		13			
		X-chain		$t_{11}, t_{12}, t_{11}^2, t_{11}^2$	X-chain	$t_{11}, t_{11}^2, t_{11}^2$
		Y-chain		$t_{11}, t_{11}^2, t_{11}^2$	Y-chain	$t_{11}, t_{11}^2, t_{11}^2$
		Z-chain		$t_{11}, t_{11}^2, t_{11}^2$	Z-chain	$t_{11}, t_{11}^2, t_{11}^2$
Robot mobility	14a		14b			
		X-chain		$t_{11}, t_{11}^2, t_{11}^2$	X-chain	$t_{11}, t_{11}^2, t_{11}^2$
		Y-chain		$t_{11}, t_{11}^2, t_{11}^2$	Y-chain	$t_{11}, t_{11}^2, t_{11}^2$
		Z-chain		$t_{11}, t_{11}^2, t_{11}^2$	Z-chain	$t_{11}, t_{11}^2, t_{11}^2$
Robot mobility	15		16			
		X-chain		$t_{11}, t_{11}^2, t_{11}^2$	X-chain	$t_{11}, t_{11}^2, t_{11}^2$
		Y-chain		$t_{11}, t_{11}^2, t_{11}^2$	Y-chain	$t_{11}, t_{11}^2, t_{11}^2$
		Z-chain		$t_{11}, t_{11}^2, t_{11}^2$	Z-chain	$t_{11}, t_{11}^2, t_{11}^2$

Robot mobility	6		7			
		X-chain		$t_{11}, t_{11}^2, t_{11}^2$	X-chain	$t_{11}, t_{11}^2, t_{11}^2$
		Y-chain		$t_{11}, t_{11}^2, t_{11}^2$	Y-chain	$t_{11}, t_{11}^2, t_{11}^2$
		Z-chain		$t_{11}, t_{11}^2, t_{11}^2$	Z-chain	$t_{11}, t_{11}^2, t_{11}^2$
Robot mobility	8		9			
		X-chain		$t_{11}, t_{11}^2, t_{11}^2$	X-chain	$t_{11}, t_{11}^2, t_{11}^2$
		Y-chain		$t_{11}, t_{11}^2, t_{11}^2$	Y-chain	$t_{11}, t_{11}^2, t_{11}^2$
		Z-chain		$t_{11}, t_{11}^2, t_{11}^2$	Z-chain	$t_{11}, t_{11}^2, t_{11}^2$
Robot mobility	10		11			
		X-chain		$t_{11}, t_{11}^2, t_{11}^2$	X-chain	$t_{11}, t_{11}^2, t_{11}^2$
		Y-chain		$t_{11}, t_{11}^2, t_{11}^2$	Y-chain	$t_{11}, t_{11}^2, t_{11}^2$
		Z-chain		$t_{11}, t_{11}^2, t_{11}^2$	Z-chain	$t_{11}, t_{11}^2, t_{11}^2$

























Robot mobility	34		35	
	X-chain	$t_{11}, t_{12}, t_{11}, t_{11}$	X-chain	$t_{11}, t_{12}, t_{11}, t_{12}, t_{11}$
	Y-chain	$t_{11}, t_{12}, t_{11}, t_{12}, t_{11}$	Y-chain	$t_{11}, t_{12}, t_{11}, t_{12}, t_{11}$
	Z-chain	$t_{11}, t_{12}, t_{11}, t_{12}, t_{11}$	Z-chain	$t_{11}, t_{12}, t_{11}, t_{12}, t_{11}$
	36		37	
	38		39a	
	39b		40	
	X-chain	$t_{11}, t_{12}, t_{11}, t_{12}, t_{11}$	X-chain	$t_{11}, t_{12}, t_{11}, t_{12}, t_{11}$
	Y-chain	$t_{11}, t_{12}, t_{11}, t_{12}, t_{11}$	Y-chain	$t_{11}, t_{12}, t_{11}, t_{12}, t_{11}$
	Z-chain	$t_{11}, t_{12}, t_{11}, t_{12}, t_{11}$	Z-chain	$t_{11}, t_{12}, t_{11}, t_{12}, t_{11}$

Robot mobility	29a		29b	
	X-chain	$t_{11}, t_{12}, t_{11}, t_{11}$	X-chain	$t_{11}, t_{12}, t_{11}, t_{12}, t_{11}$
	Y-chain	$t_{11}, t_{12}, t_{11}, t_{12}, t_{11}$	Y-chain	$t_{11}, t_{12}, t_{11}, t_{12}, t_{11}$
	Z-chain	$t_{11}, t_{12}, t_{11}, t_{12}, t_{11}$	Z-chain	$t_{11}, t_{12}, t_{11}, t_{12}, t_{11}$
	30a		30b	
	31		32a	
	32b		33	
	X-chain	$t_{11}, t_{12}, t_{11}, t_{12}, t_{11}$	X-chain	$t_{11}, t_{12}, t_{11}, t_{12}, t_{11}$
	Y-chain	$t_{11}, t_{12}, t_{11}, t_{12}, t_{11}$	Y-chain	$t_{11}, t_{12}, t_{11}, t_{12}, t_{11}$
	Z-chain	$t_{11}, t_{12}, t_{11}, t_{12}, t_{11}$	Z-chain	$t_{11}, t_{12}, t_{11}, t_{12}, t_{11}$



Robot mobility			
	<p><b>41</b></p> <p>X-chain <math>t_{11}, t_{12}, t_{11}^2, t_{12}^2, t_{11}t_{12}</math></p> <p>Y-chain <math>t_{11}, t_{12}, t_{11}^2, t_{12}^2, t_{11}t_{12}</math></p> <p>Z-chain <math>t_{11}, t_{12}, t_{11}^2, t_{12}^2, t_{11}t_{12}</math></p>	<p><b>42</b></p> <p>X-chain <math>t_{11}, t_{12}, t_{11}^2, t_{12}^2, t_{11}t_{12}</math></p> <p>Y-chain <math>t_{11}, t_{12}, t_{11}^2, t_{12}^2, t_{11}t_{12}</math></p> <p>Z-chain <math>t_{11}, t_{12}, t_{11}^2, t_{12}^2, t_{11}t_{12}</math></p>	<p><b>43</b></p> <p>X-chain <math>t_{11}, t_{12}, t_{11}^2, t_{12}^2, t_{11}t_{12}</math></p> <p>Y-chain <math>t_{11}, t_{12}, t_{11}^2, t_{12}^2, t_{11}t_{12}</math></p> <p>Z-chain <math>t_{11}, t_{12}, t_{11}^2, t_{12}^2, t_{11}t_{12}</math></p>
		<p><b>44</b></p>	<p><b>48a</b></p>
	<p><b>45a</b></p>	<p><b>45b</b></p>	<p><b>48b</b></p>
	<p><b>49a</b></p>	<p><b>49b</b></p>	<p><b>49c</b></p>
	<p><b>50</b></p>	<p><b>51</b></p>	<p><b>51</b></p>
	<p><b>50</b></p>	<p><b>51</b></p>	<p><b>51</b></p>
	<p><b>50</b></p>	<p><b>51</b></p>	<p><b>51</b></p>

Robot mobility	60		X-chain	Y-chain	Z-chain	61		X-chain	Y-chain	Z-chain
			$t_{11}, t_{12}, t_{11}^1, t_{11}^2$	$t_{11}, t_{12}, t_{11}^1, t_{11}^2$	$t_{11}, t_{12}, t_{11}^1, t_{11}^2$			$t_{11}, t_{12}, t_{11}^1, t_{11}^2$	$t_{11}, t_{12}, t_{11}^1, t_{11}^2$	$t_{11}, t_{12}, t_{11}^1, t_{11}^2$
	62					63				
			$t_{11}, t_{12}, t_{11}^1, t_{11}^2$	$t_{11}, t_{12}, t_{11}^1, t_{11}^2$	$t_{11}, t_{12}, t_{11}^1, t_{11}^2$			$t_{11}, t_{12}, t_{11}^1, t_{11}^2$	$t_{11}, t_{12}, t_{11}^1, t_{11}^2$	$t_{11}, t_{12}, t_{11}^1, t_{11}^2$
	64					65				
			$t_{11}, t_{12}, t_{11}^1, t_{11}^2$	$t_{11}, t_{12}, t_{11}^1, t_{11}^2$	$t_{11}, t_{12}, t_{11}^1, t_{11}^2$			$t_{11}, t_{12}, t_{11}^1, t_{11}^2$	$t_{11}, t_{12}, t_{11}^1, t_{11}^2$	$t_{11}, t_{12}, t_{11}^1, t_{11}^2$
	66					67a				
			$t_{11}, t_{12}, t_{11}^1, t_{11}^2$	$t_{11}, t_{12}, t_{11}^1, t_{11}^2$	$t_{11}, t_{12}, t_{11}^1, t_{11}^2$			$t_{11}, t_{12}, t_{11}^1, t_{11}^2$	$t_{11}, t_{12}, t_{11}^1, t_{11}^2$	$t_{11}, t_{12}, t_{11}^1, t_{11}^2$

Robot mobility	52		X-chain	Y-chain	Z-chain	53		X-chain	Y-chain	Z-chain
			$t_{11}, t_{12}, t_{11}^1, t_{11}^2$	$t_{11}, t_{12}, t_{11}^1, t_{11}^2$	$t_{11}, t_{12}, t_{11}^1, t_{11}^2$			$t_{11}, t_{12}, t_{11}^1, t_{11}^2$	$t_{11}, t_{12}, t_{11}^1, t_{11}^2$	$t_{11}, t_{12}, t_{11}^1, t_{11}^2$
	54					55				
			$t_{11}, t_{12}, t_{11}^1, t_{11}^2$	$t_{11}, t_{12}, t_{11}^1, t_{11}^2$	$t_{11}, t_{12}, t_{11}^1, t_{11}^2$			$t_{11}, t_{12}, t_{11}^1, t_{11}^2$	$t_{11}, t_{12}, t_{11}^1, t_{11}^2$	$t_{11}, t_{12}, t_{11}^1, t_{11}^2$
	56					57				
			$t_{11}, t_{12}, t_{11}^1, t_{11}^2$	$t_{11}, t_{12}, t_{11}^1, t_{11}^2$	$t_{11}, t_{12}, t_{11}^1, t_{11}^2$			$t_{11}, t_{12}, t_{11}^1, t_{11}^2$	$t_{11}, t_{12}, t_{11}^1, t_{11}^2$	$t_{11}, t_{12}, t_{11}^1, t_{11}^2$
	58					59				
			$t_{11}, t_{12}, t_{11}^1, t_{11}^2$	$t_{11}, t_{12}, t_{11}^1, t_{11}^2$	$t_{11}, t_{12}, t_{11}^1, t_{11}^2$			$t_{11}, t_{12}, t_{11}^1, t_{11}^2$	$t_{11}, t_{12}, t_{11}^1, t_{11}^2$	$t_{11}, t_{12}, t_{11}^1, t_{11}^2$



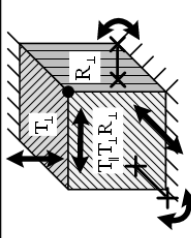



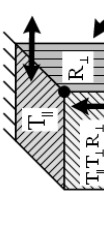

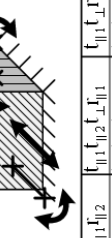



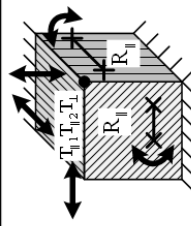

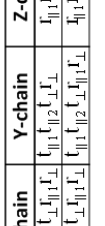

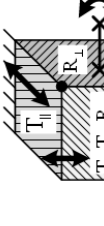

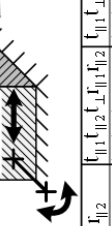





Robot mobility	22a		22b	
	X-chain	Y-chain	Z-chain	X-chain
	$f_{  1} f_{\perp 1} f_{\perp 2}$ $f_{  1} f_{\perp 1}$	$f_{  1} f_{\perp 1} f_{\perp 2}$ $f_{  1} f_{\perp 1} f_{\perp 2} f_{\perp 1}$	$f_{  1} f_{\perp 1} f_{\perp 2}$ $f_{  1} f_{\perp 1} f_{\perp 2} f_{\perp 1}$	$f_{  1} f_{\perp 1} f_{\perp 2}$ $f_{  1} f_{\perp 1}$
	<b>23</b>			
	$f_{  1} f_{\perp 1} f_{\perp 2}$ $f_{  1} f_{\perp 1}$	$f_{  1} f_{\perp 1} f_{\perp 2}$ $f_{  1} f_{\perp 1} f_{\perp 2} f_{\perp 1}$	$f_{  1} f_{\perp 1} f_{\perp 2}$ $f_{  1} f_{\perp 1} f_{\perp 2} f_{\perp 1}$	$f_{  1} f_{\perp 1} f_{\perp 2}$ $f_{  1} f_{\perp 1}$
	<b>26</b>			
	$f_{  1} f_{\perp 1}$ $f_{  1} f_{\perp 1} f_{\perp 2}$	$f_{  1} f_{\perp 1} f_{\perp 2} f_{\perp 1}$ $f_{  1} f_{\perp 1} f_{\perp 2} f_{\perp 1}$	$f_{  1} f_{\perp 1}$ $f_{  1} f_{\perp 1} f_{\perp 2}$	$f_{  1} f_{\perp 1}$ $f_{  1} f_{\perp 1} f_{\perp 2}$
	<b>27</b>			
	$f_{  1} f_{\perp 1} f_{\perp 2}$ $f_{  1} f_{\perp 1} f_{\perp 2}$	$f_{  1} f_{\perp 1} f_{\perp 2} f_{\perp 1}$ $f_{  1} f_{\perp 1} f_{\perp 2} f_{\perp 1}$	$f_{  1} f_{\perp 1}$ $f_{  1} f_{\perp 1} f_{\perp 2}$	$f_{  1} f_{\perp 1}$ $f_{  1} f_{\perp 1} f_{\perp 2}$

Robot mobility	15		16	
	X-chain	Y-chain	Z-chain	X-chain
	$f_{  1} f_{\perp 1} f_{\perp 2}$ $f_{  1} f_{\perp 1}$	$f_{  1} f_{\perp 1} f_{\perp 2}$ $f_{  1} f_{\perp 1} f_{\perp 2} f_{\perp 1}$	$f_{  1} f_{\perp 1} f_{\perp 2}$ $f_{  1} f_{\perp 1} f_{\perp 2} f_{\perp 1}$	$f_{  1} f_{\perp 1} f_{\perp 2}$ $f_{  1} f_{\perp 1} f_{\perp 2}$
	<b>17</b>			
	$f_{  1} f_{\perp 1} f_{\perp 2}$ $f_{  1} f_{\perp 1}$	$f_{  1} f_{\perp 1} f_{\perp 2}$ $f_{  1} f_{\perp 1} f_{\perp 2} f_{\perp 1}$	$f_{  1} f_{\perp 1} f_{\perp 2}$ $f_{  1} f_{\perp 1} f_{\perp 2} f_{\perp 1}$	$f_{  1} f_{\perp 1} f_{\perp 2}$ $f_{  1} f_{\perp 1}$
	<b>19</b>			
	$f_{  1} f_{\perp 1} f_{\perp 2}$ $f_{  1} f_{\perp 1} f_{\perp 2}$	$f_{  1} f_{\perp 1} f_{\perp 2} f_{\perp 1}$ $f_{  1} f_{\perp 1} f_{\perp 2} f_{\perp 1}$	$f_{  1} f_{\perp 1} f_{\perp 2}$ $f_{  1} f_{\perp 1} f_{\perp 2} f_{\perp 1}$	$f_{  1} f_{\perp 1} f_{\perp 2}$ $f_{  1} f_{\perp 1}$
	<b>20</b>			
	$f_{  1} f_{\perp 1} f_{\perp 2}$ $f_{  1} f_{\perp 1} f_{\perp 2}$	$f_{  1} f_{\perp 1} f_{\perp 2} f_{\perp 1}$ $f_{  1} f_{\perp 1} f_{\perp 2} f_{\perp 1}$	$f_{  1} f_{\perp 1}$ $f_{  1} f_{\perp 1} f_{\perp 2}$	$f_{  1} f_{\perp 1}$ $f_{  1} f_{\perp 1}$

<p>Robot mobility</p>	<p>34</p> 	<p>35</p> 	
	<p>X-chain</p> $T_{11}T_{12}T_{13}$ $T_{11}T_{12}T_{13}$ $T_{11}T_{12}T_{13}$	<p>Y-chain</p> $T_{11}T_{12}T_{13}$ $T_{11}T_{12}T_{13}$ $T_{11}T_{12}T_{13}$	<p>Z-chain</p> $T_{11}T_{12}T_{13}$ $T_{11}T_{12}T_{13}$ $T_{11}T_{12}T_{13}$
	<p>36</p> 	<p>37</p> 	
	<p>38a</p> 	<p>38b</p> 	
	<p>39</p> 	<p>40</p> 	

<p>Robot mobility</p>	<p>29a</p> 	<p>29b</p> 	
	<p>X-chain</p> $T_{11}T_{12}T_{13}$ $T_{11}T_{12}T_{13}$ $T_{11}T_{12}T_{13}$	<p>Y-chain</p> $T_{11}T_{12}T_{13}$ $T_{11}T_{12}T_{13}$ $T_{11}T_{12}T_{13}$	<p>Z-chain</p> $T_{11}T_{12}T_{13}$ $T_{11}T_{12}T_{13}$ $T_{11}T_{12}T_{13}$
	<p>30</p> 	<p>31</p> 	
	<p>32</p> 	<p>33a</p> 	
	<p>33b</p> 	<p>33c</p> 	





Robot mobility	61	62
Robot mobility		
Robot mobility		
Robot mobility		
Robot mobility		







Robot mobility	10	11
6 DOF 3 translations 3 rotations Tx, Ty, Tz, Rx, Ry, Rz		
1		
2		
3		
4		
5		
6		
7		
8		
9		
10		
11		
12		
13		
14		
15		
16		
17		
18		
19		
20		

Robot mobility	30		31		
	X-chain	$t_{11}, t_{12}, t_{11}^T, t_{12}^T$	Y-chain	$t_{11}, t_{12}, t_{11}^T, t_{12}^T$	Z-chain
	32		33		
	34		35		
	36		37		
	38		39		
		$t_{11}, t_{12}, t_{11}^T, t_{12}^T$		$t_{11}, t_{12}, t_{11}^T, t_{12}^T$	

Robot mobility	20		21		
	X-chain	$t_{11}, t_{12}, t_{11}^T, t_{12}^T$	Y-chain	$t_{11}, t_{12}, t_{11}^T, t_{12}^T$	Z-chain
	22		23		
	24		25		
	26		27		
	28		29		
		$t_{11}, t_{12}, t_{11}^T, t_{12}^T$		$t_{11}, t_{12}, t_{11}^T, t_{12}^T$	







Robot mobility				
	80	81	82	83

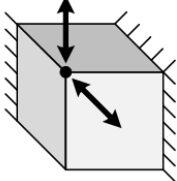
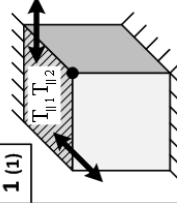
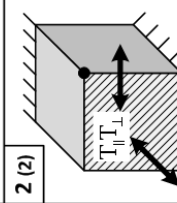

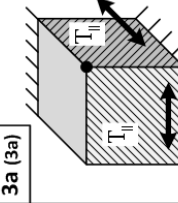
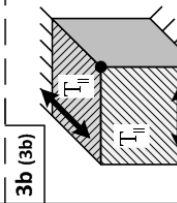
## Appendix C

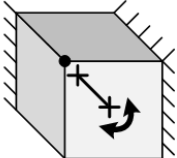
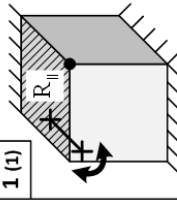
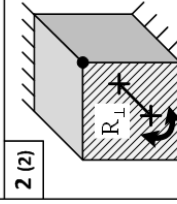
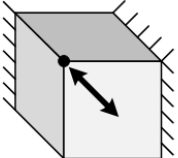
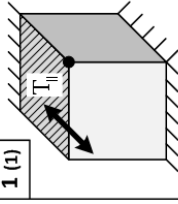
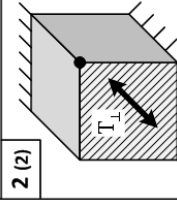
# Reduced solution catalogue for ultra-high precision

This appendix features the reduced conceptual solution catalogue for ultra-high precision, which solely includes the kinematic solutions which are exclusively composed of the building bricks which have been selected for ultra-high precision applications (see chapter 4).

As in appendix B, the kinematic arrangements of active bricks are graphically represented and arranged according to the mobility which the robot end-effector performs, whereas the corresponding passive bricks solutions are simply listed. Moreover, the orientations of the motions along the x, y and z axes have been arbitrarily set: a simple rotation of the robot cube allows to reorient the mobility along the desired directions.

Note that each solution features a double numbering system: the plain numeral stands for the position of the solution in the reduced catalogue, whereas the number in parentheses refers to its rank in the exhaustive catalogue.

Robot mobility	Active bricks arrangement	X-chain passive brick	Y-chain passive brick	Z-chain passive brick
 <p>2 DOF 2 translations Tx, Ty</p>	<p><b>1 (1)</b></p> 			
	<p><b>2 (2)</b></p> 			
	<p><b>3a (3a)</b></p> 	$t_{11}, t_{12}, t_{13}, t_{21}, t_{22}, t_{23}, t_{31}, t_{32}, t_{33}$	$t_{11}, t_{12}, t_{13}, t_{21}, t_{22}, t_{23}, t_{31}, t_{32}, t_{33}$	
	<p><b>3b (3b)</b></p> 	$t_{11}, t_{12}, t_{13}, t_{21}, t_{22}, t_{23}, t_{31}, t_{32}, t_{33}$		
		$t_{11}, t_{12}, t_{13}, t_{21}, t_{22}, t_{23}, t_{31}, t_{32}, t_{33}$		
		$t_{11}, t_{12}, t_{13}, t_{21}, t_{22}, t_{23}, t_{31}, t_{32}, t_{33}$		

Robot mobility	Active bricks arrangement	X-chain passive brick	Y-chain passive brick	Z-chain passive brick
 <p>Revolute joint 1 DOF 1 rotation: Rx</p>	<p><b>1 (1)</b></p> 			
	<p><b>2 (2)</b></p> 			
 <p>Prismatic joint 1 DOF 1 translation: Tx</p>	<p><b>1 (1)</b></p> 			
	<p><b>2 (2)</b></p> 			







































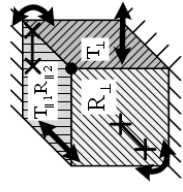
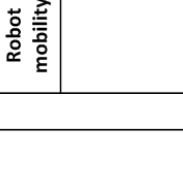
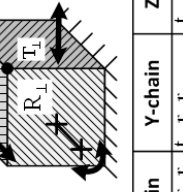
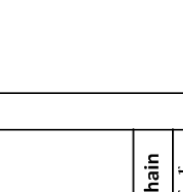
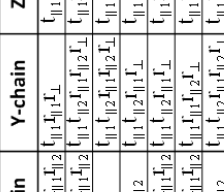
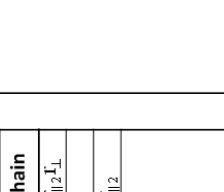

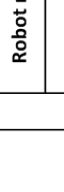


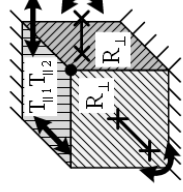
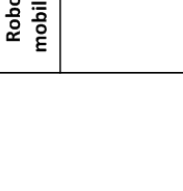
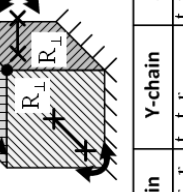

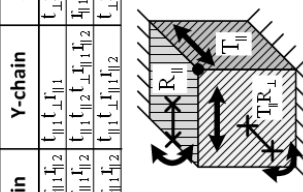

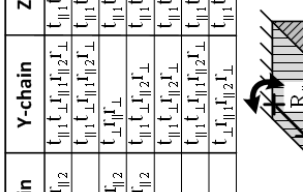

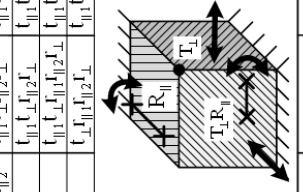

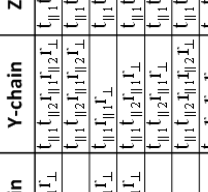





<p>Robot mobility</p> <p>4 DOF 2 translations 2 rotations Tx, Ty, Rz, Ry</p>	<p>1 (7)</p>	<p>2 (8)</p>	<p>3 (9)</p>	<p>4 (10)</p>																																			
	<table border="1"> <thead> <tr> <th>X-chain</th> <th>Y-chain</th> <th>Z-chain</th> </tr> </thead> <tbody> <tr> <td><math>f_{11}^1, f_{11}^2, f_{11}^3, f_{11}^4</math></td> <td><math>f_{11}^1, f_{11}^2</math></td> <td><math>f_{11}^1, f_{11}^2, f_{11}^3, f_{11}^4</math></td> </tr> <tr> <td><math>f_{11}^1, f_{11}^2, f_{11}^3, f_{11}^4</math></td> <td><math>f_{11}^1, f_{11}^2, f_{11}^3, f_{11}^4</math></td> <td><math>f_{11}^1, f_{11}^2, f_{11}^3, f_{11}^4</math></td> </tr> </tbody> </table>	X-chain	Y-chain	Z-chain	$f_{11}^1, f_{11}^2, f_{11}^3, f_{11}^4$	$f_{11}^1, f_{11}^2$	$f_{11}^1, f_{11}^2, f_{11}^3, f_{11}^4$	$f_{11}^1, f_{11}^2, f_{11}^3, f_{11}^4$	$f_{11}^1, f_{11}^2, f_{11}^3, f_{11}^4$	$f_{11}^1, f_{11}^2, f_{11}^3, f_{11}^4$	<table border="1"> <thead> <tr> <th>X-chain</th> <th>Y-chain</th> <th>Z-chain</th> </tr> </thead> <tbody> <tr> <td><math>f_{11}^1, f_{11}^2, f_{11}^3, f_{11}^4</math></td> <td><math>f_{11}^1, f_{11}^2, f_{11}^3, f_{11}^4</math></td> <td><math>f_{11}^1, f_{11}^2, f_{11}^3, f_{11}^4</math></td> </tr> <tr> <td><math>f_{11}^1, f_{11}^2, f_{11}^3, f_{11}^4</math></td> <td><math>f_{11}^1, f_{11}^2, f_{11}^3, f_{11}^4</math></td> <td><math>f_{11}^1, f_{11}^2, f_{11}^3, f_{11}^4</math></td> </tr> </tbody> </table>	X-chain	Y-chain	Z-chain	$f_{11}^1, f_{11}^2, f_{11}^3, f_{11}^4$	$f_{11}^1, f_{11}^2, f_{11}^3, f_{11}^4$	$f_{11}^1, f_{11}^2, f_{11}^3, f_{11}^4$	$f_{11}^1, f_{11}^2, f_{11}^3, f_{11}^4$	$f_{11}^1, f_{11}^2, f_{11}^3, f_{11}^4$	$f_{11}^1, f_{11}^2, f_{11}^3, f_{11}^4$	<table border="1"> <thead> <tr> <th>X-chain</th> <th>Y-chain</th> <th>Z-chain</th> </tr> </thead> <tbody> <tr> <td><math>f_{11}^1, f_{11}^2, f_{11}^3, f_{11}^4</math></td> <td><math>f_{11}^1, f_{11}^2, f_{11}^3, f_{11}^4</math></td> <td><math>f_{11}^1, f_{11}^2, f_{11}^3, f_{11}^4</math></td> </tr> <tr> <td><math>f_{11}^1, f_{11}^2, f_{11}^3, f_{11}^4</math></td> <td><math>f_{11}^1, f_{11}^2, f_{11}^3, f_{11}^4</math></td> <td><math>f_{11}^1, f_{11}^2, f_{11}^3, f_{11}^4</math></td> </tr> </tbody> </table>	X-chain	Y-chain	Z-chain	$f_{11}^1, f_{11}^2, f_{11}^3, f_{11}^4$	$f_{11}^1, f_{11}^2, f_{11}^3, f_{11}^4$	$f_{11}^1, f_{11}^2, f_{11}^3, f_{11}^4$	$f_{11}^1, f_{11}^2, f_{11}^3, f_{11}^4$	$f_{11}^1, f_{11}^2, f_{11}^3, f_{11}^4$	$f_{11}^1, f_{11}^2, f_{11}^3, f_{11}^4$	<table border="1"> <thead> <tr> <th>X-chain</th> <th>Y-chain</th> <th>Z-chain</th> </tr> </thead> <tbody> <tr> <td><math>f_{11}^1, f_{11}^2, f_{11}^3, f_{11}^4</math></td> <td><math>f_{11}^1, f_{11}^2, f_{11}^3, f_{11}^4</math></td> <td><math>f_{11}^1, f_{11}^2, f_{11}^3, f_{11}^4</math></td> </tr> <tr> <td><math>f_{11}^1, f_{11}^2, f_{11}^3, f_{11}^4</math></td> <td><math>f_{11}^1, f_{11}^2, f_{11}^3, f_{11}^4</math></td> <td><math>f_{11}^1, f_{11}^2, f_{11}^3, f_{11}^4</math></td> </tr> </tbody> </table>	X-chain	Y-chain	Z-chain	$f_{11}^1, f_{11}^2, f_{11}^3, f_{11}^4$	$f_{11}^1, f_{11}^2, f_{11}^3, f_{11}^4$	$f_{11}^1, f_{11}^2, f_{11}^3, f_{11}^4$	$f_{11}^1, f_{11}^2, f_{11}^3, f_{11}^4$	$f_{11}^1, f_{11}^2, f_{11}^3, f_{11}^4$
X-chain	Y-chain	Z-chain																																					
$f_{11}^1, f_{11}^2, f_{11}^3, f_{11}^4$	$f_{11}^1, f_{11}^2$	$f_{11}^1, f_{11}^2, f_{11}^3, f_{11}^4$																																					
$f_{11}^1, f_{11}^2, f_{11}^3, f_{11}^4$	$f_{11}^1, f_{11}^2, f_{11}^3, f_{11}^4$	$f_{11}^1, f_{11}^2, f_{11}^3, f_{11}^4$																																					
X-chain	Y-chain	Z-chain																																					
$f_{11}^1, f_{11}^2, f_{11}^3, f_{11}^4$	$f_{11}^1, f_{11}^2, f_{11}^3, f_{11}^4$	$f_{11}^1, f_{11}^2, f_{11}^3, f_{11}^4$																																					
$f_{11}^1, f_{11}^2, f_{11}^3, f_{11}^4$	$f_{11}^1, f_{11}^2, f_{11}^3, f_{11}^4$	$f_{11}^1, f_{11}^2, f_{11}^3, f_{11}^4$																																					
X-chain	Y-chain	Z-chain																																					
$f_{11}^1, f_{11}^2, f_{11}^3, f_{11}^4$	$f_{11}^1, f_{11}^2, f_{11}^3, f_{11}^4$	$f_{11}^1, f_{11}^2, f_{11}^3, f_{11}^4$																																					
$f_{11}^1, f_{11}^2, f_{11}^3, f_{11}^4$	$f_{11}^1, f_{11}^2, f_{11}^3, f_{11}^4$	$f_{11}^1, f_{11}^2, f_{11}^3, f_{11}^4$																																					
X-chain	Y-chain	Z-chain																																					
$f_{11}^1, f_{11}^2, f_{11}^3, f_{11}^4$	$f_{11}^1, f_{11}^2, f_{11}^3, f_{11}^4$	$f_{11}^1, f_{11}^2, f_{11}^3, f_{11}^4$																																					
$f_{11}^1, f_{11}^2, f_{11}^3, f_{11}^4$	$f_{11}^1, f_{11}^2, f_{11}^3, f_{11}^4$	$f_{11}^1, f_{11}^2, f_{11}^3, f_{11}^4$																																					
<p>5 (21)</p>	<p>6 (22)</p>																																						
<table border="1"> <thead> <tr> <th>X-chain</th> <th>Y-chain</th> <th>Z-chain</th> </tr> </thead> <tbody> <tr> <td><math>f_{11}^1, f_{11}^2, f_{11}^3, f_{11}^4</math></td> <td><math>f_{11}^1, f_{11}^2, f_{11}^3, f_{11}^4</math></td> <td><math>f_{11}^1, f_{11}^2, f_{11}^3, f_{11}^4</math></td> </tr> <tr> <td><math>f_{11}^1, f_{11}^2, f_{11}^3, f_{11}^4</math></td> <td><math>f_{11}^1, f_{11}^2, f_{11}^3, f_{11}^4</math></td> <td><math>f_{11}^1, f_{11}^2, f_{11}^3, f_{11}^4</math></td> </tr> </tbody> </table>	X-chain	Y-chain	Z-chain	$f_{11}^1, f_{11}^2, f_{11}^3, f_{11}^4$	$f_{11}^1, f_{11}^2, f_{11}^3, f_{11}^4$	$f_{11}^1, f_{11}^2, f_{11}^3, f_{11}^4$	$f_{11}^1, f_{11}^2, f_{11}^3, f_{11}^4$	$f_{11}^1, f_{11}^2, f_{11}^3, f_{11}^4$	$f_{11}^1, f_{11}^2, f_{11}^3, f_{11}^4$	<table border="1"> <thead> <tr> <th>X-chain</th> <th>Y-chain</th> <th>Z-chain</th> </tr> </thead> <tbody> <tr> <td><math>f_{11}^1, f_{11}^2, f_{11}^3, f_{11}^4</math></td> <td><math>f_{11}^1, f_{11}^2, f_{11}^3, f_{11}^4</math></td> <td><math>f_{11}^1, f_{11}^2, f_{11}^3, f_{11}^4</math></td> </tr> <tr> <td><math>f_{11}^1, f_{11}^2, f_{11}^3, f_{11}^4</math></td> <td><math>f_{11}^1, f_{11}^2, f_{11}^3, f_{11}^4</math></td> <td><math>f_{11}^1, f_{11}^2, f_{11}^3, f_{11}^4</math></td> </tr> </tbody> </table>	X-chain	Y-chain	Z-chain	$f_{11}^1, f_{11}^2, f_{11}^3, f_{11}^4$	$f_{11}^1, f_{11}^2, f_{11}^3, f_{11}^4$	$f_{11}^1, f_{11}^2, f_{11}^3, f_{11}^4$	$f_{11}^1, f_{11}^2, f_{11}^3, f_{11}^4$	$f_{11}^1, f_{11}^2, f_{11}^3, f_{11}^4$	$f_{11}^1, f_{11}^2, f_{11}^3, f_{11}^4$																				
X-chain	Y-chain	Z-chain																																					
$f_{11}^1, f_{11}^2, f_{11}^3, f_{11}^4$	$f_{11}^1, f_{11}^2, f_{11}^3, f_{11}^4$	$f_{11}^1, f_{11}^2, f_{11}^3, f_{11}^4$																																					
$f_{11}^1, f_{11}^2, f_{11}^3, f_{11}^4$	$f_{11}^1, f_{11}^2, f_{11}^3, f_{11}^4$	$f_{11}^1, f_{11}^2, f_{11}^3, f_{11}^4$																																					
X-chain	Y-chain	Z-chain																																					
$f_{11}^1, f_{11}^2, f_{11}^3, f_{11}^4$	$f_{11}^1, f_{11}^2, f_{11}^3, f_{11}^4$	$f_{11}^1, f_{11}^2, f_{11}^3, f_{11}^4$																																					
$f_{11}^1, f_{11}^2, f_{11}^3, f_{11}^4$	$f_{11}^1, f_{11}^2, f_{11}^3, f_{11}^4$	$f_{11}^1, f_{11}^2, f_{11}^3, f_{11}^4$																																					

<p>Robot mobility</p>	<p>24b (55b)</p>	<p>25 (56)</p>																	
	<table border="1"> <thead> <tr> <th>X-chain</th> <th>Y-chain</th> <th>Z-chain</th> </tr> </thead> <tbody> <tr> <td><math>f_{11}^1, f_{11}^2, f_{11}^3, f_{11}^4</math></td> <td><math>f_{11}^1, f_{11}^2, f_{11}^3, f_{11}^4</math></td> <td><math>f_{11}^1, f_{11}^2, f_{11}^3, f_{11}^4</math></td> </tr> <tr> <td><math>f_{11}^1, f_{11}^2, f_{11}^3, f_{11}^4</math></td> <td><math>f_{11}^1, f_{11}^2, f_{11}^3, f_{11}^4</math></td> <td><math>f_{11}^1, f_{11}^2, f_{11}^3, f_{11}^4</math></td> </tr> </tbody> </table>	X-chain	Y-chain	Z-chain	$f_{11}^1, f_{11}^2, f_{11}^3, f_{11}^4$	$f_{11}^1, f_{11}^2, f_{11}^3, f_{11}^4$	$f_{11}^1, f_{11}^2, f_{11}^3, f_{11}^4$	$f_{11}^1, f_{11}^2, f_{11}^3, f_{11}^4$	$f_{11}^1, f_{11}^2, f_{11}^3, f_{11}^4$	$f_{11}^1, f_{11}^2, f_{11}^3, f_{11}^4$	<table border="1"> <thead> <tr> <th>X-chain</th> <th>Y-chain</th> <th>Z-chain</th> </tr> </thead> <tbody> <tr> <td><math>f_{11}^1, f_{11}^2, f_{11}^3, f_{11}^4</math></td> <td><math>f_{11}^1, f_{11}^2, f_{11}^3, f_{11}^4</math></td> <td><math>f_{11}^1, f_{11}^2, f_{11}^3, f_{11}^4</math></td> </tr> <tr> <td><math>f_{11}^1, f_{11}^2, f_{11}^3, f_{11}^4</math></td> <td><math>f_{11}^1, f_{11}^2, f_{11}^3, f_{11}^4</math></td> <td><math>f_{11}^1, f_{11}^2, f_{11}^3, f_{11}^4</math></td> </tr> </tbody> </table>	X-chain	Y-chain	Z-chain	$f_{11}^1, f_{11}^2, f_{11}^3, f_{11}^4$	$f_{11}^1, f_{11}^2, f_{11}^3, f_{11}^4$	$f_{11}^1, f_{11}^2, f_{11}^3, f_{11}^4$	$f_{11}^1, f_{11}^2, f_{11}^3, f_{11}^4$	$f_{11}^1, f_{11}^2, f_{11}^3, f_{11}^4$
X-chain	Y-chain	Z-chain																	
$f_{11}^1, f_{11}^2, f_{11}^3, f_{11}^4$	$f_{11}^1, f_{11}^2, f_{11}^3, f_{11}^4$	$f_{11}^1, f_{11}^2, f_{11}^3, f_{11}^4$																	
$f_{11}^1, f_{11}^2, f_{11}^3, f_{11}^4$	$f_{11}^1, f_{11}^2, f_{11}^3, f_{11}^4$	$f_{11}^1, f_{11}^2, f_{11}^3, f_{11}^4$																	
X-chain	Y-chain	Z-chain																	
$f_{11}^1, f_{11}^2, f_{11}^3, f_{11}^4$	$f_{11}^1, f_{11}^2, f_{11}^3, f_{11}^4$	$f_{11}^1, f_{11}^2, f_{11}^3, f_{11}^4$																	
$f_{11}^1, f_{11}^2, f_{11}^3, f_{11}^4$	$f_{11}^1, f_{11}^2, f_{11}^3, f_{11}^4$	$f_{11}^1, f_{11}^2, f_{11}^3, f_{11}^4$																	
<p>26a (59a)</p>	<p>26b (59b)</p>																		
<table border="1"> <thead> <tr> <th>X-chain</th> <th>Y-chain</th> <th>Z-chain</th> </tr> </thead> <tbody> <tr> <td><math>f_{11}^1, f_{11}^2, f_{11}^3, f_{11}^4</math></td> <td><math>f_{11}^1, f_{11}^2, f_{11}^3, f_{11}^4</math></td> <td><math>f_{11}^1, f_{11}^2, f_{11}^3, f_{11}^4</math></td> </tr> <tr> <td><math>f_{11}^1, f_{11}^2, f_{11}^3, f_{11}^4</math></td> <td><math>f_{11}^1, f_{11}^2, f_{11}^3, f_{11}^4</math></td> <td><math>f_{11}^1, f_{11}^2, f_{11}^3, f_{11}^4</math></td> </tr> </tbody> </table>	X-chain	Y-chain	Z-chain	$f_{11}^1, f_{11}^2, f_{11}^3, f_{11}^4$	$f_{11}^1, f_{11}^2, f_{11}^3, f_{11}^4$	$f_{11}^1, f_{11}^2, f_{11}^3, f_{11}^4$	$f_{11}^1, f_{11}^2, f_{11}^3, f_{11}^4$	$f_{11}^1, f_{11}^2, f_{11}^3, f_{11}^4$	$f_{11}^1, f_{11}^2, f_{11}^3, f_{11}^4$	<table border="1"> <thead> <tr> <th>X-chain</th> <th>Y-chain</th> <th>Z-chain</th> </tr> </thead> <tbody> <tr> <td><math>f_{11}^1, f_{11}^2, f_{11}^3, f_{11}^4</math></td> <td><math>f_{11}^1, f_{11}^2, f_{11}^3, f_{11}^4</math></td> <td><math>f_{11}^1, f_{11}^2, f_{11}^3, f_{11}^4</math></td> </tr> <tr> <td><math>f_{11}^1, f_{11}^2, f_{11}^3, f_{11}^4</math></td> <td><math>f_{11}^1, f_{11}^2, f_{11}^3, f_{11}^4</math></td> <td><math>f_{11}^1, f_{11}^2, f_{11}^3, f_{11}^4</math></td> </tr> </tbody> </table>	X-chain	Y-chain	Z-chain	$f_{11}^1, f_{11}^2, f_{11}^3, f_{11}^4$	$f_{11}^1, f_{11}^2, f_{11}^3, f_{11}^4$	$f_{11}^1, f_{11}^2, f_{11}^3, f_{11}^4$	$f_{11}^1, f_{11}^2, f_{11}^3, f_{11}^4$	$f_{11}^1, f_{11}^2, f_{11}^3, f_{11}^4$	$f_{11}^1, f_{11}^2, f_{11}^3, f_{11}^4$
X-chain	Y-chain	Z-chain																	
$f_{11}^1, f_{11}^2, f_{11}^3, f_{11}^4$	$f_{11}^1, f_{11}^2, f_{11}^3, f_{11}^4$	$f_{11}^1, f_{11}^2, f_{11}^3, f_{11}^4$																	
$f_{11}^1, f_{11}^2, f_{11}^3, f_{11}^4$	$f_{11}^1, f_{11}^2, f_{11}^3, f_{11}^4$	$f_{11}^1, f_{11}^2, f_{11}^3, f_{11}^4$																	
X-chain	Y-chain	Z-chain																	
$f_{11}^1, f_{11}^2, f_{11}^3, f_{11}^4$	$f_{11}^1, f_{11}^2, f_{11}^3, f_{11}^4$	$f_{11}^1, f_{11}^2, f_{11}^3, f_{11}^4$																	
$f_{11}^1, f_{11}^2, f_{11}^3, f_{11}^4$	$f_{11}^1, f_{11}^2, f_{11}^3, f_{11}^4$	$f_{11}^1, f_{11}^2, f_{11}^3, f_{11}^4$																	

<p><b>Robot mobility</b></p>	<p><b>13 (37)</b></p> 	<p><b>14 (38)</b></p> 
<p><b>Robot mobility</b></p>	<p><b>13 (37)</b></p> 	<p><b>14 (38)</b></p> 
<p><b>Robot mobility</b></p>	<p><b>4 DOF</b> 1 translation 3 rotations Tx, Rx, Ry, Rz</p> 	<p><b>2 (26)</b></p> 
<p><b>Robot mobility</b></p>	<p><b>1 (25)</b></p> 	<p><b>2 (26)</b></p> 

<p><b>Robot mobility</b></p>	<p><b>7 (23)</b></p> 	<p><b>8 (24)</b></p> 
<p><b>Robot mobility</b></p>	<p><b>9 (29)</b></p> 	<p><b>10 (30)</b></p> 
<p><b>Robot mobility</b></p>	<p><b>11 (33)</b></p> 	<p><b>12 (34)</b></p> 
<p><b>Robot mobility</b></p>	<p><b>11 (33)</b></p> 	<p><b>12 (34)</b></p> 
<p><b>Robot mobility</b></p>	<p><b>11 (33)</b></p> 	<p><b>12 (34)</b></p> 
<p><b>Robot mobility</b></p>	<p><b>11 (33)</b></p> 	<p><b>12 (34)</b></p> 

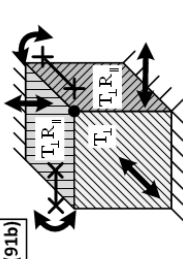
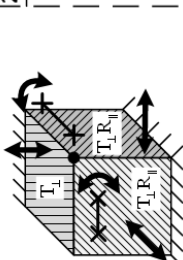
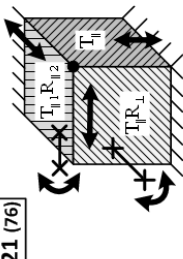
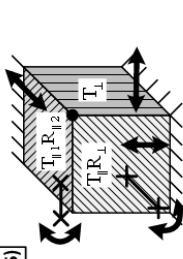
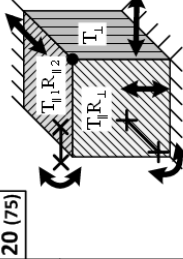
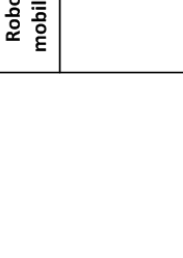



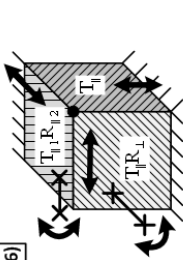
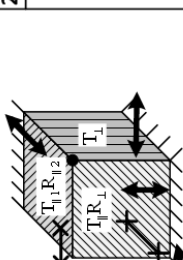
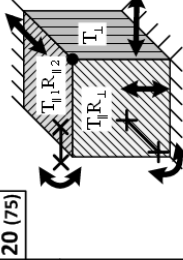
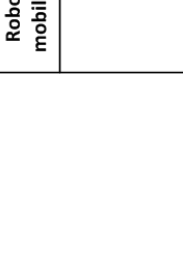

<p><b>Robot mobility</b></p> <p>5 DOF 3 translations 2 rotations Tx, Ty, Tz, Rx, Ry</p>	<p><b>1 (3)</b></p>	<p><b>2 (4)</b></p>
	<p><b>3 (16)</b></p>	<p><b>4 (17)</b></p>
<p><b>5a (18a)</b></p>	<p><b>5b (18b)</b></p>	<p><b>6 (30)</b></p>
<p><b>7 (31)</b></p>	<p><b>7 (31)</b></p>	

<p><b>Robot mobility</b></p>	<p><b>5 (59)</b></p>	<p><b>6 (60)</b></p>
	<p><b>7 (61)</b></p>	<p><b>8 (62)</b></p>
<p><b>9 (82)</b></p>	<p><b>10 (83)</b></p>	<p><b>11 (90)</b></p>
<p><b>12 (91)</b></p>	<p><b>12 (91)</b></p>	





Robot mobility	27a (91a)		27b (91b)	
	<p><b>Robot mobility</b></p> <p>6 DOF 3 translations 3 rotations Tx, Ty, Rz, Rx, Ry, Rz</p>		<p><b>Robot mobility</b></p> <p>6 DOF 3 translations 3 rotations Tx, Ty, Rz, Rx, Ry, Rz</p>	
	<p><b>X-chain</b> <math>t_{11}, t_{12}, t_{11}^2, t_{11}^3</math></p> <p><b>Y-chain</b> <math>t_{11}, t_{12}, t_{11}^2, t_{11}^3</math></p> <p><b>Z-chain</b> <math>t_{11}, t_{12}, t_{11}^2, t_{11}^3</math></p>	<p><b>X-chain</b> <math>t_{11}, t_{12}, t_{11}^2, t_{11}^3</math></p> <p><b>Y-chain</b> <math>t_{11}, t_{12}, t_{11}^2, t_{11}^3</math></p> <p><b>Z-chain</b> <math>t_{11}, t_{12}, t_{11}^2, t_{11}^3</math></p>	<p><b>X-chain</b> <math>t_{11}, t_{12}, t_{11}^2, t_{11}^3</math></p> <p><b>Y-chain</b> <math>t_{11}, t_{12}, t_{11}^2, t_{11}^3</math></p> <p><b>Z-chain</b> <math>t_{11}, t_{12}, t_{11}^2, t_{11}^3</math></p>	<p><b>X-chain</b> <math>t_{11}, t_{12}, t_{11}^2, t_{11}^3</math></p> <p><b>Y-chain</b> <math>t_{11}, t_{12}, t_{11}^2, t_{11}^3</math></p> <p><b>Z-chain</b> <math>t_{11}, t_{12}, t_{11}^2, t_{11}^3</math></p>
	21 (76)		23 (79)	
	20 (75)		22 (77)	
	24 (80)		24 (80)	
	25a (87a)		26 (88)	
	25b (87b)		4 (30)	
	2 (23)		3 (27)	
	5 (34)		5 (34)	

Robot mobility	20 (75)		21 (76)	
	<p><math>t_{11}, t_{12}, t_{11}^2, t_{11}^3</math></p> <p><math>t_{11}, t_{12}, t_{11}^2, t_{11}^3</math></p> <p><math>t_{11}, t_{12}, t_{11}^2, t_{11}^3</math></p>	<p><math>t_{11}, t_{12}, t_{11}^2, t_{11}^3</math></p> <p><math>t_{11}, t_{12}, t_{11}^2, t_{11}^3</math></p> <p><math>t_{11}, t_{12}, t_{11}^2, t_{11}^3</math></p>	<p><math>t_{11}, t_{12}, t_{11}^2, t_{11}^3</math></p> <p><math>t_{11}, t_{12}, t_{11}^2, t_{11}^3</math></p> <p><math>t_{11}, t_{12}, t_{11}^2, t_{11}^3</math></p>	<p><math>t_{11}, t_{12}, t_{11}^2, t_{11}^3</math></p> <p><math>t_{11}, t_{12}, t_{11}^2, t_{11}^3</math></p> <p><math>t_{11}, t_{12}, t_{11}^2, t_{11}^3</math></p>
	22 (77)		23 (79)	
	24 (80)		24 (80)	
	25a (87a)		26 (88)	
	25b (87b)		4 (30)	
	2 (23)		3 (27)	
	5 (34)		5 (34)	





# Appendix D

## Mechanical design of the active bricks for ultra-high precision

In this appendix, the considerations which have led to the Legolas 5 prototype, such as force alignment, compactness, and gravity compensation (see section 6.3), are applied to each of the active bricks for ultra-high precision. Subtleties in the geometric arrangement of the mechanisms proposed in chapter 5 are highlighted, thus leading to several possible design directions.

### D.1 $R_{\parallel}$ and $R_{\perp}$ bricks

The design principle of these bricks actuating a single rotation, which has been detailed in section 5.2.2.1, stems from the same solution as the  $T_{\parallel}R_{\perp}$  brick thoroughly developed in section 6.3.1.3. Consequently, the choice of the parameter  $d$  (the orthogonal distance between the rotation centre and the actuation direction) and of the actuator stroke can be straightforwardly derived from section 6.3.1.1.

As for the geometric arrangement of the  $R_{\parallel}$  and  $R_{\perp}$  bricks design, the following options are possible:

- **Fully planar design**, which thus directly consists in the design proposed in figure 5.8, recollected here as figure D.1: this solution presents the advantage of allowing to align the brick plane with the end-effector, thus suppressing parasitic transverse forces. Nonetheless, this fully planar design necessitates a high value of  $d$ , which can be fulfilled only with small rotation angles or with a high stroke actuator.
- **2-plane design**: this solution is similar to the design of the  $T_{\parallel}R_{\perp}$  brick included in the Legolas 5 robot (see figures 6.11 and D.2): one plane contains the actuation sub-brick, whereas the second features both parts of the RCM mechanism, namely the leaf springs defining the rotation centre and the leaf spring transforming the actuation force into a moment. This design presents the advantages of being efficient regardless the value of the parameter  $d$ , and of allowing for a high compactness. Nevertheless,

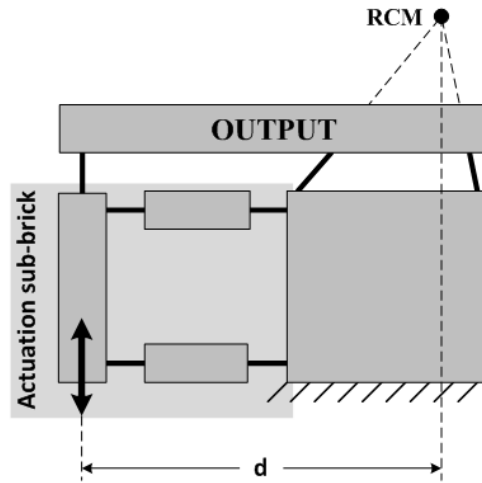


Figure D.1: Sketch of the  $R_{\parallel}$  and  $R_{\perp}$  bricks design principle, including the actuation sub-brick and a Remote Centre of Motion

the force alignment must be carefully performed to limit parasitic displacements due to transverse forces: designing leaf springs with a non-constant breadth is an efficient way to overcome this issue (see section 6.3.4.1).

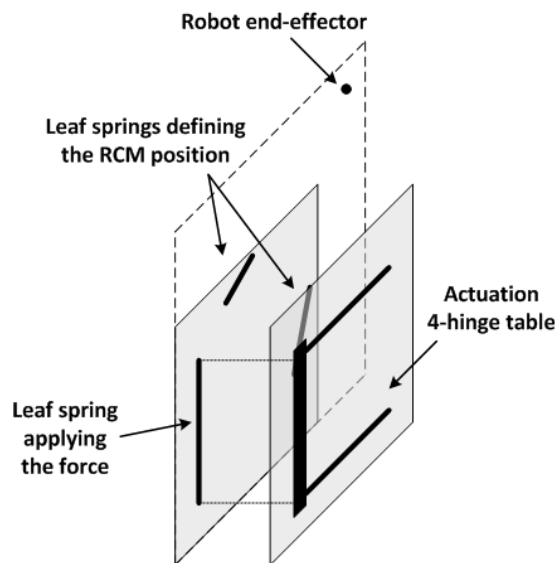


Figure D.2: Geometric arrangement and force alignment of the 2-plane design principle

Lastly, gravity compensation of these bricks must be performed in the following cases:

- *The actuation sub-brick translation is vertical:* a traction spring with minimal stiffness must be added in parallel to the 4-hinge table.
- *The plane which includes the RCM leaf springs is vertical:* the weight of both the RCM

mechanism and the serially arranged passive brick can be simultaneously counter-acted by adding a traction spring between the output of the actuation sub-brick and the passive brick.

## D.2 $T_{\parallel}$ and $T_{\perp}$ bricks

The design of these bricks has been fully detailed in section 5.2.1 for the actuation sub-brick design, and in section 5.2.2.2 for its integration as an active brick in the Legolas 5 prototype. The shape of the leaf springs, *i.e.* their non-constant breadth, is to be adapted according to the force alignment of the whole robot. Furthermore, gravity compensation is necessary only if the actuated translation is vertical.

## D.3 $T_{\parallel 1} T_{\parallel 2}$ and $T_{\parallel} T_{\perp}$ bricks

Two possible designs have been proposed in section 5.2.2.3 for these bricks actuating two translations: the first, recollected in figure D.3, includes two collinear actuators, whereas in the second (see figure D.5), their directions are orthogonal.

As for gravity compensation of these bricks, it must be performed in the following cases (see sections 6.3.3.3 and D.1 for the advocated counteractions):

- *One or both sub-bricks actuate a vertical translation*
- *The plane which includes the lever mechanism is vertical*

### D.3.1 Solution featuring two collinear actuators

This design principle accepts three chief geometric arrangements:

- **Fully planar design:** this option simply consists in the design proposed in figure D.3, left. The main advantage of this fully planar design lies in the possibility of aligning the plane with the robot end-effector to suppress parasitic forces. Furthermore, both actuation sub-bricks can be imbricated to increase the compactness of the mechanism, as proposed in [43] (figure D.3, right): this structure is however not adapted if EC actuators are integrated between both arms of the 4-hinge tables, as discussed in section 6.5, or if high translation strokes must be performed.
- **2-plane design** (figure D.4, left): this solution consists in including the lever mechanism in one plane, and the actuation sub-bricks in a second one, thus allowing for a more compact design. Depending on the selected actuators, the tables can be either imbricated or separated. Furthermore, as the lever mechanism is the part which is the most sensitive to parasitic forces, its plane must be aligned with the robot end-effector.

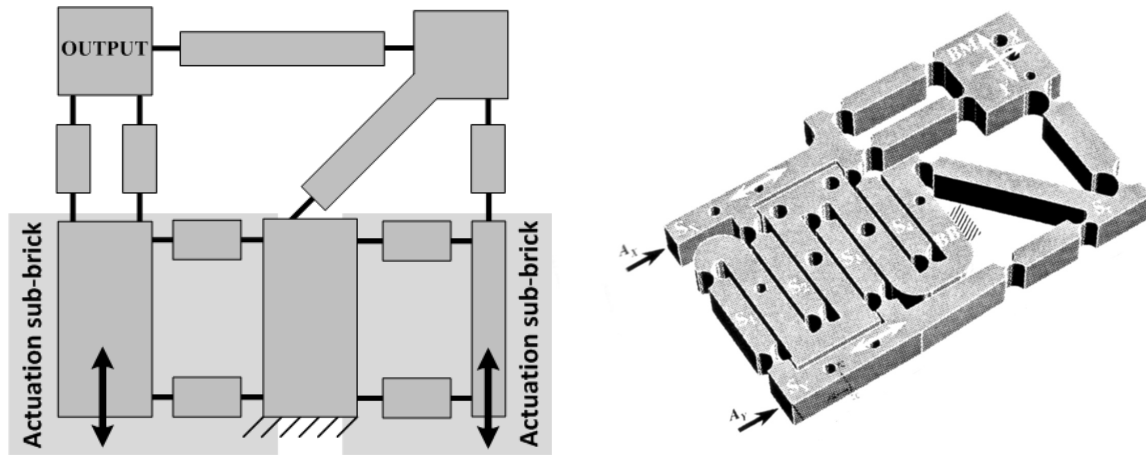


Figure D.3: Sketch of the  $T_{\parallel} T_{\parallel 2}$  and  $T_{\parallel} T_{\perp}$  bricks first design principle, including two actuators oriented in the same direction (left) and illustration of the flexure-based mechanism developed in [43] (right)

- **3-plane design** (figure D.4, right): this last option maximises the compactness of the design by separating the actuation sub-bricks into two different planes; the resulting arrangement is alike the  $T_{\parallel} R_{\perp}$  brick design which has been integrated into the Legolas 5 prototype. This solution presents the key advantages of allowing for any type of actuation (integrated or not), and of being adapted to high translation strokes. As in the previous case, the lever mechanism plane must be aligned with the robot end-effector to minimise parasitic effects.

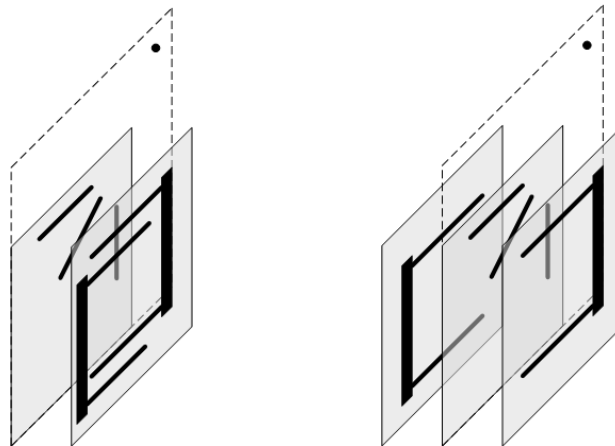


Figure D.4: Geometric arrangement and force alignment of the 2-plane (left) and 3-plane (right) design principles

### D.3.2 Solution featuring two orthogonal actuators

The integration of two orthogonal actuators does not permit an imbricated design, which thus inevitably increases the volume of the fully planar and 2-plane designs. Consequently,

if this option is selected, the most efficient solution consists in the 3-plane design, which is illustrated in figure D.5, right; the same force alignment considerations as previously detailed apply.

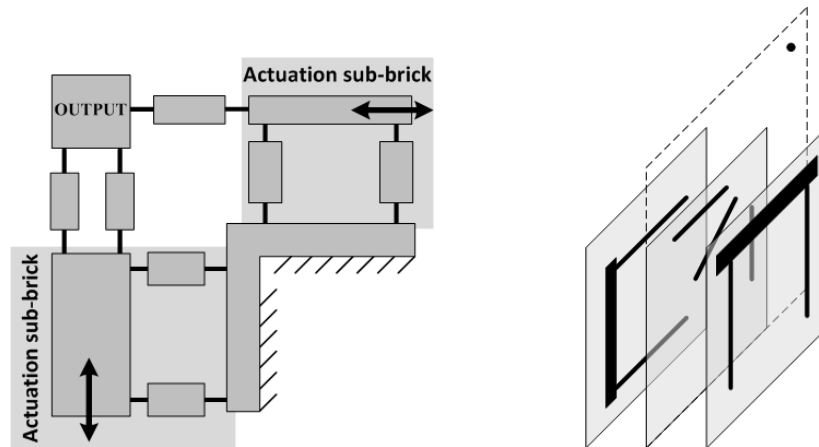


Figure D.5: Sketch of the  $T_{\parallel 1}T_{\parallel 2}$  and  $T_{\parallel}T_{\perp}$  bricks second design principle (left); geometric arrangement and force alignment of the 3-plane design (right)

## D.4 $T_{\parallel}R_{\perp}$ , $T_{\perp}R_{\parallel}$ and $T_{\parallel 1}R_{\parallel 2}$ bricks

The mechanical design of these active bricks accepts two geometric arrangements:

- **A 3-plane arrangement**, which has been integrated into the Legolas 5 prototype (see section 6.3.1.3): this solution allows for a compact design and is efficient independently from the value of the parameter  $d$ . As for the force alignment, the robot end-effector must belong to the plane which includes the RCM mechanism to limit parasitic displacements.
- **A fully planar design**, simply consisting in the solution proposed in figure 5.12, allows for a compact integration of the mechanism, but is only adapted if high values of the parameter  $d$  can be selected. Furthermore, this design can be challenging, depending on the location of the RCM relatively to the active brick: the position of the leaf springs defining the rotation centre must be carefully determined to simultaneously maximise the angle between them and avoid mechanical interferences during the motion. Nonetheless, parasitic displacements can be avoided by aligning the mechanism plane with the robot end-effector.

Similarly to the bricks actuating only a rotation, gravity compensation must be performed in the following cases:

- *The sub-bricks actuate vertical translations*
- *The plane which includes the RCM leaf springs is vertical*

## D.5 $T_{\parallel 1} T_{\parallel 2} R_{\perp}$ and $T_{\parallel 1} T_{\perp} R_{\parallel 2}$ bricks

The design of these active bricks is highly challenging in order to create a compact mechanism which is efficient and robust to forces misalignment: figure D.6 recollects the solution which has been proposed in section 5.2.2.5.

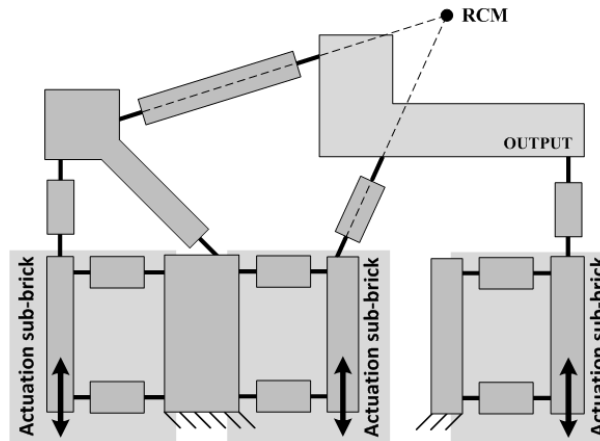


Figure D.6: Sketch of the  $T_{\parallel 1} T_{\parallel 2} R_{\perp}$  and  $T_{\parallel 1} T_{\perp} R_{\parallel 2}$  bricks design principle with RCM

All possible geometric arrangements must include the lever and RCM mechanisms in the same plane, which has to be aligned with the robot end-effector to minimise the effects of parasitic forces. Three main solutions are recommended, namely:

- **A fully planar design**, which simply consists in the solution presented in figure D.6: although this mechanism is efficient regarding the force alignment of the robot, its poor compactness limits its integration into a complete machine, along with other active and passive bricks.
- **2-plane designs** (figure D.7 left and middle), which consist in including the lever and RCM mechanisms in one plane, and the three actuation sub-bricks in a second one. These last can be imbricated if necessary, thus limiting the achievable strokes and rejecting integrated EC actuators, but increasing the compactness of the brick.
- **A 3-plane design**, which consists in the advocated solution (figure D.7, right): the high-stroke sub-brick, which simultaneously actuates a translation and a rotation, is included in a separate plane, which allows to freely chose the parameter  $d$  of the RCM. Moreover, both low-stroke sub-bricks can be imbricated or separated, depending on the actuator choice and of the required strokes.

Similarly to the previous bricks, gravity compensation must be performed in the following cases:

- *The sub-bricks actuate vertical translations*
- *The plane which includes the RCM and lever mechanisms is vertical*

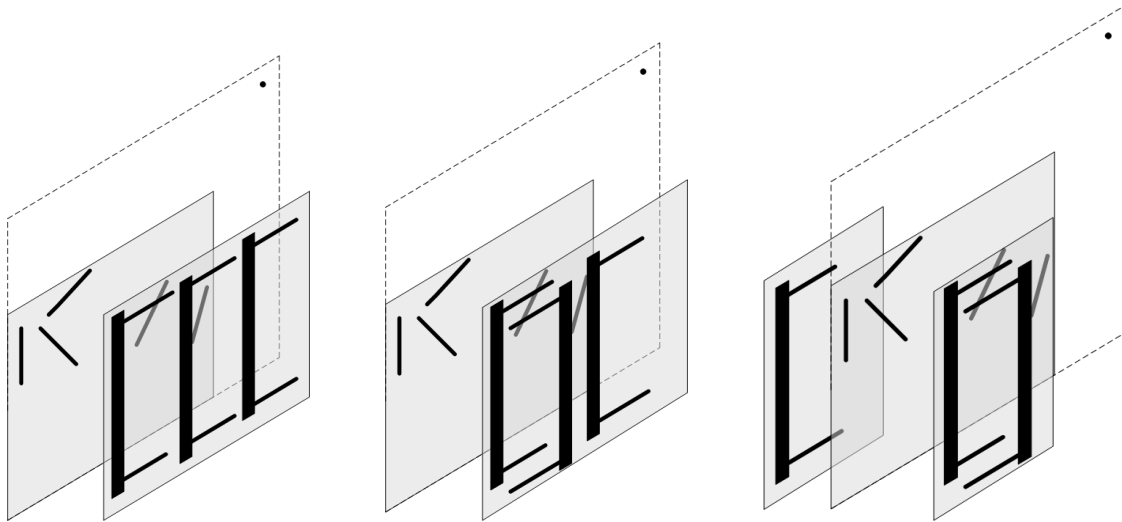


Figure D.7: *Geometric arrangement and force alignment of the 2-plane design with separated actuation (left), with imbricated actuation (middle), and of the 3-plane design (right)*





## Appendix E

# Legolas, ultra-high precision parallel robots family

This appendix completes section 6.2.3 by detailing the arrangements and mechanical designs of the ultra-high precision Legolas family robots: each mobility includes both the selected kinematic solution, excerpted from the catalogues, and the robot design principle. The double numbering of the kinematic arrangements refer to the reduced (first number) and exhaustive (number in brackets) solution catalogues. Figure 3.1 is repeated here to recollect the system coordinates and the notations of the kinematic chains.

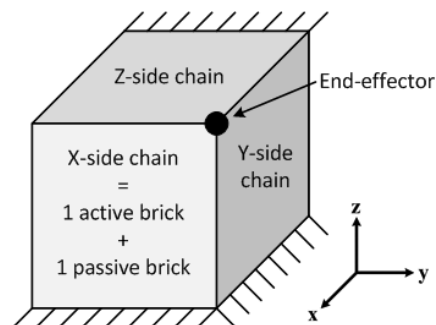


Figure E.1: Symbolism of the parallel robot designed with the modular concept

Furthermore, the mechanical solutions feature the following active and passive bricks:

- $T_{\parallel}$  active brick (violet), whose mechanical design has been detailed in section 6.3.1.2
- $R_{\perp}$  active brick (brown, section D.1)
- $T_{\parallel}R_{\perp}$  active brick (violet and brown, section 6.3.1.3)
- $t_{\parallel}t_{\perp}r_{\parallel}r_{\perp}2$  passive brick (green, section 6.3.2)
- $t_{\parallel}r_{\perp}$  and  $t_{\perp}r_{\parallel}$  passive bricks (blue, see figure E.2 for their detailed mechanical design)

The design outlines include key characteristics of the robots, such as compact arrangement and force alignment to minimise parasitic displacements due to forces and torques applied to the robot end-effector. The latter, although not entirely designed, is symbolised in the figures by a red area; the precise position of the Remote Centres of Motion (RCM) must thus be adapted to each specific case, depending on the robot output detailed design.

Furthermore, as stated in section 6.2.3, the design of the Legolas robots is outlined for identical requirements as the 5-DOF case detailed in chapter 6, namely for translational strokes of  $\pm 5$  mm and rotation angles of  $\pm 10^\circ$  (see section 6.1 for the complete specifications). Moreover, the mechanical solutions presented here include the same sensors and actuators as the Legolas 5 prototype.

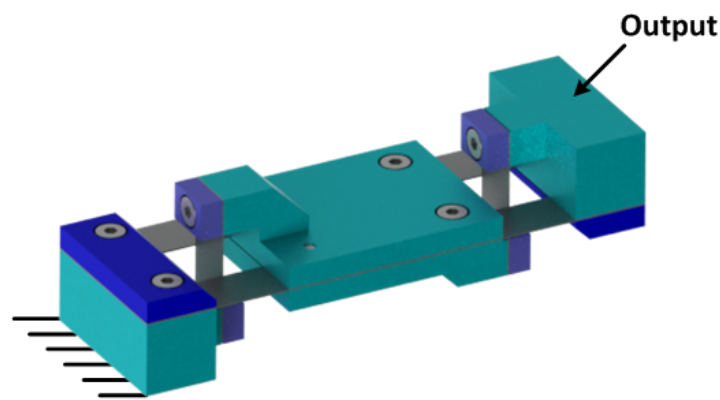


Figure E.2: Detailed mechanical design of the  $t_{\parallel}r_{\perp}$  and  $t_{\perp}r_{\parallel}$  bricks

### E.1 1 DOF: Rx

This robot simply consists in the  $R_{\perp}$  active brick.

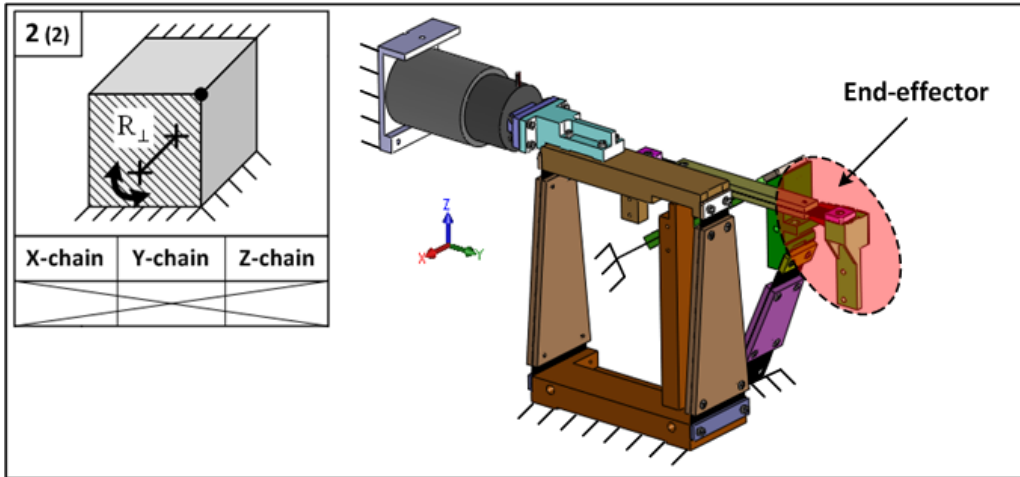


Figure E.3: 1-DOF (Rx) robot

### E.2 1 DOF: Tx

This robot simply consists in the  $T_{\parallel}$  active brick.

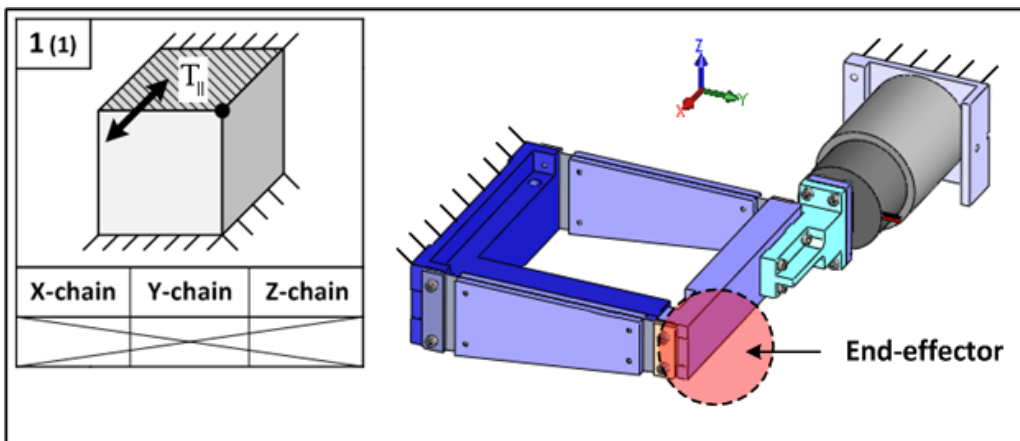


Figure E.4: 1-DOF (Tx) robot

### E.3 2 DOF: $T_x, T_y$

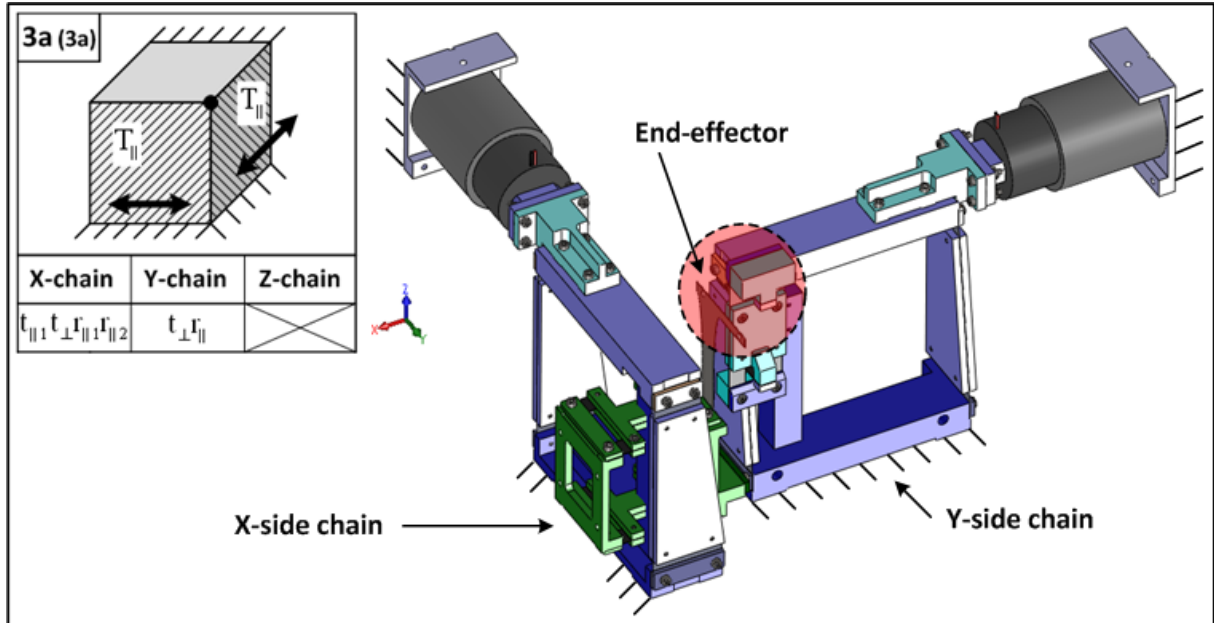


Figure E.5: 2-DOF ( $T_x, T_y$ ) robot

### E.4 2 DOF: $T_x, R_x$

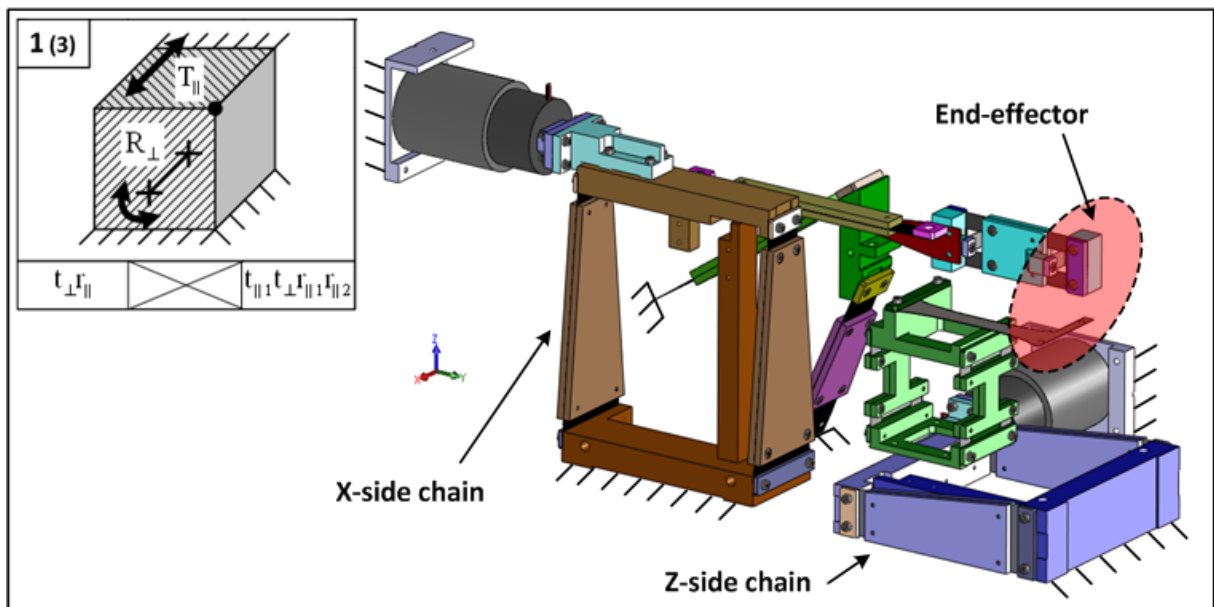


Figure E.6: 2-DOF ( $T_x, R_x$ ) robot

### E.5 2 DOF: Tx, Ry

This robot simply consists in the  $T_{\parallel}R_{\perp}$  active brick.

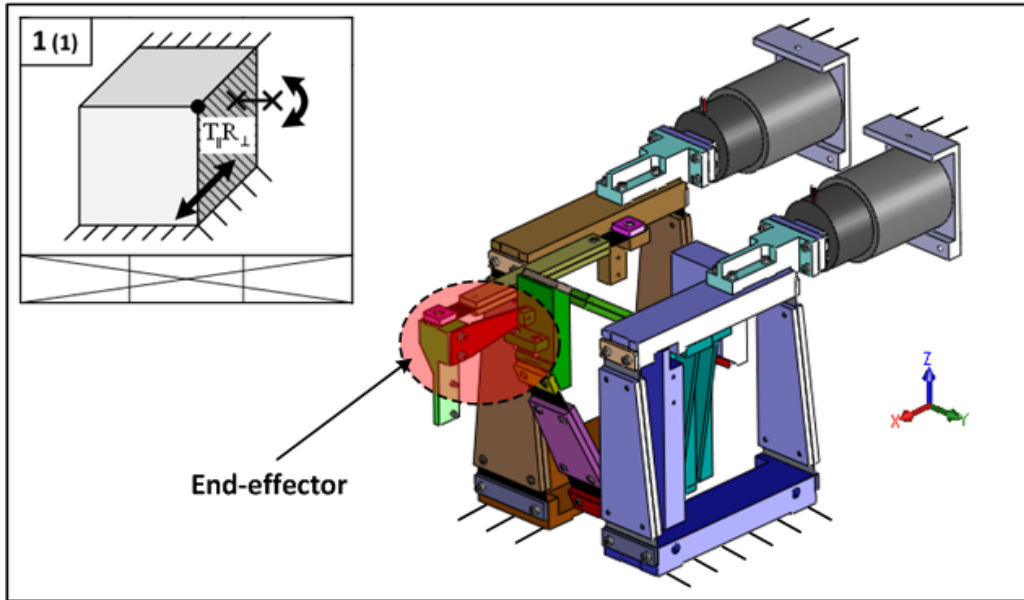


Figure E.7: 2-DOF (Tx, Ry) robot

### E.6 2 DOF: Rx, Ry

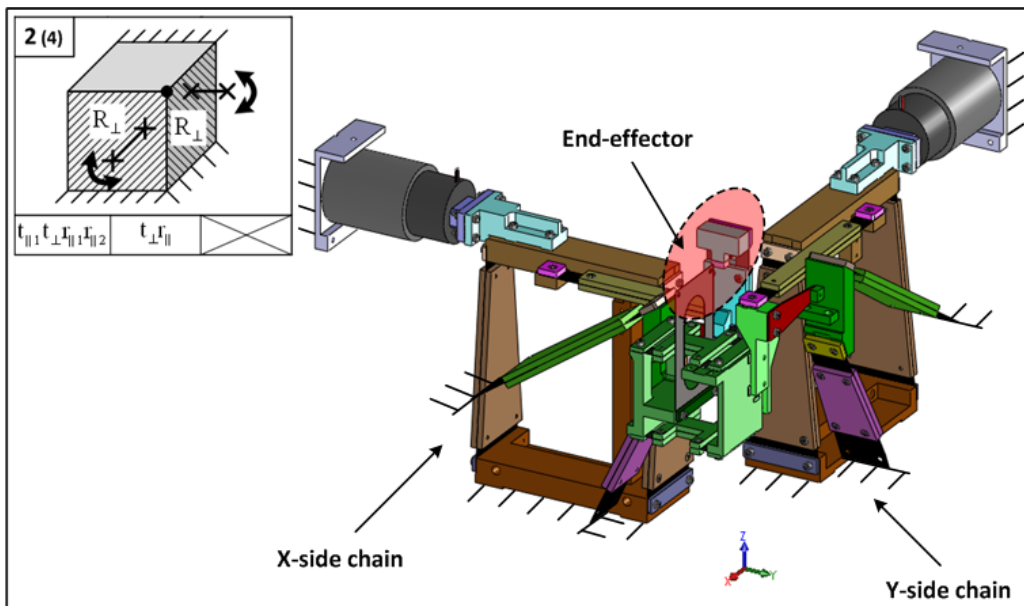


Figure E.8: 2-DOF (Rx, Ry) robot

## E.7 3 DOF: $T_x, T_y, T_z$

This robot, actuating three translations, is the Legolas adaptation of the orthogonal Delta kinematics (see figures 1.4, 2.17 and 2.18): the mechanical design of the space parallelogram ( $t_{\parallel 1} t_{\perp 1} r_{\parallel 1} r_{\parallel 2}$  passive brick) consists in the key difference between this robot and the former Delta<sup>3</sup> prototypes. Furthermore, the transformation of the 5-DOF Legolas 5 detailed in chapter 6 into this mobility is straightforward: it simply consists in replacing both  $T_{\parallel R_{\perp}}$  active bricks by two  $T_{\parallel}$  bricks (see figure E.9).

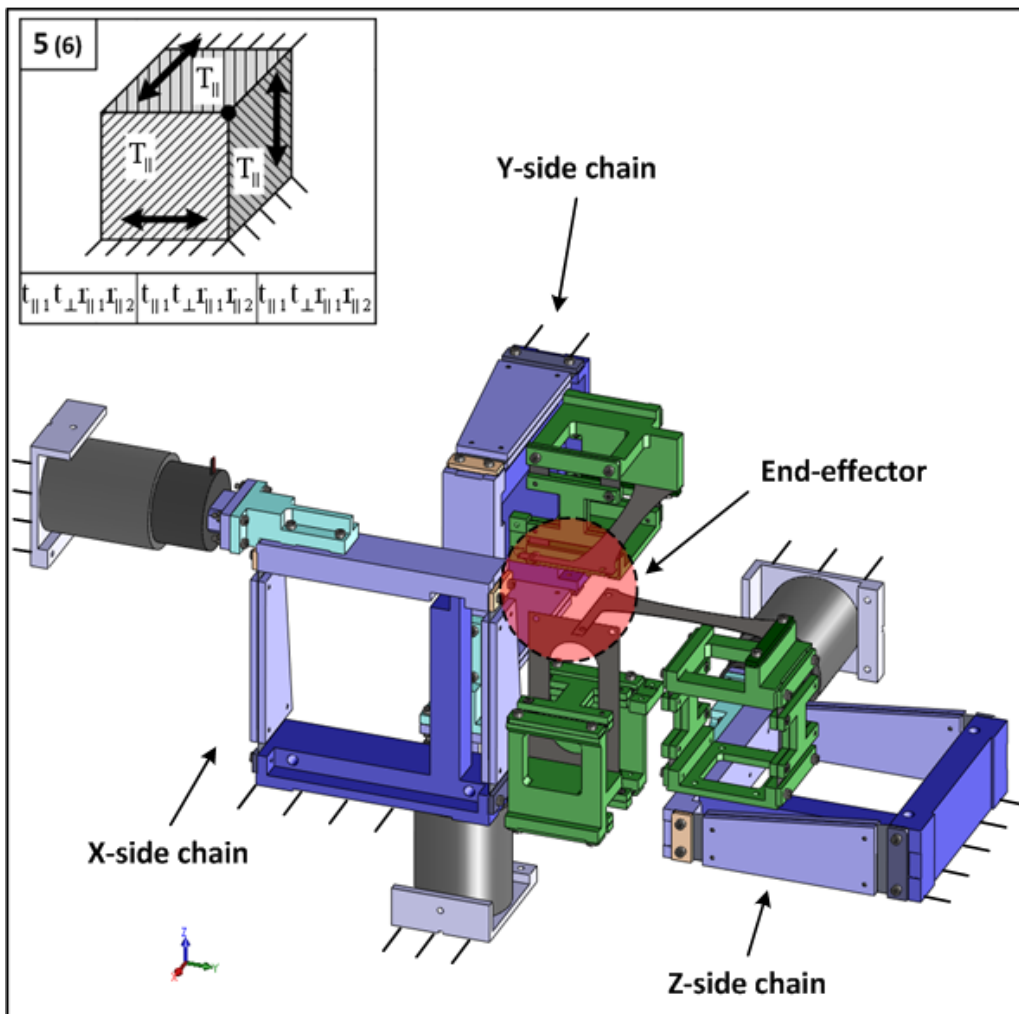


Figure E.9: 3-DOF ( $T_x, T_y, T_z$ ) robot



**E.8 3 DOF:  $T_x, T_y, R_x$**

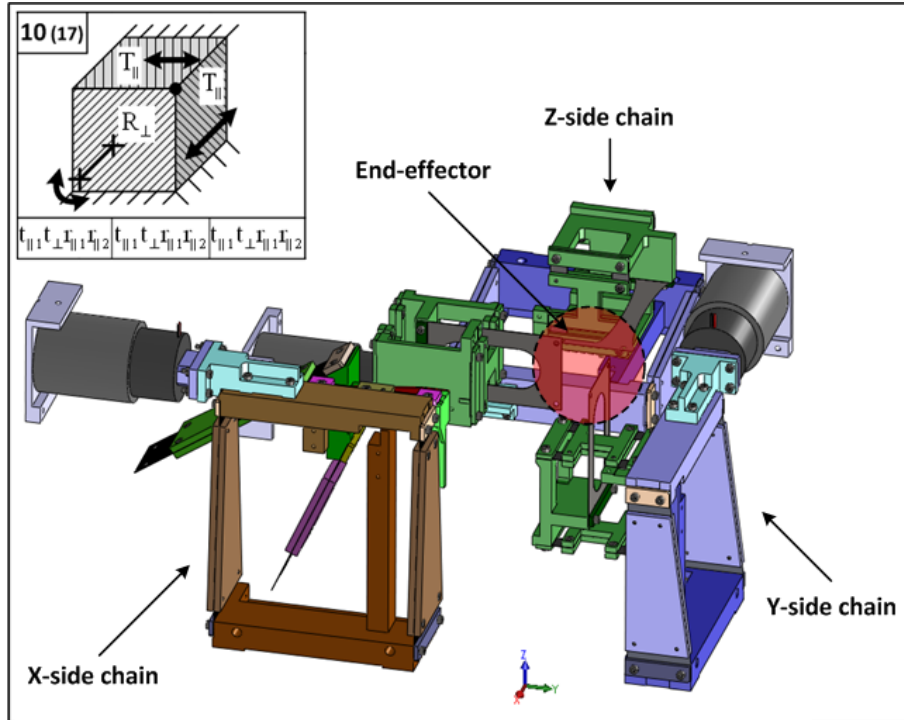


Figure E.10: 3-DOF ( $T_x, T_y, R_x$ ) robot

**E.9 3 DOF:  $T_y, T_z, R_x$**

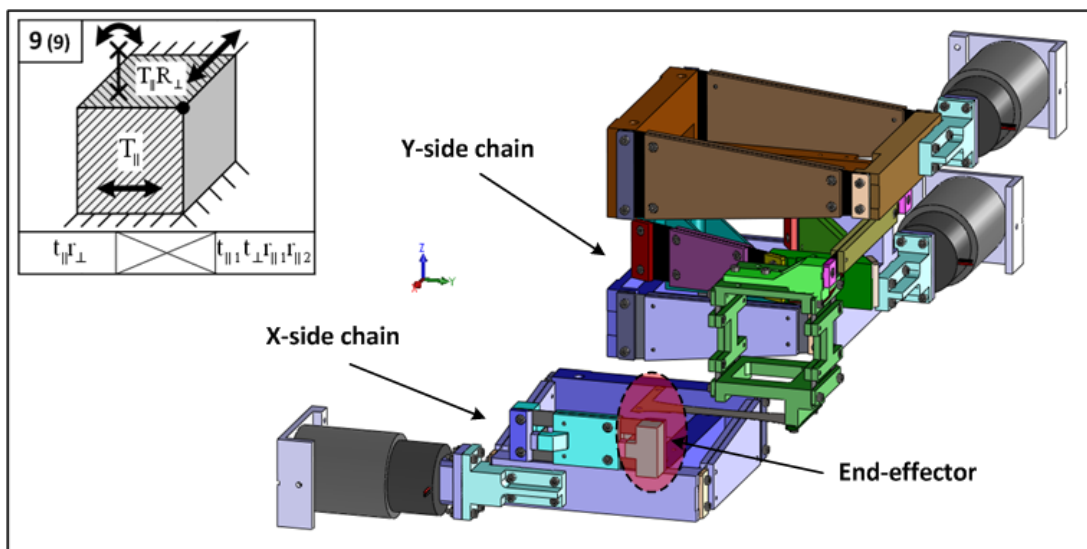


Figure E.11: 3-DOF ( $T_y, T_z, R_x$ ) robot

### E.10 3 DOF: $T_z, R_x, R_y$

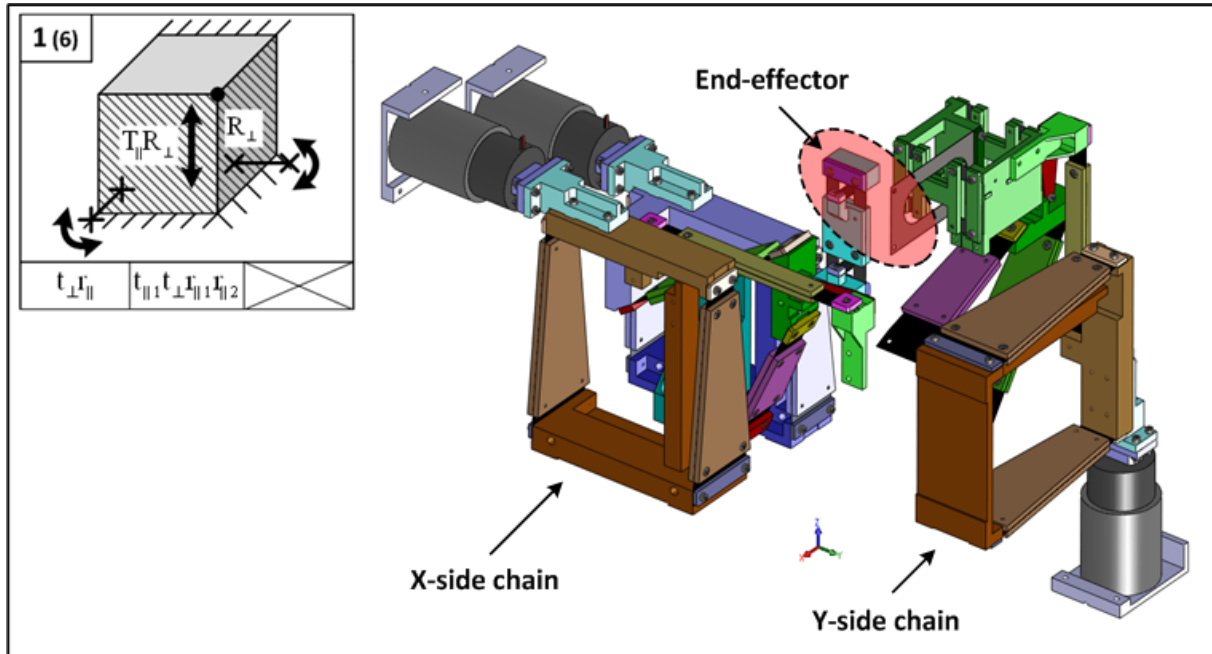


Figure E.12: 3-DOF ( $T_z, R_x, R_y$ ) robot

### E.11 3 DOF: $T_x, R_x, R_y$

This 3-DOF robot consists in the Legolas 5 kinematics where both  $T_{\parallel}R_{\perp}$  active bricks have been replaced by  $R_{\perp}$  bricks. Furthermore, the Y-side and the Z-side kinematic chains have been swapped to allow for a more compact arrangement.

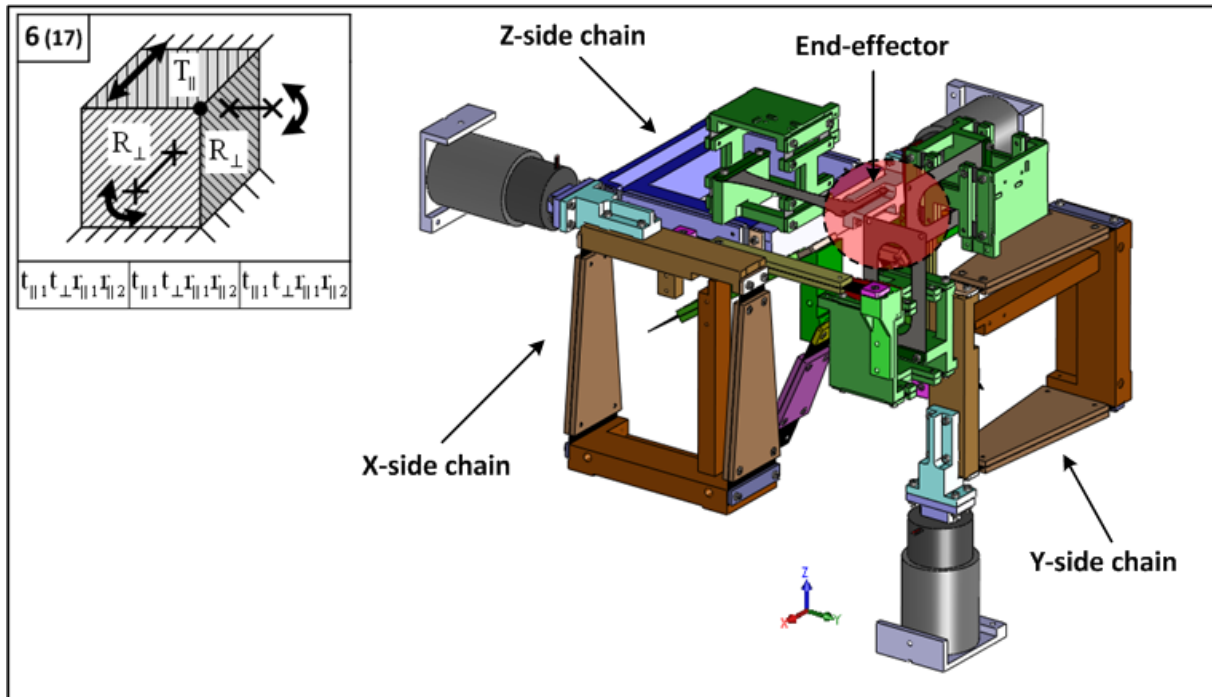


Figure E.13: 3-DOF ( $T_x, R_x, R_y$ ) robot

E.12 3 DOF:  $R_x, R_y, R_z$

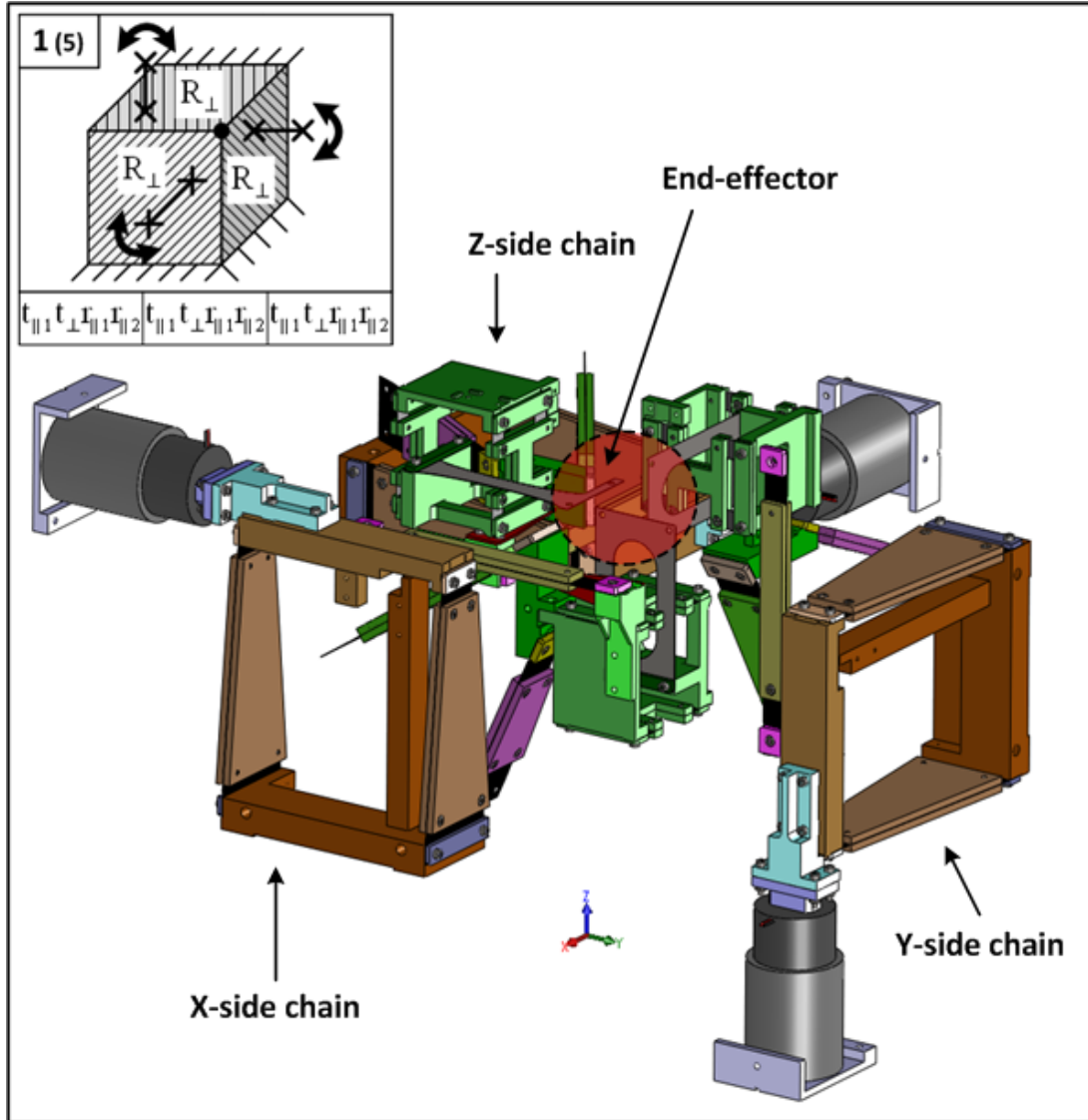


Figure E.14: 3-DOF ( $R_x, R_y, R_z$ ) robot

### E.13 4 DOF: $T_x, T_y, T_z, R_x$

This 4-DOF robot consists in the Legolas 5 kinematics where a  $T_{\parallel}R_{\perp}$  active brick has been replaced by a  $T_{\parallel}$  brick. Furthermore, the Y-side and the Z-side kinematic chains have been swapped to allow for a more compact arrangement.

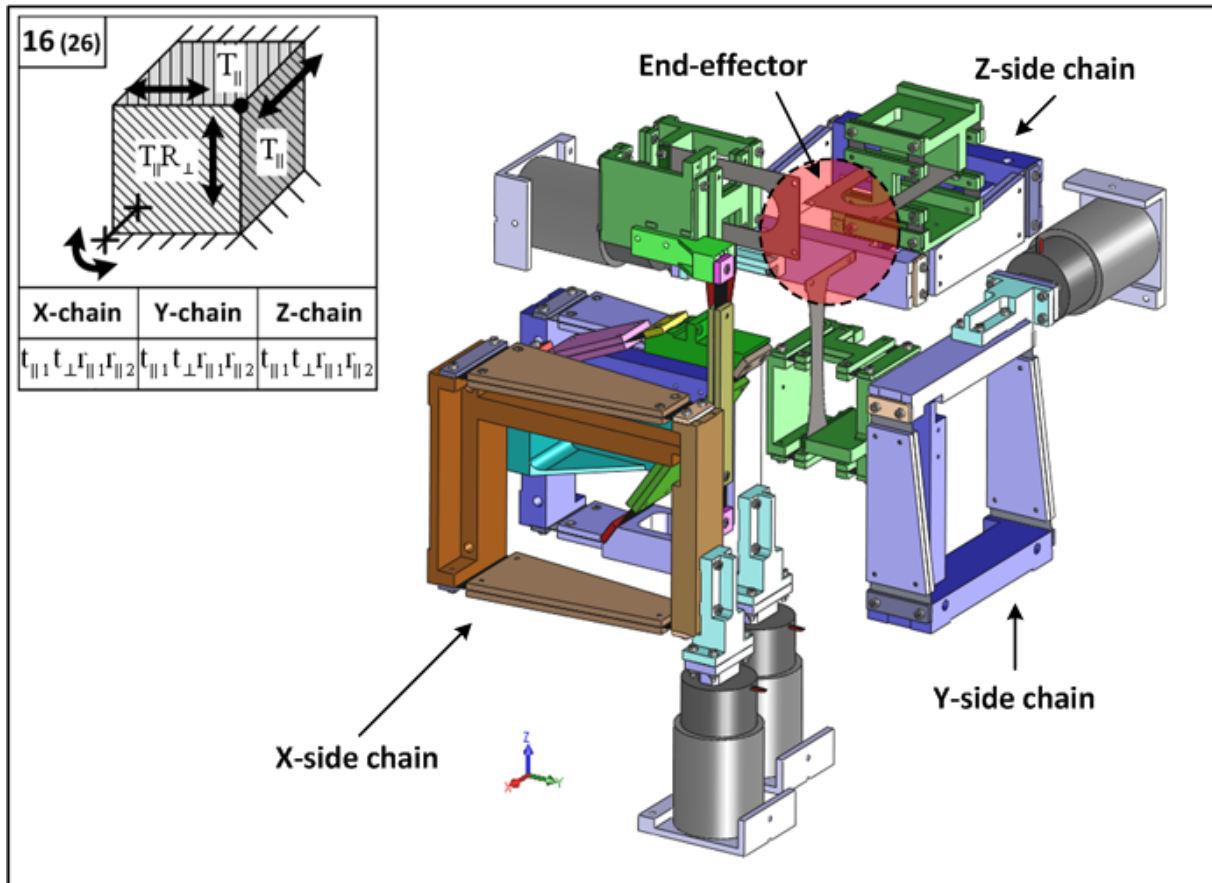


Figure E.15: 4-DOF ( $T_x, T_y, T_z, R_x$ ) robot

### E.14 4 DOF: $T_x, T_z, R_x, R_y$

This 4-DOF robot consists in the Legolas 5 kinematics where a  $T_{\parallel}R_{\perp}$  active brick has been replaced by a  $R_{\perp}$  brick.

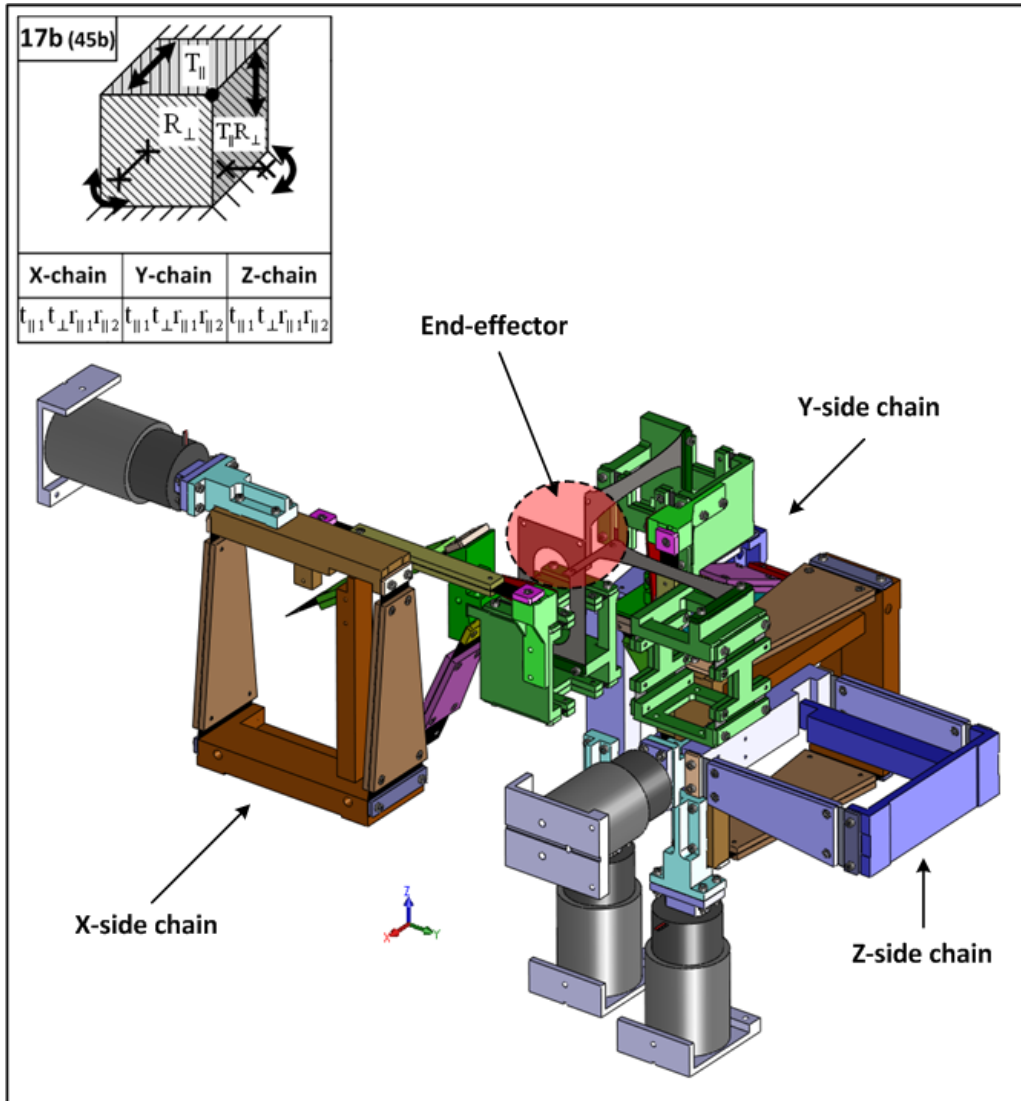


Figure E.16: 4-DOF ( $T_x, T_z, R_x, R_y$ ) robot

**E.15 4 DOF:  $T_x, T_y, R_x, R_y$**

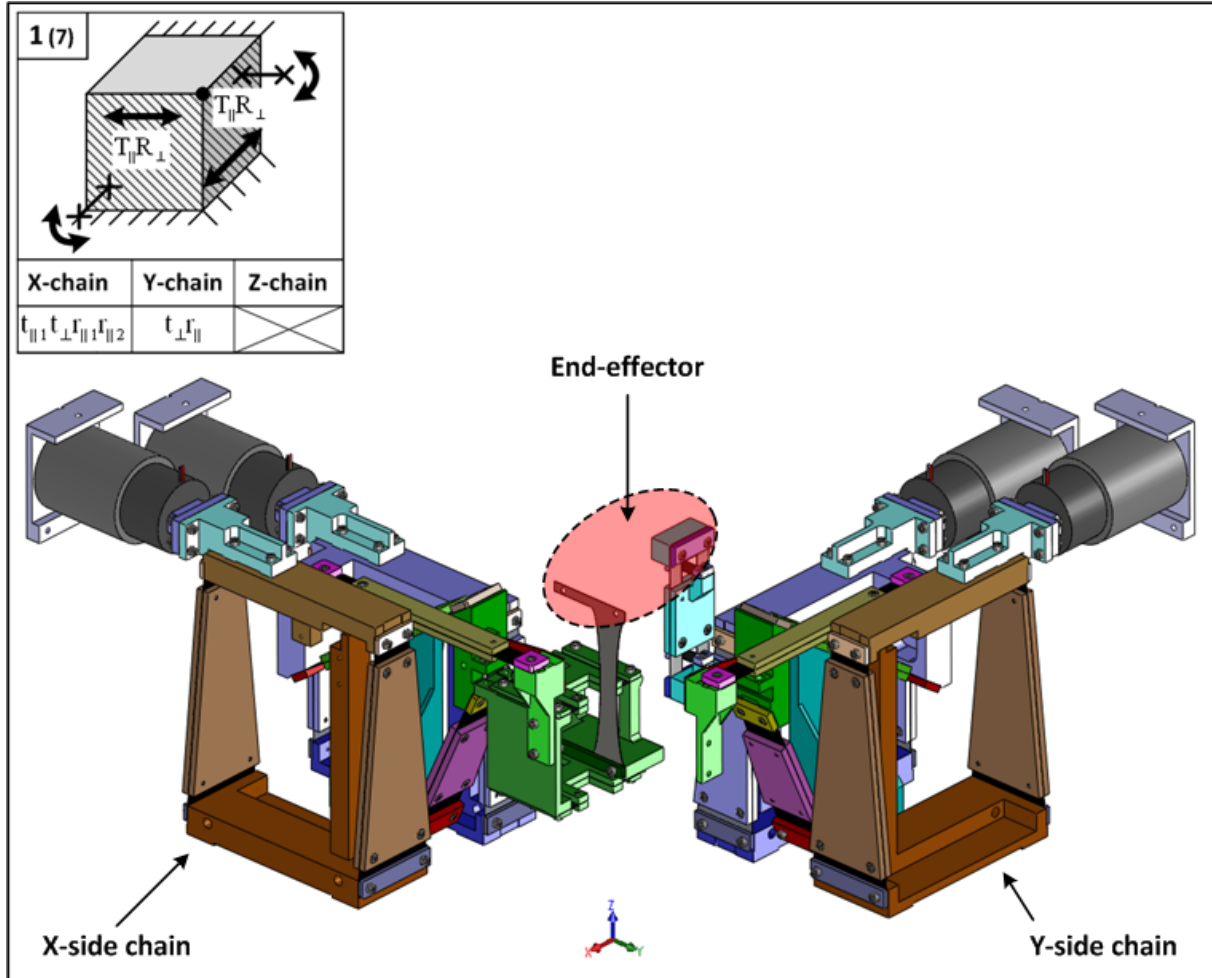


Figure E.17: 4-DOF ( $T_x, T_y, R_x, R_y$ ) robot



E.16 4 DOF:  $T_x, R_x, R_y, R_z$

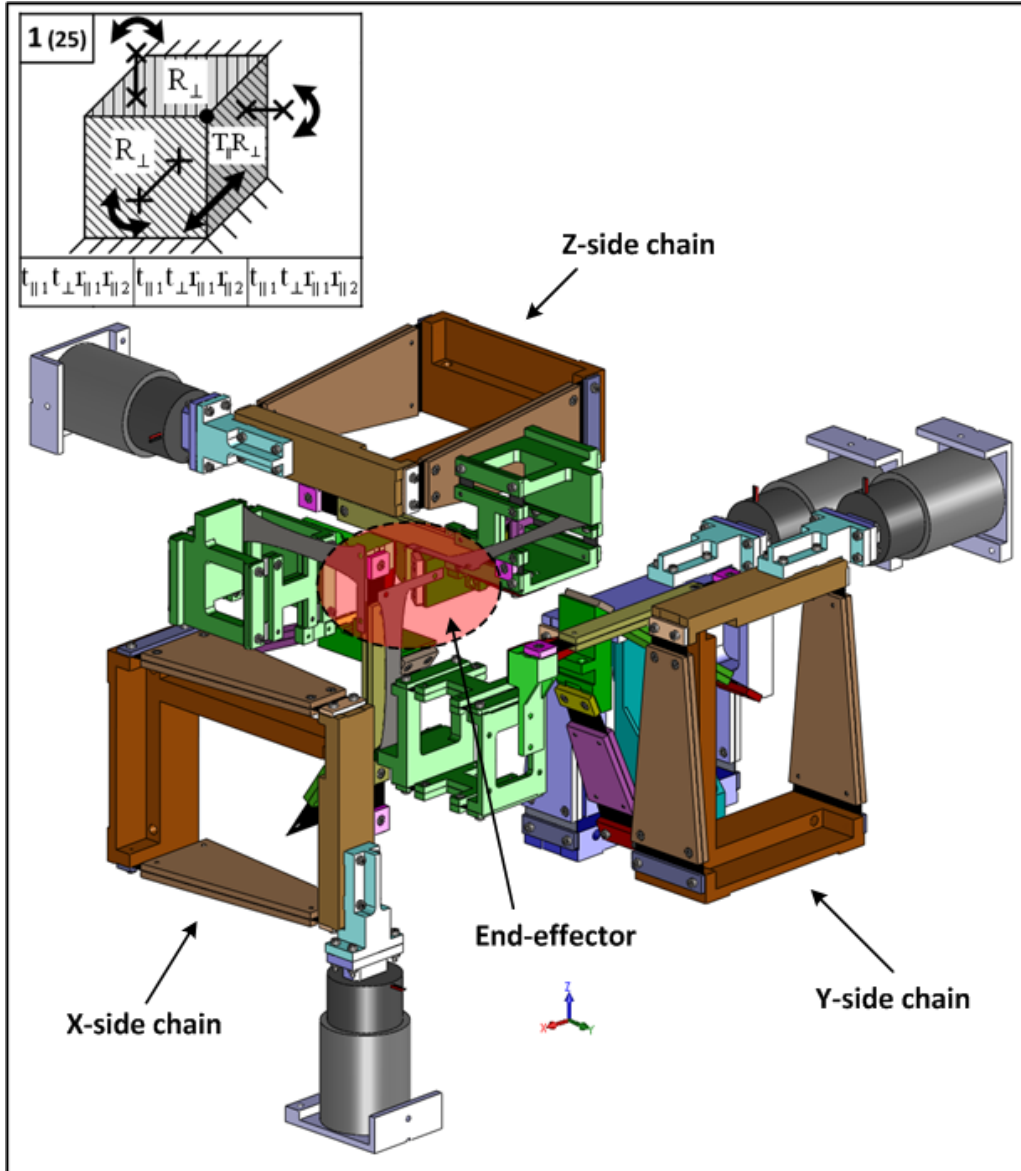


Figure E.18: 4-DOF ( $T_x, R_x, R_y, R_z$ ) robot

E.17 5 DOF:  $T_x, T_y, R_x, R_y, R_z$

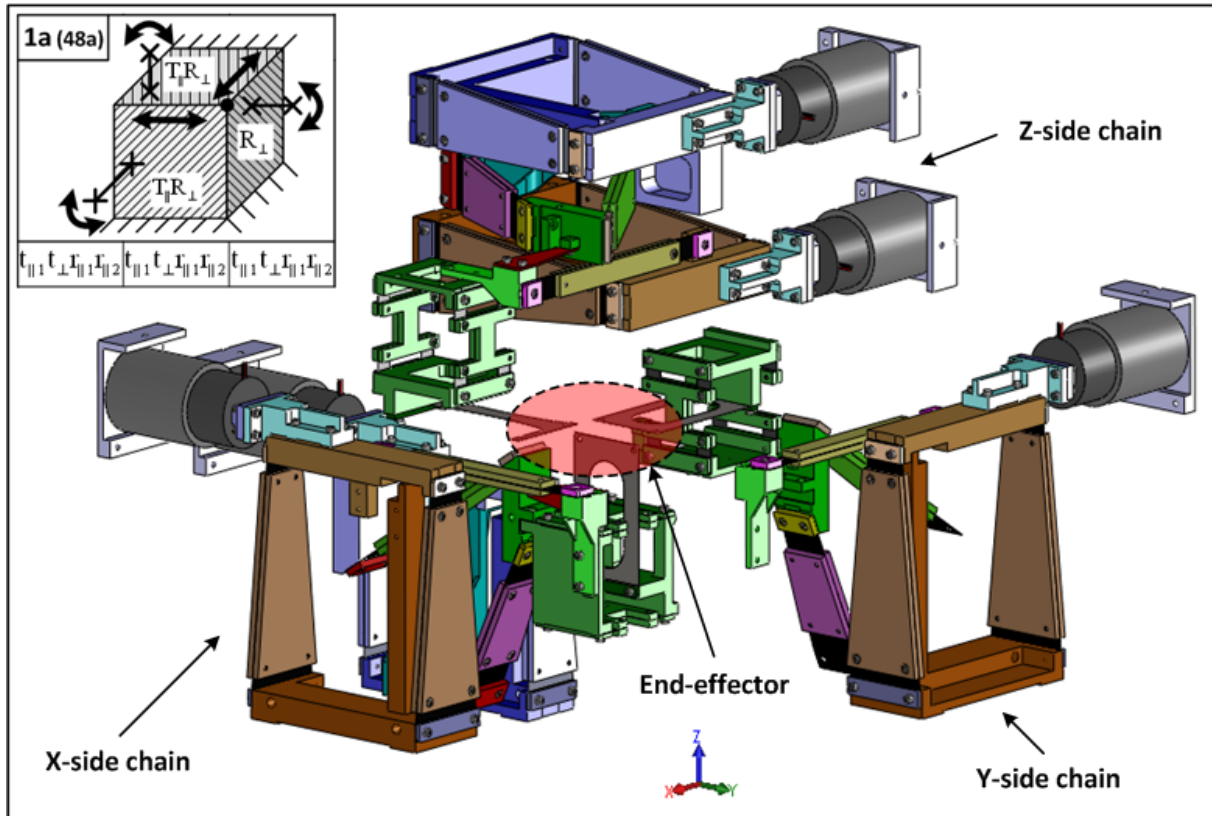


Figure E.19: 5-DOF ( $T_x, T_y, R_x, R_y, R_z$ ) robot

### E.18 5 DOF: $T_x, T_y, T_z, R_x, R_y$

This robot consists in the Legolas 5 prototype, whose mechanical design has been detailed in chapter 6.

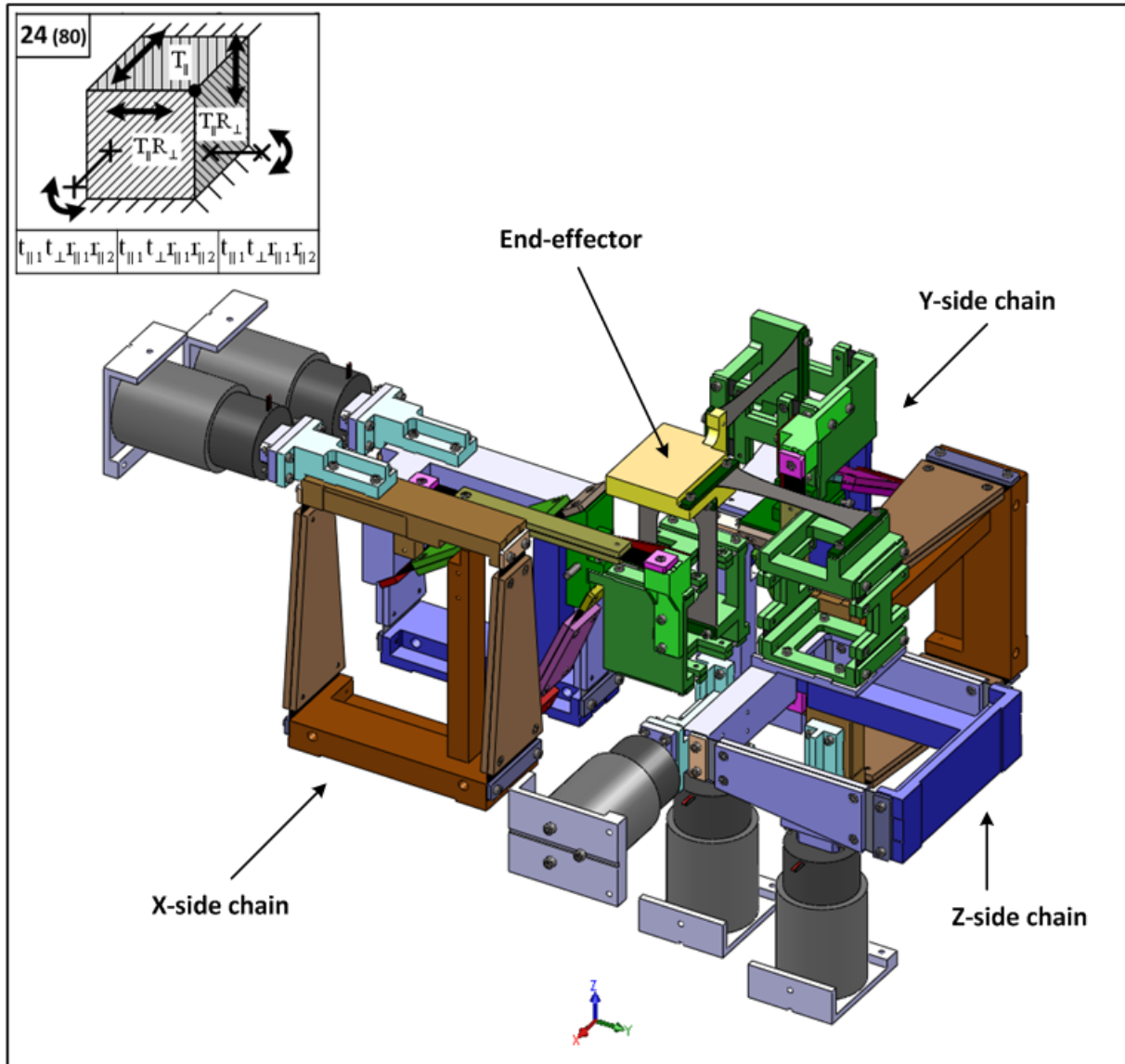


Figure E.20: 5-DOF ( $T_x, T_y, T_z, R_x, R_y$ ) robot

**E.19 6 DOF:  $T_x, T_y, T_z, R_x, R_y, R_z$**

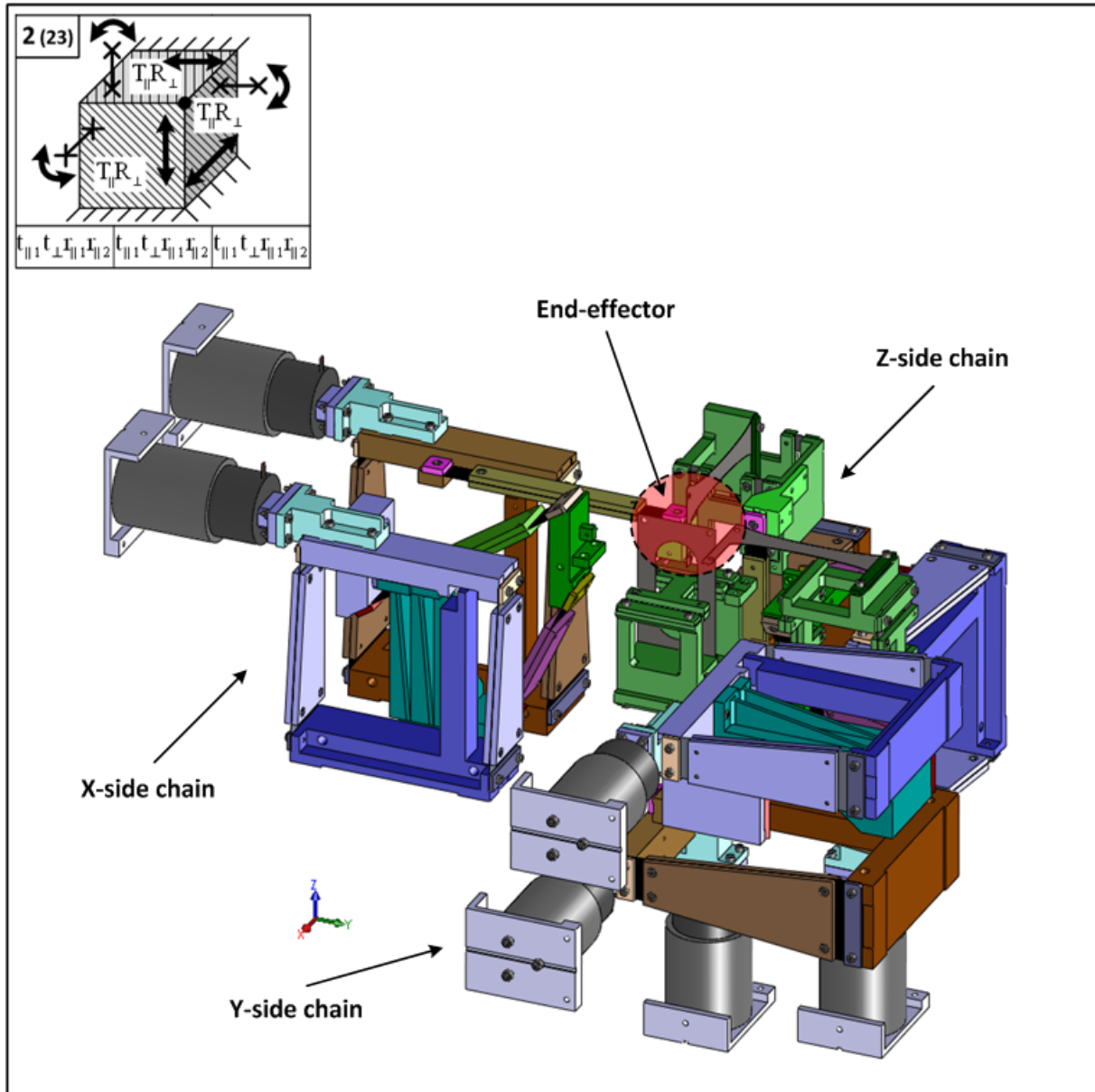


Figure E.21: 6-DOF ( $T_x, T_y, T_z, R_x, R_y, R_z$ ) robot



# Bibliography

- [1] G. Accaccia, L. Bruzzone, R. Razzoli, *A modular robotic system for industrial applications*, Assembly Automation, Emerald, Vol. 28, No. 2, 151-162, 2008.
- [2] D. S. Ackerson, D. R. Harry, *Theory, Experimental Results, and Recommended Standards Regarding the Static Positioning and Orienting Precision of Industrial Robots*, Robotics and Computer-Integrated Manufacturing, Pergamon Journals Ltd, Vol. 2, No. 3/4, 247-259, 1985.
- [3] GF AgieCharmilles, <http://www.gfac.com>, January 2012.
- [4] I. Asimov, *The Roving Mind*, Prometheus Books, New York, 1997.
- [5] J.-P. Bacher, S. Bottinelli, J.-M. Breguet, R. Clavel, *Delta<sup>3</sup>, a New Ultra-high Precision Micro-Robot: Design and Control of a Flexure Mechanism*, Journal Européen des Systèmes Automatisés, Vol. 36, No. 9, 1263-1275, 2002.
- [6] J.-P. Bacher, *Conception de robots de très haute précision à articulations flexibles : interaction dynamique-commande*, Ph. D. Thesis, No. 2907, Ecole Polytechnique Fédérale de Lausanne (EPFL), 2003.
- [7] A. K. Banerjee, S. Nagarajan, *Efficient Simulation of Large Overall Motion of Beams Undergoing Large Deflection*, Multibody System Dynamics, Kluwer Academic Publishers, Vol. 1, 113-126, 1997.
- [8] BEI Kimco Magnetics website, <http://www.beikimco.com>, February 2012.
- [9] Y. Bellouard, *Conception de dispositifs en alliage à mémoire de forme en microtechnique*, Ph. D. Thesis, No. 2308, Ecole Polytechnique Fédérale de Lausanne (EPFL), 2000.
- [10] Y. Bellouard, *Microrobotics: Methods and Applications*, CRC Press, Boca Raton, 2010.
- [11] B. Benhabib, G. Zak, M. G. Lipton, *A Generalized Kinematic Modeling Method for Modular Robots*, Journal of Robotic Systems, John Wiley & Sons, Vol. 6, 545-571, 1989.
- [12] B. Benhabib, M. Q. Dai, *Mechanical Design of a Modular Robot for Industrial Applications*, Journal of Manufacturing Systems, Elsevier, Vol. 10, No. 4, 297-306, 2003.

- [13] S. Bottinelli, S. Henein, C. Aymon, R. Clavel, *Movement transmission unit and movement transmission apparatus employing the same*, US Patent US006453566B1, 24<sup>th</sup> September 2002.
- [14] D. M. Brouwer, *Design Principles for Six Degrees-of-Freedom MEMS-based Precision Manipulators*, Ph. D. Thesis, University of Twente, 2007.
- [15] Brüel & Kjær Sound & Vibration Measurement A/S. website, <http://www.bksv.com>, February 2012.
- [16] L. Bruzzone, R. M. Molfino, M. Zoppi, *A Cartesian Parallel Robot with Flexure Joints for Miniaturized Assembly Applications*, Proceedings of the 5<sup>th</sup> Chemnitz Parallel Kinematics Seminar, Vol. 33, 835-838, 2006.
- [17] L. Bruzzone, R. Molfino, *A novel parallel robot for current microassembly applications*, Assembly Automation, Emerald, Vol. 26, No. 4, 299-306, 2006.
- [18] J. Bryant, C. Sangwin, *How Round Is Your Circle ? Where Engineering and Mathematics Meet*, Princeton University Press, 2008.
- [19] A. Burisch, J. Wrege, A. Raatz, J. Hesselbach, R. Degen, *PARVUS - miniaturised robot for improved flexibility in micro production*, Assembly Automation, Emerald, Vol. 27, No. 1, 65-73, 2007.
- [20] J. R. Cannon, *Compliant Mechanisms to perform Bearing and Spring Functions in High Precision Applications*, Master of Science Thesis, Dept. of Mechanical Engineering, Brigham Young University, 2004.
- [21] D. Chablat, P. Wenger, *A New Concept of Modular Parallel Mechanism for Machining Applications*, Proceedings of the IEEE International Conference on Robotics and Automation, 3965-3970, 2003.
- [22] R. Clavel, *Conception d'un robot parallèle rapide à 4 degrés de liberté*, Ph. D. Thesis, No. 925, Ecole Polytechnique Fédérale de Lausanne (EPFL), 1991.
- [23] F. Cosandier, V. Chatagny, A. Eichenberger, H. Baumann, R. Clavel, *Optimizing the Design of the 13-Hinge Rectilinear Stage for High Straightness Translation*, Proceedings of the 13<sup>th</sup> World Congress in Mechanism and Machine Science, A23-437, 2011.
- [24] G. Danescu, *Une méthode algébrique de synthèse et conception des mécanismes articulés*, Ph. D. Thesis, No. 460, U.F.R. des Sciences et Techniques de l'Université de Franche-Comté, 1995.
- [25] M. Del Pedro, T. Gmür, *Eléments de Mécanique des Structures*, Presses Polytechniques et Universitaires Romandes, 2001.
- [26] J. van Eijk, *On the design of plate-spring mechanisms*, Ph. D. Thesis, No. 172, Dept. of Mechanical Engineering, Delft University of Technology, 1985.



- [27] Etel SA website, <http://www.etel.ch>, February 2012.
- [28] Y. Fang, L.-W. Tsai, *Structure Synthesis of a Class of 4-DoF and 5-DoF Parallel Manipulators with Identical Limb Structures*, International Journal of Robotics Research, Sage, Vol. 21, 799-810, 2002.
- [29] N. Fazenda, T. Niaritsiry, R. Clavel, *Simulation-based kinematic modeling of a high precision parallel manipulator*, Proceedings of the 9<sup>th</sup> IEEE International Conference on Methods and Models in Automation and Robotics, Vol. 2, 1051-1058, 2003.
- [30] N. Fazenda, *Calibration of high-precision flexure parallel robots*, Ph. D. Thesis, No. 3712, Ecole Polytechnique Fédérale de Lausanne (EPFL), 2007.
- [31] G. Gogu, *Structural Synthesis of Parallel Robots, Part I - Methodology, Part II - Translational Topologies with Two and Three Degrees of Freedom, Part III - Topologies with planar motion of the moving platform*, Springer, 2008-2010.
- [32] L. C. Hale, *Principles and Techniques for Designing Precision Machines*, Ph. D. Thesis, Dept. of Mechanical Engineering, Massachusetts Institute of Technology, 1999.
- [33] P. Helmer, Y. Mabillard, R. Clavel, S. Bottinelli, *High precision apparatus for imposing or measuring a position or of a force*, US Patent US2004025569A1, 23<sup>rd</sup> December 2004.
- [34] P. Helmer, *Conception systématique de structures cinématiques orthogonales pour la micro-robotique*, Ph. D. Thesis, No. 3365, Ecole Polytechnique Fédérale de Lausanne (EPFL), 2006.
- [35] S. Henein, *Conception des structures articulées à guidages flexibles de haute précision*, Ph. D. Thesis, No. 2194, Ecole Polytechnique Fédérale de Lausanne (EPFL), 2000.
- [36] S. Henein, *Conception des guidages flexibles*, Presses Polytechniques et Universitaires Romandes, Collection Meta, 2001.
- [37] S. Henein, P. Spanoudakis, S. Droz, L. I. Myklebust, E. Onillon, *Flexure Pivot for Aerospace Mechanisms*, Proceedings of the 10<sup>th</sup> European Space Mechanisms and Tribology Symposium, Spain, 2003.
- [38] S. Henein, *Flexures: simply subtle*, Proceedings of the 6<sup>th</sup> International Conference on Mechanical Engineering Design of Synchrotron Radiation Equipment and Instrumentation (MEDSI), 2010.
- [39] S. Henein, F. Barrot, S. Jeanneret, R. Fournier, L. Giriens, M. Gumy, S. Droz, M. Toimil, *Silicon Flexures for the Sugar-Cube Delta Robot*, Proceedings of the 11<sup>th</sup> euspen International Conference, Vol. 2, 6-9, 2011.
- [40] J. Hesselbach, A. Raatz, *Compliant parallel robot with 6 DOF*, Microrobotics and Microassembly III, Proceedings of SPIE, Vol. 4568, 143-150, 2001.

- [41] J. Hesselbach, A. Raatz, *Performance of Pseudo-Elastic Flexure Hinges in Parallel Robots for Micro-Assembly Tasks*, CIRP Annals - Manufacturing Technology, Elsevier, Vol. 53, No. 1, 329-332, 2004.
- [42] J. Hesselbach, J. Wrege, A. Raatz, O. Becker, *Aspects on design of high precision parallel robots*, Assembly Automation, Emerald, Vol. 24, No. 1, 49-57, 2004.
- [43] A. Hodac, *A macro/micro-manipulator for high speed and accurate pick and place operations*, Diss. ETH No. 13148, Swiss Federal Institute of Technology Zurich (ETHZ), 1999.
- [44] J. B. Hopkins, R. M. Panas, *Design of Flexure-based Precision Transmission Mechanisms using Screw Theory*, Proceedings of the 11<sup>th</sup> euspen International Conference, Vol. 2, 443-446, 2011.
- [45] J. B. Hopkins, M. L. Culpepper, *Synthesis of Multi-Degree-of-Freedom Precision Flexure Concepts via Freedom and Constraint Topologies*, Proceedings of the American Society for Precision Engineering, 2007.
- [46] L. L. Howell, *Compliant Mechanisms*, Wiley-Interscience, 2001.
- [47] R. V. Jones, I. R. Young, *Some parasitic deflexions in parallel spring movements*, Journal of Scientific Instruments, IOP Science, Vol. 33, No. 1, 11-15, 1956.
- [48] C. Joseph, *Contribution à l'accroissement des performances du processus de  $\mu$ EDM par l'utilisation d'un robot à dynamique élevée et de haute précision*, Ph. D. Thesis, No. 3281, Ecole Polytechnique Fédérale de Lausanne (EPFL), 2005.
- [49] P. Kobel, R. Clavel, *Miniaturization Challenges and Their Impact on the Micro-factory Concept and Manipulators*, Japan Society of Precision Engineering, Vol. 77, No. 3, 263-268, 2011.
- [50] M. P. Koster, *Constructieprincipes voor het nauwkeurig bewegen en positioneren*, Twente University Press, 2000.
- [51] J. Lemay, L. Notash, *Configuration engine for architecture planning of modular parallel robots*, Mechanism and Machine Theory, Elsevier, Vol. 39, 101-117, 2004.
- [52] N. Lobontiu, *Compliant Mechanisms: Design of flexure hinges*, CRC Press, Boca Raton, 2002.
- [53] E. Lubrano, R. Clavel, *Thermal Calibration of a 3 DOF Ultra High-Precision Robot Operating in Industrial Environment*, Proceedings of the 2010 IEEE International Conference on Robotics and Automation, IEEE, 3692-3697, 2010.
- [54] E. Lubrano, *Calibration of Ultra-high-precision Robots Operating in an Unsteady Environment*, Ph. D. Thesis, No. 5098, Ecole Polytechnique Fédérale de Lausanne (EPFL), 2011.

- [55] J. M. McCarthy, *Geometric Design of Linkages*, Interdisciplinary Applied Mathematics, Springer, Vol. 11, 2000.
- [56] Measurement Specialities<sup>TM</sup>, <http://www.meas-spec.com/>, February 2012.
- [57] Mecartex SA website, <http://www.mecartex.com>, February 2012.
- [58] J. Meng, G. F. Liu, Z. Li, *A Geometric Theory for Synthesis and Analysis of Sub-6 DoF Parallel Manipulators*, Proceedings of the IEEE International Conference on Robotics and Automation, 2938-2943, 2005.
- [59] J. Meng, G. F. Liu, Z. Li, *A Geometric Theory for Synthesis and Analysis of Sub-6 DoF Serial Manipulator Subchains*, Proceedings of the IEEE International Conference on Robotics and Automation, 4716-4721, 2005.
- [60] J.-P. Merlet, *Les robots parallèles*, 2<sup>e</sup> édition, Hermès, Collection robotique, Paris, 1997.
- [61] J.-P. Merlet, *DEMOCRAT: A DDesign MethOdology for the Conception of Robot with parallel ArchiTecture*, Proceedings of the IEEE International Conference on Intelligent Robots and Systems, Vol. 3, 1630-1636, 1997.
- [62] J.-P. Merlet, *Determination of the optimal geometry of modular parallel robots*, Proceedings of the 2003 IEEE International Conference on Robotics & Automation, 1197-1202, 2003.
- [63] PI miCos GmbH website, <http://www.pimicos.com>, February 2012.
- [64] Y.-M. Moon, S. Kota, *Design of Compliant Parallel Kinematic Machines*, Proceedings of the ASME 27<sup>th</sup> Biennial Mechanisms and Robotics Conference, 2002.
- [65] R. Neugebauer, D. Weidlich, H. Zickner, S. Hensel, S. Ihlenfeldt, T. Polzin, *A Virtual Reality-Based Engineering Tool for Fast Configuration of Machine Tools with Parallel Kinematics - VRAx<sup>®</sup>*, Proceedings of the 5<sup>th</sup> Chemnitz Parallel Kinematics Seminar, Vol. 33, 39-62, 2006.
- [66] R. Neugebauer, H.-J. Koriath, M. Richter, M. Müller, *Miniature 3-DOF planar parallel kinematics with large work space for precision positioning of endeffectors*, Proceedings of the 11<sup>th</sup> euspen International Conference Vol. 1, 315-318, 2011.
- [67] Newport Corporation website, <http://www.newport.com>, February 2012.
- [68] T. Niaritsiry, N. Fazenda, R. Clavel, *Study of the sources of inaccuracy of a 3 DOF flexure hinge-based parallel manipulator*, Proceedings of the IEEE International Conference on Robotics and Automation ICRA'04, Vol. 4, 4091-4096, 2004.
- [69] T. Niaritsiry, *Optimisation de la conception du robot parallèle Delta Cube de très haute précision*, Ph. D. Thesis, No. 3567, Ecole Polytechnique Fédérale de Lausanne (EPFL), 2006.

- [70] T. Noll, K. Holldack, G. Reichardt, O. Schwarzkopf, T. Zeschke, *Parallel kinematics for nanoscale Cartesian motions*, Precision Engineering, Elsevier, Vol. 33, No. 3, 291-304, 2009.
- [71] Numerik Jena GmbH, <http://numerik.cycro-project.de>, February 2012.
- [72] C. B. Patil, *Robust Design of Selectively Compliant Flexure-based Precision Mechanisms*, Ph. D. Thesis, University of Texas, 2008.
- [73] E. Pernette, *Robot de Haute Précision à 6 degrés-de-liberté pour l'Assemblage des Microsystèmes*, Ph. D. Thesis, No. 1909, Ecole Polytechnique Fédérale de Lausanne (EPFL), 1998.
- [74] H.-H. Pham, H.-C. Yeh, I. Chen, *Micromanipulation System Design Based on Selective Actuation Mechanisms*, The International Journal of Robotics Research, Vol. 25, No. 2, 171-186, 2006.
- [75] P. Pham, *Design of Hybrid-Kinematic Mechanisms for Machine Tools*, Ph. D. Thesis, No. 4314, Ecole Polytechnique Fédérale de Lausanne (EPFL), 2009.
- [76] C. Pozna, *The Modular Robots Kinematics*, Acta Polytechnica Hungarica, Vol. 4, No. 2, 5-18, 2007.
- [77] C. Pozna, *Modular Robots Design Concepts and Research Directions*, Proceedings of the 5<sup>th</sup> International Symposium on Intelligent Systems and Informatics, 113-118, 2007.
- [78] G. Pritschow, K.-H. Wurst, *Modular Robots for Flexible Assembly*, Proceedings of the 28<sup>th</sup> International Seminar on Manufacturing Systems, 153-158, 1996.
- [79] A. Raatz, F. Trauden, N. Plitea, J. Hesselbach, *Design and Modeling of Compliant High Precision Parallel Robots*, Proceedings of the 5<sup>th</sup> Chemnitz Parallel Kinematics Seminar, Vol. 33, 233-252, 2006.
- [80] M. Richard, R. Clavel, *A new concept of modular kinematics to design ultra-high precision flexure-based robots*, in Proceedings for the Joint Conference of the 41<sup>st</sup> International Symposium of Robotics and the 6<sup>th</sup> German Conference on Robotics, Munich, Germany, pp. 940-947, 2010.
- [81] M. Rösner, R. Lammering, *Basic principles and aims of model reduction in compliant mechanisms*, Proceedings of the Second International Symposium on Compliant Mechanisms, Delft, 2011.
- [82] J. W. Ryu, D.-G. Gweon, *Error analysis of a flexure hinge mechanism induced by machining imperfection*, Precision Engineering, Elsevier Science Inc, Vol. 21, 83-89, 1997.
- [83] P. Schellenkens, N. Rosielle, M. Vermeulen, S. Wetzels, W. Pril, *Design for Precision: current status and trends*, Annals of the CIRP, Vol. 47/2, 1998.

- [84] K. Schöttler, A. Raatz, J. Hesselbach, *Size-adapted Parallel and Hybrid Parallel Robots for Sensor Guided Micro Assembly*, Parallel Manipulators, Towards New Applications, edited by H. Wu, I-Tech Education and Publishing, 225-244, Vienna, 2008.
- [85] K.-H. Sieker, *Lehrbücher des Feinwerktechnik, Band 16: Getriebe mit Energiespeichern*, C. F. Winterische Verlagshandlung, Füssen, 1954.
- [86] Sios Messtechnik GmbH website, <http://www.sios.de>, February 2012.
- [87] S. T. Smith, D. G. Chetwynd, *Foundations of Ultraprecision Mechanism Design*, Developments in Nanotechnology, Taylor & Francis, Vol. 2, 1992.
- [88] S. T. Smith, *Flexures: Elements of Elastic Mechanisms*, CRC Press, Boca Raton, 2000.
- [89] X. Tang, I. Chen, *A Large-Displacement 3-DOF Flexure Parallel Mechanism with Decoupled Kinematics Structure*, Proceedings of the 2006 IEEE International Conference on Intelligent Robots and Systems, 1668-1673, 2006.
- [90] M. Thurneysen, *Méthode Systématique de Conception de Cinématiques Parallèles*, Ph. D. Thesis, No. 3009, Ecole Polytechnique Fédérale de Lausanne (EPFL), 2004.
- [91] S. Timoshenko, *Strength of Materials*, Parts I and II, Second Edition, D. Van Nostrand Company, 1940.
- [92] D. Tolfree, *Commercialising Nanotechnology, concepts - products - markets*, International Journal of Nanomanufacturing, Vol. 1, No. 1, 117-133, 2006.
- [93] I. Verettas, *Microfabrique: méthodologie de conception de systèmes de production miniaturisés et modulaires, disposant d'un environnement salles blanches*, Ph. D. Thesis, No. 3549, Ecole Polytechnique Fédérale de Lausanne (EPFL), 2006.
- [94] C. Wang, L. Wang, *A Novel CAD System for Modular Reconfigurable Parallel Robots*, Proceedings of the 2010 International Conference On Computer Design and Applications (ICCD 2010), Vol. 4, 159-163, 2010.
- [95] Y. Wu, Z. Li, H. Ding, Y. Lou, *Quotient Kinematics Machines: Concept, Analysis and Synthesis*, Proceedings of the IEEE International Conference on Intelligent Robots and Systems, 1964-1969, 2008.
- [96] G. Yang, I. Chen, W. Lim, S. Yeo, *Kinematic Design of Modular Reconfigurable In-Parallel Robots*, Autonomous Robots, Kluwer Academic Publishers, Vol. 10, 83-89, 2001.
- [97] G. Yang, I. Chen, W. Chen, S. H. Yeo, *Design and Analysis of a 3-RPRS Modular Parallel Manipulator for Rapid Deployment*, Proceeding of the 2003 IEEE/ASME International Conference on Advanced Intelligent Mechatronics (AIM 2003), 1250-1255, 2003.
- [98] G. Yang, T. J. Teo, W. Lin, I. Chen, *Analysis and Design of a 3-DOF Flexure-based Zero-torsion Parallel Manipulator for Nano-alignment Applications*, Proceedings of the 2011 IEEE International Conference on Robotics and Automation, 2751-2756, 2011.





# Curriculum Vitae

*Murielle Richard*  
Avenue d'Ouchy 24C  
CH - 1006 Lausanne

Nationality: Swiss  
Born: 4<sup>th</sup> December 1984  
Civil status: Single



## Studies

04/2008 – 05/2012 **EPFL - Ecole Polytechnique Fédérale de Lausanne** (Switzerland):  
Ph.D. in Manufacturing Systems and Robotics

10/2006 – 02/2008 **EPFL - Ecole Polytechnique Fédérale de Lausanne** (Switzerland):  
M.Sc. in Microengineering, specialisation in Robotics and Autonomous Systems.  
Nominated for an excellence scholarship at Master level.

10/2003 – 10/2006 **EPFL - Ecole Polytechnique Fédérale de Lausanne** (Switzerland):  
B.Sc. in Microengineering

## Professional Experience

04/2008 – 04/2012 **EPFL - Ecole Polytechnique Fédérale de Lausanne** (Switzerland),  
**Laboratory of Robotic Systems:** Research assistant for Prof. Reymond Clavel:  
helps Bachelor students achieve practical projects in mechanical design (Micro-  
engineering Components course). Supervises Master students in the frame of  
academic and industrial research projects.

## Skills

- **Languages:** French (mother tongue), English (C1 level, Cambridge Advanced Certificate obtained in March 2009), German (B2 level), Swiss German (basic understanding)
- **Engineering software:** SolidWorks, ProE Wildfire, Comsol Multiphysics, Abaqus, Ansys, Matlab, Mathematica, C/C++
- **Office automation software:** Microsoft Office, Lyx, Latex (basics), Adobe Photoshop, Adobe Premiere



## Publications

- M. Richard, R. Clavel, *A new concept of modular kinematics to design ultra-high precision flexure-based robots*, in Proc. for the Joint Conference of the 41<sup>st</sup> Int. Symposium of Robotics and the 6<sup>th</sup> German Conference on Robotics, Munich, Germany, pp. 940-947, 2010.
- M. Richard, R. Clavel, *Concept of modular flexure-based mechanisms for ultra-high precision robot design*, in Proc. of the 2<sup>nd</sup> International Symposium on Compliant Mechanisms, Delft, Netherlands, 2011.
- M. Richard, R. Clavel, *Concept of modular flexure-based mechanisms for ultra-high precision robot design*, Mechanical Sciences, vol. 2, Special Issue on Future directions in compliant mechanisms, pp. 99-107, 2011.
- M. Richard, R. Clavel, *Modularity and parallel kinematics: an original design methodology applied to high precision*, in Proc. of the 14<sup>th</sup> Int. Conference on Climbing and Walking Robots (CLAWAR 2011), Special Session on Parallel Kinematic Machines: Recent and Future Trends, Paris, France, pp. 933-940, 2011.
- E. Lubrano, M. Richard, R. Clavel, *Design and Calibration of Ultra-High-Precision industrial robots*, in Robotics and Automation, submitted.
- M. Richard, R. Clavel, *Modular methodology to design high precision parallel robots and application to a 5-Degree of Freedom flexure-based manipulator*, in Transactions in Robotics, submitted.
- R. Clavel, F. Cosandier, P. Helmer, S. Henein, M. Richard, edited by S. Henein, *Flexures: Simply subtle: essentials of flexure-mechanism design*, Presses Polytechniques et Universitaires Romandes (PPUR), to be published in 2013.
- S. Régnier et al., *Structures flexibles - Applications à la manipulation robotique multi-échelle*, Hermes Science, to be published.

## Extra-scholar activities

- 06/2007      **Participates to the SmartRob contest** (EPFL, Switzerland): designs and programs four autonomous robots, along with three other Master students.
- 2004 – 2007      **Comitee member of Robopoly, EPFL robotics club** (Switzerland): in charge of sponsoring (material, fundraising). Teaches the members on a weekly basis and trains them to assemble and program mobile robots.